# SYNTHESIS OF ALUMINUM INCORPORATED MESOPOROUS CATALYSTS FOR PYROLYSIS OF POLYPROPYLENE

A THESIS SUBMITTED TO
THE GRADUATE SCHOOL OF NATURAL AND APPLIED SCIENCES
OF
MIDDLE EAST TECHNICAL UNIVERSITY

BY

ZEYNEP OBALI

IN PARTIAL FULFILLMENT OF THE REQUIREMENTS
FOR
THE DEGREE OF DOCTOR OF PHILOSOPHY
IN
CHEMICAL ENGINEERING

APRIL 2010

Approval of the thesis:

**SYNTHESIS OF ALUMINUM INCORPORATED MESOPOROUS CATALYSTS FOR PYROLYSIS OF POLYPROPYLENE**

submitted by **ZEYNEP OBALI** in partial fulfillment of the requirements for the degree of **Doctor of Philosophy in Chemical Engineering Department, Middle East Technical University** by,

Prof. Dr. Canan Özgen
Dean, Graduate School of **Natural and Applied Sciences** _____

Prof. Dr. Gürkan Karakaş
Head of Department, **Chemical Engineering** _____

Assoc.Prof. Dr. Naime Aslı Sezgi
Supervisor, **Chemical Engineering Dept., METU** _____

Prof. Dr. Timur Doğu
Co-supervisor, **Chemical Engineering Dept., METU** _____

**Examining Committee Members:**

Prof. Dr. Güzide Çalık
Chemical Engineering Dept., Ankara University _____

Assoc. Prof. Dr. Naime Aslı Sezgi
Chemical Engineering Dept., METU _____

Prof. Dr. Suna Balcı
Chemical Engineering Dept., Gazi University _____

Prof. Dr. Gürkan Karakaş
Chemical Engineering Dept., METU _____

Assoc. Prof. Dr. Göknur Bayram
Chemical Engineering Dept., METU _____

**Date:** 01.04.2010

**I hereby declare that all information in this document has been obtained and presented in accordance with academic rules and ethical conduct. I also declare that, as required by these rules and conduct, I have fully cited and referenced all material and results that are not original to this work.**

Name, Last name : Zeynep Obalı

Signature :

# ABSTRACT

## SYNTHESIS OF ALUMINUM INCORPORATED MESOPOROUS CATALYSTS FOR PYROLYSIS OF POLYPROPYLENE

Obalı, Zeynep
Ph.D., Department of Chemical Engineering
Supervisor : Assoc. Prof. Dr. Naime Aslı Sezgi
Co-supervisor : Prof. Dr. Timur Doğu

April 2010, 202 pages

The total amount of plastic wastes produced by our society has been growing rapidly. The low biodegradability of these wastes creates a serious environmental problem that is directing the governments and environmental agencies to take serious measures to solve the problem of the plastic wastes. Landfilling or incineration of these wastes are not the right solutions, because the former has the danger of leaching and soil impregnation of its degradation products and the latter produce air pollution problems due to the possible emissions of toxic and acid gases. An alternative approach to the solution of problem caused by these wastes is the recycling of them by chemical recovery. In this method, the waste plastics are thermally non-catalytically or catalytically degraded into gases and oils.

In this study, pure and aluminum containing ordered mesoporous materials *MCM-type* and *SBA-type*, were synthesized using different aluminum sources

and aluminum loadings in order to be tested in catalytic degradation of polypropylene. These catalysts, except aluminum containing SBA-type catalysts, were synthesized by hydrothermal synthesis method. Aluminum containing SBA-type catalysts were synthesized by impregnation method. Tetraethyl orthosilicate was used as the Si source and aluminum nitrate, aluminum sulphate and aluminum isopropoxide were used as the Al source. It was observed that these materials had high surface areas and exhibited Type IV isotherms. In MCM-type materials, the aluminum incorporated more effectively into the structure at low concentrations but not effectively at high concentrations. On the other hand, in SBA-type catalysts, the aluminum incorporation into structure was very effective. $^{27}$Al MAS NMR spectra of the catalysts exhibited a mixture of tetrahedral and octahedral aluminum. TEM images showed well-ordered hexagonal arrays of mesopores.

As an initial step, the activation energy value of polypropylene pyrolysis reaction in the presence of synthesized catalysts was determined by the help of a thermal analyzer and these TGA results showed a marked reduction in the degradation temperature. In the case of using aluminum containing MCM-type materials, the activation energy values decreased to about 68-126 kJ/mol. On the other hand, when aluminum containing SBA-type catalysts were used, the activation energy values decreased from 172 kJ/mol to a value in the range of 51 – 89 kJ/mol.

Heavier molecules degraded into lighter hydrocarbons in the presence of catalysts and they gave high ethylene selectivity among the gaseous products. Additionally, butane selectivity increased with the use of catalysts. SBA-type catalysts showed higher selectivity to lighter hydrocarbons ($<C_{14}$). $C_7$ selectivity among the liquid products was high when aluminum isopropoxide was used in the synthesis of catalysts and $C_{18}$ selectivity increased significantly when aluminum nitrate was used in the synthesis of MCM-type catalysts.

Keywords: Pyrolysis, Catalytic Thermal Degradation, Polypropylene, Mesoporous materials, MCM-41, SBA-15, Characterization, TGA

# öz

## POLİPROPİLENİN PİROLİZİ İÇİN ALÜMİNYUM İÇERİKLİ MEZOGÖZENEKLİ KATALİZÖRLERİN SENTEZİ

Obalı, Zeynep
Doktora, Kimya Mühendisliği Bölümü
Tez Yöneticisi : Doç.Dr. Naime Aslı Sezgi
Ortak Tez Yöneticisi : Prof. Dr. Timur Doğu

Nisan 2010, 202 sayfa

Toplum tarafından oluşturulan plastik atık miktarı hızla artmaktadır. Bu atıkların doğadaki çözünürlüğünün yok denecek kadar az olması, hükümetleri ve çevre örgütlerini bu atıklar konusunda ciddi önlemler almaya yöneltmektedir. Gömerek veya yakarak yok etme yöntemleri çok doğru çözümler değildir, çünkü plastik atıklar toprağa gömüldükleri zaman bu atıkların bozunması sonucu ortaya çıkan ürünler gömüldükleri alanda toprağı kirletebilmektedirler, diğer yandan bu atıklar yakıldıkları zaman atmosfere zehirli gaz salınımı olmaktadır. Bu sebeplerden dolayı, plastik atıklarının geri kazanımı yönteminin, kirlilik probleminin çözümüne daha fazla katkı sağlayacağı düşünülmektedir. Isıl yolla ve/veya katalizörlü ortamda bozundurma bu yöntemlerden ikisidir.

Bu çalışmada, saf ve alüminyum içerikli mezogözenekli malzemeler, *MCM-tipi* ve *SBA-tipi*, sentezlenerek polipropilenin bozunma reaksiyonundaki aktiviteleri

incelenmiştir. Alüminyum içeren SBA-tipi katalizörünlerin dışındakiler hidrotermal sentez yöntemiyle, alüminyum içeren SBA-tipi katalizörler ise emdirme yöntemi ile sentezlenmiştir. Silika kaynağı olarak tetraetil ortosilikat, alüminyum kaynağı olarak ise alüminyum nitrat, alüminyum sülfat ve alüminyum izopropoksit kullanılmıştır. Bu malzemeler yüksek yüzey alanı değerlerine sahip olup, Tip IV izotermi ortaya koymuşlardır. EDS sonuçlarına göre, düşük alüminyum derişimlerinde MCM-tipi malzemelerde alüminyumun yapıya daha etkin bir şekilde girdiği görülmüştür. Diğer yandan, SBA-tipi malzemelerde, her koşulda, alüminyumun yapıya verimli bir şekilde girdiği görülmüştür. $^{27}$Al MAS NMR sonuçları, sentezlenen katalizörlerin yapısındaki alüminyumun tetrahedral alüminyum ve oktahedral alüminyum olarak bulunduğunu göstermektedir. TEM fotoğrafları, düzgün, altıgen yapıların oluştuğunu göstermektedir.

İlk adım olarak, sentezlenen bu katalizörlerin polipropilenin bozunmasındaki aktiviteleri termal analiz cihazında incelenmiştir. Elde edilen sonuçlara göre, katalizörlü ortamda polimerin bozunma sıcaklığında belirgin bir düşüş gözlenmiştir. Alüminyum içeren *MCM-tipi* katalizörler kullanıldığında, reaksiyonun aktivasyon enerjisi 172 kJ/mol' den 68-126 kJ/mol değerine, alüminyum içerikli *SBA-tipi* katalizörler kullandığında ise bu değer 51–89 kJ/mol aralığına düşmüştür.

Katalizörlü ortamda, ağır hidrokarbonlar parçalanarak küçük moleküllere dönüşmüş ve etilen seçimliliği artmıştır. Buna ilaveten, katalizörlü ortamda bütan gazı oluşumu katalizörsüz ortama göre etkin bir şekilde artmıştır. SBA-tipi katalizörler $C_{14}$'den küçük moleküllere daha çok seçimlilik göstermiştir. Son olarak, alüminyum kaynağı olarak aluminyum izopropoksit kullanıldığında, MCM hem de SBA-tipi katalizörlerin sentezinde, $C_7$ seçimliliği diğer ürünlere göre çok daha yüksek çıkmıştır, diğer yanda alüminyum nitrat kullanılarak sentezlenen katalizörlerde Al/Si oranı arttıkça $C_{18}$ seçimliliği belirgin bir şekilde artmıştır.

Anahtar sözcükler: Piroliz, Katalitik Parçalanma, Polipropilen, Mezogözenekli malzemeler, MCM-41, SBA-15, Karakterizasyon, Termal analiz

*To my family and best friends Canan Şener and Buğçe Aydemir*

# ACKNOWLEDGEMENTS

First of all, I would like to express my sincere gratitude to my supervisor Assoc. Prof. Dr. Naime Aslı Sezgi for her guidance, interest and suggestions throughout this study. I would also like to thank my co-supervisor Prof. Dr. Timur Doğu for his suggestions and criticisms during each step of my research.

I would like to thank Prof.Dr.Güzide Çalık and Assoc.Prof.Dr.Göknur Bayram for their suggestions and criticisms during each step of my research. I would like to extend my thanks to Prof. Dr. Gülşen Doğu and Gazi University Research Group for their support in this study.

I would like to thank here my family, for their big supports, patience and faith in me, in every moment throughout my education. Thanks for their big love…

I would like to thank my best friends Canan Şener, Buğçe Aydemir and Zeynep Özaydın for their supports, suggestions and solutions to my problems. Additionally, thanks for loving and helping me all the time. Thanks also to my lab mates, Cem Tokay, Ayça Arınan and Ayşegül Çiftçi for their helpful and enjoyable friendships throughout this study.

I would like to thank specialist Gülten Orakçı for her helps in surface area analysis. I wish to thank specialist Cengiz Tan for his helps in Scanning Electron Microscopic analysis. I would also thank Necmi Avcı for his helps in X-ray diffraction analysis. I would like to thank Machine Shop for their help in constructing various set-up components and their availability to every call for help. I am also thankful to all staff of Department of Chemical Engineering and Central Laboratory for their helps throughout the study. I would like to thank Esra Eren from Turkish Petroleum Corporation in GC-MS analysis.

I would also like to thank Dr.Lucian Barbu-Tudoran from Babes-Bolyai University (Romania) for her helps in Transmission Electron Microscopy analysis.

I would like to thank The Scientific and Technological Research Council of Turkey (TÜBİTAK) for their financial support through 107M303 project.

# TABLE OF CONTENTS

# LIST OF TABLES

TABLES

# LIST OF FIGURES

FIGURES

# LIST OF SYMBOLS

| | |
|---|---|
| a | : Lattice parameter (nm) |
| A | : Pre-exponential factor |
| $d_{pore}$ | : Pore diameter (nm) |
| $E_A$ | : Activation energy (kJ/mol) |
| M | : Molarity (mol/l) |
| $M_W$ | : Weight-average molecular weight |
| n | : Order of reaction |
| PA | : MCM-41 type mesostructured aluminosilicate catalyst |
| q | : Heating rate (°C/min) |
| R | : Gas constant (J/mol.K) |
| $S_i$ | : Selectivity of ith component |
| T | : Temperature (°C) |
| $y_i$ | : Mole fraction of ith gas component |
| $w_i$ | : Weight fraction of ith component |

*Greek Letters*

| | |
|---|---|
| $\rho$ | : Density of polymer (g/ml) |
| $\delta$ | : Pore wall thickness (nm) |
| $\lambda$ | : Wavelength (Å) |
| $\beta$ | : Calibration factor for gas chromatography |

*Abbreviations*

| | |
|---|---|
| BET | : Brunauer-Emmett-Teller |
| BJH | : Barrett-Joyner-Halenda |
| CTMABr | : Cetyltrimethylammonium bromide |
| CTMACl | : Cetyltrimethylammonium chloride |

| | |
|---|---|
| DRIFT | : Diffuse reflectance fourier transform infrared |
| EDS | : Energy dispersive X-ray spectroscopy |
| FCC | : Fluid catalytic cracking |
| FSM | : Folded sheet mesoporous material |
| GC | : Gas chromatography |
| HDPE | : High density polyethylene |
| HPLC | : High performance liquid chromatography |
| IUPAC | : International union of pure and applied chemistry |
| LCT | : Liquid crystal templating mechanism |
| LDPE | : Low density polyethylene |
| MAS NMR | : Magic angle spinning nuclear magnetic resonance |
| PE | : Polyethylene |
| PET | : Poly(ethylene terephthalate) |
| PP | : Polypropylene |
| PS | : Polystyrene |
| PVC | : Poly(vinyl chloride) |
| SEM | : Scanning electron microscopy |
| SLC | : Silicatropic liquid crystal |
| TEM | : Transmission electron microscopy |
| TEOS | : Tetraethyl orthosilicate |
| TMOS | : Tetramethyl orthosilicate |
| TGA | : Thermogravimetric analysis |
| XRD | : X-ray diffraction |

# CHAPTER 1

# INTRODUCTION

In any society of today's modern world, plastics provide an essential contribution to all daily activities like packaging, building materials, agriculture, automobile industry and so on. As only a small amount of waste plastics is recycled and most plastics are not biodegradable, all these daily activities have led to the generation of huge amount of waste plastics [1]. These waste plastics are composed of polyethylene, polystyrene, polypropylene, poly(vinyl chloride), and poly(ethylene terephthalate), the sum of which is nearly 70% of the total waste plastics [2].

Measures have to be taken to reduce negative impact of waste plastics on the environment. Landfilling or incineration of the waste plastics is not the right solutions, because the former has the danger of leaching and soil impregnation of its degradation products. Additionally, the available space in landfill is decreasing around the world as time goes on [3, 4]. Incineration is strongly rejected by public opinion, due to the risk of the possible emission of toxic chemicals like dioxins, furans, nitrous and sulfur oxides and dusts. Therefore this method only shifts a solid waste problem to an air pollution one [4].

Different alternatives are currently beginning to be considered for reducing the environmental impact of waste plastics. Primary recycling (mechanical) consists of grinding the plastics and producing new goods with the recycled material, but this method can be applied up to a certain limit due to the

difficulties in processing mixtures of different plastics [4, 5]. Additionally, the quality of the recycled material is lower than that of fresh material.

The secondary recycling is incineration. In this recycling, calorific energy is generated. The calorific value of the plastics is comparable to that of fuels around 46 MJ/kg, but uncontrolled incineration may produce different harmful pollutants which are toxic at very low concentrations [4, 5].

Pyrolysis is tertiary recycling process where the polymer sample is heated in an inert atmosphere under moderate conditions of pressure and temperature causing the conversion of polymers into more valuable chemicals or fuels, technological implementations depending on the type of polymers to be recycled [3-6]. The simplest method of plastic feedstock recycling is non-catalytic thermal degradation. This method leads towards a broad distribution of hydrocarbons up to waxy products and high temperatures greater than 500°C are needed to receive more oily products [7]. In contrast, catalytic thermal degradation process allows the plastic degradation to be performed at lower temperatures, while the product distribution can be controlled by a right selection of the catalyst type being used [8]. The most commonly used catalysts in the catalytic degradation of polyolefins are solid acids $SiO_2$-$Al_2O_3$, HZSM-5, HY zeolites, etc. [6-9].

Zeolites show excellent properties as catalysts for the degradation of waste plastics. *HZSM-5* zeolite has proved to be an efficient catalyst for catalytic thermal degradation of polymers because of its strong acidity for the carbon-carbon bond scission and unique pore structure to reduce coke formation. However, the pore size of the zeolites is limited to a maximum value of about 1.0 nm, and in the case of *HZSM-5* the pore size is 0.5 nm, which hinders the access of bulky molecules to the acid sites located inside the channels [4].

The discovery of mesoporous materials in 1992 and 1998 (*MCM-41 and SBA-15*) has opened the way to new zeo-type molecular sieves with ordered mesoporous channel system. These materials possess highly regular arrays of uniform pore channels ranging from 1.5 nm to 10 nm in size and large surface area. But, the usage of these materials as catalysts in purely siliceous form is

now to some extent restricted by its relative low acidity, in comparison with those of microporous zeolites such as *HZSM-5* [4].

Since the discovery of the possible incorporation of aluminum and other metal ions ($Fe^{+3}$, $V^{+5}$, $Co^{+2}$, etc.) into the framework of these materials, the interest in the substituted material has been growing. Tetrahedrally coordinated aluminum ions make the way for the creation of Brönsted acid sites solving the problem of the low acidity that present in these materials [4].

In addition to the degradation reaction of waste plastics, these mesoporous materials are used in different processes as listed below [10, 11]:

- Oxidation Reactions: Olefin epoxidation, oxidation of large organic molecules, liquid-phase oxidation of aniline
- Acid-Catalyzed Reactions: Gasoil cracking, hydrogenation reaction, acetal production, tetrahydropyranylation of alcohols, Friedel-Crafts alkylation
- Hydroxylation Reactions
- Polymerization Reactions
- Membrane Applications: Gas separation processes
- Electronic/Optical Applications: New generation low-*k* dielectric materials for integrated circuits, dye inclusion, photochromic materials, chemical sensors
- Sorption and Chromatographic Separations: Enzyme immobilization, removal of heavy metals from fresh water resources, monolithic silica columns with a disordered templated mesoporous structure used in HPLC for the separation of proteins

In this study, the catalytic activity of ordered mesoporous materials*, MCM-type* and *SBA-type*, in polymer degradation reaction was investigated. For this purpose, aluminium containing *MCM-type* and *SBA-type* catalysts were synthesized and their activity was tested in polypropylene degradation reaction using a thermal analyzer. After that, the effect of these catalysts on product distribution was investigated in polypropylene degradation reaction system. To make a reasonable comparison, non-catalytic thermal degradation (blank) reactions were carried out in the same system.

# CHAPTER 2

# DEGRADATION OF POLYMERS

## 2.1 Polymers

A polymer is a macromolecule (from the Greek *poly* meaning "many" and *meros* meaning "parts") composed of repeating structural units typically connected by covalent chemical bonds. While *polymer* in popular usage suggests plastic, the term actually refers to a large class of natural and synthetic materials with a variety of properties [12, 13].

Due to the extraordinary range of properties accessible in polymeric materials, they have come to play an essential and important role in everyday life. A simple example is polyethylene, whose repeating unit is based on ethylene monomer and another example is polypropylene, which has a repeating unit based on propylene monomer. Most commonly, as in these examples, the continuously linked backbone of a polymer consists of mainly carbon atoms. However, other structures do exist; for example, elements such as silicon form familiar materials such as silicones, examples being silly putty and waterproof plumbing sealant. The backbone of DNA is in fact based on a phosphodiester bond, and repeating units of polysaccharides (e.g. cellulose) are joined together by glycosidic bonds via oxygen atoms [12].

Natural polymeric materials such as gum mastic, amber, natural rubber and asphalt have been in use for centuries. Biopolymers such as proteins and nucleic acids play crucial roles in biological processes. A variety of other

natural polymers exist, such as cellulose, which is the main constituent of wood and paper.

The list of synthetic polymers includes synthetic rubber, Bakelite, neoprene, nylon, PVC, polystyrene, polyacrylonitrile, polyethylene, polypropylene and many others [12, 14].

### 2.1.1 Historical Development of Polymers

Starting in 1811, Henri Braconnot did pioneering work in derivative cellulose compounds, perhaps the earliest important work in polymer science. The development of vulcanization later in the 19$^{th}$ century improved the durability of the natural polymer rubber, signifying the first popularized semi-synthetic polymer. In 1907, Leo Baekeland created the first completely synthetic polymer, Bakelite, by reacting phenol and formaldehyde at precisely controlled temperature and pressure. Bakelite was then introduced to public in 1909 [12].

Despite significant advances in synthesis and characterization of polymers, a correct understanding of polymer molecular structure did not emerge until the 1920s. Before then, scientists believed that polymers were clusters of small molecules (colloids), without definite molecular weights, held together by an unknown force, a concept known as association theory. In 1922, Hermann Staudinger proposed that polymers consisted of long chains of atoms held together by covalent bonds, an idea which did not gain wide acceptance for over a decade and for which Staudinger was ultimately awarded the Nobel Prize. Work by Wallace Carothers in the 1920s also demonstrated that polymers could be synthesized rationally from their constituent monomers. An important contribution to synthetic polymer science was made by the Italian chemist Giulio Natta and the German chemist Karl Ziegler, who won the Nobel Prize in Chemistry in 1963 for the development of the Ziegler-Natta catalyst. Further recognition of the importance of polymers came with the award of the Nobel Prize in Chemistry in 1974 to Paul Flory, whose extensive work on polymers included the kinetics of step-growth and addition polymerization,

chain transfer, excluded volume, the Flory-Huggins solution theory, and the Flory convention [12].

Synthetic polymer materials such as nylon, polyethylene and Teflon have formed the basis for a developing polymer industry. These years have also shown significant developments in rational polymer synthesis. Most commercially important polymers today are entirely synthetic and produced in high volume on appropriately scaled organic synthetic techniques [12].

### 2.1.2 Application Areas of Polymers

Synthetic polymers today find application in nearly every industry and area of life. Polymers are widely used as adhesives and lubricants, as well as structural components for products ranging from children's toys to aircraft. They have been employed in a variety of biomedical applications ranging from implantable devices to controlled drug delivery. Polymers such as poly(methyl methacrylate) find application as photoresist materials used in semiconductor manufacturing and low-k dielectrics for use in high-performance microprocessors. Polyethylene finds application in consumer products (shopping bags, water bottles, etc.). Polypropylene is used in a wide variety of applications, including packaging, textiles (e.g. ropes, thermal underwear and carpets), stationery, plastic parts and reusable containers of various types, laboratory equipment, loudspeakers, automotive components, and polymer banknotes. Polystyrene is used in disposable cutlery, plastic models, CD and DVD cases, smoke detector housings, packing materials, insulation, and foam drink cups. Polyvinyl chloride is used in household sewerage pipes. Also, it is popular for window and door frames. Poly(ethylene terephthalate) is mostly used in soft drinks bottles and thin film applications. Recently, polymers have also been employed as flexible substrates in the development of organic light-emitting diodes for electronic displays [12, 15-17].

### 2.1.3 Some Important Polymers

#### 2.1.3.1 Polyethylene

*Polyethylene* is a polymer consisting of long chains of the monomer *ethylene*, IUPAC name: ethene, $CH_2{=}CH_2$. The recommended scientific name *polyethene* is systematically derived from the scientific name of the monomer [15, 18]. Space-filling model of *ethylene* and *polyethylene* is given in Figure 2.1 (Black and white balls represent carbon and hydrogen atoms, respectively).

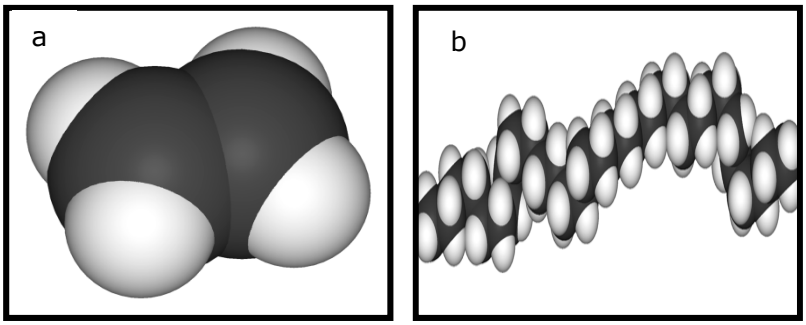


Figure 2.1 Space-filling model of (a) *ethylene*, (b) *polyethylene* (adapted from [15])

Polyethylene is classified into several different categories based on its density and branching:

The first *polyethylene* that was made is what we now call "low density" polyethylene (branched polyethylene), or *LDPE*. It is soft, waxy and flexible. The main reason that it exhibits these properties is that the polymer chains have many branches with varying lengths from the main polymer backbone. These branches cause the molecule to resemble a tangled ball of yarn, and prevent the strands from arranging themselves into any kind of order. After a period of relatively slow growth in the 1940's, the production of branched

polyethylene expanded rapidly. It is used for the lids of margarine containers, for trash bags, squeeze bottles, and plastic film [14, 18].

In the 1950's, Robert Banks and J. Paul Hogan at Phillips Petroleum discovered a catalyst (chromium trioxide based) that could prevent most of the branching that occurs when ethylene polymerizes. In 1953, the German chemist Karl Ziegler developed a catalytic system based on titanium halides and organoaluminium compounds that worked at even milder conditions than the Phillips catalyst [15,18]. This new material, "high density" polyethylene (HDPE), that is produced as a result of that catalytic reaction has the same chemical composition as does *LDPE*, but it is much stronger and more rigid, as well as being more dense. Many packages, including milk jugs, food and bleach containers, garbage containers, water pipes, shipping drums, wire and cable insulation, extrusion coating and automobile gasoline tanks are made of *HDPE* [14, 15, 18].

Depending on the crystallinity and molecular weight, a melting point and glass transition may or may not be observable. The temperature at which these occur varies strongly with the type of polyethylene. For common commercial grades of high-density polyethylene (*HDPE*), the melting point is typically in the range of 120 to 130°C. The melting point for average, commercial, low-density polyethylene (*LDPE*) is typically 105 to 115 °C. Most LDPE and HDPE grades have excellent chemical resistance and do not dissolve at room temperature because of their crystallinity. Usually, they can be dissolved at elevated temperatures in aromatic hydrocarbons such as toluene or xylene, or in chlorinated solvents such as trichloroethane or trichlorobenzene [15].

A newer and third type of *polyethylene* is *linear low density polyethylene, LLDPE*. It is a copolymer of ethylene and 1-hexene. The branched chains from the 1-hexene attached to the polyethylene chain to provide branches of a defined length. This reduces the ease of molecular packing and gives a very low density product. This polymer was produced in a catalytic system, based on metallocenes which was discovered in 1976 in Germany by Walter Kaminsky and Hansjörg Sinn [15, 18]. *LLDPE* has higher tensile strength than *LDPE*. Lower thickness (gauge) films can be blown, compared with *LDPE*, with

better environmental stress cracking resistance but is not as easy to process. *LLDPE* is used in packaging, particularly film for bags and sheets.

### 2.1.3.2 Polypropylene

*Polypropylene* is a thermoplastic and it consists of long chains of the monomer, *propylene*, $C_3H_6$ [19]. Space-filling model of *propylene* and *polypropylene* is given in Figure 2.2 (Black and white balls represent carbon and hydrogen atoms, respectively).

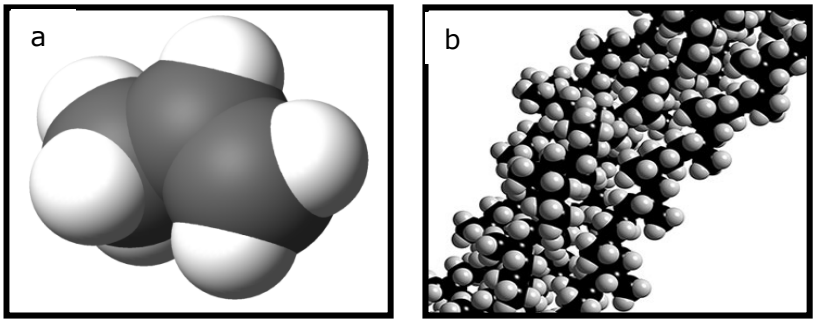


Figure 2.2 Space-filling model of (a) *propylene,* (b) *polypropylene* (adapted from [20-21])

Polypropylene(PP) was first polymerized in 1954 by Giulio Natta in Spain, and the commercial production began in 1957 [16, 19]. It was manufactured from propylene gas in the presence of a catalyst such as titanium chloride.

The large number of end use applications for PP is often possible because of the ability to tailor grades with specific molecular properties and additives during its manufacture. For example, antistatic additives can be added to help PP surfaces resist dust and dirt. Many physical finishing techniques can also be used on PP, such as machining. Surface treatments can be applied to PP parts in order to promote adhesion of printing ink and paints.

This polymer is the lightest major plastic, with a density of 0.905. Its high crystallinity imparts to its high tensile strength, stiffness and hardness. The high melting point of PP (~160-165°C) allows well-molded parts to be sterilized, and the polymer retains high tensile strength at high temperatures. It is non-toxic and highly resistant to most alkalis and acid, organic solvent, degreasing agent and electrolytic attack. On the other hand, this polymer is less resistant to aromatic, aliphatic and chlorinated solvents and UV [14, 19].

This polymer can be used for housewares, packing, film tapes, cassette holders, fibers, automotive parts, pipes, containers, seat shells and filament (rope, cordage and webbing). Additionally, polypropylene is the major polymer used in nonwovens, with over 50% used for diapers or sanitary products where it is treated to absorb water (hydrophillic) rather than naturally repelling water (hydrophobic) [14, 16, 19].

#### 2.1.3.3 Polystyrene

*Polystyrene* is an aromatic polymer made from the aromatic monomer *styrene* ($C_6H_5CH=CH_2$), a liquid hydrocarbon that is commercially manufactured from petroleum by the chemical industry. Polystyrene is one of the most widely used kinds of plastic [17]. Space-filling model of *styrene* and *polystyrene* is given in Figure 2.3 (Black ball represents carbon atom, white ball represents hydrogen atom).

*Polystyrene* was discovered in 1839 by Eduard Simon, a pharmacist in Berlin. From storax, the resin of the Turkish sweetgum tree, he distilled an oily substance, a monomer which he named styrol. Several days later, Simon found that the styrol had thickened, presumably from oxidation, into a jelly he dubbed styrol oxide ("Styroloxyd"). By 1845 English chemist John Blyth and German chemist August Wilhelm von Hofmann showed that the same transformation of styrol took place in the absence of oxygen. They called their substance metastyrol. Analysis later showed that it was chemically identical to Styroloxyd. In 1866 Marcelin Berthelot correctly identified the formation of metastyrol from styrol as a polymerization process. About 80 years went by before it was realized that heating of styrol starts a chain reaction which

produces macromolecules, following the thesis of German organic chemist Hermann Staudinger. This eventually led to the substance receiving its present name, *polystyrene*. The company I. G. Farben began manufacturing *polystyrene* in Ludwigshafen, Germany, in 1931. By 1937, American chemist Robert Dreisbach and others at the Dow Chemical Company's physics laboratory had obtained purified styrene monomer through the dehydrogenation of ethylbenzene and developed a pilot polymerization process. By 1938 polystyrene was being produced commercially [17, 24].

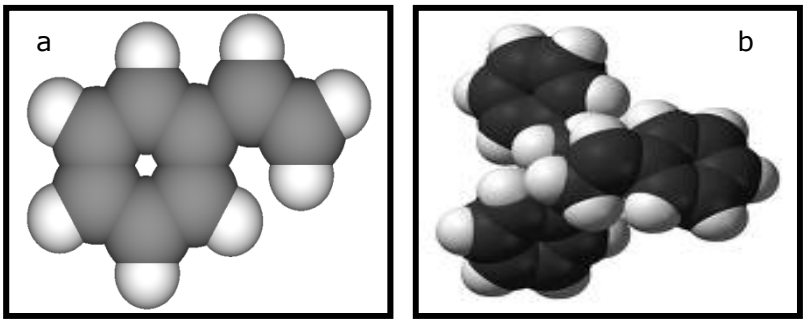


Figure 2.3 Space-filling model of (a) *styrene,* (b) *polystyrene* (adapted from [22,23])

*Polystyrene* is a thermoplastic substance, which is in solid (glassy) state at room temperature, but flows if heated above its glass transition temperature (~95°C), and becomes solid again when cooling off. Pure solid polystyrene is a colorless, hard plastic with limited flexibility. It can be cast into molds with fine detail. *Polystyrene* can be transparent or can be made to take on various colors. It is quite resistant to alkalis, halide acids, and oxidizing and reducing agents. It can be nitrated by fuming $HNO_3$, and sulfonated by concentrated $H_2SO_4$ at 100°C to water soluble resin. Its high refractive index (1.60) makes it useful for plastic optical components [14,17].

Foaming with pentane or carbondioxide gas, *PS* is made into insulation and packaging materials as well as food containers such as beverage cups, egg cartons, and disposable plates and trays [24]. Additionally, solid polystyrene

is used in disposable cutlery, plastic models, CD and DVD cases, and smoke detector housings [17].

#### 2.1.3.4 Poly(vinyl chloride)

*Poly(vinyl chloride)*, commonly abbreviated *PVC*, is the third most widely used thermoplastic polymer after polyethylene and polypropylene. In terms of revenue generated, it is one of the most valuable products of the chemical industry [25]. It is produced by polymerization of the *vinyl chloride* monomer ($C_2H_3Cl$). Since about 57% of its mass is chlorine, creating a given mass of PVC requires less petroleum than many other polymers. Space-filling model of *vinyl chloride* and *poly(vinyl chloride)* is given in Figure 2.4 (Black, white and green balls represent carbon, hydrogen and chlorine atoms, respectively).

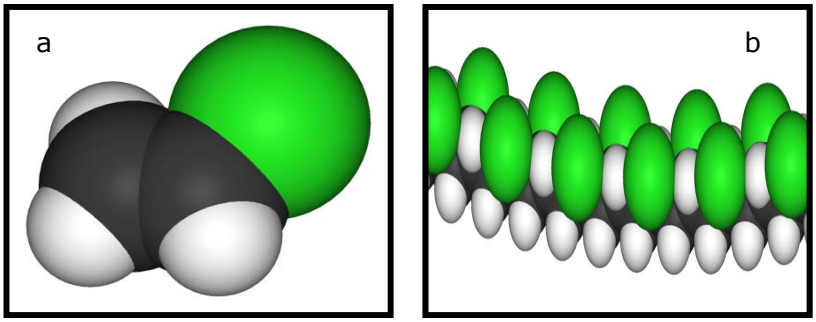


Figure 2.4 Space-filling model of (a) *vinyl chloride,* (b) *poly(vinyl chloride)* (adapted from [25,26])

*PVC* was accidentally discovered on at least two different occasions in the 19$^{th}$ century, first in 1835 by Henri Victor Regnault and in 1872 by Eugen Baumann. On both occasions, the polymer appeared as a white solid inside flasks of vinyl chloride that had been left exposed to sunlight. In the early 20$^{th}$ century, the Russian chemist Ivan Ostromislensky and Fritz Klatte of the German chemical company Griesheim-Elektron both attempted to use *PVC* in

commercial products, but difficulties in processing the rigid, sometimes brittle polymer blocked their efforts. In 1926, Waldo Semon and the B.F. Goodrich Company developed a method to plasticize *PVC* by blending it with various additives. The result was a more flexible and more easily-processed material that soon achieved widespread commercial use [25].

*PVC* is tough and flame resistant. It is compatible with other additives that can provide *PVC* clear or colored, rigid or flexible. It has excellent electrical insulation properties and this makes it ideal to be used in cables. PVC has impact strength and resistance to bad weather conditions therefore it is appropriate to be used as a construction material. It shows resistance to grease, oil and chemicals [27].

*PVC*'s intrinsic properties make it suitable for a wide variety of applications. It is biologically and chemically resistant, as mentioned above, making it the plastic of choice for most household sewerage pipes and other pipe applications where corrosion would limit the use of metal. With the addition of impact modifiers and stabilizers, it becomes a popular material for window and door frames. By adding plasticizers, it can become flexible enough to be used in cabling applications as a wire insulator. *PVC* is finding increased use as a composite for the production of accessories or housings for portable electronics. It is also commonly used in figurines and in inflatable products such as waterbeds and pool toys [25].

#### 2.1.3.5 Poly(ethylene terephthalate)

*Poly(ethylene terephthalate)*, commonly abbreviated *PET*, is a thermoplastic polymer resin of the polyester family and is used in synthetic fibers; beverage, food and other liquid containers; thermoforming applications; and engineering resins often in combination with glass fiber. Depending on its processing and thermal history, poly(ethylene terephthalate) may exist both as an amorphous (transparent) and as a semi-crystalline material. The semi crystalline material might appear transparent (particle size < 500nm) or opaque and white (particle size up to few microns) depending on its crystal structure and particle size. The semi-crystalline *PET* has good strength,

ductility, stiffness and hardness. The amorphous PET has better ductility but less stiffness and hardness. Its monomer (bis-ß-hydroxyterephthalate) can be synthesized by the esterification reaction between terephthalic acid and ethylene glycol with water as a byproduct, or by transesterification reaction between ethylene glycol and dimethyl terephthalate with methanol as a byproduct [28, 29].

The main virtue of *PET* is that it is fully recyclable. Unlike other plastics, its polymer chains can be recovered for additional use. It can be semi-rigid to rigid, depending on its thickness, and it is very lightweight. It makes a good gas and fair moisture barrier, as well as a good barrier to alcohol and solvents. It is strong and impact-resistant. It is naturally colorless and transparent. *PET* film (***Mylar***) is often coated with aluminium to reduce its permeability, and to make it reflective and opaque. For soft drink bottles, *PET* is often blended with polyvinyl alcohol to reduce its carbon dioxide permeability. When filled with glass particles or fibers, it becomes significantly stiffer and more durable. This glass-filled plastic, in a semi-crystalline formulation, is sold under the tradename ***Rynite****. PET* was patented in 1941 by the Calico Printer's Association of Manchester. The *PET* bottle was patented in 1973 [30].

The majority of the world's *PET* production is for synthetic fibers (in excess of 60%) with bottle production accounting for around 30% of global demand. In discussing textile applications, *PET* is generally referred to as simply "polyester" while *PET* is used most often to refer to packaging applications. Some of the trade names of *PET* products are ***Dacron****,* ***Diolen****,* ***Tergal****,* ***Terylene***, and ***Trevira*** fibers, ***Cleartuf****,* ***Eastman PET*** and ***Polyclear*** bottle resins, ***Hostaphan****,* ***Melinex***, and ***Mylar*** films. The polyester industry makes up about 18% of world polymer production and is third after *PE* and *PP* [28].

## 2.2 Degradation of Polymers

In today's modern societies, plastic materials become necessary in everyday life. As a result of this, a continuous increase in the consumption plastics causes an increase in the amount of plastic wastes [31]. The growing amount of these wastes is creating more and more environmental problems worldwide. Suitable waste management is an important factor for a sustainable economical development. Waste plastics represent a considerable part of municipal wastes. In addition to these wastes, large amounts of waste plastics arise as a by-product or defective product in industry [32]. As a result of these, the disposal of waste plastics has created serious social and environmental arguments. At present, both landfilling and incineration of waste plastics are generally practiced [33]. Landfill space is becoming scarce and expensive, a problem intensified by the fact that plastic waste is more voluminous than other waste type, therefore landfilling of waste plastics is expected to decrease in the future [33, 34]. Incineration of waste plastics with other municipal solid wastes may be increasingly practiced, because the high calorific value can improve the heating value of municipal solid waste, while their energy content can also recovered. But the potential relationship between plastics fed into an incinerator and the formation of some highly toxic pollutants like polyaromatic hydrocarbons, dioxins and furans is still unclear [31,33]. It is suggested that the chlorine content in PVC and other plastics is related to the formation of dioxins and furans, which are chlorinated polynuclear aromatic compound, and although there is considerable proof that these pollutants would still be generated in the absence of plastics, environmental pressures against incineration have never completely disappeared [33].

It is, therefore, desired to develop an alternative technology to recycle or reuse waste plastics. Plastics can be recycled by three different methods: mechanical (primary) recycling, energy recovery (secondary recycling), and chemical (tertiary or feedstock) recycling [35, 36]. Since primary recycling by simply remelting and shaping waste plastics usually results in a low-quality product, its application is highly limited. Energy recovery through combustion means a loss of potential for use as resources and may contribute to an

environmental pollution caused by the generation of harmful materials [35,37]. Owing to these restrictions, chemical recycling has been growing in importance. By this way, waste plastics can be converted into monomers, fuels or valuable chemicals for petrochemistry. To achieve this, different solutions have been considered and they are given below [37].

Depolimerization converts mainly condensation polymers (*polyurethane, PET*, *nylon*, etc.) into monomers or polymer precursors by thermal (pyrolysis) or chemical pathways like methanolysis, glycolysis, hydrolysis, etc. Unfortunately it can only be applied to clean and homogeneous plastic wastes and mixed plastics are not recommended [37]. Therefore, there has been a growing interest in non-catalytic and catalytic thermal degradation processes [37-39].

### 2.2.1 Non-Catalytic Thermal Degradation

Non-catalytic thermal degradation of plastics has been studied extensively in the past [31, 32, 40-44]. Four types of mechanisms are proposed for non-catalytic thermal degradation [33]:

- End-chain scission: In this mechanism, the polymer is broken up from the end groups successively yielding the corresponding monomers.
- Random-chain scission: The polymer chain broken up randomly into fragments of uneven length. It results both in monomers and oligomers [45, 46].
- Chain-stripping: In this mechanism, reactive substitutes or side groups are eliminated, leading to the evolution of a cracking product on one hand, and a charring polymer chain on the other.
- Cross-linking: Formation of a chain network, which often occurs for thermosetting polymers when heated.

The non-catalytic thermal degradation of PP and PE is known to follow the random chain scission route, resulting in mainly oligomers and dimers [46]. This mechanism is shown for PE and PP in Figures 2.5 and 2.6, respectively.

Peterson *et. al.* observed that PE decomposition by thermogravimetry yielded mainly 1-hexene and propene [47]. Additionally, in the thermal pyrolysis of PP, the main products were pentane, 2-methyl-1-pentene and 2,4-dimethyl-1-heptene [47].

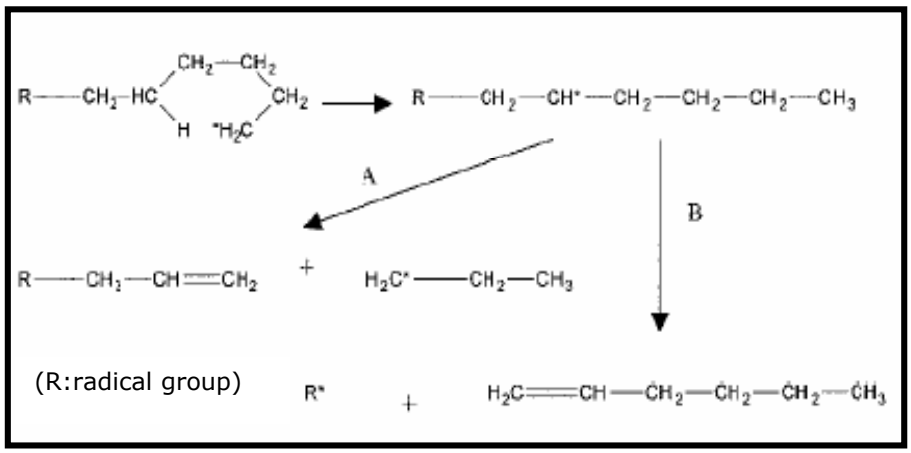


Figure 2.5 Random-chain scission in *PE* (adapted from [47])

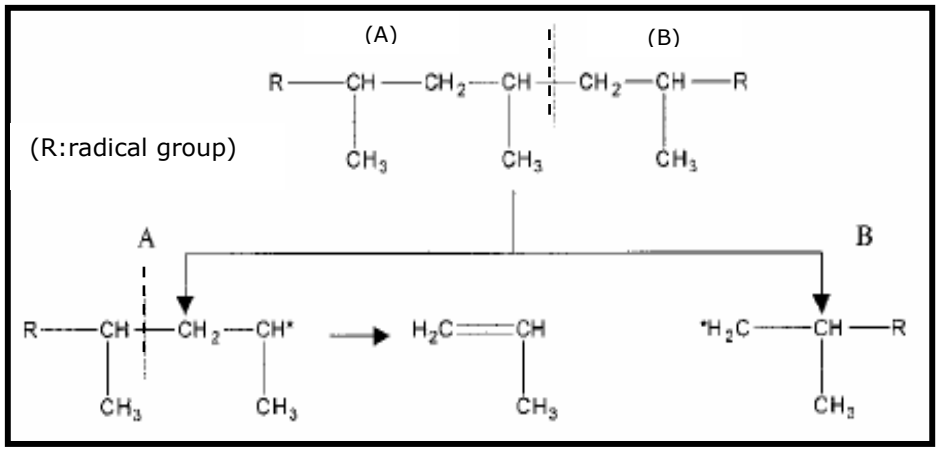


Figure 2.6 Random-chain scission in *PP* (adapted from [47])

The non-catalytic thermal degradation is a high-energy, endothermic process requiring high temperatures, typically more than 500°C and even up to 900°C [46,48] and the products of this process are distributed over a wide range of carbon numbers and their commercial value is low, requiring upgrading for effective usage as fuel or other valuable chemicals in petrochemical industry [34,49].

### 2.2.2 Catalytic Thermal Degradation

Catalytic thermal degradation of polymers has shown the greatest potential to be developed into a commercialized process [46]. In comparison to non-catalytic thermal degradation, the addition of catalysts in polymer degradation processes has the following advantages:

- It reduces the degradation temperature significantly. A significant reduction in the temperature and reaction time under catalytic conditions results in an increase in the conversion rates for most of the polymers [46, 49-51].
- The oils produced by the catalytic thermal degradation are known to contain a relatively narrow distribution of hydrocarbons and the selectivity of products in the gasoline range ($C_5$-$C_{12}$) are much more enhanced by the presence of catalysts [46, 52, 53].
- The presence of a catalyst increases the gaseous product yields [46, 54-56].
- The catalytic thermal degradation process increases the product yield in the gasoline range whereas a non-catalytic thermal degradation process produces more light gas oils [51]. Oils obtained by catalytic degradation contain less olefins and more aromatic content [50].

There are different methods for performing the catalytic degradation of polymers: catalytic thermal degradation of waste plastics-liquid streams mixtures, non-catalytic thermal degradation plus catalytic upgrading, catalytic thermal degradation of waste plastics by direct contact with the catalyst.

A simpler way of processing the plastics via catalytic thermal degradation would consist in mixing the plastic wastes with a fluid catalytic cracking (FCC) feed, forming slurry that is treated conventionally in the FCC unit of a refinery. The principal limitations to this solution are the transportation costs of the plastics from origin to the refinery, the need of important refining liquid streams necessary taking into account the limited amount of plastics that can be mixed, and restricted use of chlorine and other heteroatoms contained in the plastics that can be negatively affect the FCC unit and catalyst [37]. Another possibility involves a non-catalytic thermal degradation of waste plastics (mainly polyolefins like PE, PP, etc.) for producing low quality hydrocarbons that are treated directly afterwards in a catalytic reactor for upgrading and reforming into high quality liquid transportation fuels [37, 50, 57]. This option involves a high economical cost because of the infrastructure needed in each treatment center or because of the cost of plastic transportation to a centeralized plant. Nevertheless, it should be possible to separate the non-catalytic thermal degradation from the catalytic thermal degradation operation by means of condensing pyrolyzed products so that liquid products are feed to a catalytic cracking reactor [37].

Another advantage of catalytic thermal degradation is the possibility of processing chlorine containing plastics, provided that the gas and liquid streams from the thermal reactor are dechlorinated. Another option is based on catalytic thermal degradation of plastic wastes by direct contact with a cracking catalyst, without any thermal degradation. Liquid products generated are transported to a refinery where they are upgraded conventionally. This option reduces energy costs in comparison with thermal plus catalytic degradation because temperature or residence time can be reduced. Here the important point is that, catalyst cost can affect the process economy considerably. The most commonly used catalysts in the catalytic thermal degradation of polymers are solid acids ($SiO_2$-$Al_2O_3$, HZSM-5, HY zeolites, etc.) and activated carbon [37, 52-54, 58-60].

However, due to the bulky nature of the polymer molecules, the degradation reaction is strongly controlled by the pore size of the catalysts. Amorphous $SiO_2$-$Al_2O_3$ usually present a wide distribution of pore radius whereas zeolites

are microporous materials having a maximum pore size of approximately 0.75 nm [56, 61]. This fact is responsible for the appearance of steric hindrances in the degradation of bulky polymeric molecules. This problem can be solved using catalysts of larger pores (mesoporous catalysts). This approach has demonstrated to be successful in the catalytic thermal degradation of polymers over mesoporous catalysts like MCM-41 [49, 56, 61-65]. Detailed information about these porous materials and their uses is given in the next chapter.

# CHAPTER 3

# POROUS MATERIALS

Porous solids are studied intensively by material scientists with regard to technical applications as catalysts, catalysts supports, ion exchange material and adsorbents [66].

According to IUPAC definition, porous materials can be classified into three groups [67]:

- Microporous materials: their pore diameters are less than 2 nm,
- Mesoporous materials: their pore diameters are ranging from 2-50 nm,
- Macroporous materials: they have pore diameters larger than 50 nm.

Porous materials according to their pore sizes are given in Figure 3.1.

Microporous materials involve amorphous silica, inorganic gels, pillared clays and crystalline materials such as zeolites, gallophosphates and aluminophosphates. Among these materials, zeolites are the most widely studied ones due to their advantageous properties such as high adsorption capacities, large surface areas and shape selective properties [10, 67].

## 3.1 Zeolites

These materials occur in nature and have been known for almost 250 years as aluminosilicate minerals. Faujasite, mordenite, ferrierite and erionite can be given as examples for these materials. Today, these and other zeolite structures are of great interest in catalysis, in spite of their naturally occurring

forms are of limited value, because (i) they always contain undesired impurity phases, and (ii) nature did not optimize their properties for catalytic applications [68].

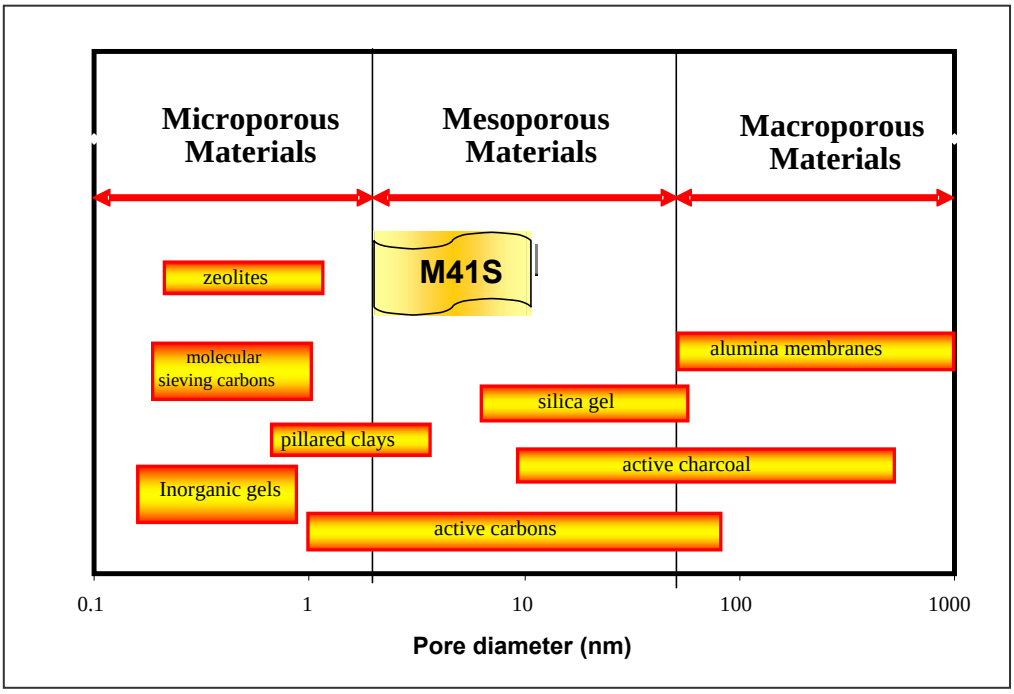


Figure 3.1 Porous materials as classified by their pore sizes [69]

It was only with the introduction of the synthetic zeolites, from 1948 to 1955, that this class of porous materials began to play an important role in catalysis. The turning point event was the introduction of synthetic faujasites (zeolites X and Y) on an industrial scale in FCC of heavy petroleum distillates in 1962, one of the most important chemical processes throughout the world. These new zeolitic catalysts were not only orders of magnitude more active than the previously used amorphous $SiO_2/Al_2O_3$ catalysts, but they also brought about a significant increase in the yield of gasoline which is the most valuable product from the FCC plants. In the period after 1962, zeolites rapidly

conquered additional processes in the fields of petroleum refining and petrochemistry [68, 70].

Some of advantages of the zeolites are summarized as below [10, 68, 70]:

- They have thermal and hydrothermal stability,
- They have controllable adsorption properties variable from hydrophilic to hydrophobic,
- The dimensions of their channels are close to the kinetic diameter of many molecules (0.5-1.2 nm),
- The unique pore structure makes these materials able to recognize molecules.

However, these catalysts present severe limitations when large reactant molecules are involved, especially in liquid-phase reactions as is frequently the case in the synthesis of fine chemicals due to the fact that mass transfer limitations are very severe for microporous materials [66]. Hence, it has been an important field of research to synthesize materials that would both resemble zeolites structurally and have larger pore systems. Most of the organic surfactants used to synthesize zeolites involve gel formation and act as void fillers in the growing porous solids. As a result, researchers attempted to employ larger organic surfactants to result in larger voids in synthesized molecular sieves. The presence of mesopores in these materials allows them to catalyze larger molecules [69]. As it was reported in the literature, amorphous $SiO_2/Al_2O_3$ materials with a narrow pore size distribution in the mesoporous region also have similar catalytic properties to zeolites, but these materials do not have uniform pore structure to affect the selectivity for catalysis. Therefore, number of researchers tried to synthesize mesoporous materials with a uniform pore structure [10, 68-71].

### 3.2 Mesoporous Materials

A continuous research in developing materials with constantly larger pores finally led to the development of materials with mesopores (2 nm<$d_{pore}$<50 nm) and these materials were designated as ***M41S***. These materials were synthesized firstly by ExxonMobil researchers in 1992 [72, 73]. The main

groups of this family are *MCM-41* (short for **M**obile **C**rystalline **M**atter, No.41), which shows a highly ordered hexagonal array of unidimensional pores with a very narrow pore size distribution, *MCM-48*, which has a three-dimensional, cubic-ordered pore structure and *MCM-50*, which has an unstable lamellar structure [10, 66, 74]. Their structures are given in Figure 3.2.

*M41S* family of materials is mainly made up of $SiO_2$. Silica has specific advantages as a support such as: excellent thermal and chemical stability and ease of handling. Also, it has a rather rigid structure and does not swell in solvents, so it may be used both at high and low temperatures. *MCM-41* becomes the most popular member of this family because of its flexible synthesis conditions and advantageous properties such as exceptionally high surface area and narrow pore size distribution and *MCM-41* bridges the gap between microporous and macroporous materials [75]. This material consists of an amorphous (alumino, metalo)-silicate framework, forming hexagonal pores (Figure 3.3a) and its structure is unidirectional and arranged in honeycomb structure (Figure 3.3b).

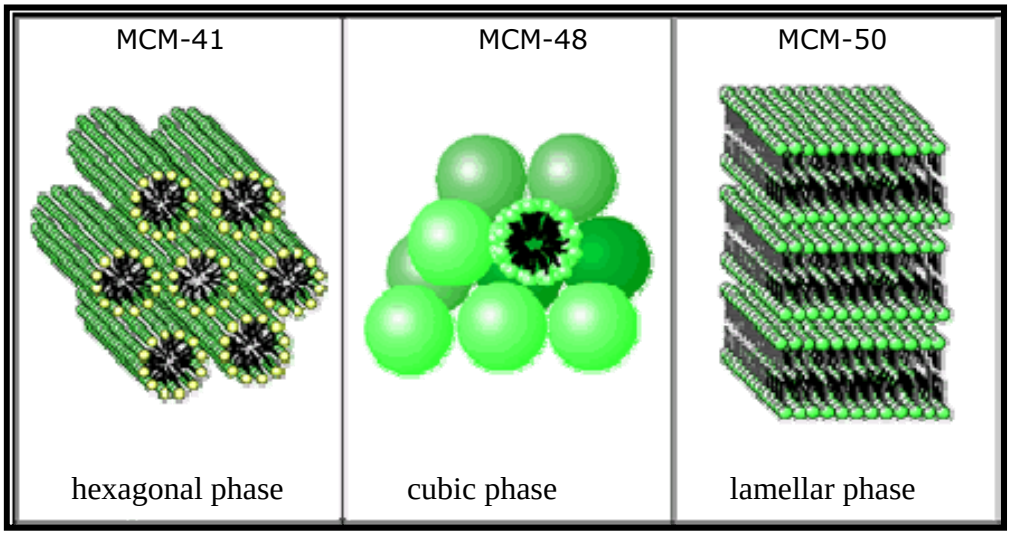


Figure 3.2 The important members of *M41S* family (adapted from [69])

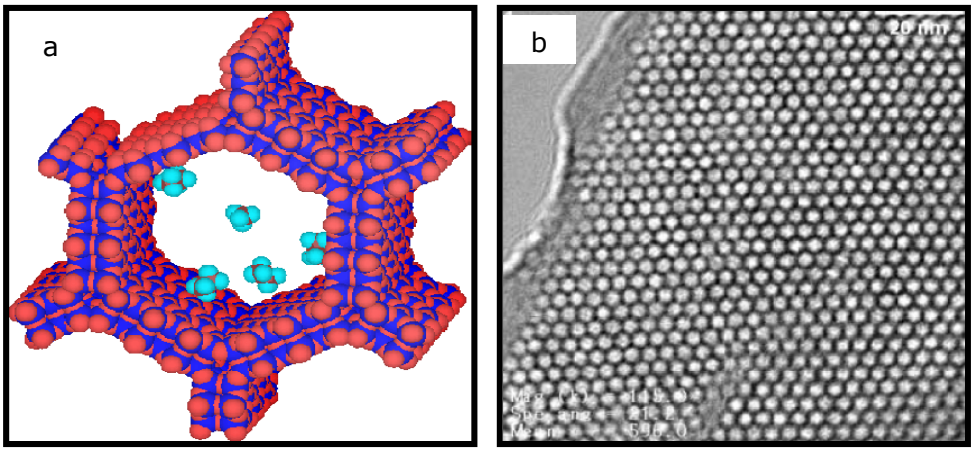


Figure 3.3 (a) Schematical representation of *MCM–41*, (b) TEM image of *MCM–41* (adapted from [69])

The hexagonal shape of the pore (Figure 3.3a) makes the pore surface heterogeneous. In the corners of the pore an enhanced presence of siloxane bridges has been detected [76]. These bridges help to create hydrophobic portions on the pore surface whereas the flat areas of the pore surface are hydrophilic due to the presence of hydroxyl groups.

All these characteristics open up new applications in acid, base or redox catalysis. However, for this material to be useful for catalytic applications, it is essential to incorporate metal ions ($Co^{+2}$, $V^{+5}$, $Fe^{+3}$, $Al^{+3}$, etc.) into silica framework. Also, the incorporation of these metal ions into the silica framework increases the acidity and ion exchange capacity of the mesoporous silica molecular sieves [10, 66, 77].

*M41S* materials are advantageous in many reactions, as mentioned above, but they are limited to a pore diameter of approximately 80 Å, and furthermore, they have significant external surface areas. These characteristics limit usage of these materials in size-selective reactions [78, 79]. To overcome this situation, Zhao and his co-workers extended the family of highly ordered mesoporous silicates by synthesizing ***S**anta **B**arbara **A**morphous (**SBA**)* type materials in 1998 [80, 81]. These materials have pore sizes between 20 and 300Å, and non-ionic block copolymers as structure

directing agents were used. These materials are synthesized in highly acidic media.

*SBA-15* is the most popular member of this family. It is synthesized using tri-block copolymer poly(ethylene oxide)-poly(propylene oxide)-poly(ethylene oxide). Another feature of *SBA-15* is the existence of micropores interconnecting hexagonally ordered mesopores (Figure 3.4a), which make it more suitable for catalysis because these interconnections facilitate diffusion inside the entire porous structure [82]. Additionally, these materials possess large BET surface area (>700 $m^2/g$) with large pore diameter and large pore wall thickness. The large wall thickness results in higher hydrothermal stability than M41S materials [78].

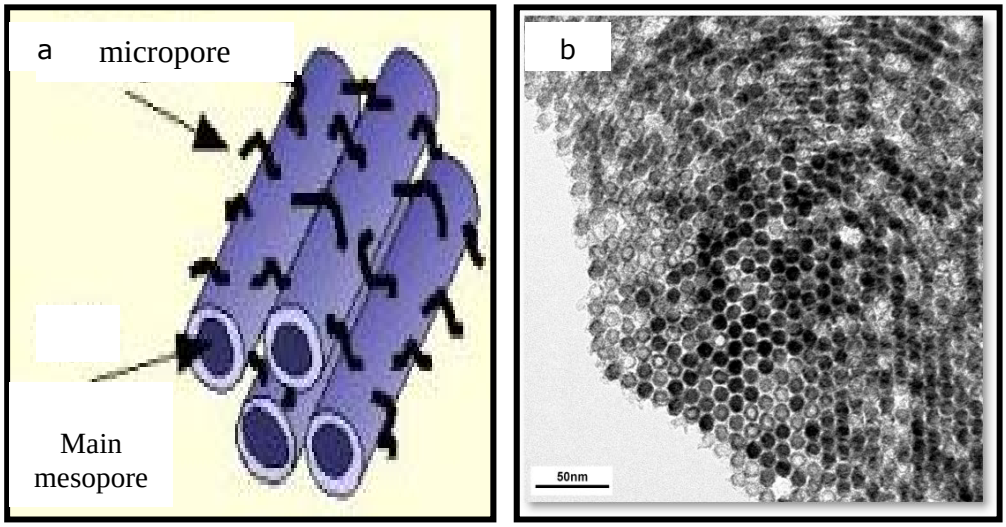


Figure 3.4 (a)Schematical representation of *SBA–15*,(b)TEM image of *SBA–15* (adapted from [83])

## 3.3 Synthesis of Mesoporous Materials

Mesoporous materials are synthesized by polymerizing a silica source around an organic surfactant in an aqueous solvent. In order to empty the pores, the organic surfactant is removed by the help of calcination. However, the interaction between the organic surfactant molecules and the silicate framework is influenced by the synthesis parameters [10]. Therefore, it is important to understand and control these parameters to obtain the desired structure [67, 69].

### 3.3.1 Components of Mesoporous Material Synthesis

The four main components of the synthesis of mesoporous materials (*MCM-41, SBA-15*, etc.) are a silica source, a structure-directing agent, a solvent and a mineralizing agent (acid or base).

#### 3.3.1.1 Silica Source

Sodium silicate ($Na_4O_4Si$), sodium metasilicate ($Na_2SiO_3$), tetraethyl orthosilicate (TEOS), tetramethyl orthosilicate (TMOS), fumed silica, colloidal silica and Ludox are the silica sources which are used in the synthesis of mesoporous materials. TEOS is usually used in mesoporous material synthesis under acidic conditions and the others are generally preferred for basic conditions [71, 84].

#### 3.3.1.2 Structure-directing Agents (Surfactants)

The term surfactant is the reduced form of "surface active agent" and refers to a class of chemical compounds known as amphiphiles (come from two Greek words meaning they are not certain what they like). The molecules of surfactants contain two parts: one part is polar (dipole or charged group), and the other part is non-polar (usually a hydrocarbon or halocarbon chain). The polar part is hydrophilic and the non-polar part is hydrophobic (Figure 3.5), therefore the molecule self-organizes itself in water in such a way as to minimize contact between incompatible ends [69, 84].

Ionic surfactants such as cetyltrimethylammonium chloride (CTMACl) and cetyltrimethyl bromide (CTMABr) are the most commonly used surfactants for the synthesis of *MCM-41*. In general, the use of low-molecular-weight amphiphiles with the formula of $C_nH_{2n+1}(CH_3)_3N^+$ (n=8-22) or $C_nH_{2n+1}C_5H_5N^+$ (n=12 or 16) is reported to result in the formation of MCM-41 [84]. The formation mechanism of MCM-41 is based on the electrostatic interactions between negatively charged silicate species and the positively charged surfactants in solution.

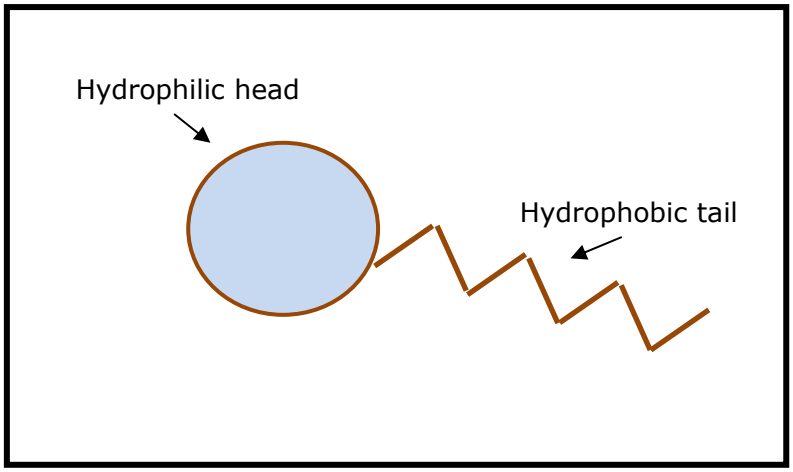


Figure 3.5 A typical surfactant (adapted from [69])

Mobil researchers showed that the pore diameter of *MCM-41* increases as the alkyl chain length of the surfactant increases. Furthermore, mesitylene was solubilized into the micelles. This made the micelles more voluminous and materials with pore diameter as large as 12 nm were prepared [10]. Table 3.1 lists some pore diameter values reported by Beck et al. [72] obtained for MCM-41 materials using different surfactants with different alkyl chain lengths. It is clearly seen that the values of the pore diameters increase with an increase in the lengths of the surfactant alkyl chains, as mentioned above.

Poly(ethylene oxide) is also a versatile surfactant used in the synthesis of mesoporous materials. Poly(ethylene oxide) monoethers were used to form materials showing worm-like disordered or hexagonally ordered mesopores with pore sizes of being around 5 nm [66, 81]. One of the most useful groups of surfactant is the triblock co-polymers made of poly(ethylene oxide)$_x$-poly(propylene oxide)$_y$-poly(ethylene oxide)$_x$, (PEO)$_x$(PPO)$_y$(PEO)$_x$, (trade name: Pluronics) which show the ability to form liquid-crystal structures. They can be used to synthesize sort of different mesoporous materials with preferably large pores in several framework compositions under strongly acidic conditions [66, 81, 85]. During the synthesis reaction of these materials, the ethylene oxide (EO) units and the cationic silicate species interact to form mesostructured assembly. *SBA-15* material formed through this pathway, showing a thick wall of 3-7 nm thickness and large pore sizes adjustable between 6 and about 15 nm [66].

Table 3.1 Pore sizes of *MCM-41* materials synthesized using different surfactants (adapted from [72])

| **Surfactant chain length n** $C_nH_{2n+1}(CH_3)_3N^+$ | **Average pore size (nm)** |
|---|---|
| 8 | 1.8 |
| 9 | 2.1 |
| 10 | 2.2 |
| 12 | 2.2 |
| 14 | 3.0 |
| 16 | 3.7 |

#### 3.3.1.3 Solvent

In the synthesis of *MCM-41*, water is used as the solvent. The amount of water used for the synthesis mixture is critical [84]. In the synthesis of *SBA-15*, HCl solution is used as the solvent. For both materials, the pH of the solution used for the synthesis mixture is critical [86].

#### 3.3.1.4 Mineralizing Agents

The mineralizing agent can be either an acid or base. Mineralizing agents mineralize the silica sources into soluble species with suitable morphologies capable of associating with surfactant molecules to form various periodic mesophases. For this purpose, sodium hydroxide, tetramethylammonium hydroxide or tetraethylammonium hydroxide can be used as basic additives and HCl, HF or $HNO_3$ can be used as acidic additives [10, 84].

### 3.3.2 Formation Mechanism of MCM-41

The original *MCM-41* synthesis is performed in water under alkaline conditions [72, 73]. Surfactants function as templates forming an ordered organic-inorganic composite material. Via calcination the surfactant is removed, leaving the porous silicate network, as mentioned before. The first mechanism proposed for the *MCM-41* synthesis is described by Beck *et al*. [72]. This formation mechanism is named as liquid crystal templating mechanism and it is shown in Figure 3.6.

Beck and his coworkers [72], proposed that the *MCM-41* structure is defined by the organization of surfactant molecules into liquid crystals which serve as templates for the formation of the *MCM-41* structure. The first step in the synthesis of *MCM-41* is the formation of a micellar rod. In the second step formation of a hexagonal array of rods by the incorporation of an inorganic array of silica or silica-alumina around the rod-like structures is reported (Figure 3.6). They also proposed an alternative pathway for the formation of *MCM-41* (Figure 3.6). This pathway shows a silicate anion initiated mechanism

in which the whole amount of cationic surfactant molecules in combination with anionic silicate species form a supramolecular structure [69].

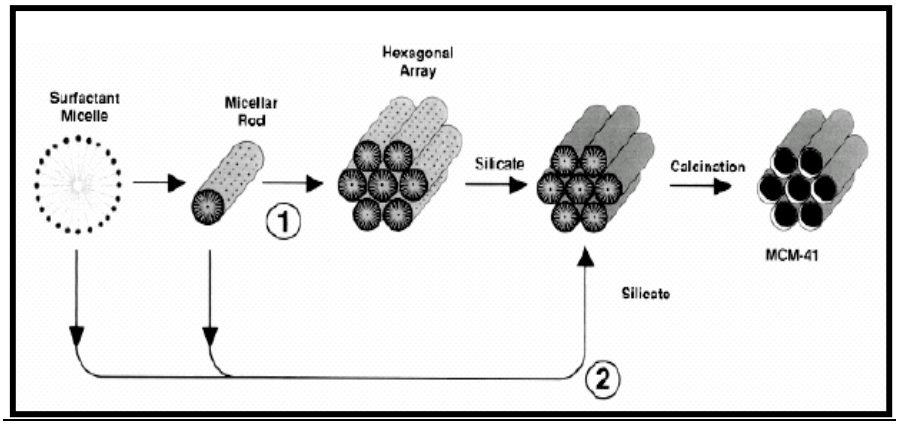


Figure 3.6 LCT mechanism proposed by Beck et al. [72] showing two possible pathways for the formation of *MCM-41*: (1) liquid-crystal-initiated and (2) silicate-initiated

It is now known that first pathway (liquid crystal initiated) did not take place because the surfactant concentrations used were far below the critical micelle concentration required for hexagonal liquid crystal formation [87].

Another formation mechanism was proposed by Stucky and coworkers and it is called as cooperative organization of inorganic and organic molecular species into three dimensional structured arrays [69]. In this mechanism, the formation process of MCM-41 was divided into three reaction steps, as shown in Figure 3.7: 1) Prior to silica addition, the surfactant is assumed to be in a dynamic equilibrium between spherical or cylindrical micelles and single molecules, 2) Upon addition of a silica source, the predominantly multicharged silicate species exchange with the $OH^-$ or $Br^-$ anions of surfactants to form organic-inorganic ion pairs accompanied by dissociation of the organic micelles and aggregation of the ion pairs into a new mesophase,

3) The silicatropic liquid crystal assembly process involving multidentate interaction controls the number of surfactant molecules that can bind to a given inorganic species and determines the interface packing density and ultimately the biphase morphology.

## 3.4 Control of Local Environment and Morphology of Mesoporous Materials

Recently, thermal, hydrothermal and mechanical stabilities of several mesoporous silicas (*MCM-41, SBA-15, FSM-16*, etc.) have been studied in literature [88, 89]. It was discovered that the thermal stability strongly depends on the wall thickness of the mesoporous materials and the silica source used in the synthesis.

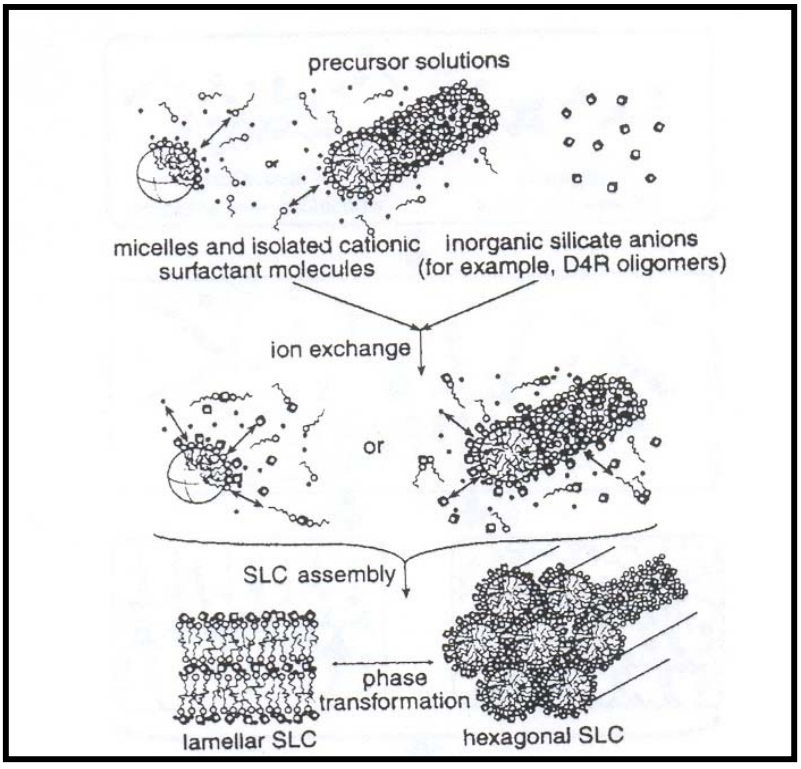


Figure 3.7 Formation of a silicatropic liquid crystal phase (adapted from [87])

Hydrothermal stability is also influenced by the wall thickness. In addition to this, the degree of silica polymerization has a very strong influence on hydrothermal stability. Mechanical stability, on the other hand, is only little influenced by the nature of the mesoporous materials and is usually sufficient for application of ordered mesoporous solids in most catalytic applications.

Since hydrothermal stability is necessary for most applications of mesoporous materials in catalysis, several approaches were developed to improve this property. The strategies that were investigated include the addition of salts during the hydrothermal synthesis, modification of surface by silylation or incipient wetness impregnation of inorganic compounds to increase the wall thickness [90-92].

In order to decrease the population of surface silanol groups, which influences the structural stability, silylation of surface hydroxyls is mostly used [89]. This treatment significantly increases the surface hydrophobicity, and therefore, the resulting materials have improved hydrothermal stabilities. Direct incorporation of organic compounds, either pending on the wall or incorporated as bridges between silicon atoms in the wall is possible. Impregnation of inorganic components, such as Al, V, Cu, Ni, etc. is also effective in achieving surface silanol modification [66].

### 3.5 Modification of Mesoporous Materials for Catalytic Purposes

Purely siliceous mesoporous materials do not have enough activity in many catalytic processes. Catalytic activity is, however, improved by modification of the siliceous framework by other elements. This may be done in various ways [10, 71]. One way is direct addition of the active sites to the structure during the synthesis. Therefore, these active sites are incorporated into the structure. Another way is to modify these materials after a desired structure has been synthesized [10]. A third method is the deposition of active sites in the structure by the incipient wetness impregnation technique [10, 69].

Metal or metal oxide incorporated mesoporous materials having high surface areas and narrow pore size distributions attracted major attention of catalysis

researchers in recent years [93-97]. The most studied of the modified mesoporous materials are those containing aluminum [77, 79, 97-100]. These materials are acidic and it is generally accepted that tetrahedral aluminum is incorporated into the wall structure, while octahedral aluminum is regarded as extra framework species [10, 75]. The significance of different aluminum sources were investigated, but the conclusions are not clear [101-103]. This may be due to different synthesis conditions.

Vanadium-containing *MCM-41* materials can be used as selective oxidation catalysts [84, 94] and copper-incorporated MCM-41 materials can be used as sorbents for removal of toxic gases [95]. Supported Pd catalysts are mostly used in number of hydrogenation, in organic synthesis and in steam reforming of ethanol. Due to its unique property for absorbing large quantities of hydrogen, this metal has also applications in purification and storage of hydrogen [69, 93].

### 3.6 Characterization Techniques for Mesoporous Materials

Many different experimental techniques are utilized to characterize mesoporous materials. Often several techniques are used in combination, in order to provide clear, understandable structural information.

#### 3.6.1 X-Ray Diffraction (XRD)

XRD provides direct information of the pore architecture of the materials. For mesoporous materials, the diffraction patterns only have reflection peaks in the low Bragg angle range (less than 10). These reflections are due to the ordered hexagonal array of paralel silica tubes [10, 67]. A well ordered two-dimensional hexagonal structure gives a sharp (100) plane diffraction peak and the diffraction peaks of higher Miller index planes, (110), (200) and (210) [69].

From $d_{100}$ value, calculation of lattice parameter *a* in a hexagonal lattice is done by using the following formula,

$$a = 2 \times d_{100} / \sqrt{3} \tag{3.1}$$

Here, the lattice parameter refers to the constant distance between unit cells in a crystal lattice. Pore wall thickness, $\delta$, can be calculated using the formula given below

$$\delta = a - 2 \times r \tag{3.2}$$

where *r* is the pore radius.

### 3.6.2 Nitrogen Physisorption

Physisorption is a primary method for characterization of porous materials. It is used to determine the porosity and specific surface area of materials. Different models for calculating the pore size distributions were developed [104]. The most common adsorbate is mostly $N_2$, at 77K. According to IUPAC classification, mesoporous materials exhibit a Type IV adsorption-desorption isotherm [10]. A typical example is given in Figure 3.8. At low relative pressures, the adsorption only occurs as a thin layer on the walls. On the other hand, a sharp increase is seen at relative pressures from 0.6 to 0.8, depending on pore size. This may due to the capillary condensation of $N_2$ in the mesopores. The sharpness of the inflection reflects the uniformity of the pore size and the height indicates the pore volume [10].

### 3.6.3 NMR Technique

Another important technique for the characterization of mesoporous materials is solid state NMR. $^{29}$Si-MAS-NMR spectroscopy is used to study the degree of condensation in the pore walls. The structure of these is found to be quite similar to amorphous silica, and usually two or three broad signals, at -89/-92, -98/-102 and -108/-111, are observed. These are assigned to $Si(OSi)_2(OH)_2$, $Si(OSi)_3(OH)$ and $Si(OSi)_4$ groups, respectively [10, 105].

$^{27}$Al-MAS-NMR is employed to distinguish between tetrahedrally and octahedrally coordinated aluminum in the framework (at approx. 50 and 0

ppm, respectively). Hence, the amount of framework aluminum can be determined. Dealumination processes can also be followed [10, 75].

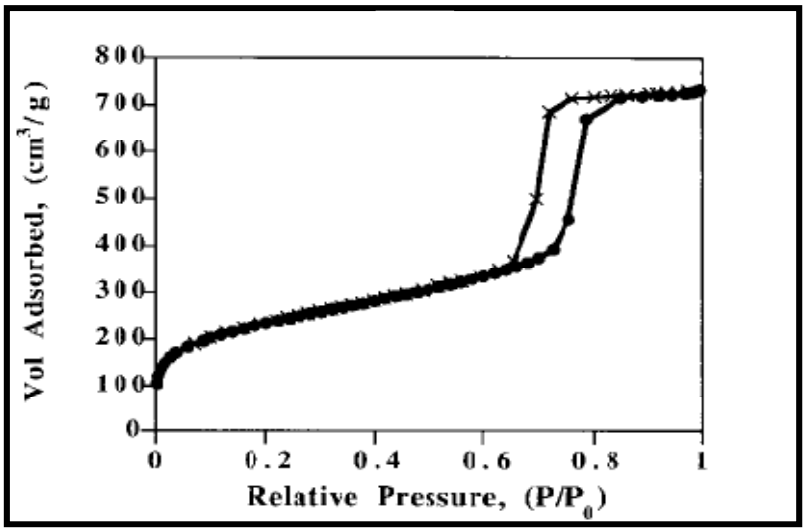


Figure 3.8 The $N_2$ adsorption-desorption isotherm for a siliceous *SBA-15* sample (adapted from [80])

### 3.6.4 Transmission Electron Microscopy (TEM)

One of the standard methods to characterize mesoporous materials is transmission electron microscopy. In this method, a thin solid specimen (≤200 nm thick) is bombarded in vacuum with a highly focused, monoenergetic beam of electrons (100-200 keV). The beam has sufficient energy to propagate through the specimen. A series of electromagnetic lenses then magnifies this transmitted electron signal. Diffracted electrons are observed in the form of a diffraction pattern beneath the specimen. This information is used to determine the atomic structure of the material in the sample [106].

### 3.6.5 Scanning Electron Microscopy (SEM)

SEM is often the first analytical instrument used when a "quick look" at a material is required and the light microscope cannot provide adequate resolution. In the SEM, an electron beam is focused into a fine probe and subsequently raster scanned over a small rectangular area. As the beam interacts with the sample, it creates various signals. These signals are highly localized to the area directly under the beam. By using these signals to modulate the brightness of a cathode-ray tube, which is raster scanned in synchronism with the electron beam, an image is formed on the screen [106].

### 3.6.6 Diffuse Reflactance Fourier Transform Infrared (DRIFT)

This method is used for measurement of fine particles and powders, as well as rough surface (e.g., the interaction of a surfactant with the inner particle, the adsorption of the molecules on the particle surface). In addition to this, presence of acid sites (Brönsted, Lewis or both) can be detected by DRIFT analysis [10]. For this purpose, adsorption studies using bases such as ammonia and pyridine were carried out [67].

## 3.7 Potential Applications of Mesoporous Materials

### 3.7.1 Acid Catalysis

These materials have been examined with regard to their use in cracking and hydrocracking reactions [66]. Corma *et al.* [107], have compared *AlMCM-41*, amorphous silica-alumina and zeolite Y (USY zeolite) in the catalytic cracking of n-heptane and vacuum gas oil. The activity of *AlMCM-41* was higher than for the amorphous silica-alumina and approached that for USY zeolite in the processing of large gas oil molecules. The selectivity of aluminum containing *MCM-41* in the gas oil cracking resulted in more liquid fuels and less gases and coke compared to the amorphous $SiO_2/Al_2O_3$. Compared with the USY zeolite, the diesel formation was higher and it gives less gasoline and more coke [10].

For small molecules, such as n-hexane, n-heptane or small cyclic hydrocarbons such as tetralin and decaline, the cracking activity of *MCM-41* is much lower than that of USY zeolite. In addition, steam treatment, which was used as way to simulate fluidized catalytic cracking, results in a collapse of the mesopore structure and a decrease in activity far below that of steam-treated aluminosilicate [66].

There are refining processes which do not demand the kind of acidity and hydrothermal stability of the catalysts as catalytic cracking does. These are for instance hydrocracking, olefin oligomerization and hydroisomerization. The hydrocracking process involves an upgradation of resids and gas oils to lighter products. Mild hydrocracking is a process where hydrocracking is performed in reactors usually utilized in hydrodesulfurization of feed. At these conditions, the hydrodesulfurization of the feed is obtained simultaneously to some hydrocracking of the feed, resulting in increase of diesel amount. The reaction is carried out over a mildly acidic catalyst deposited with NiO and $Mo_2O_3$ [10].

Important properties of hydrocracking catalysts are the distribution of metal sites at the surfaces and the proximity of these to acidic cracking sites. Consequently, *AlMCM-41* has been considered as a good candidate for mild hydrocracking processes. This support is mildly acidic and it has a large surface area [10].

Oligomerization of butane at 150°C and 1.5-2 MPa has been investigated over zeolites, amorphous silica-alumina, and ordered mesoporous aluminosilicates. The mesoporous catalyst showed high selectivity and good stability with time for the production of branched dimmers, while strongly adsorbed residue was formed over microporous zeolites and amorphous silica-alumina and fast deactivation occurred over these catalysts [66].

Sulfated $ZrO_2$ supported on *MCM-41* shows comparable activity with bulk sulfated $ZrO_2$ catalyst in both cumene and 1,3,5-triisopropylbenzene cracking. Catalyst deactivation was slower for the supported catalyst compared to bulk sulfated $ZrO_2$ [66]. In the condensation of *tert*-butanol and methanol over

sulfated $ZrO_2$ supported on *SBA-15*, the supported catalyst showed about 2 times higher yield of methyl *tert*-butyl ether (MTBE) than bulk zirconia [108].

Acidic *MCM-41* materials have also a great potential in the field of organic synthesis and production of fine chemicals. Some of the reactions that are investigated are Friedel-Crafts alkylation, acylation and acetalyzation reactions. In all these reactions, when the size of the reacting molecules increases, the activity of *MCM-41* catalysts increases [10].

### 3.7.2 Redox Catalysis

There are numerous reports in the literature about redox reactions on framework modified ordered mesoporous materials or materials which had been changed by grafting of active species [66]. In many cases, it is very difficult to judge the performance of such materials, because the reaction conditions are not comparable with each other most of the times.

Selective oxidation reactions of paraffins, olefins and alcohols have been carried out over titanium-silicalite. In order to be able to process larger molecules, investigations have been made to extend the pore sizes of this type of catalyst. For example, Ti-β-zeolite has been synthesized, and in 1994 the first mesoporous templated silicates containing tetrahedral titanium was prepared according to two independent procedures with different surfactant templating mechanisms [71]. It was shown that *Ti-MCM-41* could selectively oxidize olefins to epoxides using $H_2O_2$ or organic hydroperoxides as the oxidizing agent. Furthermore, bulky sulfides have been oxidized to the corresponding sulfoxides and sulfones [66, 71].

The success of titanium in the mesoporous structures initiated an interest for incorporating other transition metals into the structures as well. A major problem with mesoporous transition metal catalysts, however, is the strong decrease in activity and selectivity when the metal content is increased. Another drawback is the alternation of the oxidation state of the metals during calcinations and regeneration [10, 71].

### 3.7.3 Other Applications

The *MCM-41* type of materials has also been investigated with respect to somewhat exotic applications. Some of these are shortly presented below [10].

*AlMCM-41* was used as a stationary phase in normal phase HPLC. It was found to have acidic and basic properties which made it suitable in the chromatographic separation of acidic, neutral and basic compounds [10].

Conducting polyaniline and carbon fibers have been synthesized within the pore system of *AlMCM-41*. The microwave conductivity of polyacrylonitrile was found to be 10 times higher than that of bulk carbonized polyacrylonitrile. This type of molecular and quantum wires may have many applications within high technology electronic equipment [10].

Controlled shape selective polymerization of styrene, methyl methacrylate and vinyl acetate has been performed in *MCM-41* materials. Finally, their large surface areas make mesoporous materials very attractive as supports for active phases. They have been applied as support for acids, bases and metals or metal oxides [10].

# CHAPTER 4

# LITERATURE SURVEY

The disposal of municipal and industrial plastic waste is recognized to be a major environmental problem. Recycling of these waste polymers by chemical recovery is a promising approach to the solution of pollution problem. In this method, the waste plastics are thermally or catalytically degraded into gases and liquids which can be utilized as fuels or chemicals. Catalytic degradation by contacting the polymers directly with an acidic catalyst is preferred more than thermal degradation because the latter one requires higher working temperatures and gives low-quality products. The most commonly used catalysts in the catalytic degradation of polymers are zeolites but in recent years, acidic mesoporous catalysts (MCM-41, SBA-15, etc.) have been utilized in polymer cracking reactions. Studies about non-catalytic and catalytic degradation of polymers are reviewed below.

Jakab *et al.*[41] studied the thermal decomposition of polypropylene in the presence of wood flour, lignin cellulose and charcoal in order to understand the pyrolytic behavior of the mixture of these components occurring in the waste. It was found that activated charcoal had the most significant effect on the decomposition profile and the product distribution of polypropylene. In the presence of charcoal, the decomposition shifted to lower temperature and the presence of this material promoted the formation of monomer and dimer. The effect of wood flour, lignin and cellulose was less pronounced. In the presence of these additives, the temperature of the maximum decomposition rate and the char yields did not change significantly.

Walendziewski [43] performed two series of experiments for cracking of waste polymers (PS, PE and PP). The first series of polymer cracking experiments were carried out in a glass reactor at atmospheric pressure and in a temperature range of 350 to 420°C, the second one in autoclaves under hydogen pressure in the temperature range of 380 to 440°C. Application of catalyst increases gas product yields but no visible influence of catalyst on gas composition was observed. In comparison to the atmospheric process, the cracking of waste plastics in autoclaves under pressure at long contact time and high temperature resulted in larger conversion level, larger gas and gasoline fraction yields and relatively lower boiling and lower freezing points however lower cetane number of diesel fuel fractions.

Peterson *et al.*[47] studied the kinetics of thermal degradation of PS, PE and PP under both inert nitrogen and air atmospheres using TGA and DSC. Here DSC was employed to elucidate the decomposition steps observed in the TGA data. The isoconversional method has been employed to calculate the activation energies as a function of the extent of degradation. This method permits the effective activation energy of a process to be unambiguously estimated as a function of the extent of conversion. It can be effectively applied to the overall as well as species-specific data. The results showed that lower values were observed for the initial stages of the thermal degradation of PE and PS: this suggested that degradation was initiated at weak links and under nitrogen, the thermal degradation of polymers followed a random scission pathway.

Puente *et al*.[5] studied the performance of various acidic catalysts in recycling of polystyrene (PS) into fuels. Commercial FCC catalyst and various acidic catalysts like zeolites (ZSM-5), mordenite, Y, and a sulfur-promoted zirconia were tested in the conversion of polystyrene to fuel products at 550°C in a fluidized-bed batch reactor. Main products were in the gasoline range, including benzene, toluene, ethylbenzene, styrene and minor amounts of $C_{9-12}$ aromatics and light $C_{5-}$ compounds. Also coke formation was observed in significant amounts. Styrene would be mainly produced in this system from thermal cracking of the polymer as the initial step. Even though sulfur-promoted zirconia was highly acidic, the low proportion of Brönsted-type acid

sites did not allow the occurrence of secondary styrene reactions. It was shown that most favorable product distributions (higher yields of desirable products) were obtained on equilibrium commercial FCC catalysts.

Van Grieken *et al.*[6] studied both the non-catalytic and catalytic thermal degradation of high and low-density polyethylene. HZSM-5 and HY zeolites, amorphous alumina-silica, activated carbon and MCM-41 catalysts were employed. The best results achieved in the LDPE degradation with regard to stability and homogeneity of the waxy product were obtained using MCM-41 as catalyst. On the other hand, the product obtained from HDPE had a higher homogeneity than that of coming from LDPE, leading to a waxy product with better quality.

Kaminsky *et al.*[7] studied the performance of Lewis acids and mixtures of Ziegler-Natta catalysts such as $TiCl_4$, $AlCl_3$ in the pyrolysis of polypropylene. The reactions were carried out in a batch reactor. It was found that the pyrolysis temperature decreased by 100°C in the presence of catalysts compared to the runs without catalysts. Additionally, a significant increase in the amount of low boiling compounds ($C_4$ hydrocarbons) was observed by the use of the catalysts, and when the amount of catalyst loading was increased, light oil and gas fraction amounts increased.

Takuma *et al.*[35] studied degradation of LDPE, HDPE and PP in a fixed-bed flow reactor system with and without H-gallosilicate catalyst at 375-550°C to investigate the product distribution and catalyst stability. The catalytic degradation over the gallosilicate yielded lighter hydrocarbon mixtures that were rich in valuable aromatic components, mostly benzene, toluene, and xylenes. The product distribution was influenced little by the structure of the polymers to be degraded because the catalytic degradation of polyolefins proceeds through similar intermediates regardless of the structure of the degrading polymers, leading to almost the same product distributions. The gallosilicate exhibited a stable catalytic activity for the degradation of polyolefins when reused, because of a very low yield of coke deposited on the catalyst surface.

Uçar *et al*.[36] studied the processability of low density polyethylene (LDPE) and polypropylene (PP) in the hydrocracking unit of a refinery. For this purpose, the polymer blends were thermally and catalytically cracked over different catalysts using a batch autoclave at 425-450°C under hydrogen atmosphere. The catalysts used were HZSM-5, cobalt loaded active carbon (Co-Ac) and commercial silica-alumina catalyst (DHC-8). HZSM-5 gave higher gas yields than the other catalysts. When using Co-Ac and DHC-8 catalysts, the gas and liquid yields depend on the polymer type as well as temperature. In thermal cracking, the product distribution obtained from cracking of PP did not change with temperature whereas the temperature had an effect on the product distribution for the LDPE cracking. Also, they observed that the thermal run gave higher gas+liquid yields than the catalytic run above 425°C, because in catalytic cracking waxy compounds were formed in larger amounts than in thermal cracking.

Cardona *et al.*[37] studied the catalytic cracking of polypropylene in a semi-batch reactor. The influence of the cracking catalyst's nature and the reaction conditions on conversion and selectivity was studied. Large pore zeolites, amorphous and ordered silica-aluminas were used as catalysts, in order to better study the influence of pore size, crystallite size and the number and strength of the active acid sites. Also, a catalytic cracking was performed on a spent equilibrium catalyst coming from a FCC unit. The results showed that by working with zeolite with unit cell size, it was proven that neither the total amount nor the strength of the acid sites was the most determinant factors for cracking PP. Also, it was shown that amorphous or ordered silica-aluminas were very active catalysts. However, a FCC equilibrium catalyst could be better option from economical point of view since it gave a very good selectivity, and even if its activity was lower than that of the silica-aluminas, this could be compensated by increasing the catalyst to PP ratio. As a result, a kinetic model including both thermal and catalytic cracking and catalyst decay was developed for this system. The kinetic model fitted very well the experimental results and was able to simulate the process in a wide range of operating conditions.

Serrano *et al.* [38] studied recycling of plastic film waste, mixture of low-density polyethylene (LDPE) and ethylene-vinyl acetate copolymer, over several acid catalysts at 420°C. They used zeolite (HZSM5) and mesoporous catalysts (Al-SBA-15 and Al-MCM-41) for this purpose. They found that mesoporous solids were practically inactive with the plastic film waste probably due to their medium acid strength along with a deactivation phenomenon caused by the presence of EVA copolymer in the raw refuse. However, HZSM5 zeolite was able to degrade completely the film waste using a very small amount of catalyst. In addition, more than 55 wt% of $C_3$-$C_5$ hydrocarbons were obtained over H-ZSM5 catalyst at 420°C, the majority of them being valuable olefins.

Williams *et al.* [39] investigated the yield and composition of oils and gases derived from the pyrolysis and catalytic pyrolysis of PS performed in a fixed bed reactor. Two catalysts were used, zeolite ZSM-5 and Y-zeolite. The influence of the catalyst's temperature, the amount of catalyst loading and the use of a catalyst mixture was investigated. The main product from the uncatalysed pyrolysis of PS was oil mostly composed of styrene and other aromatic hydrocarbons. The gases were found to consist of methane, ethane, ethene, propane, propene, butane and butene. In the presence of catalyst, an increase in the yield of gas and decrease in the amount of oil produced was observed.

Sharratt *et al.*[48] studied the pyrolysis of PE over HZSM-5 catalyst using a specially developed laboratory fluidized-bed reactor operating at ambient pressure. The influence of reaction conditions including temperature, ratios of PE to catalyst feed, and flow rates of fluidizing gas was examined. HZSM-5 catalyzed degradation resulted in much greater amounts of volatile hydrocarbons compared with degradation over silicalite. The systematic experiments carried out with HZSM-5 showed that the use of catalyst reduced the required reaction temperature, improved the yield of volatile products, and provided selectivity in the product distributions. The selectivity could be further influenced by changes in reactor conditions: in particular, olefins and *i*-olefins were produced using low temperatures and short contact times. It

was concluded that, under appropriate conditions the resource potential of polymer waste could be recovered.

Garforth *et al.* [49] investigated the activity of various solid acid catalysts (HZSM5 and HY zeolites, amorphous $SiO_2$-$Al_2O_3$, MCM-41, Al-MCM-41) in the degradation of high density polyethylene (HDPE). For this purpose, thermogravimetric analysis was used. They found that amorphous $SiO_2$-$Al_2O_3$ significantly reduced the apparent activation energy as compared with uncatalysed thermal processes. Zeolites HY and HZSM5 further reduced the activation energy resulting in more rapid degradation. Aluminum containing MCM-41 was found to be more active in the degradation of HDPE at a rate similar to that of HZSM5. On the other hand, siliceous form of MCM-41, containing virtually no aluminum, had a minimal effect on HDPE with degradation occurring at a temperature similar to that of non-catalytic thermal cracking.

Ohkita *et al.* [50] studied the relationship between the acid strengths and amounts of silica-alumina catalysts and the compositions of products formed by the catalytic degradation of PE at 400°C. Although the resulting products was composed of gases, oils and wax, they found that the fraction of gases increased and inversely, the fraction of oils decreased, as the acid amounts over the catalysts increased. On the other hand, the fraction of aromatics in the oils was enhanced as the acid sites over the catalysis increased.

Sakata *et al.*[51] studied the thermal and catalytic degradation of plastic polymers, PE at 430°C and PP at 380°C into fuel oil which was carried out in batch reactor. The catalysts employed were acid-catalysts silica-alumina, zeolite ZSM-5 and non-acidic mesoporous silica catalysts (silicalite, mesoporous silica gel and mesoporous folded silica (FSM)). The yields of product gas, liquid and residues; recovery rate of liquid products, and boiling point distribution of liquid products by catalytic degradation were compared with those of non-catalytic thermal degradation. For PP degradation in liquid phase contact with silica-alumina, the yield of liquid hydrocarbons was obtained with 69 wt.%, and the boiling point of the oil ranged between 36 and 270°C, equivalent to the boiling point of normal paraffins n-$C_6$ to n-$C_{15}$. The

liquid products from catalytic degradation have a carbon number distribution very similar to commercial automobile gasoline. Catalysts possessing strong acid sites such as zeolite ZSM-5 accelerated the degradation of PP and PE into gases which resulted in low liquid yields. For FSM, which possesses no acid sites, the initial rates of PP and PE degradation into liquid were as fast as that over an acid catalyst (silica-alumina) and the liquid yields were higher.

Sakata *et al.*[54] performed the degradation of PP at 380°C by batch operation using silica-alumina catalyst in liquid phase contact and vapor phase contact. Also, they carried out the degradation of PP under same conditions without using catalyst. For catalytic degradation in vapor phase contact, the yield of residues did not differ significantly from that of thermal degradation, however, the yield of liquid products decreased and that of gaseous products increased. These results implied that in vapor phase contact, thermally degraded hydrocarbon underwent further decomposition into gaseous products over silica-alumina. On the other hand, for catalytic degradation in liquid phase contact, the yield of gaseous products did not differ much from that of thermal degradation, but the yield of liquid products increased at the expense of yield of residues.

Lee *et al.*[55] studied the catalytic degradation of waste plastics such as PE , PP and PS over FCC catalyst which were carried out at atmospheric pressure with a stirred semi-batch operation at 400°C. Here, the objective was to investigate the influence of plastic types on the yield, liquid product rate and liquid product distribution for catalytic degradation. The catalytic degradation of waste PE and PP with polyolefinic structure exhibited high liquid yield and very low solid yield (below 1%). Accumulative liquid product weight by catalytic degradation strongly depended on the degradation temperature of the plastics. Both PE and PP showed around 80% of olefin components in the liquid product and all polyolefinic samples had a very similar tendency for the molecular weight distributions of liquid product. The orders of gas, liquid and solid yields in the type of plastics were PE>PP>PS, PS>PP>PE and PS>PP>PE, respectively. The order of thermal degradation temperatures was obtained as PS<PP<PE, while that of the initial rate from catalytic degradation over FCC catalyst was PS>PP>PE.

Uemichi *et al.*[58] investigated the degradation of PP to aromatic hydrocarbons over activated carbon catalysts containing Pt and Fe. They compared the obtained results with those for the degradation of PE and found that the mechanism for the formation of aromatics in the degradation of PP over the Pt- or Fe-containing activated carbon catalyst was essentially the same as that for polyethylene. The mechanism seems to be applicable to the degradation of other polyolefins, taking into account the structure of the decomposed fragments. The presence of methyl branching in the polymer structure was unfavorable for the formation of aromatics not only over metal-free activated carbon but also over the Pt- and Fe-containing catalysts. Further, the added Pt was found to induce some ring expansion activity in the catalyst, while the addition of Fe had no effect on the activity.

Zhou *et al.*[60] studied the catalytic degradation of low-density polyethylene and polypropylene using a modified ZSM-5 zeolite, *DeLaZSM-5*. It was found that the degradation behaviour of LDPE and PP using this modified zeolite was quite different from those observed in thermal degradation. LDPE exhibited much higher degradation activity using the *DeLaZSM-5* than PP did, especially in relatively lower temperature stage, indicating that this catalyst showed a shape-selective effect in catalytic degradation of LDPE and PP. It was concluded that the pore structure and unique acid property of the *DeLaZSM-5* catalyst as well as proper reaction temperature were important factors to fully exert the shape-selective effect of the catalyst.

Aguado *et al.*[61] investigated the catalytic degradation of both LDPE and HDPE and PP using MCM-41, a mesoporous aluminosilicate, as catalyst. The results have been compared with those of ZSM-5 zeolite and amorphous silica-alumina. For all the studied plastics, MCM-41 was found more active than the amorphous $SiO_2$-$Al_2O_3$, as a consequence of the higher surface area and the uniform mesoporosity present in the former. Compared to ZSM-5, MCM-41 exhibited a lower activity for the degradation of linear and low branched polymers (HDPE and LDPE, respectively), which could be related to the higher strength of the zeolite acid sites. However, the opposite was observed for the cracking of highly substituted plastics such as PP due to the severe steric hindrances these molecules encountered to enter into the

narrow pores of the zeolite. Moreover, for the cracking of LDPE, HDPE, and PP, the selectivities toward hydrocarbons in the range of gasolines and middle distillates obtained over MCM-41 were clearly higher than those of ZSM-5. Therefore, MCM-41 was a catalyst potentially interesting for the conversion of polyolefinic plastic wastes into liquid fuels.

Lin *et al.* [63] studied the catalytic degradation of polypropylene in the temperature range of 290-430°C to obtain a range of volatile hydrocarbons using a laboratory catalytic fluidized-bed reactor. For this purpose, different kinds of zeolite (HZSM-5, HUSY and HMOR) and non-zeolite (SAHA and MCM-41) catalysts were used. They found that the yield of volatile hydrocarbons for zeolite catalysts was higher than that of the volatile hydrocarbons for non-zeolite catalysts. MCM-41 with large mesopores and SAHA with weaker acid sites resulted in a highly olefinic product and gave a wide carbon number distribution, whereas HUSY yielded a saturate-rich product with a wide carbon number distribution and substantial coke levels. When HZSM-5 and HMOR used as catalysts, about 60% of product selectivity in the $C_3$-$C_5$ range was obtained and HMOR generating the highest yield of i-$C_4$ among all catalysts studied.

Uddin *et al.*[109] studied the catalytic degradation of polyolefinic polymers like PE and PP at atmospheric pressure by batch operation at 430°C and 380°C using non-acidic mesoporous silica catalyst (FSM). A comparison of non-catalytic thermal degradation with catalytic degradation using solid acid catalysts (silica-alumina, ZSM-5), silicalite, and silica-gel was made. Non-acidic FSM catalyst accelerated the initial rate of degradation, increased the liquid product yield and promoted degradation into lower molecular weight products. They also repeated the batch reaction four times using the same FSM catalyst and found that the extent of the decline in the degradation rate for PE was lower than that of the decline in the degradation rate for PP.

Sakata *et al.* [110] studied the catalytic degradation of PE over mesoporous silica (KFS-16) catalyst. The product yield, composition and degradation rate of PE over KFS-16 were compared with those over solid acid catalyst (silica-alumina and zeolite) and non-catalytic thermal degradation. The initial rate of

degradation of PE over KFS-16, which possesses no acid sites was as fast as that over silica-alumina (SA-1) and the yield of liquid products was higher. But the composition of the liquid products of degradation over KFS-16 was different from that over SA-1 and similar to that of non-catalytic thermal degradation. SA-1 catalyst deactivated very rapidly due to coke deposition, whereas KFS-16 deactivated much more slowly. These findings over mesoporous silica suggested that the mesopores surrounded by the silica sheet may act as a flask for storing radical species for a long time and then long-lived radicals accelerate the degradation of plastics.

As it can be seen from this brief literature survey, much less is known about polypropylene degradation over mesoporous aluminosilicate catalysts (AlMCM-41 and AlSBA-15) which are potentially interesting for the conversion of polyolefinic plastic wastes into liquid fuels. Therefore, the objective of this study is:

- To synthesize AlMCM-41 and AlSBA-15 catalysts from different aluminum sources with different amount of aluminum loading.
- To characterize the synthesized catalysts.
- To determine the activation energy of polypropylene degradation reaction using thermal analyser (TGA).
- To design and construct a pyrolysis system.
- To get information about product distribution in polypropylene degradation reaction.

# CHAPTER 5

# EXPERIMENTAL

In this study, the catalytic activity of ordered mesoporous materials*, MCM-type* and *SBA-type*, in polypropylene degradation reaction was investigated. Experimental studies conducted in this work can be summarized in two parts. The first part is the synthesis and characterization of AlMCM-41 and AlSBA-15 catalysts. For this purpose, different aluminum sources; aluminum nitrate, aluminum isopropoxide and aluminum sulphate were used. The catalysts were synthesized at different Al/Si ratios. Physical and structural properties of these materials were determined by XRD, Nitrogen Physisorption, SEM, EDS, TEM, $^{27}$Al MAS NMR and Diffuse Reflactance FT-IR. The second part is the pyrolysis of polypropylene in the presence of these synthesized materials in order to investigate their catalytic activities. Before performing catalytic pyrolysis reactions, activation energy of pyrolysis reaction in the presence of synthesized catalysts was determined by the help of a thermal analyser. After that, the reactions were carried out and the final products were identified by the help of gas chromatography. In addition to these pyrolysis reactions, non-catalytic thermal degradation (blank) reactions were also carried out to make a reasonable comparison.

## 5.1 Synthesis of Mesoporous Aluminosilicate Catalysts

In this part, two different types of mesoporous aluminosilicate catalysts were synthesized. In the first part, pure and aluminum containing *MCM-41* catalysts

were synthesized and in the second part, pure and aluminum containing *SBA-15* catalysts were synthesized.

### 5.1.1 Synthesis of Mesoporous MCM-Type Catalysts

Mesoporous MCM-type samples were synthesized according to the procedure described by Şener *et al*. [93]. This procedure was modified in the synthesis of aluminum containing MCM-type materials. Both pure and aluminum containing MCM-type materials were synthesized using direct hydrothermal synthesis route. Different silica sources were used in the synthesis of pure MCM-type materials. In addition to this, aluminum containing MCM-type materials were synthesized at different Al/Si ratios using different aluminum sources.

#### 5.1.1.1 Reagents

Reagents used in the synthesis of mesoporous aluminosilicates are given below:

- Cetyltrimethylammonium bromide (CTMABr), $C_{16}H_{33}(CH_3)_3NBr$, 99% pure, Merck (Surfactant)
- Tetraethyl orthosilicate (TEOS), $C_8H_{20}O_4Si$, Merck (Silica source)
- Sodium silicate solution, $Na_2Si_3O_7$, 27 wt% $SiO_2$, Aldrich (Silica source)
- Aluminium nitrate nonahydrate, $Al(NO_3)_3.9H_2O$, Merck (Aluminium source)
- Aluminium isopropoxide, $C_9H_{21}AlO_3$, Merck (Aluminium source)
- NaOH, 1M, Merck
- $H_2SO_4$, 2M (prepared in the laboratory)
- Deionized water

#### 5.1.1.2 Procedure

Main steps of the synthesis of mesoporous MCM-type materials are preparation of the synthesis solution, hydrothermal synthesis, filtering the solid product, washing, drying, and calcination. Synthesis steps of MCM-type catalysts are displayed in Figure 5.1.

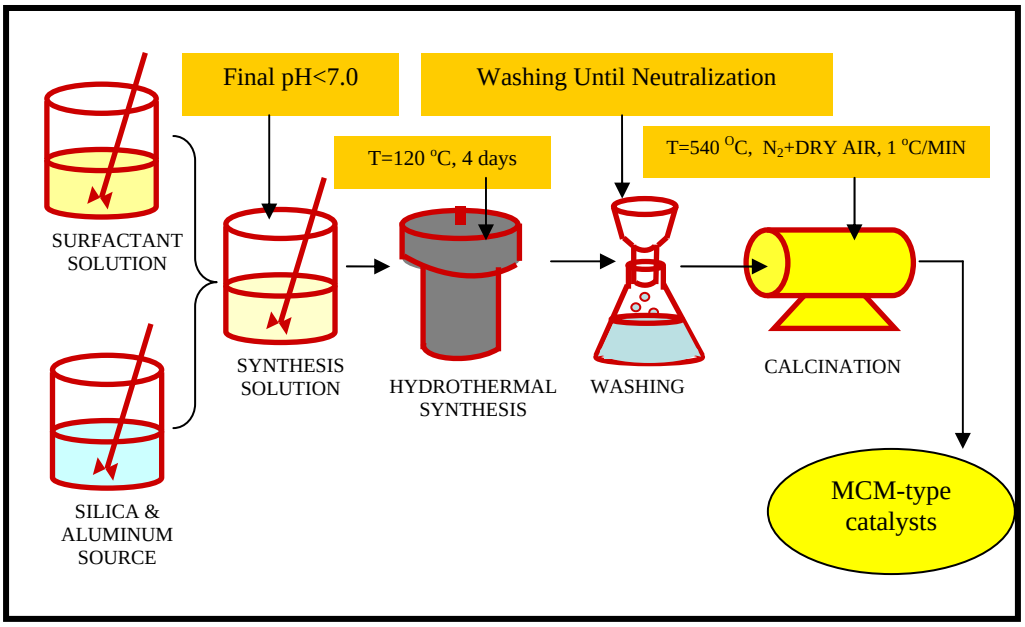


Figure 5.1 Main synthesis steps of mesoporous aluminosilicate catalysts (adapted from [69])

Details of the synthesis are described below.

#### 5.1.1.2.1 Synthesis of pure MCM-41 using sodium silicate as silica source

13.2 g of cetyltrimethylammonium bromide was dissolved in 87 ml of deionized water. The surfactant solution was continuously stirred with a rate of 500 rpm until a clear solution was obtained. Since change in temperature may cause agglomerates, solution temperature was kept at 30°C to have homogeneous solution. At the beginning of the stirring, color of the solution was white. After stirring for 45 minutes, a clear solution was obtained with a pH value of 7.3.

11.3 ml sodium silicate solution was added dropwise to the surfactant solution. By the addition of sodium silicate, the pH of the synthesis mixture increased to 12.3. After that, the pH of the solution was decreased to 11 by

adding 2M $H_2SO_4$ dropwise to the solution. Finally, the resultant mixture was stirred for 1 h and this sample was named as "*MCM-41"*.

#### 5.1.1.2.2 Synthesis of pure MCM-41 using TEOS as silica source

The same procedure mentioned in part 5.1.1.2.1 was followed for the preparation of the surfactant solution.

After preparation of the surfactant solution, 15.64 ml tetraethyl orthosilicate (TEOS) solution was added dropwise to this solution. By the addition of TEOS, the pH of the synthesis mixture decreased to 7.1. After that, two different ways were followed. In the first way, the pH of the solution was increased to 11 by adding 1M NaOH dropwise to the solution (basic route). This sample was named as "*MCM-41TB"* In the second way, the pH of the solution was decreased to 2 by adding 2M $H_2SO_4$ dropwise to the solution (acidic route). This sample was named as *"MCM-41TA"*. After that, both solutions was stirred for 1 h.

#### 5.1.1.2.3 Synthesis of Al-MCM-41 using different aluminum sources

***a) Using Aluminum Nitrate as Aluminum Source***

The same procedure mentioned in part 5.1.1.2.1 was followed for the preparation of the surfactant solution.

After preparation of the surfactant solution, 15.64 ml tetraethyl orthosilicate (TEOS) solution was dropwisely added to this solution. By the addition of TEOS, the pH of the synthesis mixture decreased to 7.1. After addition of TEOS, predetermined amount of aluminium nitrate solution was added dropwise to the synthesis solution. By addition of aluminium nitrate solution, the pH of the synthesis solution decreased to a value of around 1.5-2.5 depending on the amount of aluminium nitrate added to the synthesis solution. The resulting solution was stirred for 1 h.

***b) Using Aluminum Isopropoxide as Aluminum Source***

Firstly, certain amount of surfactant (CTABr) was dissolved in water. After obtaining a clear solution, tetraethyl orthosilicate solution was added dropwise to the surfactant solution. The amounts of the surfactant and silica source used in the synthesis are same with the amounts used in the previous part.

After addition of silica source, predetermined amount of aluminium isopropoxide was dropwisely added to the synthesis solution. By addition of this aluminium source, the pH of the synthesis solution increased to a value of around 8.5-9.0 depending on the amount of aluminium isopropoxide added to the synthesis solution. The resulting solution was stirred for 1 h. To decrease the pH of the resultant solution, 2M $H_2SO_4$ was added dropwise to adjust the pH value around 2 and the resulting solution was stirred for 1 h.

#### 5.1.1.3 Hydrothermal Synthesis

The final solution was transferred to a teflon bottle and placed in a stainless-steel autoclave. The hydrothermal synthesis was performed at 120°C for 96 h. The mesoporous MCM-type samples prepared from different aluminum sources were designated Al-*x*A and Al-*x*B, where *x* represented the Al/Si ratio of the synthesis mixture and A and B denoted $AlNO_3$ and $C_9H_{21}AlO_3$ as the aluminum source, respectively. The synthesis conditions of MCM-type materials are given in Table 5.1.

#### 5.1.1.4 Washing

The resultant solid was recovered by filtration, washed with deionized water to remove the excess template. But washing the material by adding water from the top was not succesful because the material was too concentrated and did not allow water to expose to the pores. In order to overcome this situation, material was taken into the beaker, suspended in 300 ml of water and stirred for 15 minutes. This was repeated until the pH of the residual water remained constant at a value of approximately 4.5 for acidic route

synthesis and 8.5 for basic route synthesis. After that, the synthesized material was dried at 40°C under vacuum until it dried completely.

Table 5.1 Synthesis conditions of MCM-type materials

| Sample ID | Al/Si (theoretical) | Si Source | Al Source | Synthesis Route |
|---|---|---|---|---|
| Al-1A | 1.0 | TEOS | $Al(NO_3)_3.9H_2O$ | Acidic |
| Al-0.5A | 0.5 | TEOS | $Al(NO_3)_3.9H_2O$ | Acidic |
| Al-0.1A | 0.1 | TEOS | $Al(NO_3)_3.9H_2O$ | Acidic |
| Al-0.03A | 0.03 | TEOS | $Al(NO_3)_3.9H_2O$ | Acidic |
| Al-1B | 1 | TEOS | $C_9H_{21}AlO_3$ | Acidic |
| Al-0.5B | 0.5 | TEOS | $C_9H_{21}AlO_3$ | Acidic |
| Al-0.1B | 0.1 | TEOS | $C_9H_{21}AlO_3$ | Acidic |
| Al-0.03B | 0.03 | TEOS | $C_9H_{21}AlO_3$ | Acidic |
| MCM-41 | 0 | Sodium silicate | - | Basic |
| MCM-41TA | 0 | TEOS | - | Acidic |
| MCM-41TB | 0 | TEOS | - | Basic |

#### 5.1.1.5 Calcination

Finally, in a tubular furnace, the synthesized materials prepared using aluminum nitrate were calcined at 540°C for 8 h in a flowing air medium with a flow rate of 220 ml/min to remove the excess organics but the materials synthesized using aluminum isopropoxide were calcined at 540°C for 1 h in flowing $N_2$ with a flow rate of 172 ml/min to prevent dealumination and then 7 h in a flowing air with a flow rate of 220 ml/min. During the calcination process, these samples were heated at a heating rate of 1ºC/min upto 540°C. At the end of the calcination, the furnace was switched off manually and the air continued to flow during the cooling process of the furnace to prevent gathering moisture. In addition to these catalysts, pure MCM-41 catalysts

were also calcined at 540°C for 8 h in a flowing air medium with a flow rate of 220 ml/min.

### 5.1.2 Synthesis of Mesoporous SBA-Type Catalysts

Mesoporous SBA-type catalysts were synthesized according to the procedure described by Fulvio *et al*.[82], Mirji *et al.*[111] and Kumaran *et al*.[112]. Aluminum containing SBA-type catalysts were synthesized by the modification of these procedures. Pure SBA-type catalyst was synthesized using direct hydrothermal synthesis route and the aluminum containing ones were synthesized by impregnation method. Synthesis of pure SBA-type catalyst was performed at different synthesis temperatures and durations. On the other hand, synthesis of aluminum containing SBA-type catalysts was performed at different Al/Si ratios using different aluminum sources. Synthesis conditions of pure SBA-type materials are given in Table 5.2.

Table 5.2 Synthesis conditions of pure SBA-type materials

| **Sample ID** | **Synthesis Temperature (°C)** | **Synthesis Time (hr.)** | **Synthesis Procedure (sec. *5.1.2.2.1*)** |
|---|---|---|---|
| S1 | 100 | 48 | 1 |
| S2 | 100 | 48 | 2 |
| S6 | 100 | 48 | 3 |
| S2-110 | 110 | 48 | 2 |
| S2-120 | 120 | 48 | 2 |
| S2-130 | 130 | 48 | 2 |
| S2-100(1) | 120 | 24 | 2 |
| S2-100(3) | 120 | 72 | 2 |
| S2-100(4) | 120 | 96 | 2 |

### 5.1.2.1 Reagents

Reagents used in the synthesis of mesoporous SBA-type catalysts are given below:

- Tri-block copolymer poly(ethylene oxide)-poly(propylene oxide)-poly(ethylene oxide), Sigma-Aldrich (Surfactant)
- Tetraethyl orthosilicate (TEOS), $C_8H_{20}O_4Si$, Merck (Silica source)
- Aluminum isopropoxide, $C_9H_{21}AlO_3$, Merck (Aluminium source)
- Aluminum sulphate, $Al_2(SO_4)_3.18H_2O$, Merck (Aluminium source)
- HCl, fuming, Merck
- Deionized water

### 5.1.2.2 Procedure

Main synthesis steps of the mesoporous SBA-type catalysts are similar to that of mesoporous MCM-type catalysts. These are the preparation of the synthesis solution, hydrothermal synthesis, filtering the solid product, drying and calcination. These steps are displayed in Figure 5.2.

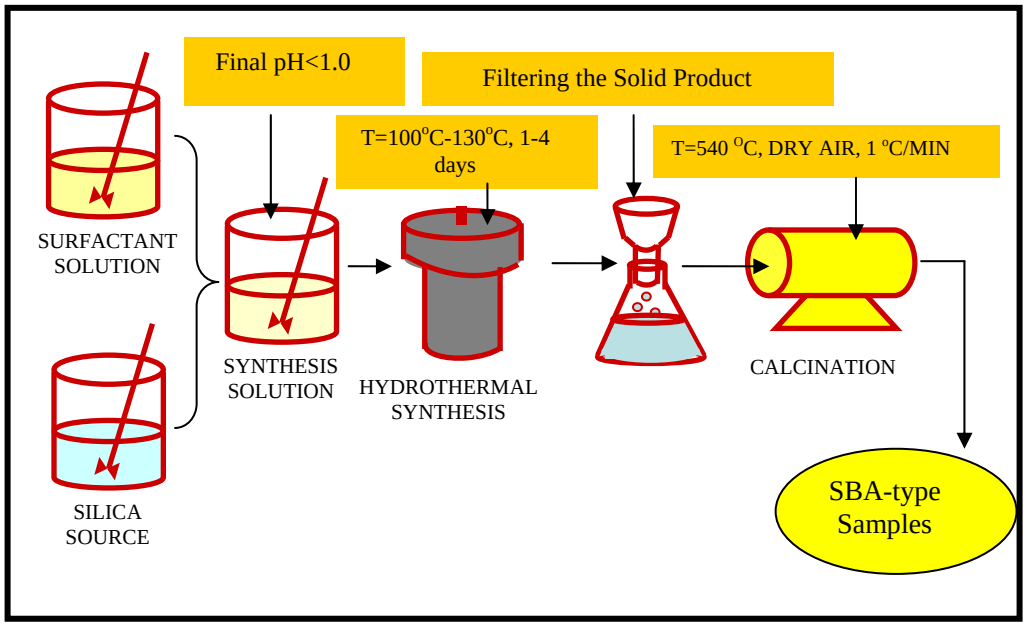


Figure 5.2 Main synthesis steps of SBA-type catalysts (adapted from [69])

Details of the synthesis are described below.

#### 5.1.2.2.1 Synthesis of pure SBA-15

Three different procedures were tried in the synthesis of pure SBA-15 and these procedures are given below.

***a) The First Synthesis Procedure***

4 g of triblock copolymer was dispersed in 30 g of deionized water and stirred for 4 h at 40°C and then 120 ml of 2M HCl solution was added and stirred for 2 h at the same temperature. Then, 8.54 g of TEOS was added to the solution under stirring at 350 rpm. The resulting gel was aged at 40°C for 24 h. After that, it was transferred into the teflon-lined stainless steel autoclave for the hydrothermal synthesis at 100°C for 48 h [111].

After hydrothermal synthesis step, the solid was filtered and washed with deionized water to remove excess HCl and dried at 80°C. Finally, the solid product was calcined at 540°C for 8 h in flowing air medium with a flow rate of 220 ml/min to decompose triblock copolymer and this sample was named as "*S1*".

***b) The Second Synthesis Procedure***

4 g of triblock copolymer was dispersed in 120 ml of 2M HCl and stirred for 4 h at 40°C. Then, 8.54 g of TEOS was added to the solution under stirring at 350 rpm. The resulting gel was aged at 40°C for 2 h. After that, it was transferred into the teflon-lined stainless steel autoclave for the hydrothermal synthesis at 100°C for 48 h [82].

After synthesis, the solid was filtered and washed with deionized water to remove excess HCl and dried at 80°C. Finally, the solid product was calcined at 540°C for 8 h in flowing air medium with a flow rate of 220 ml/min to decompose triblock copolymer and this sample was named as "*S2*".

### *c) The Third Synthesis Procedure*

In this procedure, 4 g of triblock copolymer was dispersed in 30 g of deionized water and stirred for 4 h at 40°C and then 120 ml of 2M HCl solution was added and stirred for 2 h at the same temperature. Then, 8.54 g of TEOS was added to the solution under stirring at 350 rpm. The resulting gel was aged at 40°C for 2 h. After that, it was transferred into the teflon-lined stainless steel autoclave for the hydrothermal synthesis at 100°C for 48 h [111, 112].

After synthesis, the solid was filtered and washed with deionized water to remove excess HCl and dried at 80°C. Finally, the solid product was calcined at 540°C for 8 h in flowing air medium with a flow rate of 220 ml/min to decompose triblock copolymer and this sample was named as "*S6*".

As a summary, in the second procedure, dispersion of triblock copolymer in deionized water was skipped. On the other hand, in the third procedure, aging time after adding TEOS into triblock copolymer solution was decreased from 24h to 2h.

#### 5.1.2.2.2 Synthesis of pure SBA-15 at different synthesis temperatures

*The second synthesis procedure* was followed and the hydrothermal synthesis was performed at different temperatures (100°C, 110°C, 120°C and 130°C) for 48 h. After synthesis, the solid products were filtered and washed with deionized water and dried at 80°C. Finally, the solid products were calcined at 540°C for 8 h in flowing air medium to decompose triblock copolymer and these samples were named as *"S2" ,S2-110*", *"S2-120",* and *"S2-130"*.

#### 5.1.2.2.3 Synthesis of pure SBA-15 at different synthesis durations

*The second synthesis procedure* was applied and the hydrothermal synthesis was performed at a temperature of 100°C for different synthesis durations such as 24h, 48h, 72 h, and 96 h.

After the synthesis step, the solid products were filtered and washed with deionized water to remove excess HCl and dried at 80°C. Finally, the solid products were calcined at 540°C for 8 h in flowing air medium with a flow rate of 220 ml/min to decompose triblock copolymer and these samples were named as *"S2-100(1)"*, *"S2"*, *"S2-100(3)"* and *"S2-100(4)"*.

#### 5.1.2.2.4 Synthesis of Al-SBA-15 using different aluminum sources

Aluminum containing SBA-15 catalysts were prepared by impregnation method. The main steps of this method are given in Figure 5.3. In this method, some amount of pure SBA-15, prepared according to the second synthesis procedure, was dried at 120°C under vacuum for 2 hours to remove its humidity. After that, 30 ml of deionized water was added and stirred for 2 hours. At the end of this 2 h, predetermined amount of aluminum source was added dropwise and the resulting solution was stirred for 24 h at room temperature. Then, the temperature was raised above room temperature to evaporate the solvent completely. After complete evaporation of the solvent, the solid product was dried at 120°C under vacuum for 24 h. The samples prepared from different aluminum sources were designated ALS-*x*A and ALS-*x*B, where *x* represents the Al/Si ratio of the synthesis mixture and A and B denotes $Al_2(SO_4)_3.18H_2O$ and $C_9H_{21}AlO_3$ as the aluminum source, respectively. Synthesis conditions of aluminum containing SBA-type materials are given in Table 5.3.

## 5.2 Characterization of the synthesized materials

Physical and structural properties of the synthesized materials were determined by X-Ray Diffraction (XRD), Nitrogen Physisorption, Scanning Electron Microscopy (SEM), Diffuse Reflectance Fourier Transform Infrared Spectroscopy (DRIFT) and $^{27}Al$ MAS NMR. Additionally, the commercial MCM-41 type mesostructured aluminosilicate catalyst, provided from Aldrich, was characterized with the same techniques.

Table 5.3 Synthesis conditions of Al-SBA-15 materials

| Sample ID | Al/Si(theoretical) | Al Source |
|---|---|---|
| ALS-1A | 1.0 | $Al_2(SO_4)_3.18H_2O$ |
| ALS-0.5A | 0.5 | $Al_2(SO_4)_3.18H_2O$ |
| ALS-0.2A | 0.2 | $Al_2(SO_4)_3.18H_2O$ |
| ALS-0.1A | 0.1 | $Al_2(SO_4)_3.18H_2O$ |
| ALS-0.03A | 0.03 | $Al_2(SO_4)_3.18H_2O$ |
| ALS-1B | 1 | $C_9H_{21}AlO_3$ |
| ALS-0.5B | 0.5 | $C_9H_{21}AlO_3$ |
| ALS-0.2B | 0.2 | $C_9H_{21}AlO_3$ |
| ALS-0.1B | 0.1 | $C_9H_{21}AlO_3$ |
| ALS-0.03B | 0.03 | $C_9H_{21}AlO_3$ |

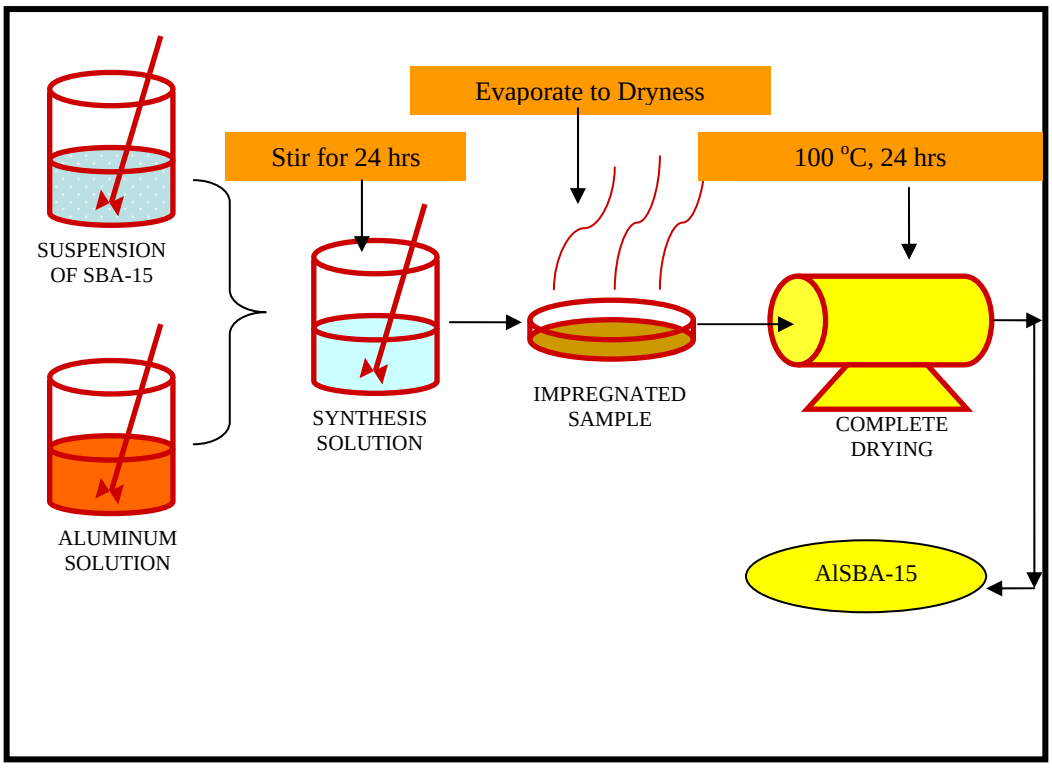


Figure 5.3 Main synthesis steps of aluminum containing SBA-15 catalysts (adapted from [69])

### 5.2.1 X-Ray Diffraction (XRD)

X-ray diffraction for the identification of the crystalline phases in the material was performed by Rigaku D/MAX2200 diffractometer with nickel filtered $CuK_\alpha$ radiation having a characteristic wavelength of 1.5406 Å in Metallurgical and Materials Engineering at METU. During the operation, the voltage and current were 40 kV and 40 mA, respectively. Diffraction patterns were recorded in the Bragg angle range of 1-10° for MCM-type catalysts and 0.8-10° for SBA-type catalysts with a scanning speed of 1° per minute.

### 5.2.2 Nitrogen Physisorption

#### 5.2.2.1 Single Point BET Surface Area Measurement

Single point BET surface area measurements were performed using Quantachrome Monosorb Surface Analyzer at Gazi University. This instrument gives rapid and accurate single point BET surface area measurement under the flow of He-$N_2$ gas mixture at the specified relative pressure of 0.30.

Before surface area measurement, every single synthesized catalyst was degassed at 140°C for 20 minutes to remove the moisture from the material under the flow of $N_2$-He gas mixture. Measurements were carried out at liquid nitrogen temperature of 77 K under the flow of gas mixture composed of 30% nitrogen and 70% helium. Before starting the measurements, the calibration of the analyzer was performed with 1 $cm^3$ of air at atmospheric pressure. The surface area value corresponding to nitrogen content of 1 $cm^3$ of air is 2.84 $m^2$. After degassing process had been completed, the sample was taken from the degassing unit and transferred to the analysis station for the measurement. To remove air entering to the system while placing the sample to the analysis station, the indicator of the analyzer was set to zero. The liquid nitrogen tank was lifted up, and the sample cell was introduced to the liquid nitrogen and then adsorption of the nitrogen to the sample began. After adsorption was completed, the liquid nitrogen tank got down and the desorption of nitrogen from the sample started at equilibrium pressure/saturation vapor pressure of the nitrogen ($P/P_o$) ratio of 0.30. The

surface area value was read from the instrument panel and then this value was divided by the weight of the sample to obtain the surface area of the material per gram.

#### 5.2.2.2 Nitrogen Adsorption/Desorption Isotherms

The average pore size, pore size distribution and pore volume of MCM-type materials were measured by Quantachrome Autosorb-1-C/MS in Central Laboratory at METU and the average pore diameter, pore size distribution and pore volume of SBA-type materials were measured by Micromeritics Gemini V1 apparatus in Chemical Engineering at METU. Materials were prepared for the analyses by drying overnight under vacuum condition at a temperature of 100°C. The analyses were carried out at a relative pressure range of 0.05 to 0.99 at liquid nitrogen temperature.

### 5.2.3 Scanning Electron Microscopy (SEM)

Scanning electron microscopy analyses were performed using JEOL 6400 and QUANTA 400F Field Emission SEM apparatus, operating at 20 and 30 kV, respectively, to determine the morphology of the synthesized materials. Elemental compositions of the synthesized materials were measured using EDS analysis coupled with JEOL 6400 apparatus at METU. All the samples were coated with gold for the analyses. The reason for coating is to prevent the accumulation of static electric charge on the specimen during electron irradiation and another reason for coating is to improve contrast and resolution of SEM images [113].

### 5.2.4 Nuclear Magnetic Resonance (NMR)

$^{27}$Al MAS NMR is employed to distinguish between tetrahedrally and octahedrally coordinated aluminum in the framework. The spectra were recorded at room temperature on a BRUKER Avance 300 Spectrometer with a resonance frequency of 78.1 MHz. The magnetic field, the spin rate of the samples and the number of scans were 7.05 T, 5 kHz and 12000,

respectively. The pulse length was adjusted to 3.86 μs with a relaxation delay of 1 s. External Al-$(H_2O)_6^{3+}$ was used as a reference.

### 5.2.5 Diffuse Reflectance FT-IR (DRIFT) Analysis

In order to get information about the Brönsted and Lewis acid sites of the synthesized materials, diffuse reflectance FT-IR (DRIFTS) analyses of the samples were carried out using a Perkin Elmer Spectrum1 FT-IR instrument installed in Chemical Engineering at METU. Before taking DRIFT spectrum, the samples were dried at 110°C overnight under vacuum. After that, 1 ml of pyridine was added dropwise to 3.5 mg of sample and left under hood for drying for 2 hours. At the end of this 2 hours, the pyridine adsorbed samples were taken and mixed with potassium bromide (KBr) with a weight ratio of 1/20. Also, pyridine free samples were mixed with KBr with the same weight ratio. Finally, DRIFT spectra of both pure (pyridine free) and pyridine adsorbed samples were recorded at room temperature and by placing sample (~75 mg) into the sample pan of the DRIFTS cell. FT-IR spectra of the samples were acquired at a wave number range of 400-4000 $cm^{-1}$ with the resolution of 4 $cm^{-1}$. At the end of the analysis, the acid sites of the synthesized materials were found from the difference between pyridine adsorbed and pyridine free spectra.

### 5.2.6 Transmission Electron Microscopy (TEM)

TEM images of the synthesized materials were obtained at the Electron Microscopy Center of the Faculty of Biology and Geology of Babes-Bolyai University in Romania. Before taking TEM images, the samples were infiltrated with Epon resin and incubated for 3 days at 70°C for polymerization. Sections of 70-80 nm thickness obtained on diatome diamond knife from a Leica Ultracut UC6 ultramicrotome were collected on 300 mesh Cu grids with collodium film. The images were taken on JEOL Model JEM 1010 transmission electron microscope equipped with SIS MegaView CCD camera.

## 5.3 Thermogravimetric Analyses (TGA)

The performance of the synthesized catalysts and the commercial MCM-41 type mesostructured aluminosilicate catalyst in the polypropylene cracking reaction was examined using Perkin-Elmer Thermal Analyzer in Central Laboratory at METU. The polypropylene used in this work was provided from Aldrich, and had the following features: isotactic, $M_w$:250,000, $\rho$:0.9 g/ml, *melt index*: 12g/10min (230°C/2.16 kg), *mp*:160-165°C, $d_p$*(avg.)*: 0.4 mm in granular form. The experiments were performed under nitrogen in the temperature range of 35-550°C with a constant heating rate of 5°C/min. In these experiments, 15 mg of sample was used with a catalyst/polymer ratio of 1/2.

## 5.4 Polymer Degradation Reaction System

The synthesized catalysts were tested in polypropylene degradation reaction system. The schematic diagram of the experimental system is given in Figure 5.4. The glass reactor was heated up to the desired reaction temperature by the help of an electric furnace (Protherm PTF 12/105/700) and the reactor temperature was measured by a thermocouple connected to digital thermometer readout. Connection line between the reactor and the condenser was heated by heating tape in order to prevent any condensation. $N_2$ gas (Air Products) with high purity was used as the carrier gas in the system to avoid the presence of oxygen. The flow rate of the carrier gas was adjusted by the help of a rotameter (Cole-Parmer). Porous glass was placed inside the glass reactor to provide the dispersion of the gas and to prevent backflow of the polymer melt. The bottom part of the reactor was designed in spiral form and filled with glass particles in order to increase the surface area to provide the carrier gas to reach the desired reaction temperature before entering the reaction part. The reactor was 109 cm in length (total) and ½ inches in diameter. The length of the reaction and spiral parts are 10 cm and 76 cm, respectively.

The vapors coming out from the reactor during the process were sent to the condenser, designed in spiral form, and the non-volatile products were

collected inside the glass vessels surrounded with water cooling jackets. The non-condensable gas products were sent to gas chromatography (Varian, CP-3800) equipped with a packed column, Porapak Q (6'x1/8", Discovery Sciences) for online analysis. Connection line between the reactor and the condenser was stainless steel tubing with ¼" diameter; the others were copper tubing with ¼" diameter. The non-volatile products and residue remaining inside the reactor were also analysed in GC (Varian, CP-3800) equipped with a capillary column HP-5 (30mx0.320mmx0.25μm, J&W Scientific).

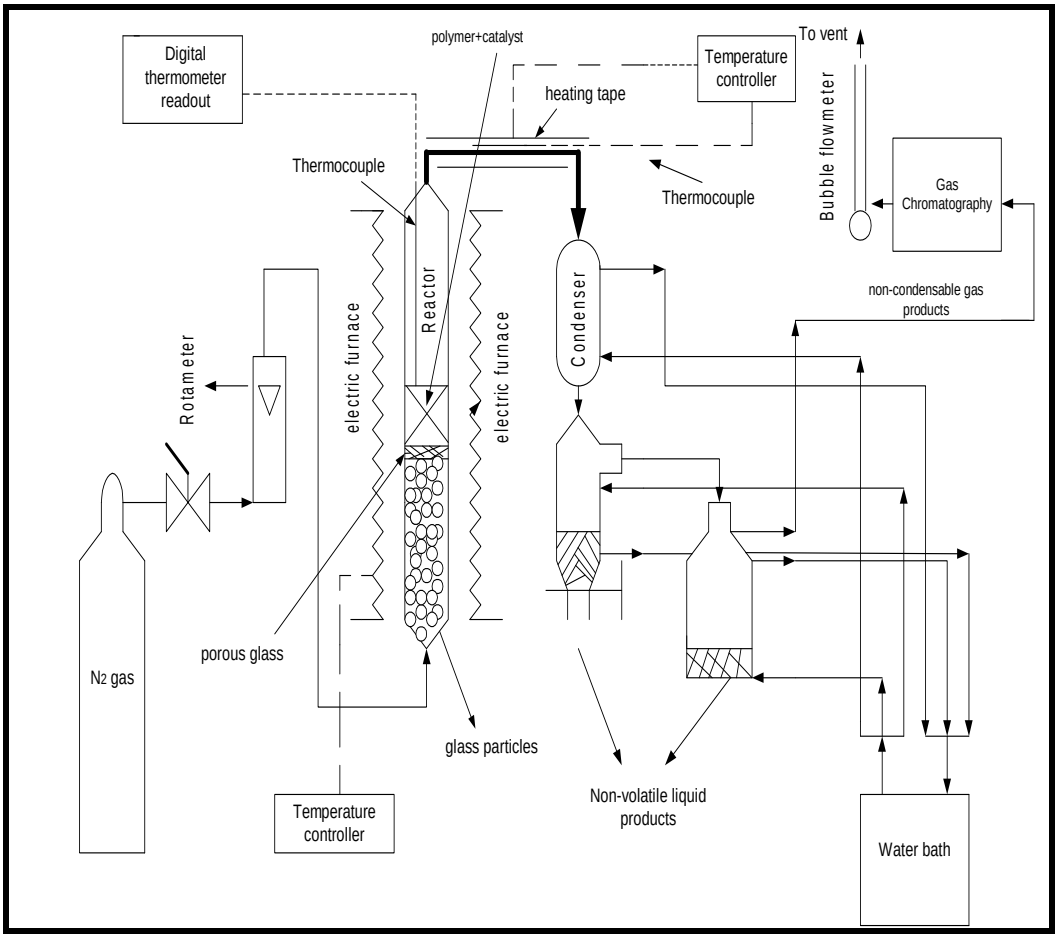


Figure 5.4 Schematic Diagram of the Experimental Apparatus

## 5.5 Experimental Procedure

The non-catalytic thermal degradation reactions were carried out in a glass semibatch reactor (Figure 5.4), at atmospheric pressure under nitrogen (carrier gas) flow. 1 g of PP was loaded to the reactor before each run and volumetric flow rate of carrier gas was set to 60 ml/min. The reaction was carried out under isothermal conditions and the furnace was heated to the desired temperature with a heating rate of 5°C/min. Reaction times and temperatures are given in Table 5.4.

Table 5.4 Experimental conditions used in non-catalytic thermal degradation reaction

| Furnace Temp. (°C) | Reaction Temp. (°C) | Reaction Time(min.) |
|---|---|---|
| 505 | 400 | 30 |
| 505 | 400 | 45 |
| 505 | 400 | 60 |
| 520 | 410 | 15 |
| 520 | 410 | 30 |
| 535 | 425 | 15 |
| 535 | 425 | 30 |

When the polymer started to melt (~165°C), the vapors coming out from the reactor began to be sent to gas chromatography equipped with Porapak Q packed column (6'x1/8") for on-line analysis. The analysis conditions of GC are given in Table 5.5. *Varian Star Chromatography Workstation Version 6.2* program was used for the data analysis. After the reaction time had completed, the furnace started to cool down to 30°C. During this cooling period, the carrier gas continued to flow in order to prevent the backflow of polymer melt through porous glass. After the cooling process, the reactor was taken from the furnace to clean up the solid residue, if any. Finally, the liquid

product collected at the end of the reaction and solid residue remained inside the reactor was weighed out using an analytical balance (Sartorius BL 210S).

Table 5.5 GC analysis conditions for gaseous products

| | |
|---|---|
| **Oven Temperature:** | 80°C (isothermal) |
| **Injection Temperature:** | 110°C |
| **Detector Type and Temperature:** | TCD, 120°C |
| **Column Pressure:** | 30 psi |
| **Duration of Analysis:** | 35 min. |
| **Carrier Gas:** | He |
| **Flow Rate of Carrier Gas:** | 30 ml/min |

After performing non-catalytic thermal degradation reactions, the catalytic thermal degradation reactions were carried out at atmospheric pressure under nitrogen flow (60 ml/min) in the same semi-batch reactor, mentioned in section 5.4. PP and catalyst mixture was loaded to the reactor before each run. In this part, again, 1 g of PP and 0.5 g of catalyst determined according to the thermogravimetric analysis results were used. Detailed information about these thermal analyses will be given in section 6.3.1 in Chapter 6. Catalysts used in the degradation reaction and reaction temperatures are given in Table 5.6. The reaction time was taken as 30 minutes in all catalytic reactions. The quantitative and qualitative chemical analyses of liquid products were performed using gas chromatography equipped with HP-5 capillary column (30mx0.320mmx0.25μm). The analysis conditions are given in Table 5.7. Again, *Varian Star Chromatography Workstation Version 6.2* program was used for the data analysis. After the reaction time had completed, the furnace started to cool down to 30°C. During this cooling period, the carrier gas continued to flow in order to prevent the backflow of polymer melt+catalyst through porous glass. After the cooling process, the reactor was taken from the furnace to clean up the polymer, if any and used

catalyst. Finally, the solid residue, the used catalyst and the liquid product collected at the end of the reaction were weighed out using an analytical balance (Sartorius BL 210S).

Table 5.6 Experimental conditions used in catalytic thermal degradation reaction

| Catalyst | Furnace Temp. (°C) | Reaction Temp. (°C) |
|---|---|---|
| Al-0.03A | 405 | 305 |
| Al-1A | 370 | 275 |
| Al-0.03B | 465 | 360 |
| Al-1B | 385 | 285 |
| ALS-0.1A | 430 | 330 |
| ALS-0.2A | 415 | 315 |
| ALS-0.1B | 400 | 300 |
| ALS-1B | 455 | 345 |

Table 5.7 GC analysis conditions for liquid products

| | |
|---|---|
| **Oven Temperature:** | 40°C (10 min hold) to 150°C at 5°C/min (15 min hold) then to 200°C at 1°C/min (70 min hold) |
| **Injection Temperature:** | 210°C |
| **Injection Amount:** | 0.1 µL |
| **Detector Type and Temperature:** | FID, 225°C |
| **Column Pressure:** | 5 psi |
| **Duration of Analysis:** | 167 min. |
| **Carrier Gas:** | He at 1.5 ml/min |
| **Split Ratio:** | 100:1 |

# CHAPTER 6

# RESULTS AND DISCUSSION

In this study, the catalytic activity of ordered mesoporous materials*, MCM-type* and *SBA-type*, in polypropylene degradation reaction was investigated. For this purpose, mesoporous *MCM* and *SBA* type catalysts were synthesized and characterized, as described in the experimental part. After that, the catalytic activity of these catalysts were investigated in polypropylene degradation reaction. In addition to these catalytic thermal degradation reactions, non-catalytic thermal degradation (blank) reactions were carried out to make a reasonable comparison.

## 6.1 Characterization of Mesoporous MCM-type Catalysts

The physical and structural properties of synthesized *MCM-type* catalysts were determined by X-Ray Diffraction, Nitrogen Physisorption, Scanning Electron Microscopy and $^{27}$Al MAS NMR techniques.

### 6.1.1 X-Ray Diffraction (XRD)

The XRD patterns of pure *MCM-41* and aluminum containing *MCM-type* catalysts prepared in this work are shown in Figures 6.1 and 6.2, respectively. For these materials, the diffraction patterns only have reflection peaks in the low Bragg angle range (less than 10). For pure *MCM-41* prepared using sodium silicate (Figure 6.1a), the XRD pattern showed the sharp characteristic peaks of this material at $2\theta$ values of 2.31, 3.91, 4.50 and 5.94º. On the

other hand, for pure *MCM-41* prepared using TEOS and following basic route (Figure 6.1b), the intensity of the peaks decreased and the 2θ position for the major peak shifted to a higher value. The major peak was at a 2θ value of 2.61° and the second peak was at 3.01°. The third and fourth peaks were observed at 4.71° and 4.91°, respectively. For the sample prepared using TEOS and following acidic route, the $d_{(100)}$ peak was observed at a 2θ value of 2.05° and it was wider (Figure 6.1b) than the corresponding peak of pure *MCM-41* following basic route (Figure 6.1a). This less intense main peaks shifted to a lower value also showed a deformation in the hexagonally ordered structure of the material. Similar results were also reported in previous studies even for pure *MCM-41* synthesized following the acidic route [93].

However, for the mesoporous aluminum containing *MCM-type* materials synthesized following the acidic procedure, the characteristic $d_{(100)}$ peak observed at a 2θ value of about 2.2º, was wider (Figure 6.2) than the corresponding peak of *MCM-41TB* (Figure 6.1b). This is an indication that the pore size distributions of the synthesized mesoporous aluminum containing *MCM-type* materials were not as narrow as pure *MCM-41* following basic route. These broader and less intense main peaks indicated a distortion of the long range ordering of the structure and/or badly built hexagonal arrays. This might be due to the structural irregularity caused by aluminum that was incorporated into the structure of the material. The second, third and fourth characteristic XRD peaks of *MCM-41* at higher 2θ values could not be observed for these samples, therefore the structure of these materials can not be considered as *MCM-41*. Additionally, in the case of using aluminum nitrate as the aluminum source, increasing aluminum loading from 3% to 50% causes a decrease in the intensity of $d_{(100)}$ peak. Same conclusion can be done for the catalysts contanining aluminum isopropoxide as the aluminum source.

The XRD pattern of commercial *MCM-41* type mesostructured aluminosilicate catalyst (PA) is given in Figure 6.3. The material gave poorer quality XRD pattern than purely siliceous *MCM-41*. The intensity of the peaks decreases and the 2θ positions shifted to a lower value. The major peak occurs at a 2θ value of 2.29° and the second peak occurs at 3.9°. The third and fourth peaks

were distorted. This may be due to the structural irregularity caused by aluminum that was incorporated into the structure of the material.

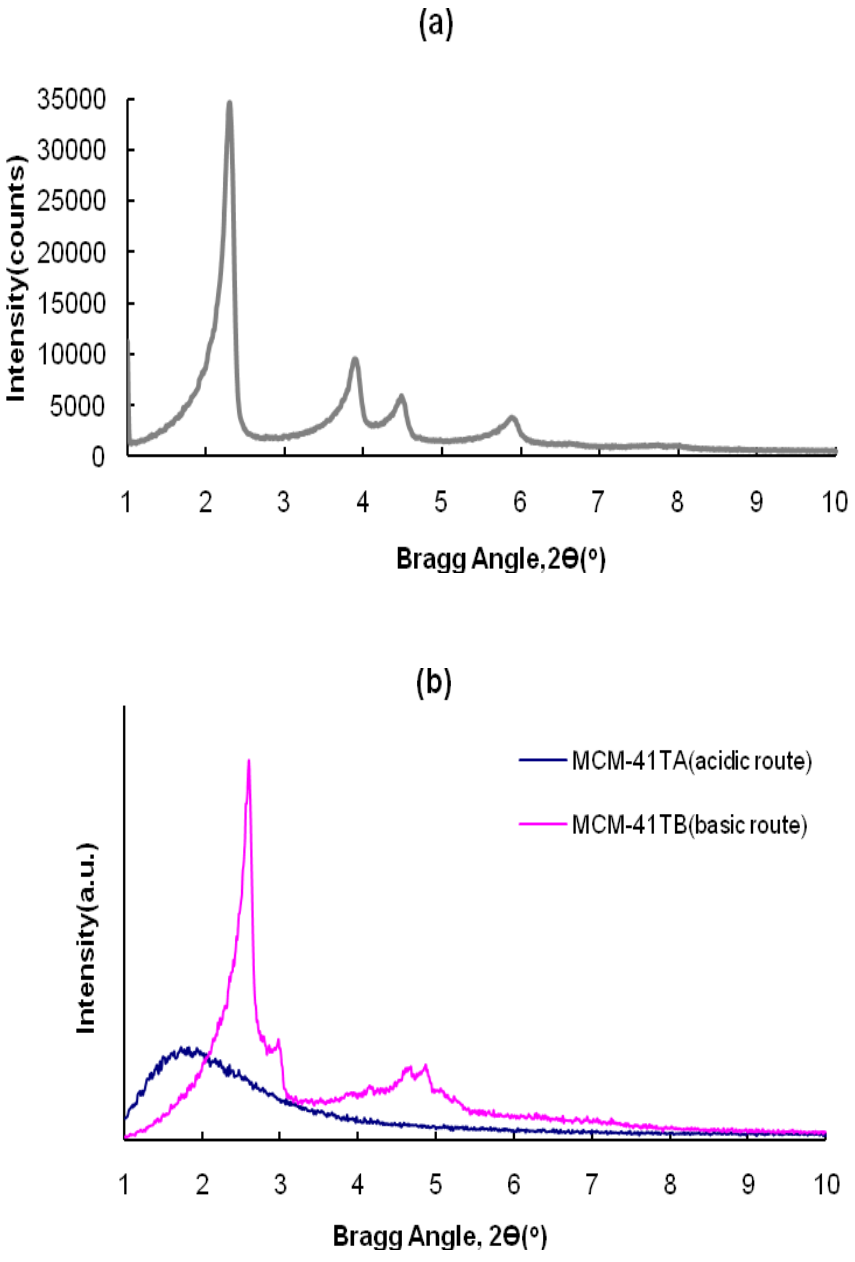


Figure 6.1 XRD patterns of pure MCM-41 synthesized using different silica sources: (a) Sodium silicate (basic route), (b) TEOS, following acidic and basic route

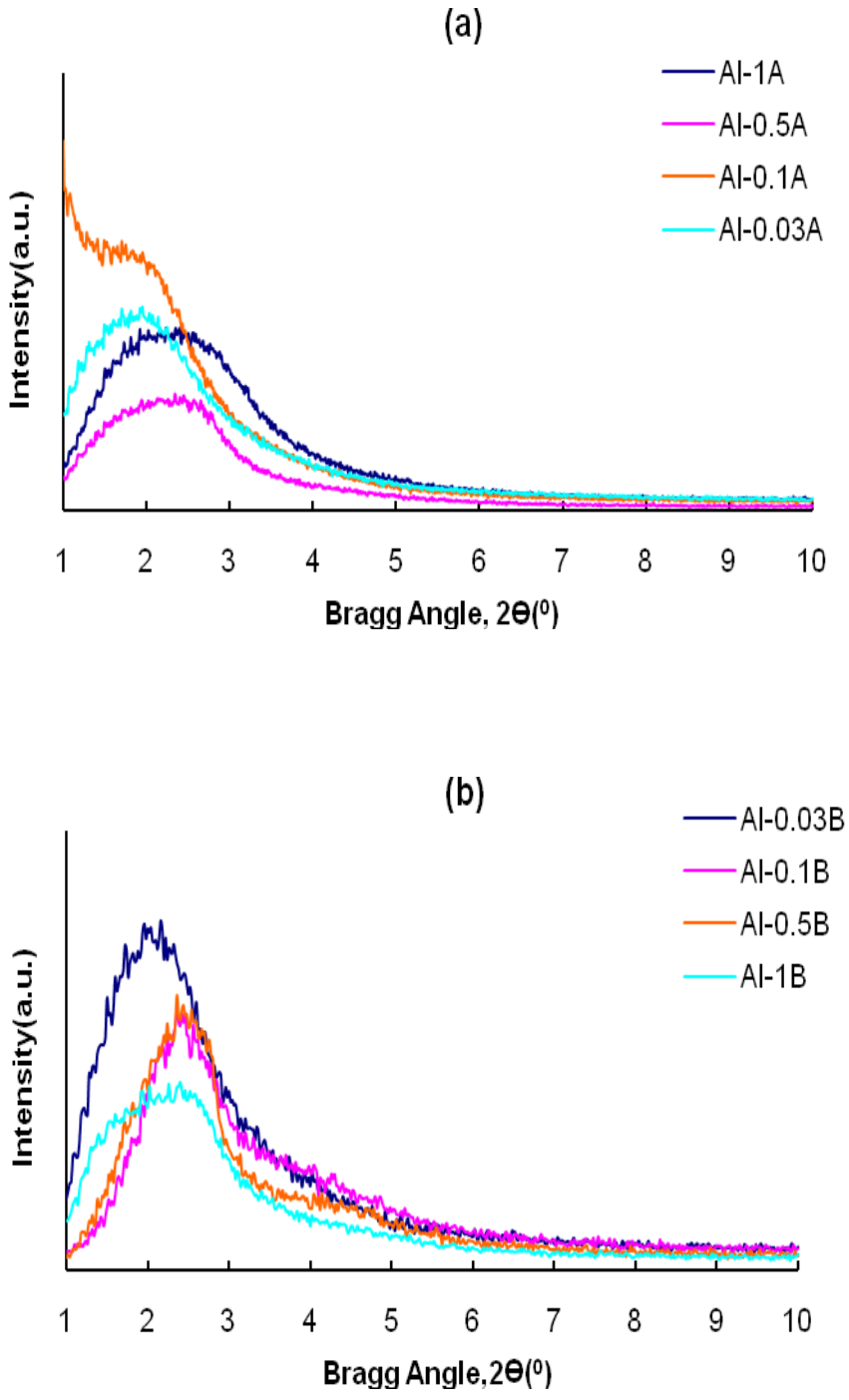


Figure 6.2 XRD patterns of aluminum containing MCM-type catalysts synthesized using different aluminum sources: (a) $Al(NO_3)_3.9H_2O$ and (b) $C_9H_{21}AlO_3$

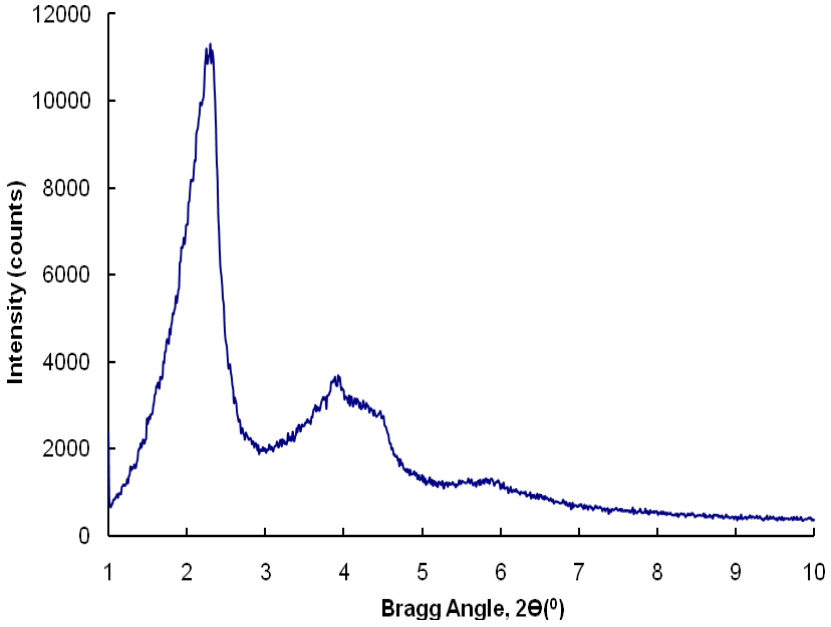


Figure 6.3 XRD pattern of commercial MCM-41 type mesostructured aluminosilicate catalyst, ***PA*** (Al/Si: 0.03)

### 6.1.2 Nitrogen Physisorption

The nitrogen sorption isotherms of synthesized materials were used to obtain information about their mesoporosity. The physical properties of the synthesized materials are given in Table 6.1 and the pore size distributions of synthesized pure and aluminum contanining *MCM-type* catalysts which were calculated by BJH model from desorption branch are given in Figures 6.4 and 6.5, respectively.

The results (Table 6.1) showed that the samples, other than *Al-1B*, had high surface area and these surface area values could be taken as a proof for the mesoporosity of these samples since for mesoporous materials surface area is generally between 600 and 1200 $m^2/g$ [69].

In other words, incorporation of Al into these *MCM-41* like mesoporous materials did not cause any significant decrease in surface area.

Table 6.1 The physical properties of the synthesized MCM-type catalysts

| Sample ID | Surface Area BET ($m^2/g$) | Pore Volume BJH Des., (cc/g) | Average Pore Diameter "*dp*" (nm) (4V/A by BET) | BJH Des. Av. Pore Diameter (nm) | Microporosity (%) |
|---|---|---|---|---|---|
| Al-1A | 819 | 0.70 | 2.6 | 2.8 | 47.0 |
| Al-0.5A | 1023 | 0.76 | 3.3 | 2.7 | 33.4 |
| Al-0.1A | 912 | 0.98 | 4.5 | 3.4 | 19.1 |
| Al-0.03A | 1001 | 1.39 | 6.6 | 4.4 | 18.9 |
| Al-1B | 520 | 0.60 | 7.4 | 5.5 | 25.7 |
| Al-0.5B | 645 | 0.90 | 5.9 | 5.0 | 24.8 |
| Al-0.1B | 977 | 1.08 | 4.2 | 3.2 | 28.1 |
| Al-0.03B | 995 | 1.14 | 5.1 | 3.7 | 24.2 |
| MCM-41TB | 1261 | 1.62 | 3.0 | 2.7 | 33.3 |
| MCM-41TA | 658 | 0.91 | 4.9 | 4.9 | 24.3 |
| MCM-41 | 889 | 1.29 | 2.9 | 2.5 | 32.9 |
| PA | 897 | 0.96 | 3.9 | 3.0 | 32.1 |

For pure *MCM-41* prepared using sodium silicate, the surface area was found to be as 889 $m^2/g$. On the other hand, for pure *MCM-41* prepared using TEOS and following basic and acidic route, the surface areas were found as 1261 $m^2/g$ and 658 $m^2/g$, respectively (Table 6.1). These results showed that the nature of the silica source used in the synthesis and route of the synthesis might have a significant effect on the physical properties of mesoporous materials.

Pure MCM-41 catalysts, synthesized using different silica sources, showed unimodal pore size distributions (Figure 6.4). The pore size distribution of *MCM-41*, prepared using sodium silicate, was narrow. On the other hand, the pore size distribution of *MCM-41TA*, prepared using TEOS and following acidic route was broader than the pore size distribution of *MCM-41TB* (basic route). The pore diameter of *MCM-41TB*, prepared using TEOS and following basic route, was 3 nm and this value increased to 4.9 nm when the same materials was prepared according to acidic route (*MCM*-41TA). Additionally, the pore

volume of pure MCM-41 decreased when acidic synthesis route was followed (Figure 6.4b). As a conclusion, the route (acidic/basic) followed during synthesis step might have significant effect on both pore diameter and volume.

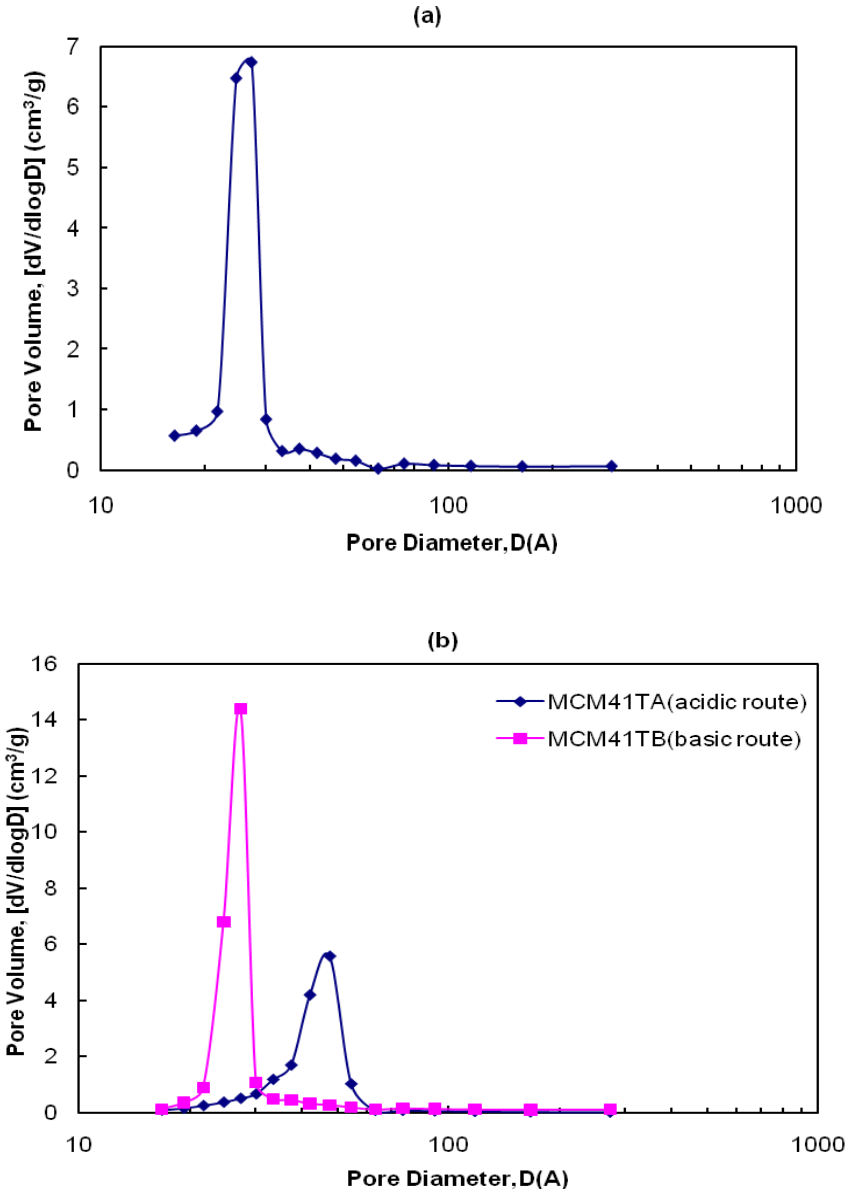


Figure 6.4 Pore size distributions of pure MCM-41 synthesized using different silica sources: (a) Sodium silicate (basic route), (b) TEOS, following acidic and basic route

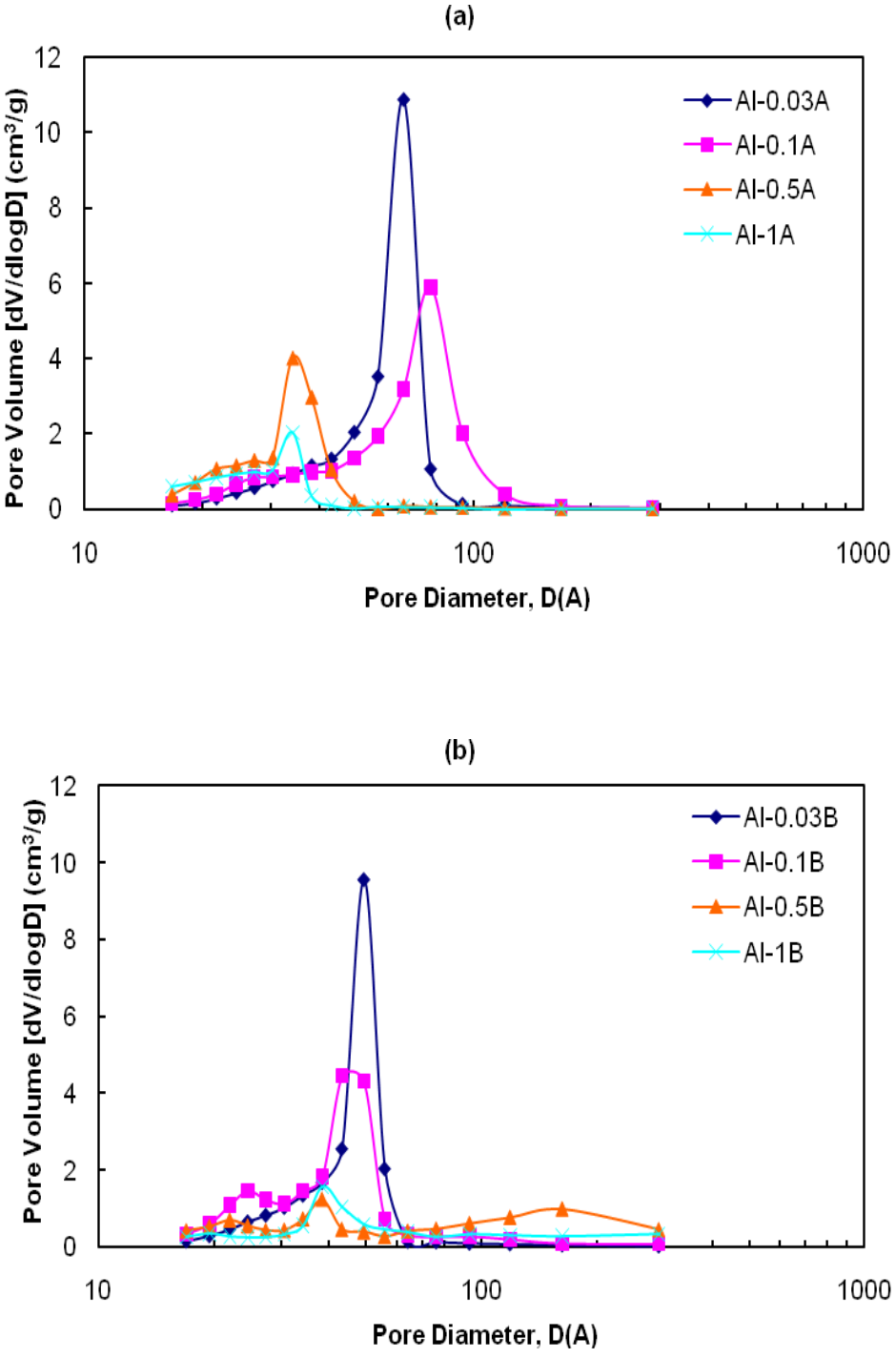


Figure 6.5 Pore size distributions of aluminum contanining MCM-type catalysts synthesized using different aluminum sources: (a) $Al(NO_3)_3.9H_2O$ and (b) $C_9H_{21}AlO_3$

The pore size distribution of catalysts synthesized using aluminum nitrate as aluminum source was much wider than that of catalyst synthesized using aluminum isopropoxide. *Al-0.1B* and *Al-0.5B* catalysts showed bimodal pore size distribution. In catalyst *Al-0.5B*, both mesoporous and macroporous structure might occur since it had low surface area and showed bimodal pore size distribution. Additionally, this catalyst contained %25 microporosity. On the other hand, in catalyst *Al-0.1B,* both microporous and mesoporous structure might occur since it had high surface area and showed bimodal pore size distribution. Additionally, the microporosity increased from 25% to 28% with a decrease in Al/Si ratio in the case of using aluminum isopropoxide as the aluminum source in the synthesis of MCM-type catalysts.

Finally, the pore size distribution of commercial *MCM-41* type mesostructured aluminosilicate catalyst (PA) is given in Figure 6.6. The material showed unimodal, narrow pore size distribution with an average pore diameter of 3.0 nm.

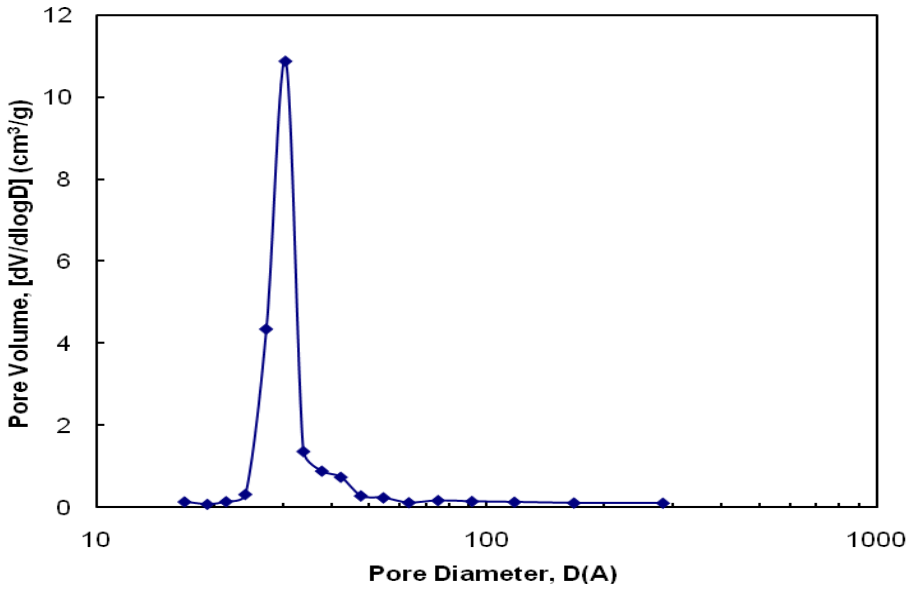


Figure 6.6 Pore size distribution of commercial MCM-41 type mesostructured aluminosilicate catalyst, ***PA*** (Al/Si: 0.03)

Additionally, both the average pore diameter values (Table 6.1) and the pore size distribution curves (Figures 6.4, 6.5, 6.6) support the mesoporosity of the materials since for mesoporous materials, the pore diameter lies between 2 and 50 nm [69].

The $N_2$ adsorption-desorption isotherms of synthesized pure and aluminum contanining *MCM-type* catalysts are given in Figures 6.7 and 6.8, respectively. Pure MCM-41 catalysts synthesized using different silica sources and following acidic and basic route exhibited *Type IV* isotherms according to the IUPAC classification. *Type IV* isotherms belong to microporous solids containing mesopores in their structure and in IUPAC classification, these types of isotherms are typical for mesoporous materials. A sharp increase in the adsorbed $N_2$ volume was observed at a narrow relative pressure range of 0.25-0.35 in both materials (Figure 6.7). This sharpness of the adsorption-desorption branches indicates a narrow pore size distribution (Figure 6.4). In other words, these materials have uniform mesopore size. This sharp increase in the adsorbed $N_2$ volume is due to capillary condensation within mesopores [106]. The catalyst *MCM*-41TA, prepared using TEOS and following acidic route, also showed the *Type IV* isotherm with hysteresis loop. According to IUPAC classification, Type H2 hysteresis was observed. It results from the differences between the adsorption and desorption mechanisms. In other words, materials are often disordered and the distribution of pore size and shape is not well defined. Additionally, the hysteresis loop is broad for *MCM-41TA* (Figure 6.7b) and the desorption branch is much steeper than the adsorption branch. This steep desorption branch indicates interconnectivity in the porous network of the material. Nitrogen condensation occurs at relative pressures much lower for the MCM-41 following basic route (*MCM-41TB*) than for the MCM-41 following acidic route (*MCM-41TA*). This indicates that the materials synthesized using acidic route induces a mesopore enlargement (Table 6.2). Finally, the pure MCM materials contained considerable amounts of micropores, as given in Table 6.2. From these results, it can be concluded that using different silica source and following the same route (*MCM-41* & *MCM-41TB*) did not change the amount of micropores but when the synthesis route was changed (*MCM-41TA*), there was a signicant decrease in the amount of micropores (Table 6.2).

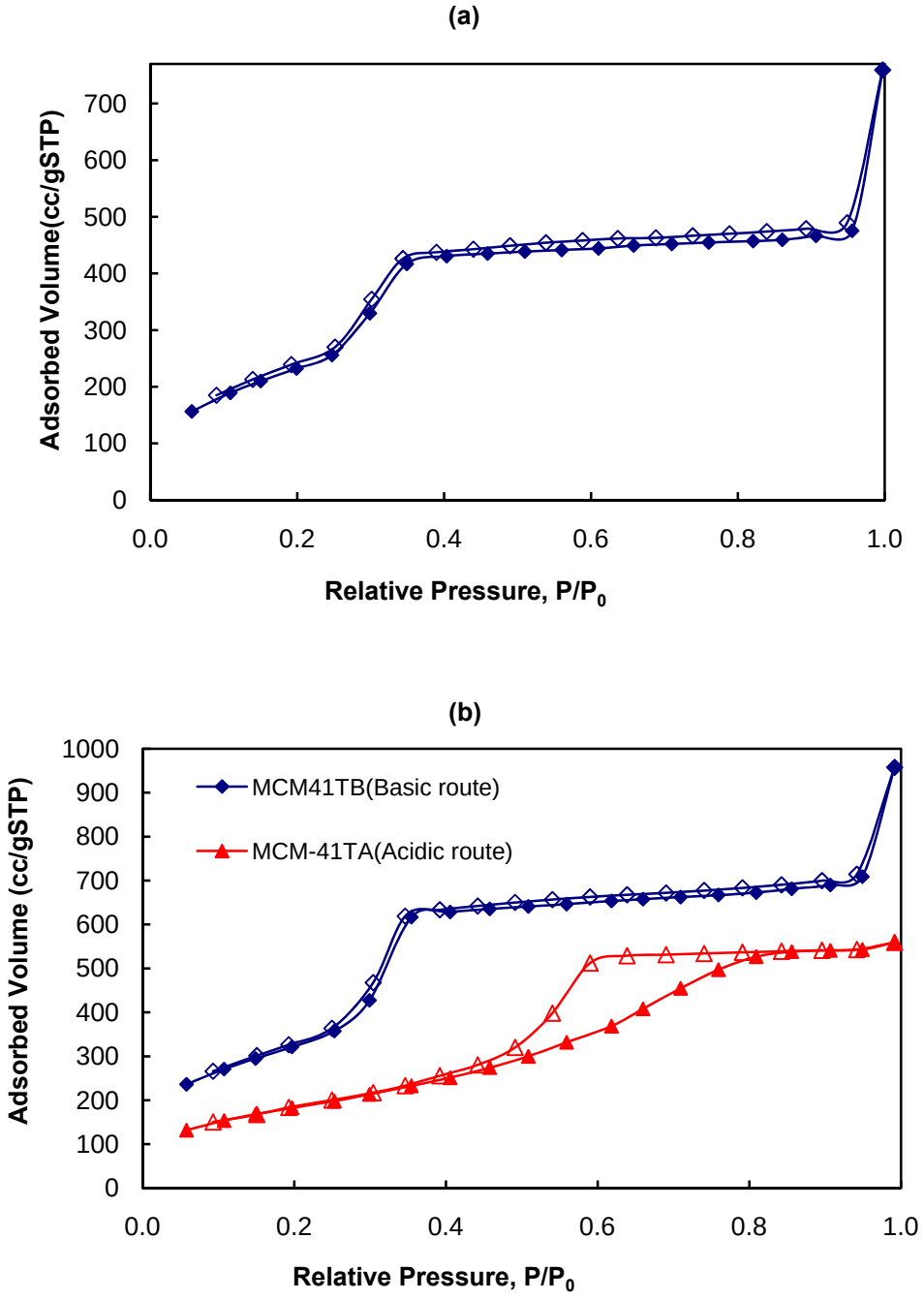


Figure 6.7 $N_2$ adsorption-desorption isotherms of pure MCM-41 synthesized using different silica sources; (a) Sodium silicate (basic route), (b) TEOS, following acidic and basic route
(solid boxes: adsorption branch; blank boxes: desorption branch)

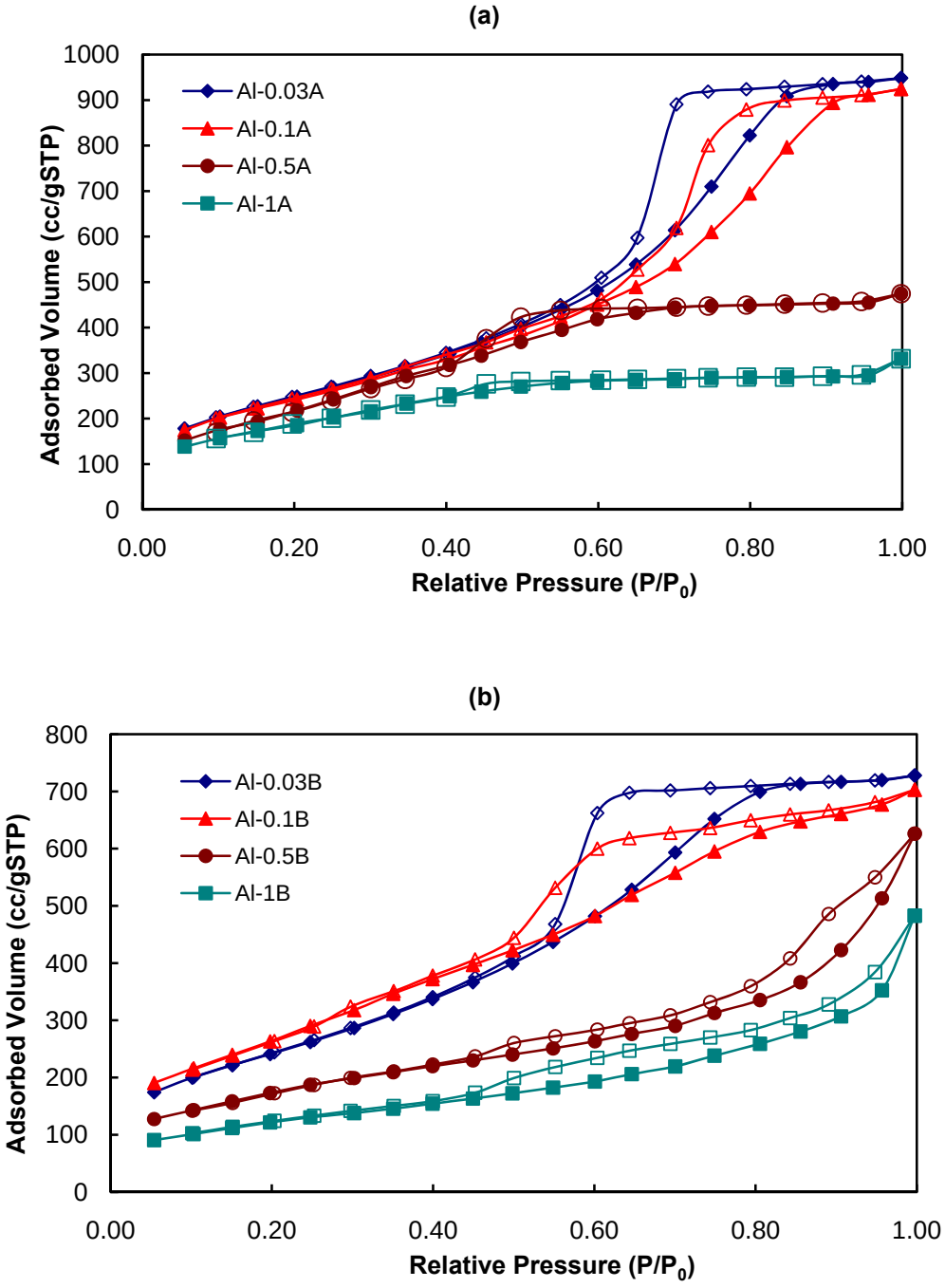


Figure 6.8 $N_2$ adsorption-desorption isotherms of aluminum containing MCM-type catalysts synthesized using different aluminum sources: (a)$Al(NO_3)_3.9H_2O$ and (b) $C_9H_{21}AlO_3$
(solid boxes: adsorption branch; blank boxes: desorption branch)

The aluminum containing *MCM-type* catalysts also exhibited *Type IV* isotherms. Nitrogen condensation occurred at relative pressures much higher for the aluminum containing materials synthesized using aluminum isopropoxide as aluminum source than for the MCM-41 following acidic route (*MCM-41TA*). In other words, loading of aluminum into MCM-41 made a mesopore enlargement. However, this enlargement was not observed for the materials synthesized using aluminum nitrate as aluminum source. Additionally, in these catalysts, hysteresis has been observed at a relative pressure greater than 0.5. Capillary condensation of nitrogen in the mesopores of the structure may cause this hysteresis formation. The hysteresis opening and the amount of nitrogen adsorbed decreased as the aluminum loading to the catalyst structure was increased (Figure 6.8). This may be due to the filling of MCM-41 pores by aluminum species. Additionally, when aluminum isopropoxide was used as the aluminum source and when the level of aluminum loading was kept at higher values (>50%), Type H3 hysteresis was observed and this type of hysteresis is specific for non-rigid aggregates of plate-like particles giving rise to slit-shaped pores. Finally, the aluminum containing MCM-type materials contained considerable amount of micropores and the amount of these micropores decreased significantly when aluminum loading increased in the materials synthesized using aluminum nitrate as aluminum source. On the other hand, when aluminum isopropoxide was used as the aluminum source, there was not a significant change in the amount of micropores. These results were consistent with the pore size distribution results given in Figure 6.5. As a conclusion, the pore size distribution and shape of the aluminum containing MCM-type catalysts were not well defined and these results were consistent with the XRD results (Figure 6.2).

The $N_2$ adsorption-desorption isotherm of commercial *MCM-41* type mesostructured aluminosilicate catalyst (PA) is given in Figure 6.9. This catalyst also showed the typical Type IV isotherm, as described by IUPAC classification. A sharp increase of the adsorbed $N_2$ volume occurred for a relative pressure larger than 0.35. This is the indication of narrow pore size distribution. This catalsyst also contained considerable amount of micropores, as given in Table 6.1.

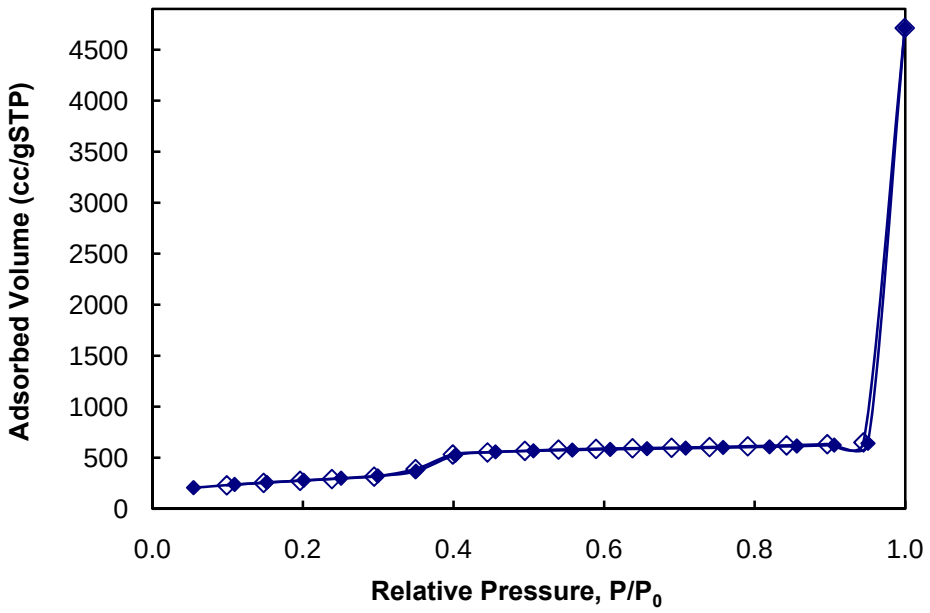


Figure 6.9 $N_2$ adsorption-desorption isotherm of commercial MCM-41 type mesostructured aluminosilicate catalyst, ***PA*** (Al/Si: 0.03)
(solid boxes: adsorption branch; blank boxes: desorption branch)

Finally, by using $N_2$ physisorption and X-ray diffraction analysis, pore wall thickness of the samples were calculated according to the relation given in section 3.6.1 (Eqn. 3.2). A sample calculation was given in Appendix A. Pore wall characteristics of synthesized catalysts are given in Table 6.2. The results showed that MCM-type catalysts had very thin pore walls and this thickness increase as the aluminum loading increased when aluminum nitrate was used as the aluminum source. On the other hand, when aluminum isopropoxide was used as the aluminum source, the wall thickness decreased as the aluminum loading was increased (Table 6.2). As a summary, the nature of aluminum source used in the synthesis of aluminum containing MCM-type materials affected the wall thickness of MCM-41 material.

Table 6.2 Pore wall properties of the synthesized MCM-type catalysts

| Sample ID | $d_{(100)}$ (nm) | Lattice Parameter, a (nm) | BJH Pore Diameter, $d_{pore}$ (nm) | Pore Wall Thickness, $\delta$ (nm) |
|---|---|---|---|---|
| Al-1A | 3.7 | 4.3 | 2.8 | 1.5 |
| Al-0.5A | 3.8 | 4.4 | 2.7 | 1.7 |
| Al-0.1A | 4.2 | 4.8 | 3.4 | 1.4 |
| Al-0.03A | 4.6 | 5.3 | 4.4 | 0.9 |
| Al-1B | 3.7 | 4.3 | 3.8 | 0.5 |
| Al-0.5B | 3.6 | 4.2 | 3.8 | 0.4 |
| Al-0.1B | 3.6 | 4.2 | 3.2 | 1.0 |
| Al-0.03B | 4.6 | 5.3 | 3.7 | 1.6 |
| MCM-41TB | 3.6 | 4.2 | 2.7 | 1.5 |
| MCM-41TA | 4.6 | 5.3 | 4.9 | 0.4 |
| MCM-41 | 3.8 | 4.4 | 2.5 | 1.9 |
| PA | 3.9 | 4.5 | 3.0 | 1.5 |

### 6.1.3 Scanning Electron Microscopy (SEM)

Morphologies of the materials were observed by SEM analyses. SEM photographs of the materials *MCM-41TB* and *Al-1A* are shown in Figure 6.10 and 6.11, respectively. These images showed that when aluminum was incorporated into the silica structure, the size of the particles became larger. For instance, for the catalyst *Al-1A*, the average particle size is approximately 7 μm (Figure 6.11b), on the other hand for *MCM-41TB,* it is much smaller than 1μm (Figure 6.10). Additionally, hexagonal-like structure was obtained in aluminum containing MCM-type materials synthesized using aluminum nitrate as aluminum source, as shown in Figure 6.11a.

The Al/Si atomic ratios in the final synthesized aluminum containing *MCM-type* samples evaluated from EDS analyses and in the synthesis solutions are reported in Table 6.3. These results showed that when aluminum nitrate was used as the aluminum source, the aluminum was incorporated into the structure more effectively at low Al loadings but at high loadings, it was concluded that most of the aluminum was not incorporated into the structure. This may be due to removal of aluminum during washing step or dealumination during calcination step. On the other hand, when aluminum

isopropoxide was used as the aluminum source, aluminum was incorporated into the structure more effectively both at low and high Al loadings. Finally, the EDS result of the commercial *MCM-41* catalyst confirms that all the aluminum in the inital synthesis solution were incorporated into the structure.

EDS spectra of all the aluminum containing *MCM-type* and commercial *MCM-41* type mesostructured aluminosilicate catalysts are given in Appendix B. In these spectra, the peaks other than aluminum and silicon, belong to gold, oxygen and carbon. Au comes from the coating of the samples with gold. Oxygen may come from the formation of $SiO_2$ in the final structure and carbon may come from the organic template that is not removed during washing or calcination step or from silica source used in the synthesis.

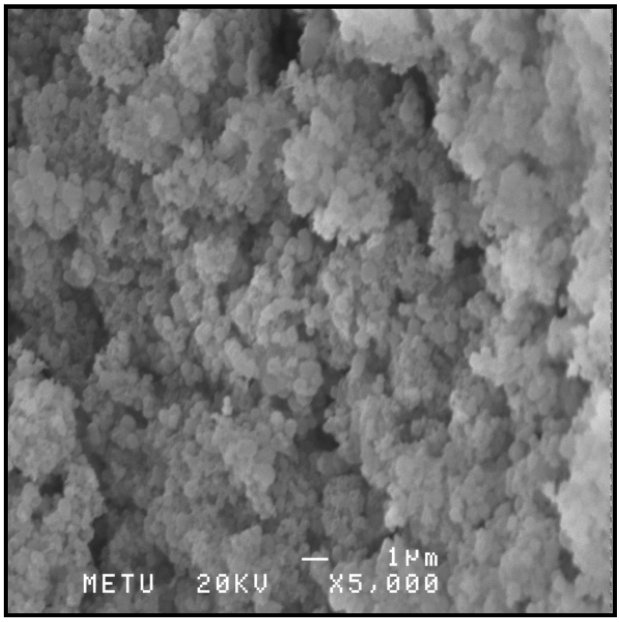


Figure 6.10 SEM image of *MCM-41TB*

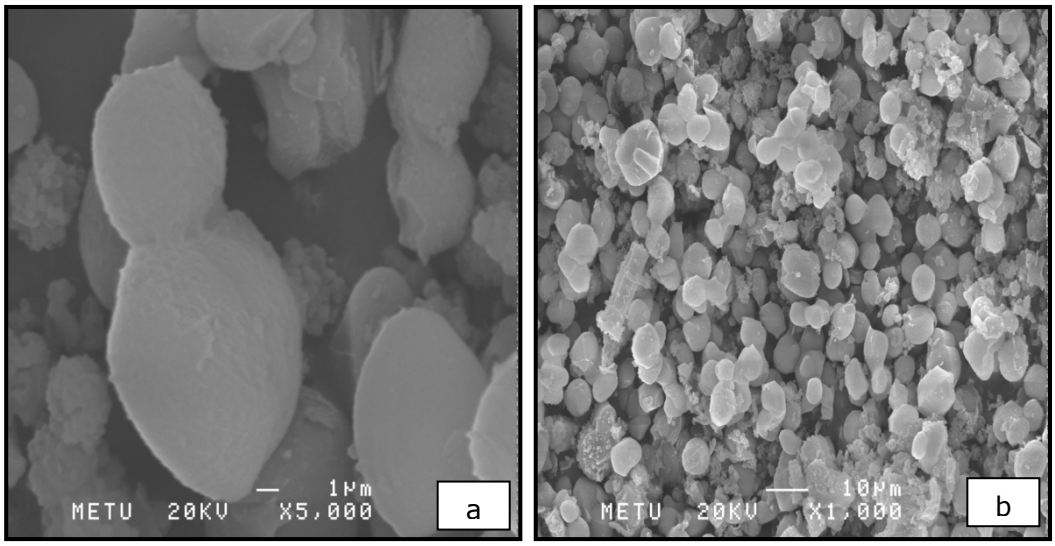


Figure 6.11 SEM image of *Al-1A* (a) 5000 times magnified
(b) 1000 times magnified

Table 6.3 Al/Si atomic ratios of synthesized Al-MCM-type catalysts

| Sample ID | Al/Si ratio (EDS) | Al/Si ratio (synthesis solution) |
|---|---|---|
| Al-1A | 0.16 | 1 |
| Al-0.5A | 0.14 | 0.5 |
| Al-0.1A | 0.08 | 0.1 |
| Al-0.03A | 0.015 | 0.03 |
| Al-1B | 0.59 | 1 |
| Al-0.5B | 0.28 | 0.5 |
| Al-0.1B | 0.05 | 0.1 |
| Al-0.03B | 0.017 | 0.03 |
| PA | 0.03 | |

### 6.1.4 $^{27}$Al MAS NMR

$^{27}$Al MAS NMR spectrum (Figure 6.12a) showed that aluminum nitrate sample (*Al-1A*) gave peaks both at 0 ppm from 6-coordinate aluminium and 50 ppm from 4-coordinate aluminium. Resonance at 50 ppm meant that most of the Al from the synthesis solution was incorporated into the framework. On the

other hand, aluminum isopropoxide gave low-intensity peak from 4-coordinate Al and high-intensity peak from 6-coordinate (Figure 6.12b and 6.12c) which meant that the most of the aluminum was not incorporated into framework of the material's structure. These results were consistent with the EDS results. EDS analyses also indicated that the aluminum was not incorporated at high aluminum loadings. Probably, it adsorbed on the material surface. In other words, the nature of the aluminum source used in the synthesis of material might affect the location of aluminum in the MCM-41 framework. $^{27}$Al MAS NMR spectrum of uncalcined *Al-1B* aluminosilicate material (Figure 6.13) also exhibited a mixture of tetrahedral and octahedral aluminum. After calcination, the sharp $^{27}$Al peak broadened and decreased in intensity (Figure 6.12c). The broadening might be a result of decreased symmetry of some aluminum sites in calcined sample. The decrease in intensity might be due to dealumination during template removal.

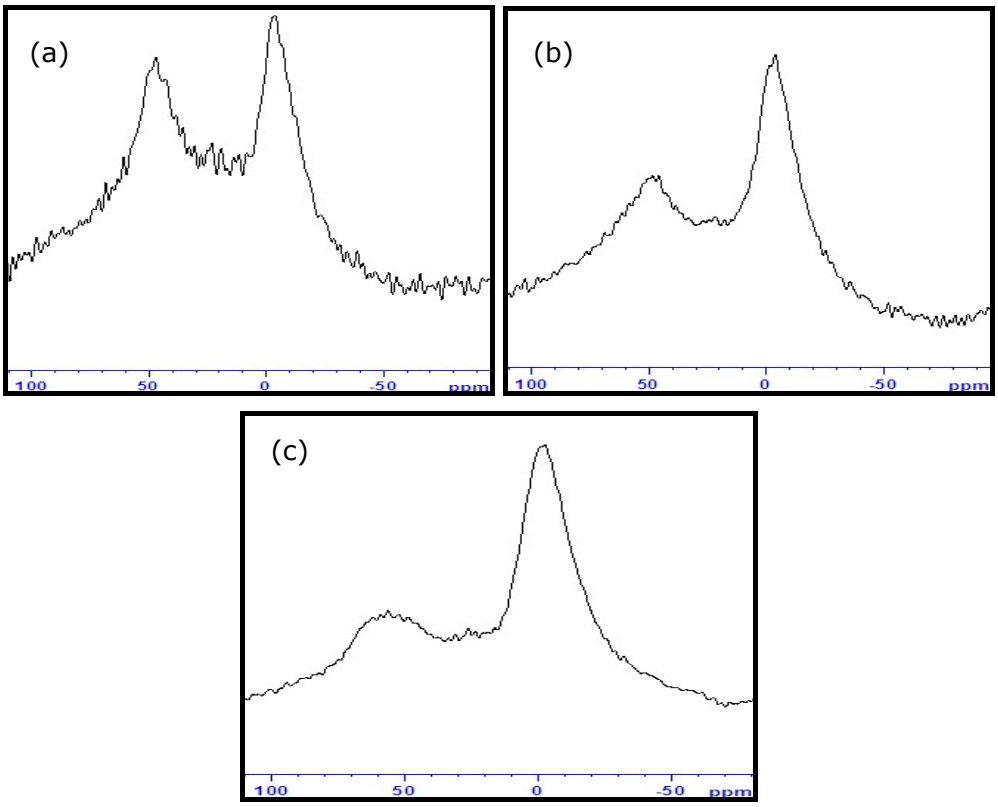


Figure 6.12 $^{27}$Al MAS NMR spectra of (a) *Al-1A*, (b) *Al-0.5B*, and (c) *Al-1B* samples.

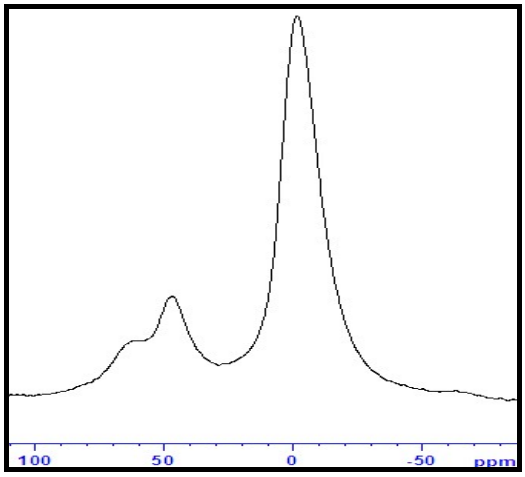


Figure 6.13 $^{27}$Al MAS NMR spectrum of uncalcined *Al-1B* MCM-type catalyst

## 6.2 Characterization of Mesoporous SBA-type Catalysts

The physical and structural properties of synthesized *SBA-type* catalysts were determined by X-Ray Diffraction, Nitrogen Physisorption, Scanning Electron Microscopy, Diffuse Reflactance Fourier Transform Infrared, $^{27}$Al MAS NMR and Transmission Electron Microscopy techniques.

### 6.2.1 X-Ray Diffraction(XRD)

The XRD patterns of SBA-type materials synthesized using three different procedures are shown in Figure 6.14. For these materials, the diffraction patterns only have reflection peaks in the low Bragg angle range (less than 10). A typical *SBA-15* shows three reflections corresponding to Bragg angle values of 0.92°, 1.60° and 1.85° [80].

For SBA-type catalyst synthesized using the first synthesis procedure (*S1*), the major peak was at a 2θ value of 1.08° and the second and the third peaks were at 1.74° and 1.94°, respectively. However, in this sample, the second and the third peaks can not be distinguished well from each other and the intensity of the peaks is too low with respect to the other two samples

(*S2&S6*). For this sample, it was concluded that a well ordered mesoporous structure was not formed. For the sample, synthesized using the second synthesis procedure (*S2*), the major peak was at a 2θ value of 0.98° and the second and the third peaks were at 1.64° and 1.86°, respectively. In this sample, the well-ordered mesoporous structure was formed with respect to the other two samples (*S1&S6*) since the intensity of the peaks was higher and they can be distinguished well from each other. For the sample, synthesized using the third synthesis procedure (*S6*), the major peak was at a 2θ value of 1.06° and the second and the third peaks were at 1.68° and 1.90°, respectively. For these three samples, the peaks were observed almost at the same Bragg angle values.

Additionally, 24 hours of mixing deteriorated the well-ordered mesoporous structure, therefore 2 hours (*S2*) of mixing instead of 24 hours (*S1*) is enough for the formation of well-ordered mesoporous structure. The highest pore wall thickness was obtained in this synthesis procedure. To obtain a well-ordered structure, the second synthesis procedure, 2 hours of mixing and using only HCl instead of HCl+$H_2O$ solution as the solvent, is the best procedure among the three procedures.

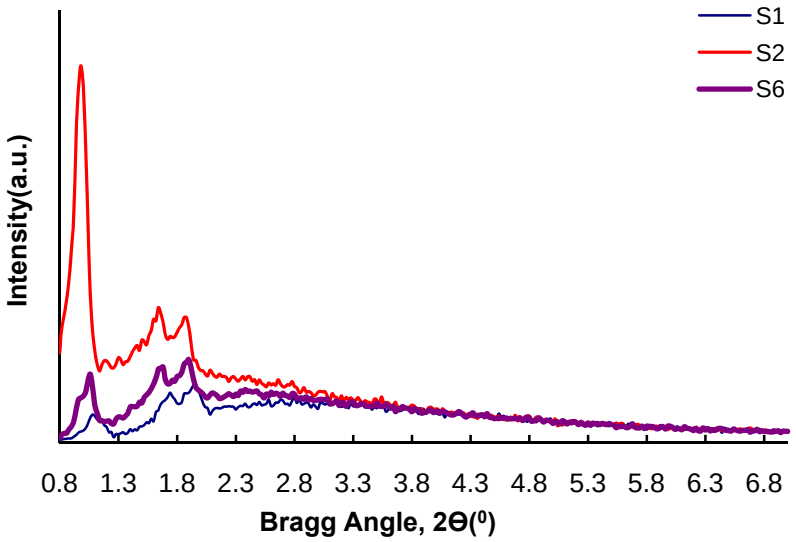


Figure 6.14 XRD patterns of *S1*, *S2* and *S6*

The XRD patterns of SBA-type samples synthesized at different hydrothermal synthesis temperatures using the second synthesis procedure are given in Figure 6.15. When the catalyst was synthesized at 110°C, the major peak was at a 2θ value of 0.94° and the second and the third peaks were at 1.64° and 1.82°, respectively. When the synthesis temperature was raised to 120°C, the intensity of the peaks increased and the major peak was observed at a 2θ value of 0.96° and the second and the third peaks were observed at a 2θ values of 1.58° and 1.78°, respectively. Finally, when the synthesis was carried out at 130°C, three clear characteristic peaks of hexagonally ordered structure disappeared. This may be due to the distortion of the long range ordering of the structure due to the temperature rise. Therefore, all these synthesized catalysts, except *S2-130*, could be considered as *SBA-15* because the characteristic XRD peaks of *SBA-15* were observed. As a conclusion, the well-ordered nature of the synthesized materials decreases when the temperature was raised from 100°C to 130°C. Shift of the major peak to a higher value with an increase in temperature caused a decrease in pore wall thickness. Additionally, these results showed that 100°C can be considered as the best synthesis temperature for SBA-15 materials synthesized using the second synthesis procedure.

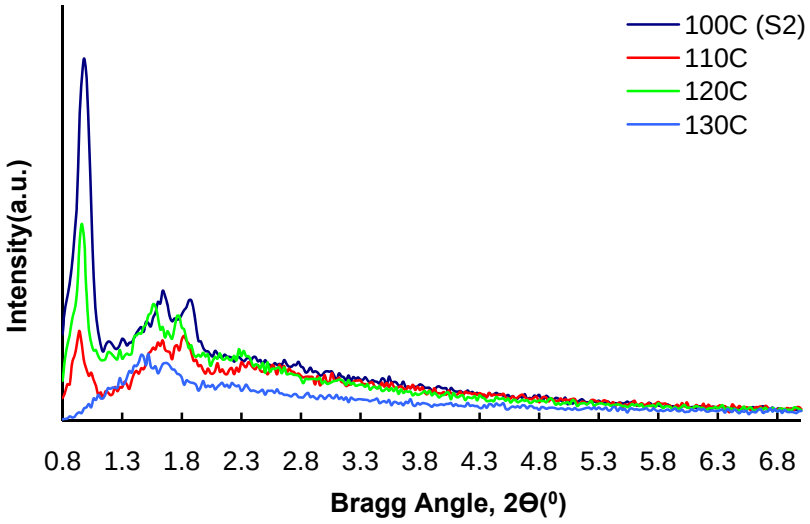


Figure 6.15 XRD patterns of materials synthesized at different temperatures using the second synthesis procedure (synthesis duration:2 days)

The XRD patterns of SBA-type samples synthesized according to the second synthesis procedure at different hydrothermal synthesis times are given in Figure 6.16. When the synthesis of the catalyst was carried out for 24 hours (1 day), the major peak was at a 2θ value of 1.06° and the second and the third peaks were at 1.66° and 1.86°, respectively. However, in this sample, the second and the third peaks can not be distinguished well from each other and the intensity of the peaks is too low with respect to the other samples. For this sample, it could be concluded that the well-ordered mesoporous structure formation was incomplete. When the synthesis time was raised to 72 hours (3 days), the intensity of the peaks increased and the major peak was observed at a 2θ value of 1.02° and the second and the third peaks were observed at 2θ values of 1.64° and 1.86°, respectively. Finally, when the synthesis time was raised to 96 hours (4 days), the major peak was observed at a 2θ value of 0.98° and the second and the third peaks were at 1.60° and 1.82°, respectively.

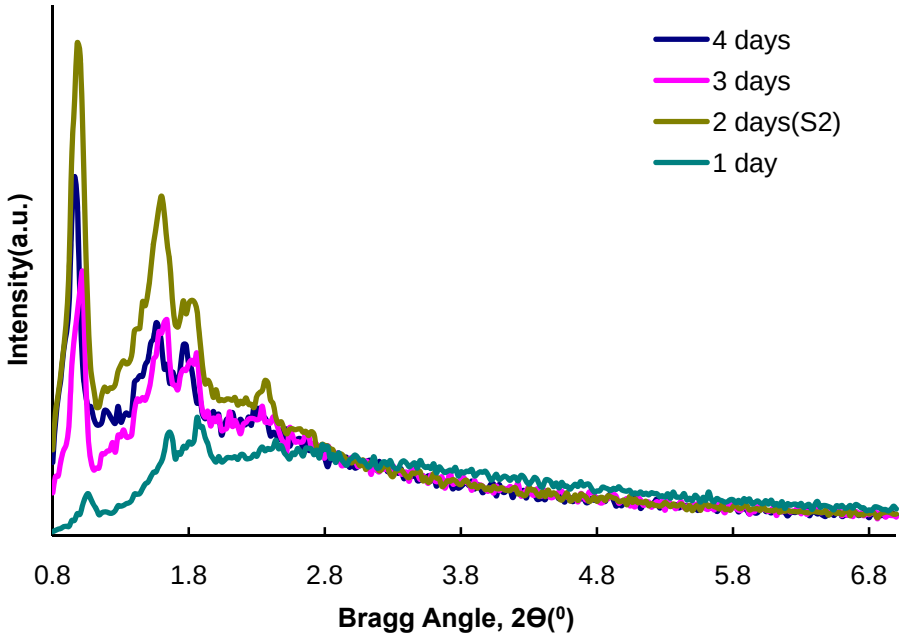


Figure 6.16 XRD patterns of materials synthesized at different times using the second synthesis procedure (synthesis temperature: 100°C)

For 2-day synthesized sample, it could be said that a well-ordered structure formed with respect to the other samples since the intensity of the peaks were high among the others and they could be distinguished well from each other. As a conclusion, in synthesizing of ordered mesoporous SBA-type materials, synthesis time is an important parameter. All these XRD patterns (Figures 6.14, 6.15 and 6.16) showed that the optimum synthesis temperature and duration to obtain well-ordered mesoporous SBA-15 catalyst were 100°C and 48 hours (2 days), respectively. In the synthesis of aluminum containing SBA-type materials, pure SBA-15 which was synthesized at these optimum conditions was used as the host material.

Finally, the XRD patterns of aluminum containing SBA-type samples synthesized using different aluminum sources are given in Figure 6.17. When $Al_2(SO_4)_3$ was used as the aluminum source and Al/Si ratio was kept at 0.03, the major peak was at a $2\theta$ value of 1° and the second and the third peaks were at 1.64° and 1.86°, respectively. When the Al/Si ratio was increased, the intensity of peaks decreased and when the Al/Si ratio was kept at 0.5 and 1, the intensity of the peaks approached to zero and they diminished. As a conclusion, after alumination, all the samples, except *ALS-0.5A* and *ALS-1A*, retain the characteristic patterns of the ordered mesostructures (Figure 6.17a).

When $C_9H_{21}AlO_3$ was used as the aluminum source and Al/Si ratio was kept at 0.03, the major peak was observed at a $2\theta$ value of 1.18° and the second and the third peaks were observed at a $2\theta$ values of 1.78° and 2°, respectively. For this sample, it could be concluded that the well ordered mesoporous structure was not formed. When the Al/Si ratio was kept at 0.1, the major peak was at a $2\theta$ value of 1.06° and the second and the third peaks were at 1.68° and 1.90°, respectively. When the Al/Si ratio was raised to 0.2, the major peak was observed at a $2\theta$ value of 1.06° and the second and the third peaks were observed at a $2\theta$ values of 1.68° and 1.92°, respectively, and when the Al/Si was raised from 0.2 to 0.5, the major peak was observed at a $2\theta$ value of 1.12° and the second and the third peaks were observed at a $2\theta$ values of 1.78° and 2.04°. Finally, when the Al/Si ratio was raised to 1, the major peak was observed at a $2\theta$ value of 1.06° and the second and the third

peaks were at 1.68° and 1.90°, respectively. For these samples, except sample *ALS-0.03B*, the peaks were observed almost at the same Bragg angle values. As a conclusion, when aluminum isopropoxide was used as the aluminum source, some deformations in the main peaks of *SBA-15* were observed which may be due to the structural irregularity, on the other hand, the well ordered structure of *SBA-15* did not deteriorate too much when the level of aluminum was kept low in the case of using aluminum sulphate as the aluminum source.

### 6.2.2 Nitrogen Physisorption

The physical properties of the synthesized materials are given in Table 6.4 and the pore size distributions of these materials are given in Figures 6.18, 6.19 and 6.20, respectively. For SBA-type catalyst, synthesized using the first synthesis procedure (*S1*), the surface area was found as 752 $m^2/g$. For the sample synthesized using the second synthesis procedure (*S2*), the surface area was found as 822 $m^2/g$ and finally, for the material synthesized using the third synthesis procedure (*S6*), the surface area was found as 799 $m^2/g$.

Table 6.4 The physical properties of the synthesized SBA-type catalysts

| Sample ID | Surface Area BET, ($m^2/g$) | Pore Volume BJH Des., (cc/g) | Average Pore Diameter "*dp*" (nm) (4V/A by BET) | BJH Des. Av. Pore Diameter (nm) | Microporosity (%) |
|---|---|---|---|---|---|
| S1 | 752 | 0.94 | 6.2 | 5.2 | 24.5 |
| S2 | 822 | 1.03 | 6.0 | 5.1 | 24.6 |
| S6 | 799 | 1.21 | 6.5 | 5.6 | 24.1 |
| S2-110 | 766 | 1.13 | 6.5 | 5.4 | 23.1 |
| S2-120 | 731 | 1.19 | 7.6 | 5.7 | 19.3 |
| S2-130 | 623 | 1.13 | 8.2 | 6.2 | 18.5 |
| ALS-0.03A | 560 | 0.87 | 6.5 | 5.4 | 23.3 |
| ALS-0.1A | 370 | 0.61 | 6.4 | 5.0 | 22.3 |
| ALS-0.2A | 200 | 0.31 | 6.2 | 5.2 | 24.7 |
| ALS-0.5A | 99 | 0.15 | 6.5 | 4.2 | 22.5 |
| ALS-1A | 44 | 0.06 | 6.9 | 4.2 | 21.5 |
| ALS-0.03B | 730 | 0.86 | 6.0 | 4.9 | 24.3 |
| ALS-0.1B | 575 | 0.84 | 6.4 | 5.2 | 23.1 |
| ALS-0.2B | 617 | 0.85 | 6.5 | 4.9 | 21.6 |
| ALS-0.5B | 383 | 0.57 | 7.4 | 5.1 | 19.2 |
| ALS-1B | 367 | 0.59 | 6.3 | 4.6 | 22.3 |

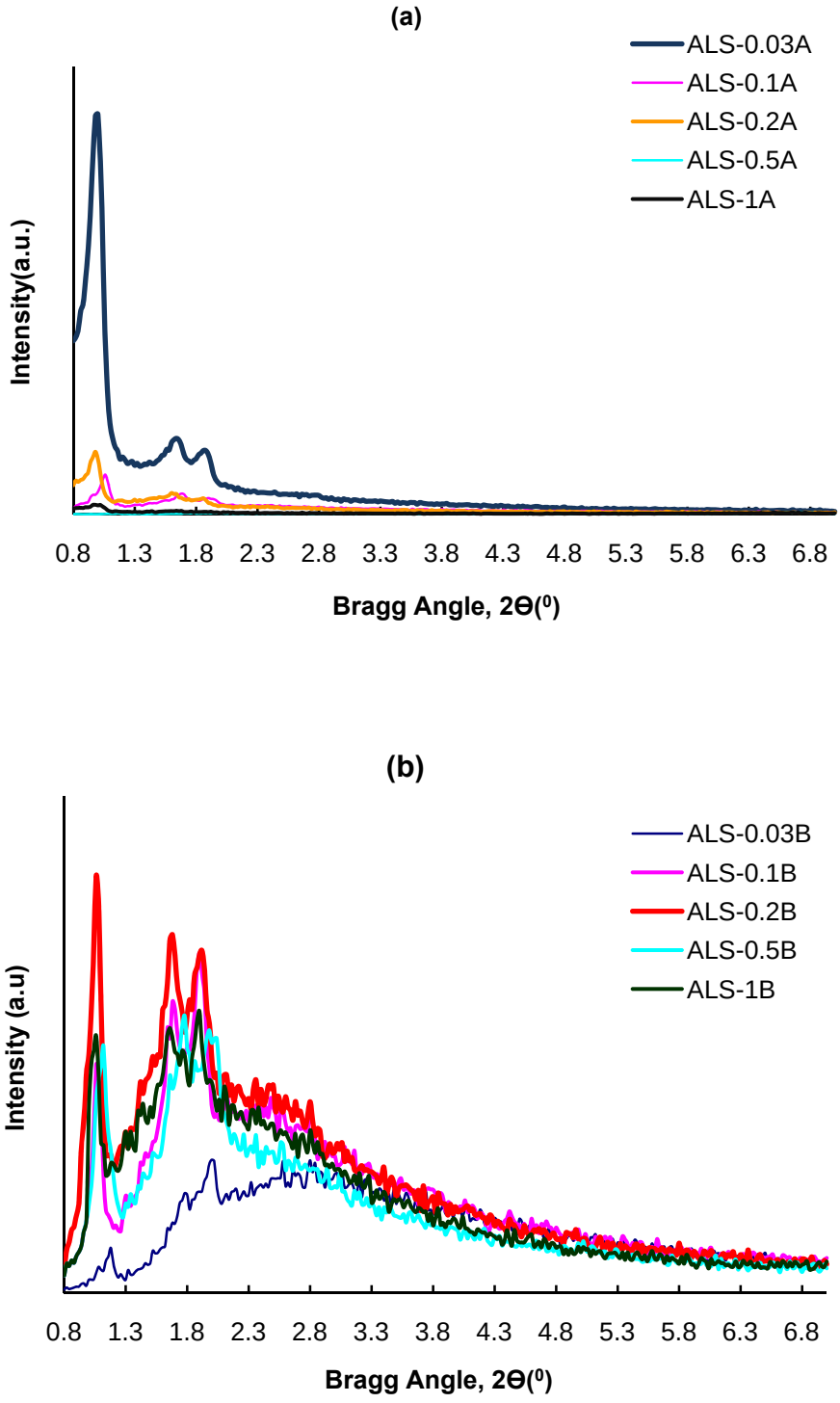


Figure 6.17 XRD patterns of aluminum containing SBA-type catalysts synthesized using different aluminum sources: (a) $Al_2(SO_4)_3.18H_2O$ and (b) $C_9H_{21}AlO_3$

These surface area values showed that 2 hours (*S2*) of mixing instead of 24 hours (*S1*) caused an increase in the surface area of pure SBA-15. Additionally, 2 hours of mixing and using only HCl (*S2*) instead of HCl+$H_2O$ solution as the solvent (*S6*) also caused an increase in the surface area of pure SBA-15. On the other hand, changing either mixing time or solvent did not cause a significant change in pore volumes and average pore diameters.

Increasing the synthesis temperature of the material which was prepared according to second synthesis procedure caused a decrease in the surface area and an increase in average pore diameters of the materials. On the other hand, increasing synthesis temperature did not cause a significant change in the pore volumes.

The BET surface areas and the pore volumes of the materials synthesized using $Al_2(SO_4)_3$ decreased with the amount of aluminum loading. This could be an indication of the aluminum incorporation into pore surface by modifying its pore diameter. Catalysts *ALS-0.2A, ALS-0.5A* and *ALS-1A* have low surface area values. This might be due to the blocking of material's pores by Al species. On the other hand, when aluminum isopropoxide was used as the aluminum source, the surface area of the materials decreased but their pore volume did not change so much when Al/Si ratio was increased from 0.03 to 0.2. This might be due to the replacement of Si atoms found in host material with Al atoms that comes from aluminum source. When Al/Si ratio was increased above 0.2, both surface area and pore volume of the materials decreased significantly. This might be due to the formation of $Al_2O_3$ on the external surface of silica based host material.

Additionally, the surface areas of SBA-type materials were much lower than the surface area of MCM-type materials because their particle diameters were high with respect to the particle diameters of MCM-type materials (Table 6.1 and 6.4)

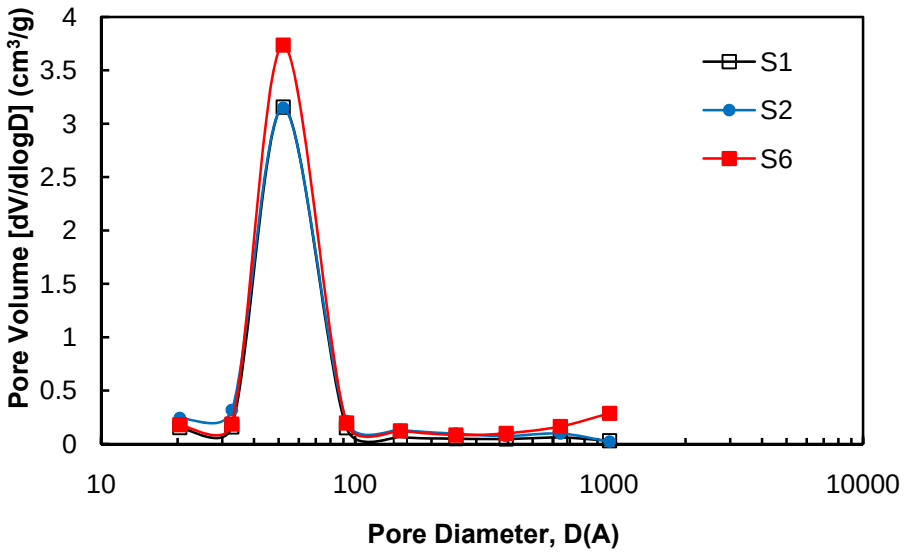


Figure 6.18 Pore size distributions of *S1*, *S2* and *S6*

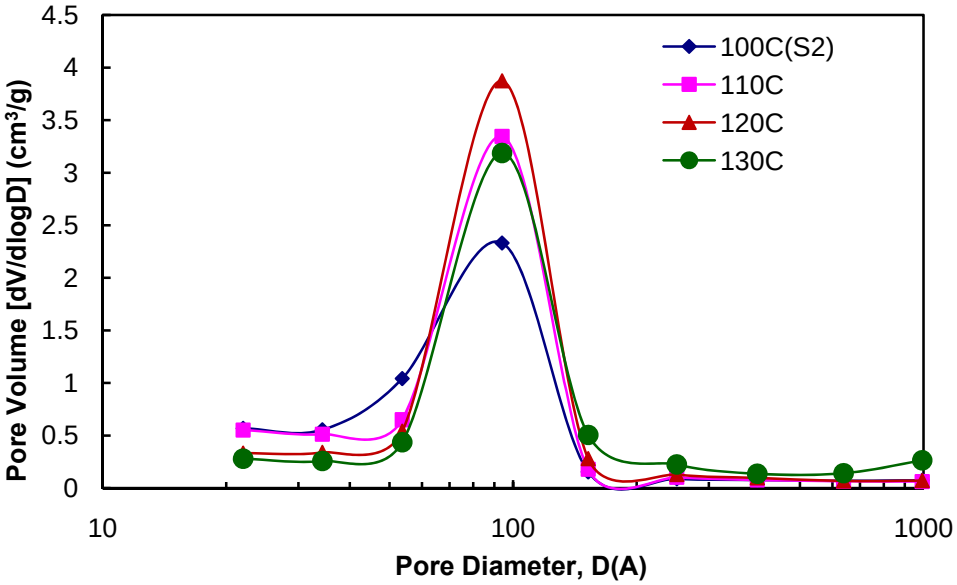


Figure 6.19 Pore size distributions of *S2,S2-110,S2-120* and *S2-130*

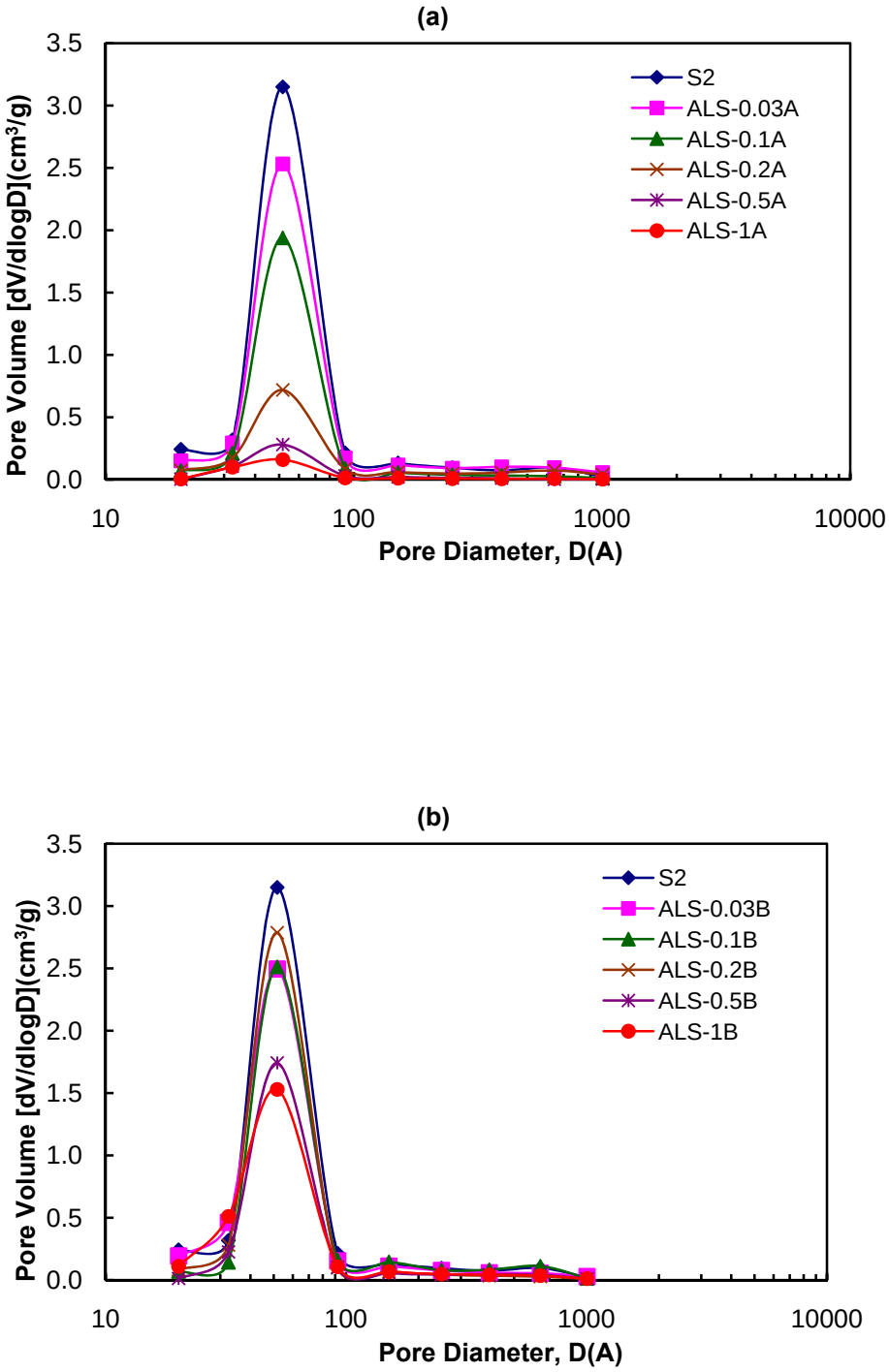


Figure 6.20 Pore size distributions of aluminum containing SBA-type catalysts synthesized using different aluminum sources;(a)$Al_2(SO_4)_3.18H_2O$ and (b) $C_9H_{21}AlO_3$

All the catalysts showed unimodal pore size distributions and their average pore diameter values and the pore size distribution curves supported the mesoporosity of the materials. When pure SBA-15 was synthesized using the first (*S1*) and second (*S2*) synthesis procedures, the pore volume of the catalysts did not change so much. On the other hand, when the third (*S6*) synthesis procedure was used for the synthesis of pure SBA-15, the pore volume slightly increased (Figure 6.18). As a conclusion, 2 hours (*S2*) of mixing instead of 24 hours (*S1*) and 2 hours of mixing and using only HCl (*S2*) instead of HCl+$H_2O$ as the solvent (*S6*) did not cause a significant change in the pore volume of pure SBA-15, as mentioned previously.

Increasing the synthesis temperature of the material prepared according to second synthesis procedure from 100°C to 130°C did not cause a significant change in the pore volumes (Figure 6.19).

When $Al_2(SO_4)_3$ was used as the aluminum source and when the Al/Si was increased from 0.03 to 0.2, pore volume of the catalysts decreased significantly (Figure 6.20a). On the other hand, when $C_9H_{21}AlO_3$ was used as the aluminum source, pore volumes of the synthesized catalysts did not change too much when Al/Si ratio was increased from 0.03 to 0.1 and slightly decreased when Al/Si ratio was increased from 0.5 to 1. Additionally, for mesoporous materials, the pore diameters lie between 2 and 50 nm. In our case, average pore diameters of the synthesized materials are in the range of 6.0 – 7.4nm. Finally, average pore diameters evaluated from the BET data and BJH desorption data (Table 6.4) agreed quite well.

The $N_2$ adsorption-desorption isotherms of the synthesized pure and aluminum containing SBA-type samples synthesized using different aluminum sources are given in Figures 6.21, 6.22 and 6.23, respectively. All the samples showed typical *Type IV* adsorption/desorption isotherm with a hysteresis loop (H1), which is characteristic of mesoporous materials [114]. This hysteresis loop was broad and the adsorption and desorption branches were parallel in most of the synthesized materials (Figures 6.21, 6.22 and 6.23). A well-defined capillary condensation step occurred at relative pressure of 0.55-0.84, indicating the uniform pore size distributions.

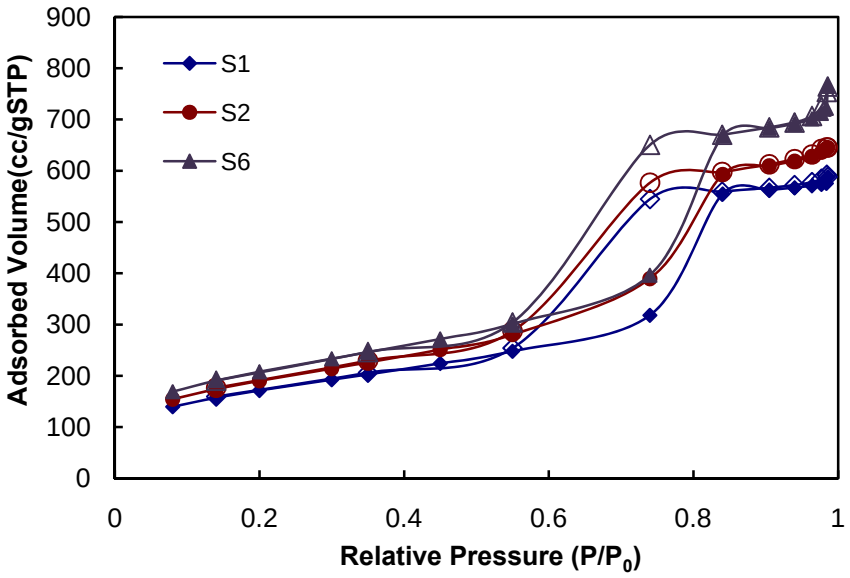


Figure 6.21 $N_2$ adsorption-desorption isotherms of *S1,S2* and *S6* (solid boxes: adsorption branch; blank boxes: desorption branch)

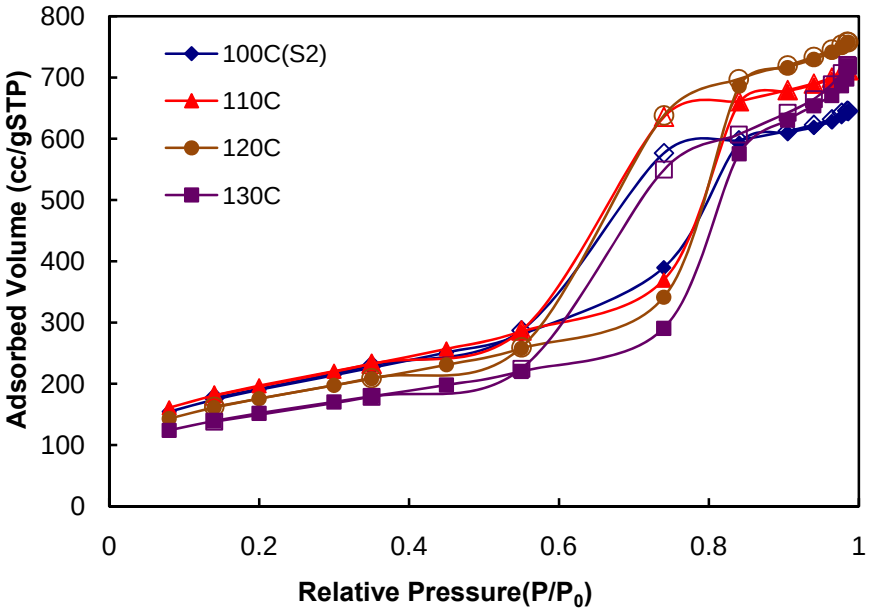


Figure 6.22 $N_2$ adsorption-desorption isotherms of *S2, S2-110, S2-120* and *S2-130*
(solid boxes: adsorption branch; blank boxes: desorption branch)

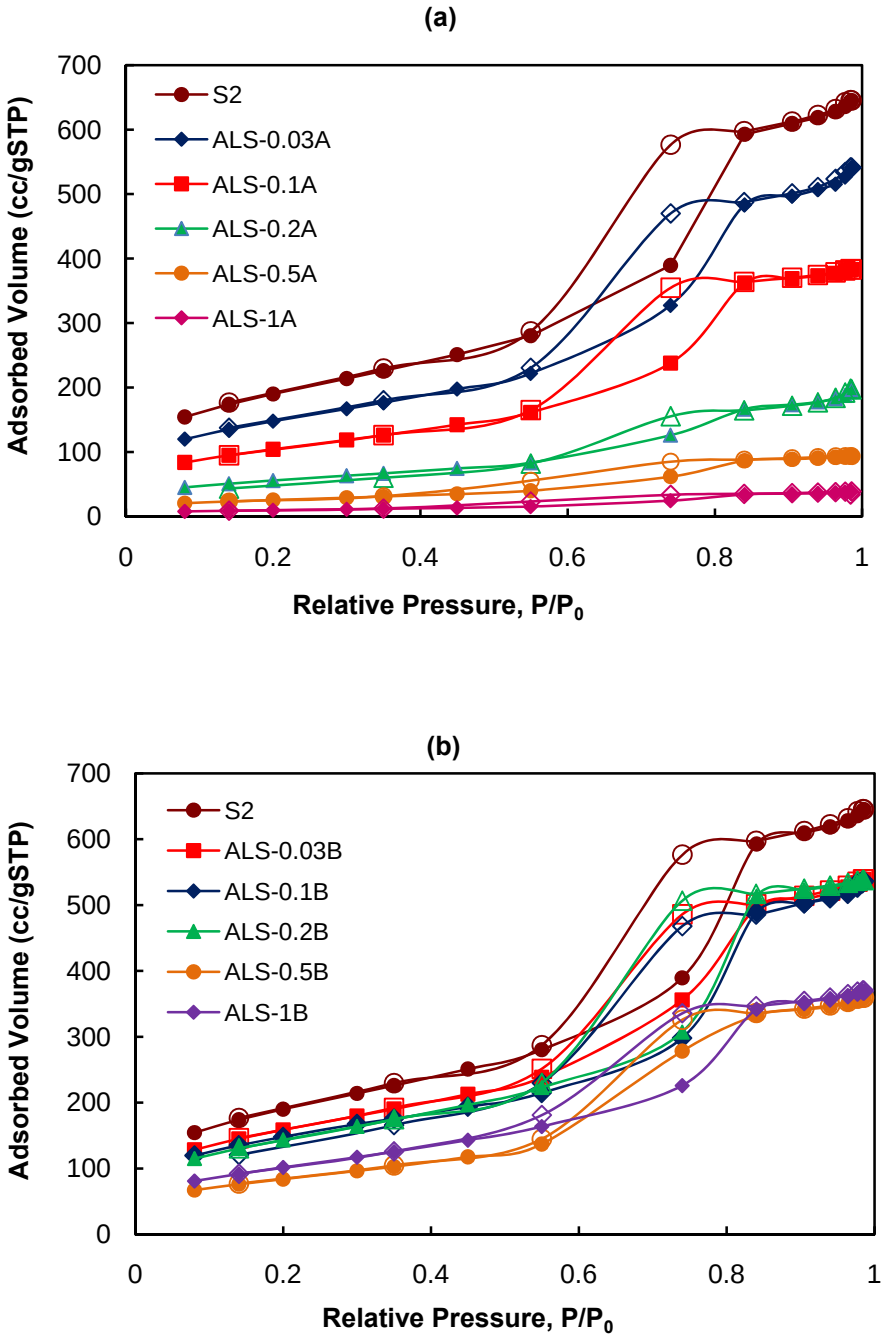


Figure 6.23 $N_2$ adsorption-desorption isotherms of aluminum containing SBA-type catalysts synthesized using different aluminum sources: (a)$Al_2(SO_4)_3.18H_2O$,and (b) $C_9H_{21}AlO_3$
(solid boxes: adsorption branch; blank boxes: desorption branch)

Additionally, the hysteresis opening decreased with an increase in aluminum loading (Figure 6.23). The adsorbed $N_2$ volumes in the materials synthesized using $Al_2(SO_4)_3$ significantly decreased with an increase in aluminum loading. This might be due to blocking of the mesopores of SBA-15 by aluminum species. However, the adsorbed $N_2$ volume in the materials synthesized using $C_9H_{21}AlO_3$ did not decrease significantly (Figure 6.23b). Finally, all the samples contained considerable amount of micropores and mixing time, solvent or aluminum source used in the synthesis of the materials did not affect the amount of the micropores in the synthesized materials. On the other hand, when the synthesis temperature was raised from 100°C to 130°C, the amount of these micropores decreased slightly. These results were consistent with the pore size distribution results given in Figure 6.20.

Finally, using $N_2$ physisorption and X-ray diffraction analysis, pore wall thickness of the samples was calculated according to the relation given in section 3.6.1 (Eqn. 3.2). Pore wall characteristics of the synthesized catalysts are given in Table 6.5. The results showed that the walls of SBA-type catalysts were much thicker than the walls of MCM-type catalysts. The thicker pore walls make these SBA-type materials more favorable at high temperature reactions such as cracking reactions. Additionally, an increase in lattice parameter ($a$) and pore wall thickness ($\delta$) of the synthesized materials caused shifts in peaks observed in XRD patterns of the synthesized materials, as given in Figure 6.17. Finally, when aluminum sulphate was used as the Al source, the pore wall of the catalyst was much thicker than the pore wall of the catalyst prepared using aluminum isopropoxide as the Al source (Table 6.5).

### 6.2.3 Scanning Electron Microscopy (SEM)

In Figure 6.24, SEM images of the AlSBA-15 materials synthesized using different aluminum sources with different aluminum loadings showed that when aluminum sulphate was used as the aluminum source, cylindrical particles were formed (Figure 6.24a,b). On the other hand, when aluminum isopropoxide was used as the aluminum source, the length of the particles shortened and hexagonal-like particles were formed (Figure 6.24c,d).

Table 6.5 Pore wall properties of the synthesized SBA-type catalysts

| Sample ID | $d_{(100)}$ (nm) | Lattice Parameter, a (nm) | BJH Pore Diameter, $d_{pore}$ (nm) | Pore Wall Thickness, δ (nm) |
|---|---|---|---|---|
| S1 | 8 | 9.2 | 5.2 | 4.0 |
| S2 | 9 | 10.4 | 5.1 | 5.3 |
| S6 | 8.7 | 10.0 | 5.6 | 4.4 |
| S2-110 | 9.5 | 11.0 | 5.4 | 5.6 |
| S2-120 | 9.2 | 10.6 | 5.7 | 4.9 |
| S2-130 | 7.7 | 8.9 | 6.2 | 2.7 |
| ALS-0.03A | 8.8 | 10.2 | 5.4 | 4.8 |
| ALS-0.1A | 8 | 9.6 | 5.0 | 4.6 |
| ALS-0.2A | 9 | 10.4 | 5.2 | 5.2 |
| ALS-0.5A | 7.6 | 8.8 | 4.2 | 4.6 |
| ALS-1A | 8.8 | 10.2 | 4.2 | 6.0 |
| ALS-0.03B | 7.7 | 8.9 | 4.9 | 4.0 |
| ALS-0.1B | 7.7 | 8.9 | 5.2 | 3.7 |
| ALS-0.2B | 8.3 | 9.6 | 4.9 | 4.7 |
| ALS-0.5B | 8.0 | 9.2 | 5.1 | 4.1 |
| ALS-1B | 8.3 | 9.6 | 4.6 | 5.0 |

For instance, for catalyst ALS-0.2B, the particle size is approximately 0.8 μm (Figure 6.24c), on the other hand for ALS-0.2A, particle size becomes approximately 1 μm (Figure 6.24a). Additionally, when Al/Si ratio was increased from 0.2 to 0.5, agglomeration was observed (Figure 6.24 b,d).

The Al/Si atomic ratios in the final synthesized aluminum containing SBA-type materials evaluated from EDS analyses and in the impregnation solutions are reported in Table 6.6 and their EDS patterns are given in Appendix C. These results showed that when aluminum isopropoxide was used as the aluminum source, the aluminum was incorporated into the structure more effectively both at low and high Al loadings. On the other hand, when aluminum sulphate was used as the aluminum source, the aluminum was only incorporated into structure more effectively at low loading, not at high loading. As a conclusion, the nature of the aluminum source used in the synthesis of catalyst has a significant effect on the level of incorporation of aluminum into the catalyst structure.

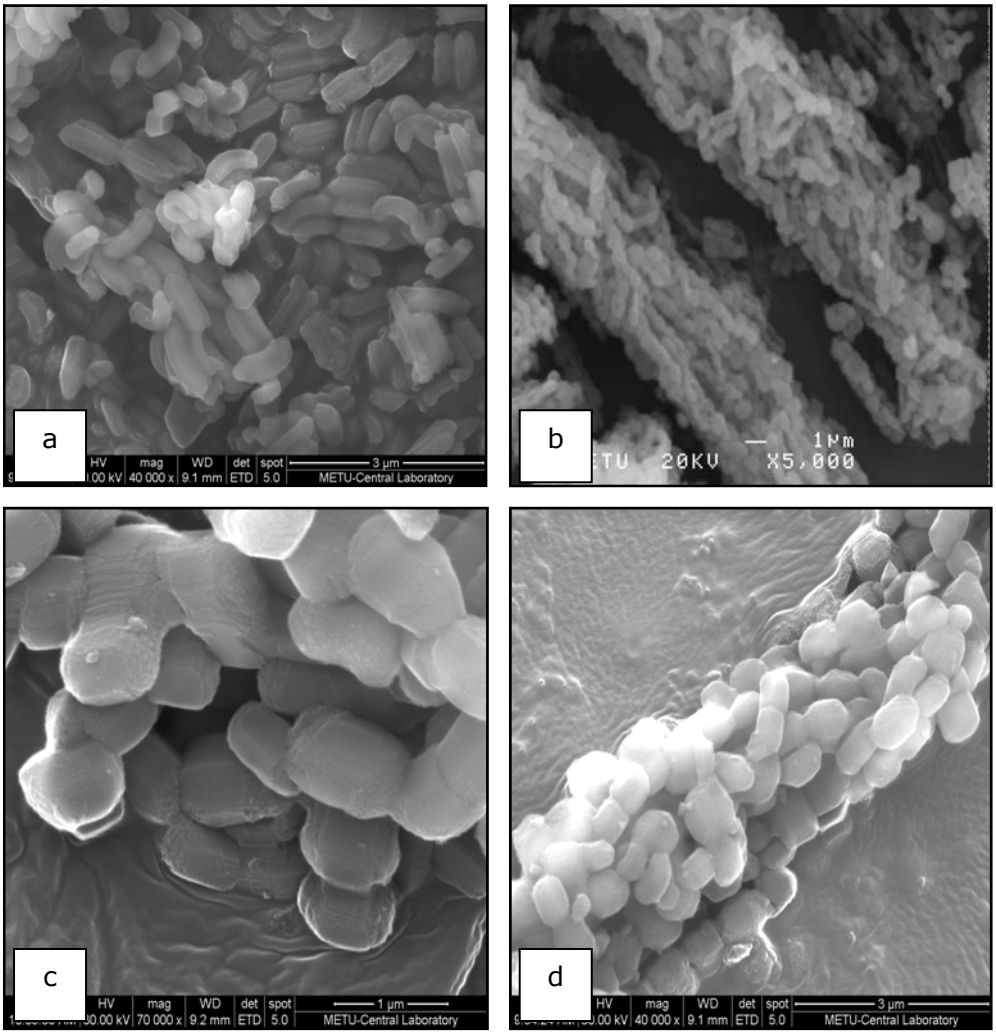


Figure 6.24 SEM images of the materials synthesized using aluminum sulphate (a) *ALS-0.2A,* (b) *ALS-0.5A*, and aluminum isopropoxide (c) *ALS-0.2B*, (d) *ALS-0.5B* as the aluminum source

Table 6.6 Al/Si atomic ratios of synthesized Al-SBA-type catalysts

| Sample ID | Al/Si (EDS) | Al/Si(impregnation solution) |
|---|---|---|
| ALS-0.03A | 0.03 | 0.03 |
| ALS-0.1A | 0.07 | 0.1 |
| ALS-0.2A | 0.17 | 0.2 |
| ALS-0.5A | 0.18 | 0.5 |
| ALS-1A | 0.22 | 1 |
| ALS-0.03B | 0.026 | 0.03 |
| ALS-0.1B | 0.08 | 0.1 |
| ALS-0.2B | 0.14 | 0.2 |
| ALS-0.5B | 0.32 | 0.5 |
| ALS-1B | 0.67 | 1 |

### 6.2.4 $^{27}$Al MAS NMR

The coordination environment of aluminum atoms in the synthesized materials was determined using $^{27}$Al MAS NMR. The spectra of these materials synthesized using different aluminum sources are given in Figures 6.25 and 6.26. The spectra of these materials showed two peaks at 0 and 50 ppm. The peak at 50 ppm is assigned to tetrahedral framework aluminum formed in the mesoporous walls of the material. The peak at 0 ppm belongs to octahedral aluminum corresponding to extra-framework aluminum species. The NMR results showed that aluminum was incorporated into the SBA-15 structure. The NMR results are consistent with the EDS results. For the materials synthesized using aluminum isopropoxide, the peak at 50 ppm was more intense than the peak at 0 ppm when the aluminum content was low (Figure 6.25a). On the other hand, for the materials synthesized using aluminum sulphate, the peak intensity at 0 ppm increased with an increase in aluminum loading (Figures 6.25b & 6.26b). In other words, the most of the aluminum was not incorporated into framework of the catalyst structure. Probably, it adsorbed on the catalyst surface. The nature of the aluminum source used in the synthesis of catalyst might affect the location of aluminum in the *SBA-15* framework. Finally, in the case of using aluminum sulphate as the aluminum source, an increase in the aluminum loading from 3% to 20% in SBA-15

material caused a significant peak shift from 0 ppm to -24 ppm (Figure 6.26b).

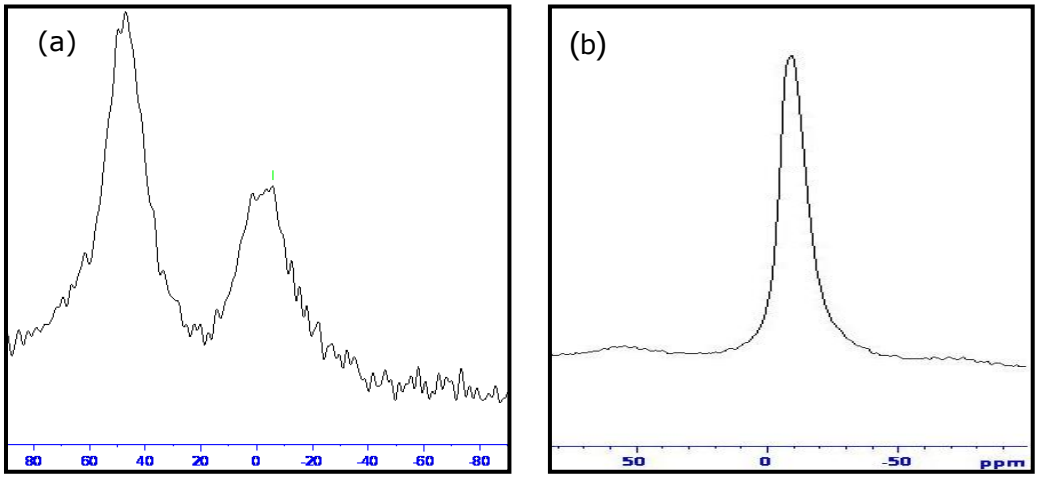


Figure 6.25 $^{27}$Al MAS NMR spectra of (a) *ALS-0.03B* and (b) *ALS-0.03A* samples

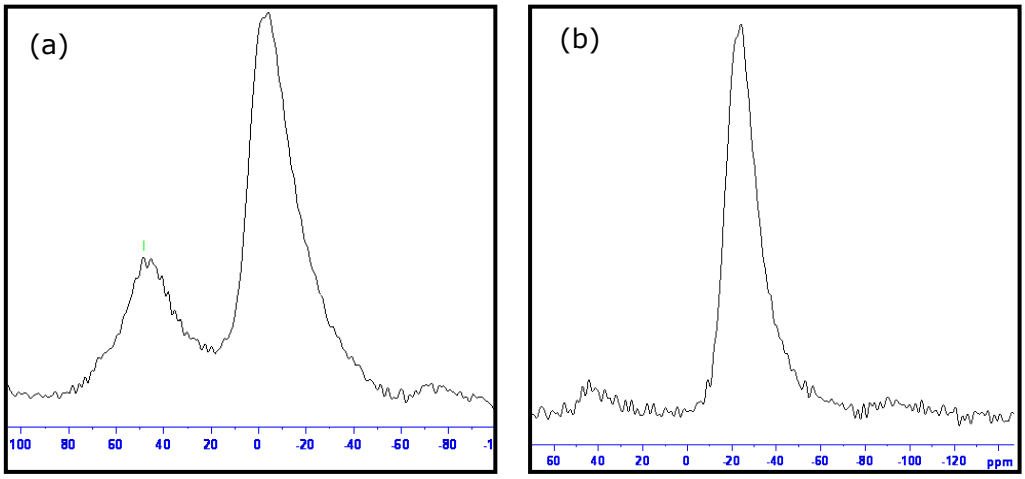


Figure 6.26 $^{27}$Al MAS NMR spectra of (a) *ALS-0.2B* and (b) *ALS-0.2A* samples

### 6.2.5 Diffuse Reflectance FT-IR (DRIFTS) Analysis

Differences of DRIFTS results obtained with pyridine adsorbed samples and fresh catalysts (Figure 6.27), gave information about the Lewis and Brönsted acid sites of these materials. DRIFTS bands observed at 1447 $cm^{-1}$ and 1598 $cm^{-1}$ correspond to the Lewis acid sites [115, 116]. On the other hand, the bands observed at 1540 $cm^{-1}$ and 1640 $cm^{-1}$ are due to the pyridinium ion adsorbed on the Brönsted acid sites on the material surface. The band observed at 1489 $cm^{-1}$ was considered to be due to the contributions of Lewis and Brönsted acid sites. This might be due to the presence of Al in the catalyst structure. When Al/Si ratio was raised to 0.5 and 1, both Brönsted (1540 and 1640 $cm^{-1}$) and Lewis (1447 $cm^{-1}$) acid sites disappeared. Additionally, the relative intensity of the band observed at 1489 $cm^{-1}$ increased up to Al/Si ratio of 0.2 and when Al/Si was raised above 0.2, the intensity of this band decreased. For these materials prepared using aluminum sulphate as the aluminum source, it is clear that Brönsted acid sites are much stronger than Lewis acids. On the other hand, when aluminum isopropoxide was used as the aluminum source, the relative intensities of the bands corresponding to the Lewis and Brönsted acid sites (1489 $cm^{-1}$) increased as the Al/Si ratio increased up to 0.2 and when Al/Si was raised to 0.5 and 1, both acid sites disappeared, as observed in the aluminum sulphate impregnated samples. Additionally, pure SBA-15 (*S2*) had low Lewis acidity with respect to the aluminum impregnated catalysts.

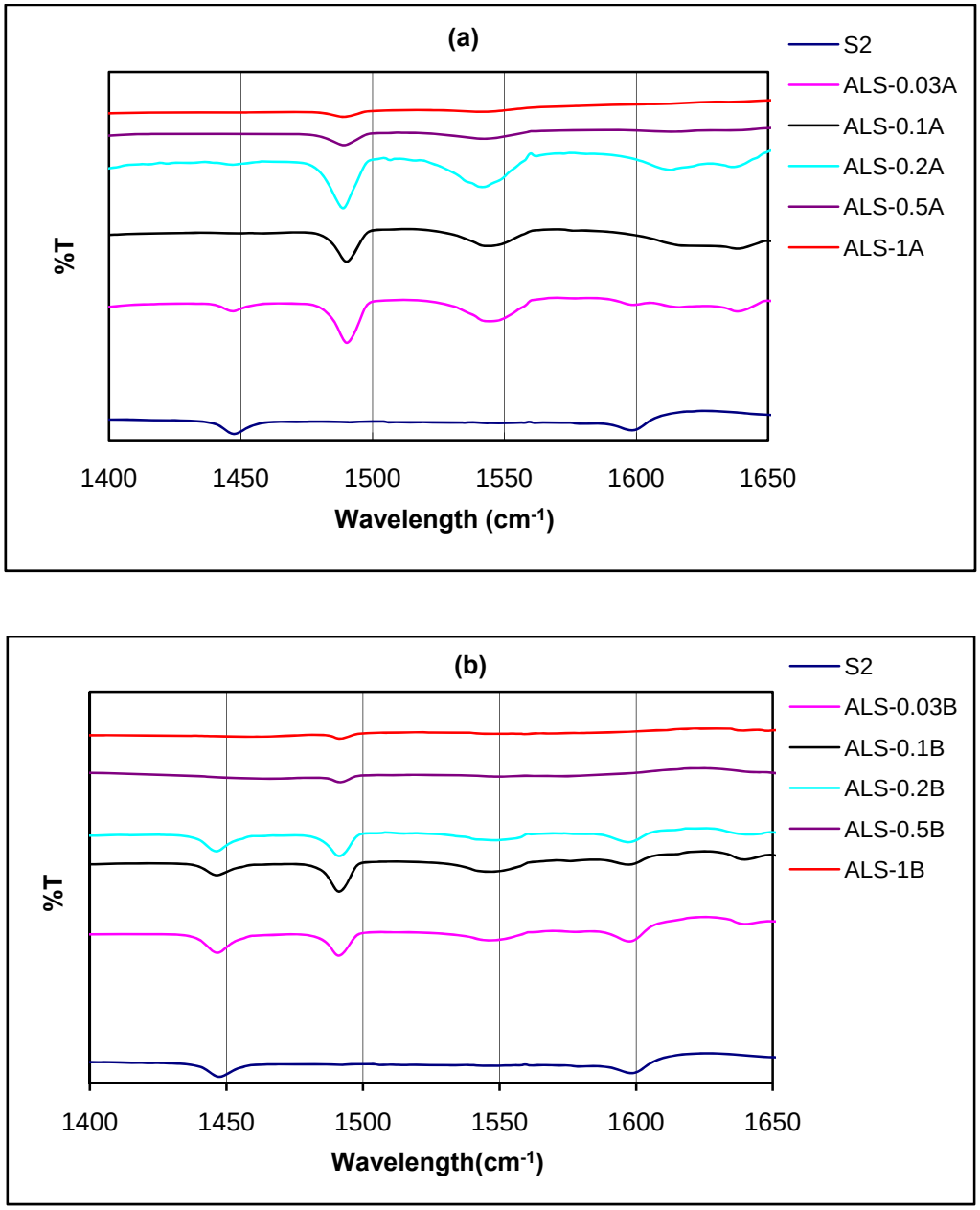


Figure 6.27 DRIFT spectra of pyridine adsorption on aluminum containing SBA-type catalysts synthesized using different aluminum sources: (a)$Al_2(SO_4)_3.18H_2O$ and (b) $C_9H_{21}AlO_3$

### 6.2.6 Transmission Electron Microscopy (TEM)

The TEM images of the synthesized materials are given in Figures 6.28 and 6.29. These images showed well-ordered hexagonal arrays of uniform mesopores with channels. The pore structure of these materials was in honeycomb form that is common for mesoporous materials. The lighter regions in Figure 6.28a indicated the presence of mesopores in the synthesized material. Figure 6.29 showed that the pore channels arranged regularly in cylindrical form both in aluminum sulphate and aluminum isopropoxide samples. These particles combined with each other and the particle size became 410 nm approximately (Figure 6.29 a,c) when aluminum sulphate was used as the aluminum source. On the other hand, these particles shortened when aluminum isopropoxide was use as the aluminum source. When aluminum sulphate was used as the aluminum source, the distance between two consecutive centers of hexagonal pores was 11.5 nm. The average thickness of the wall was 4.8 nm and the pore diameter was around 6.0 nm which is in agreement with results obtained from $N_2$ physisorption analysis (Table 6.4).

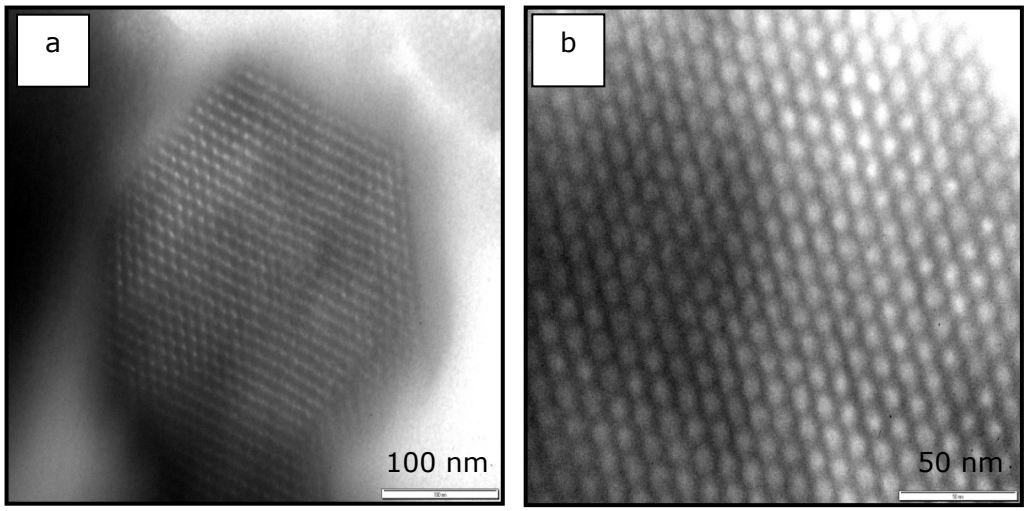


Figure 6.28 TEM image of *ALS-0.2A* (a) low magnification
(b) high magnification

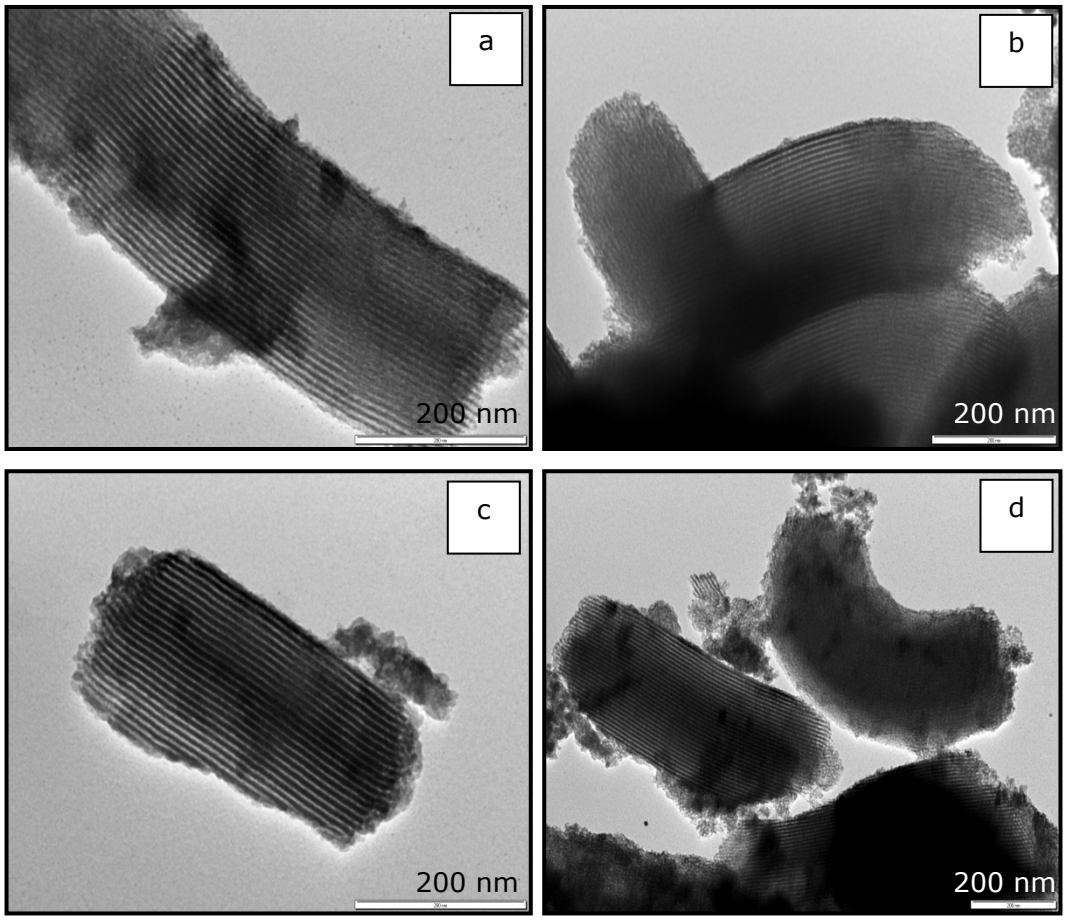


Figure 6.29 TEM images of (a) *ALS-0.2A,* (b) *ALS-0.2B*, (c) *ALS-0.03A* and (d) *ALS-0.03B*

## 6.3 Thermogravimetric Analyses

The thermogravimetry experiments were performed to test the activity of synthesized MCM-type and SBA-type catalysts in polypropylene cracking reaction under non-isothermal conditions under nitrogen flow, with a flow rate of 60 ml/min and with a constant heating rate of 5°C/min. Additionally, the activity of commercial *MCM-4*1 type mesostructured aluminosilicate catalyst was tested in the same reaction with the same analysis conditions.

### 6.3.1 Determination of Catalyst/Polymer Ratio

Before utilising the synthesized catalysts in polymer cracking reactions, catalyst/polymer ratio that will be used in degradation reaction was determined. For this purpose, the catalytic activity of commercial catalyst (PA) was tested at three different ratios. These ratios were 1/10, 1/5, and 1/2, decided according to the values used in literature [37, 109]. The TGA results are given in Figure 6.30.

The TGA results showed that when catalyst/polymer ratio was 1/10, the degradation started at 313°C (10% weight loss) and ended at 385°C (91% weight loss), on the other hand when the ratio increased to 1/5, degradation started at 292°C (10% weight loss) and ended at 386°C (81% weight loss) and when the ratio increased to 1/2, degradation started at 283°C (10% weight loss) and completed at around 340°C (71% weight loss). As a result, the catalyst/polymer ratio of 1/2 was chosen for polymer degradation reaction.

### 6.3.2 The TGA Results of the Mesoporous MCM-type Catalysts

Figure 6.31 illustrates the TGA plots resulting from both the catalytic and non-catalytic thermal cracking of polypropylene. All these TGA curves were drawn catalyst free. Table 6.7 gives the value of the temperature at which degradation starts. The results showed a marked reduction in the degradation temperature in the presence of aluminosilicate catalysts. In the absence of catalyst, degradation temperature was around 350°C. But this degradation temperature decreased to a lower value in the presence of most of the synthesized MCM-type catalysts (Figure 6.31) and these declines in temperature is in agreement with literature values [7].

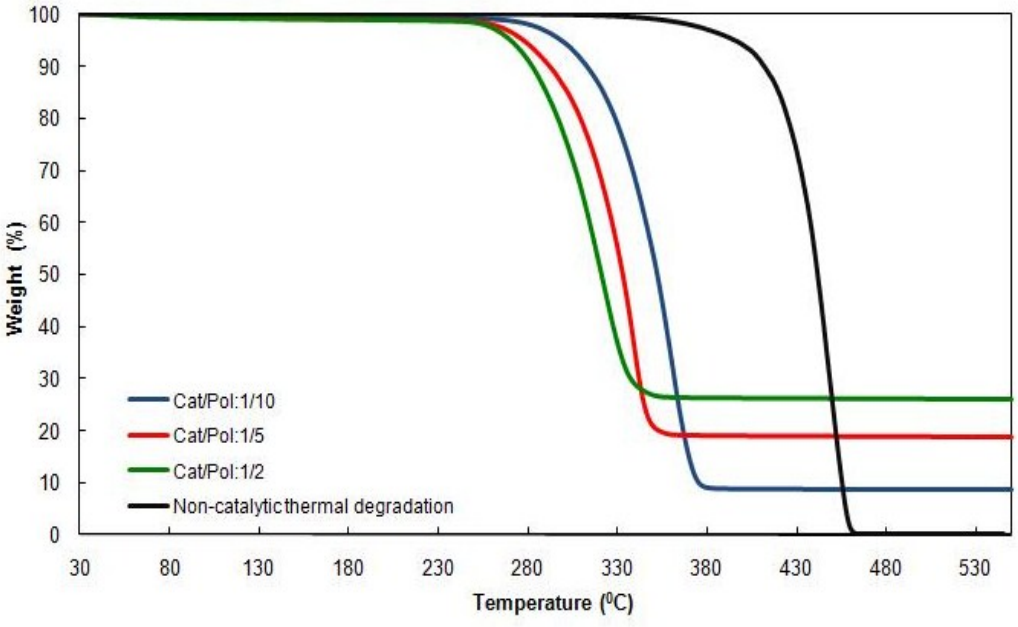


Figure 6.30 TGA curves obtained using different catalyst/polymer ratios

Table 6.7 Starting degradation temperatures of polypropylene in the presence of catalyst (at weight loss of 1%)

| Sample ID | Temperature (°C) |
|---|---|
| No Catalyst | 350 |
| MCM-41TB | 280 |
| Al-1A | 111 |
| Al-0.5A | 253 |
| Al-0.1A | 118 |
| Al-0.03A | 221 |
| Al-1B | 103 |
| Al-0.5B | 213 |
| Al-0.1B | 232 |
| Al-0.03A | 108 |

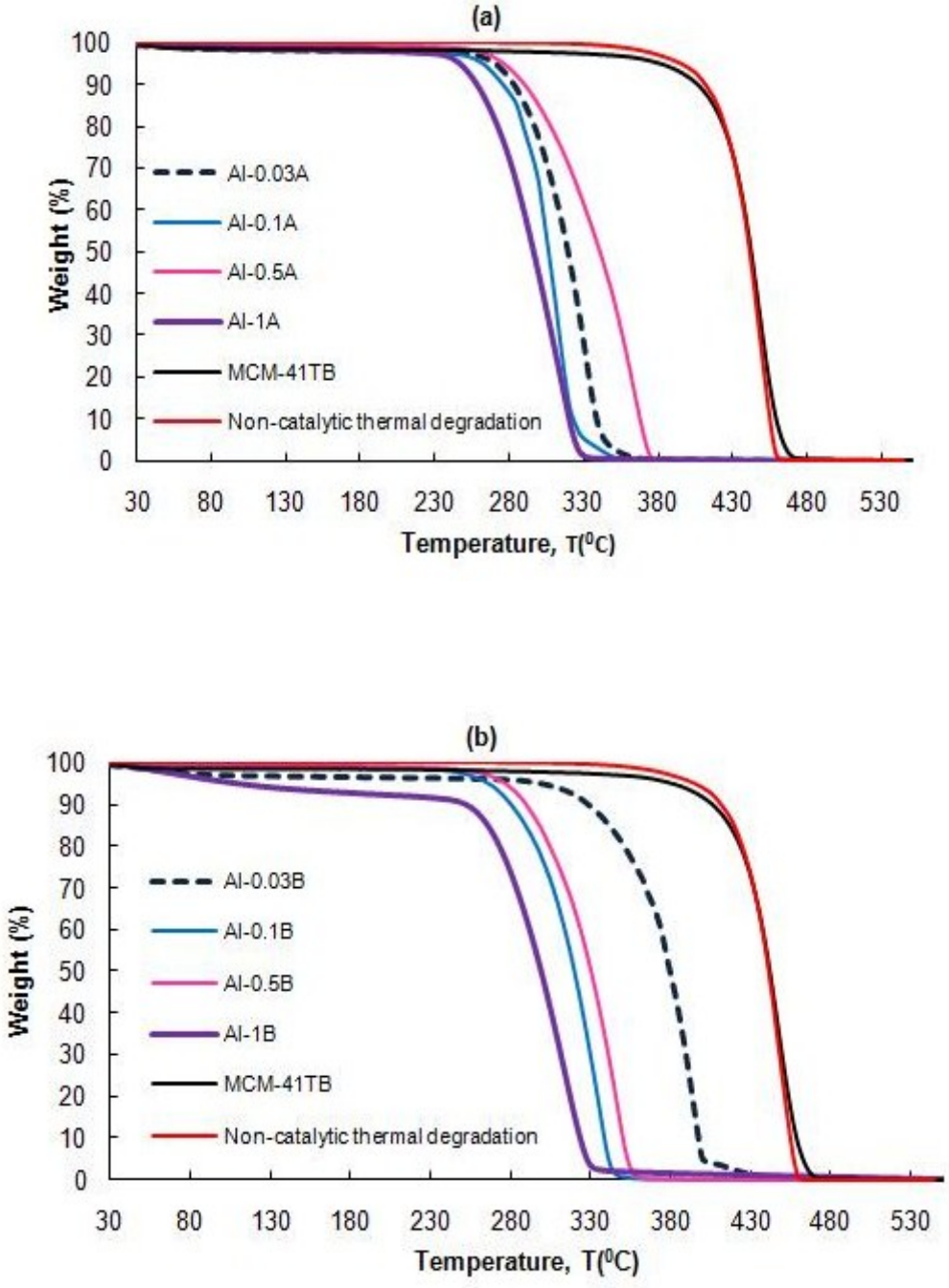


Figure 6.31 TGA plots describing the degradation of polypropylene over aluminum containing MCM-type catalysts synthesized using different aluminum sources; (a)$AlNO_3.9H_2O$ and (b)$C_9H_{21}AlO_3$

*Al-0.5A* and *Al-0.03B* catalysts showed somewhat less effective performance than the rest of the other catalysts. Decrease of Al/Si ratio is expected to cause a decrease in acidity of such catalysts and decrease of acidity is expected to have a negative effect on the activity of the catalyst for the cracking reactions. However, another important factor is the incorporation of the aluminum into the structure of these mesoporous catalysts. Degree of incorporation of Al into the catalyst structure and consequently the Al/Si ratio in the catalyst matrix are expected to have significant effects on the activity of such catalysts. Our results showed that even pure *MCM-41* exhibited an activity as the other catalysts in this polymer cracking reaction.

Using the TGA data the activation energy value of the polypropylene cracking reaction was also evaluated in the absence and presence of synthesized aluminosilicate catalyst following a similar procedure as reported in the literature [117], and it was given in Appendix D. The activation energy values are given in Table 6.8. The activation energy of the degradation reaction decreased significantly in the presence of aluminosilicate catalysts. In the case using aluminum nitrate as the aluminum source in the synthesis of the catalysts, the activation energy values of degradation were found to be decreased down to about 72-118 kJ/mol for catalysts having Al/Si ratios of 0.02-0.16 in the solid material, while the activation energy of decomposition of polypropylene in the absence of catalyst was about 172 kJ/mol. In the case of catalysts prepared using aluminum isopropoxide as the aluminum source activation energy values were obtained in the range of 68-126 kJ/mol. This might be caused by the less incorporation of aluminum into the *MCM-41* lattice during the synthesis, due to less solubility of this aluminum source than aluminum nitrate. Although *MCM-41TB* does not contain any aluminum, it also caused a decrease of activation energy from 172 kJ/mol to 143 kJ/mol.

Table 6.8 $E_A$ value for the degradation of polypropylene in the presence of MCM-type catalysts

| Sample ID | Activation Energy ($E_A$) Values (kJ/mol) |
|---|---|
| No catalyst | 172.0 |
| MCM-41TB | 142.8 |
| Al-1A | 71.8 |
| Al-0.5A | 118.1 |
| Al-0.1A | 104.7 |
| Al-0.03A | 107.9 |
| Al-1B | 67.5 |
| Al-0.5B | 81.9 |
| Al-0.1B | 86.9 |
| Al-0.03B | 125.7 |

### 6.3.3 The TGA Results of the Mesoporous SBA-type Catalysts

Figure 6.32 illustrates the TGA plots resulting from both the catalytic and non-catalytic thermal degradation of polypropylene. In the absence of catalyst, degradation temperature was around 350°C. But this degradation temperature decreased to a lower value in the presence of aluminum containing SBA-15 catalysts (Figure 6.32). Using the TGA data the activation energy value of the polypropylene degradation reaction was also evaluated in the absence and presence of synthesized aluminum containing *SBA-15* catalysts. The activation energy values are given in Table 6.9. The activation energy of the degradation reaction decreased significantly in the presence of aluminum containing *SBA-15* catalysts. In the case using aluminum isopropoxide as the aluminum source in the synthesis of the catalysts, activation energy values were obtained in the range of 53-89 kJ/mol for catalysts having Al/Si ratios of 0.026-0.67 in the solid material, while the activation energy of decomposition of polypropylene in the absence of catalyst was about 172 kJ/mol. In the case using aluminum sulphate as the aluminum source in the synthesis of the catalysts, the activation energy values of degradation were found to be decreased down to about 51-80 kJ/mol.

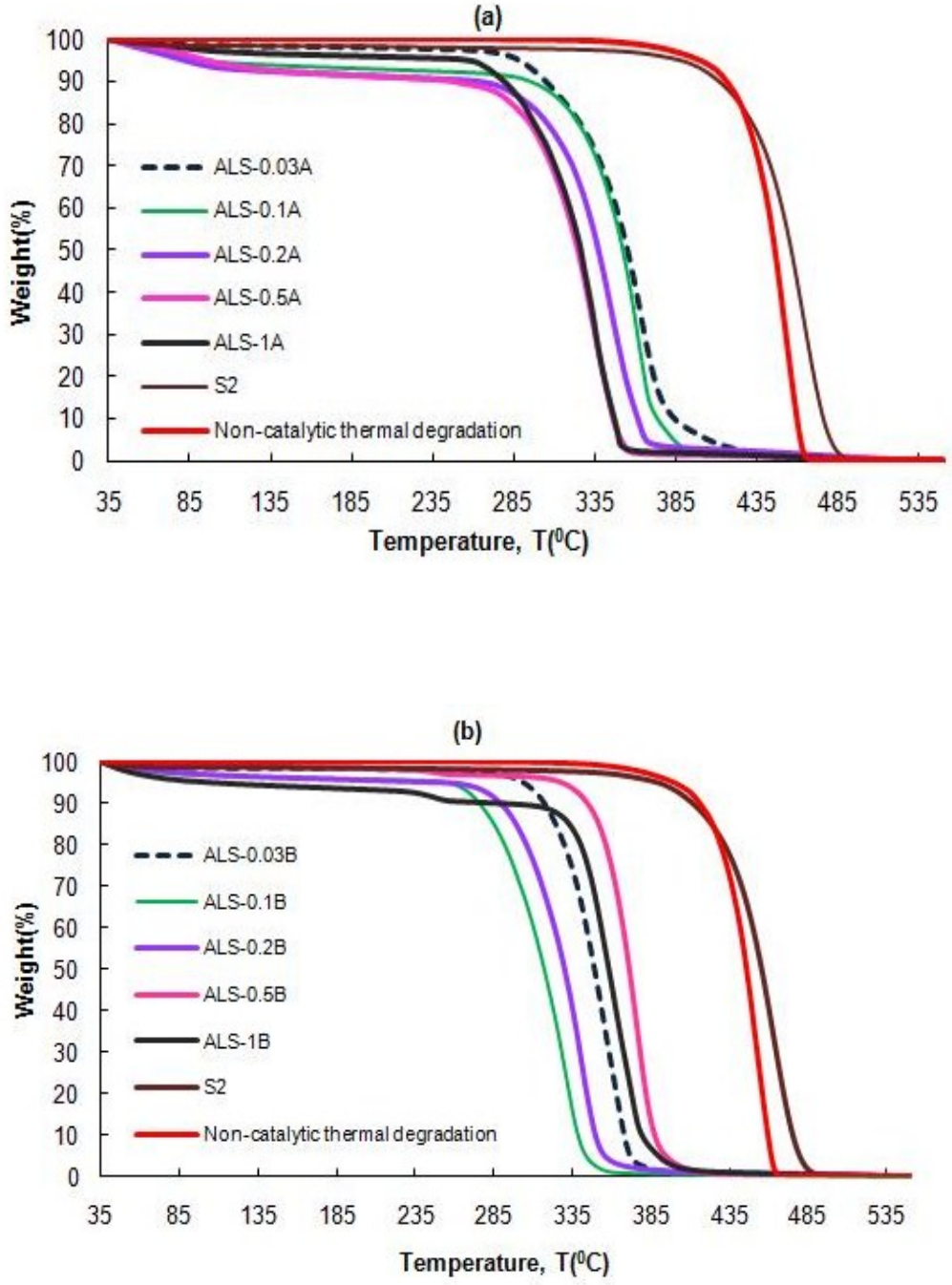


Figure 6.32 TGA plots describing the degradation of polypropylene over SBA-type catalysts synthesized using different aluminum sources: (a) $Al_2(SO_4)_3.18H_2O$, and (b)$C_9H_{21}AlO_3$

Table 6.9 $E_A$ value for the degradation of polypropylene in the presence of SBA-type catalysts

| Sample ID | Activation Energy ($E_A$) values(kJ/mol) |
|---|---|
| No catalyst | 172.0 |
| S2 | 139.7 |
| ALS-0.03A | 69.9 |
| ALS-0.1A | 56.1 |
| ALS-0.2A | 50.7 |
| ALS-0.5A | 67.8 |
| ALS-1A | 79.6 |
| ALS-0.03B | 89.2 |
| ALS-0.1B | 86.3 |
| ALS-0.2B | 81.9 |
| ALS-0.5B | 80.2 |
| ALS-1B | 53.1 |

All these results showed that increase of Al/Si ratio is expected to cause an increase in acidity of such catalysts and increase of acidity is expected to have a positive effect on the activity of the catalyst for the degradation reactions. However, another important factor is the incorporation of the aluminum into the structure of these mesoporous catalysts. Degree of incorporation of Al into the catalyst structure and consequently the Al/Si ratio in the catalyst matrix are expected to have significant effects on the activity of such catalysts. Although, pure SBA-15 (*S2*) did not show a good catalytic activity, it caused a decrease of activation energy from 172 kJ/mol to 140 kJ/mol.

## 6.4 Polymer Degradation Reaction System

Firstly, the non-catalytic thermal degradation reactions were carried out in polymer degradation reaction system. For this purpose, 1 g of polypropylene was loaded to the reactor before each run. The reaction was carried out under isothermal conditions under nitrogen, with a flow rate of 60 ml/min and a heating rate of 5°C/min. Non-catalytic pyrolysis experiments were performed

at a temperature range of 400-425°C and different reaction times (15, 30, 45 and 60 minutes). The amounts of solid residue and products produced at the end of non-catalytic thermal degradation reaction are given in Table 6.10. In this table, the amount of solid residue and liquid products were found by weighing them at the end of the reaction and the amount of gas products was found by taking the difference between the initial polymer amount (1 g) placed inside the reactor and the total amount of solid residue and liquid products.

Table 6.10 Amounts of products and solid residue at different reaction temperatures and reaction times

| **Reaction Temperature ($^0$C)** | **Reaction Time (min)** | **Gas (g)** | **Liquid (g)** | **Solid residue (g)** |
|---|---|---|---|---|
| 400 | 30 | 0.60 | 0 | 0.40 |
| | 45 | 0.58 | 0.15 | 0.27 |
| | 60 | 0.64 | 0.24 | 0.12 |
| 410 | 15 | 0.64 | 0.12 | 0.24 |
| | 30 | 0.67 | 0.31 | 0.02 |
| 425 | 15 | 0.42 | 0.58 | 0 |
| | 30 | 0.33 | 0.67 | 0 |

According to these results, with an increase in the reaction temperature and reaction time the amount of the liquid product increased while the amount of solid residue significantly decreased. When the reaction time was 15 minutes the amount of gas product decreased while liquid products increased with an increase in the reaction temperature from 410°C to 425°C. When the reaction time was increased to 30 minutes, the amount of gas product increased slightly and then decreased while the amount of liquid products increased significantly with an increase in temperature. This is probably due to the increase in the formation of heavy products (liquid) at high temperatures. Additionally, at 400°C, when the reaction time was increased from 30 minutes to higher values, the amount of liquid products increased, but solid residue

decreased. On the other hand, the amount of gas products did not change so much (Table 6.10).

At the end of these non-catalytic thermal degradation reactions, both gas and liquid products were analysed qualitatively and quantitatively. The gaseous products obtained in non-catalytic thermal degradation of polypropylene reaction are given in Table 6.11.

Table 6.11 The gaseous products obtained from the non-catalytic thermal degradation of polypropylene

| Rxn temperature | 400°C | | | 410°C | | 425°C | |
|---|---|---|---|---|---|---|---|
| Rxn time (min) | 30 | 45 | 60 | 15 | 30 | 15 | 30 |
| Methane ($CH_4$) | - | - | - | - | - | ✓ | ✓ |
| Ethane ($C_2H_6$) | ✓ | ✓ | - | ✓ | ✓ | ✓ | ✓ |
| Acetylene ($C_2H_2$) | - | - | - | - | - | ✓ | ✓ |
| Ethylene ($C_2H_4$) | ✓ | ✓ | ✓ | ✓ | ✓ | ✓ | ✓ |
| Propylene ($C_3H_6$) | ✓ | ✓ | ✓ | ✓ | ✓ | ✓ | ✓ |
| Butane (n-$C_4H_{10}$) | - | - | - | - | - | - | ✓ |

From this table, it can be concluded that both $CH_4$ and $C_2H_2$ formed when reaction temperature was increased to 425°C and at this temperature n-$C_4H_{10}$ was formed when the reaction time was increased from 15 minutes to 30 minutes. $C_2H_6$, $C_2H_4$ and $C_3H_6$ gases were observed in the studied reaction temperature range.

For the calculation of mole and weight fractions of these gas products, calibration experiments were done to obtain the calibration factors of each gas product. A sample calculation to determine calibration factors of gaseous products are given in Appendix E. After the calculation of calibration factors, the mole and weight fractions and selectivities of gas products were calculated. A sample calculation was given in Appendix F. Tabulated values of

mole and weight fractions and selectivities of gas products obtained at different temperatures and reaction times are given in Appendix G.

The variation of mole fractions and selectivities of gas products at 400°C and different reaction times is given in Figures 6.33 and 6.34. The results showed that selectivity of ethane decreased from 0.06 to 0 when the reaction time was increased to 60 minutes. On the other hand, the selectivity of ethylene increased from 0.61 to 0.75 when the reaction time was increased from 45 minutes to 60 minutes. Additionally, the selectivity of propylene decreased from 0.33 to 0.25 when the reaction time was increased to 60 minutes. Finally, carrying out the degradation reaction for 30 minutes or 45 minutes did not have any significant effect on both selectivity and fraction of gas products. As a conclusion, for the non-catalytic thermal degradation of polypropylene which was carried out at 400°C, ethylene is highly selective.

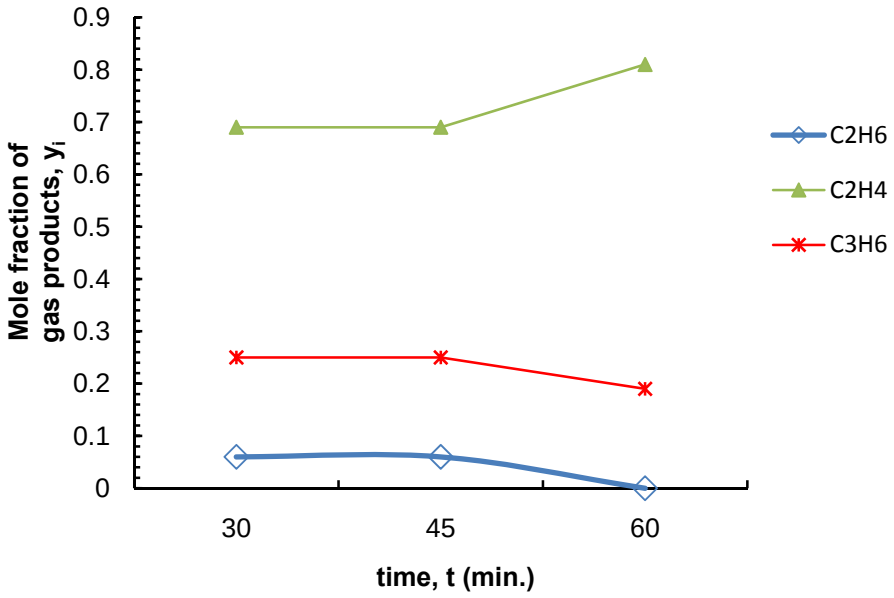


Figure 6.33 Variation of gas product mole fraction with respect to reaction time at 400°C in the non-catalytic thermal degradation of PP

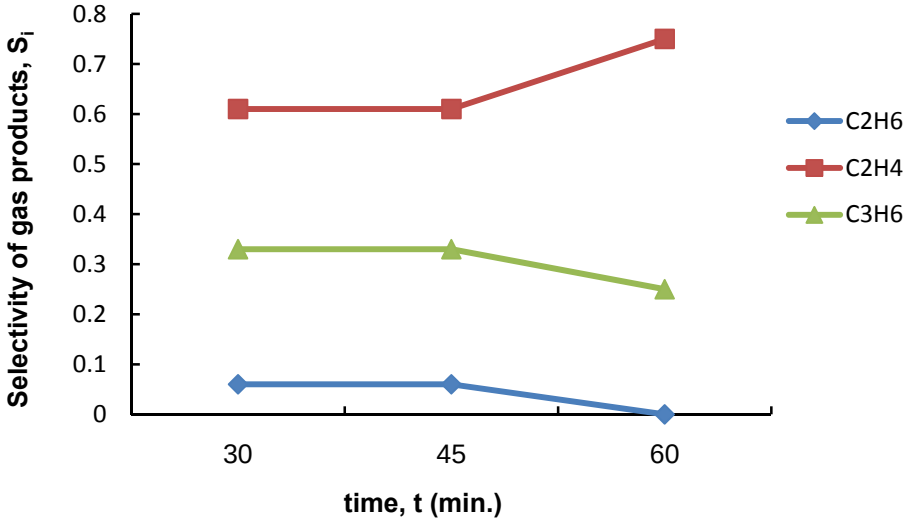


Figure 6.34 Variation of gas product selectivity with respect to reaction time at 400°C in the non-catalytic thermal degradation of PP

Variation of gas product mole fractions and selectivities at 30 minutes of reaction time and different reaction temperatures are given in Figures 6.35 and 6.36. The results showed that the mole fraction of methane, butane and acetylene gases increased with temperature. On the other hand, the amount of ethane remained constant with an increase in reaction temperature. The fraction of propylene increased significantly and then reached a constant value. Finally, the mole fraction of ethylene decreased with an increase in temperature (Figure 6.35).

The results given in Figure 6.36 showed that the selectivity of methane, butane and acetylene gases increased with temperature. On the other hand, ethane selectivity remained constant with an increase in reaction temperature. The selectivity of propylene increased significantly when the reaction temperature was raised from 400°C to 410°C but it decreased slightly when the temperature was raised to 425°C. Finally, the ethylene selectivity decreased with an increase in temperature and became constant (Figure 6.36).

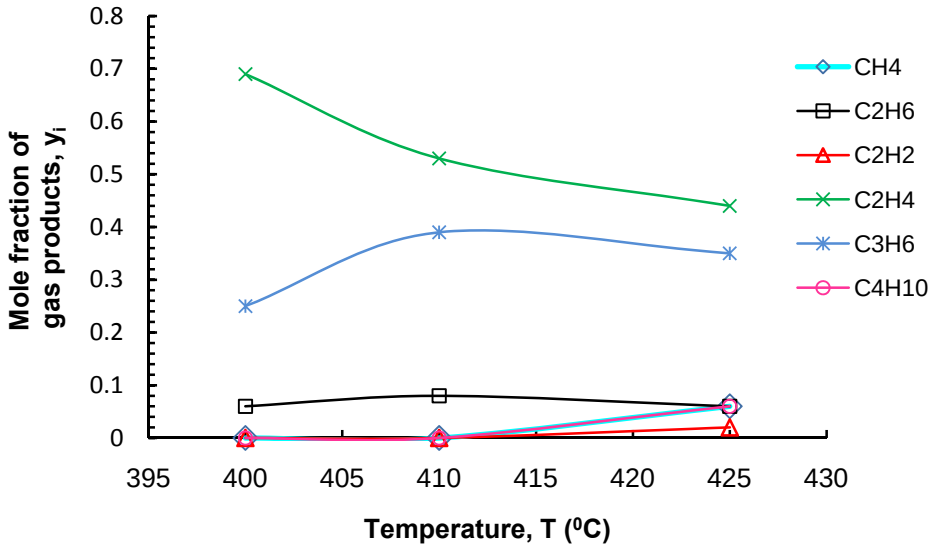


Figure 6.35 Variation of gas product mole fractions with respect to reaction temperature (t:30 minutes)

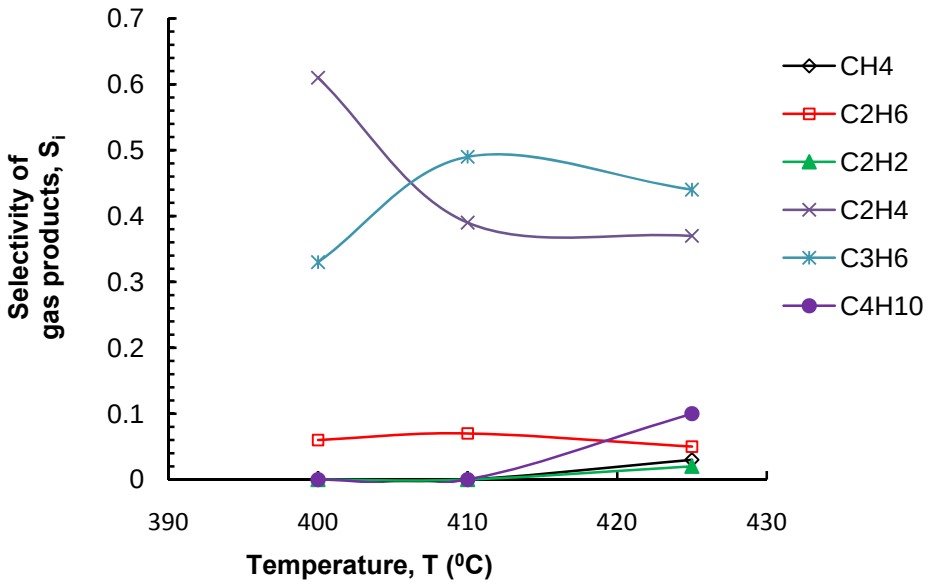


Figure 6.36 Variation of gas product selectivities with respect to reaction temperature (t:30 minutes)

After performing the non-catalytic thermal degradation reactions, catalytic degradation reactions were carried out in the same reaction system. 1 g of PP was used and the ratio of the catalyst/polymer ratio was taken as 1/2 according to the thermogravimetric analysis results given in part 6.3.1. The reaction was carried out under isothermal conditions under nitrogen, with a flow rate of 60 ml/min and a heating rate of 5°C/min. The catalysts were selected according to the activation energy results given in Tables 6.8 and 6.9. The catalysts which mostly decreased the activation energy were used in degradation reaction and the list of these catalysts was given in Table 5.6. Since in the non-catalytic thermal degradation reaction experiments, reaction temperature 425°C corresponded to 20% weight loss of the polymer and catalyst mixture, the temperatures corresponding 20% weight loss were taken as the reaction temperature in the catalytic experiments. These temperatures were determined using TGA plots (Figure 6.31 & 6.32). In all these catalytic reactions, the time was taken as 30 minutes and kept constant in all catalytic experiments. The amounts of gas and liquid products produced at the end of catalytic thermal degradation reactions are given in Table 6.12. To make a reasonable comparison, the results of non-catalytic degradation reaction performed at 425°C are also given in this table. In all catalytic experiments, no solid residue remained inside the reactor.

Table 6.12 Amounts of gas & liquid products obtained from pyrolysis reactions

| **Catalyst ID** | **Reaction Temperature (°C)** | **Amount of products (gr)** | |
|---|---|---|---|
| | | **gas** | **liquid** |
| No catalyst | 425 | 0.33 | 0.67 |
| Al-0.03A | 305 | 0.70 | 0.30 |
| Al-1A | 275 | 0.82 | 0.18 |
| Al-0.03B | 360 | 0.69 | 0.31 |
| Al-1B | 285 | 0.68 | 0.32 |
| ALS-0.1A | 330 | 0.76 | 0.24 |
| ALS-0.2A | 315 | 0.78 | 0.22 |
| ALS-0.1B | 300 | 0.77 | 0.23 |
| ALS-1B | 345 | 0.77 | 0.23 |

The results showed that using aluminum containing catalyst caused a significant increase in the amount of gas products and a significant decrease in the amount of liquid products. Catalyst in the reaction medium decomposed the heavy compounds to form smaller compounds (# of C atom<5) therefore the amount of gaseous products increased significantly in the presence of catalyst [7, 43]. Sakata and his co-workers [54] also observed the same trend in polypropylene degradation reaction in the presence of silica-alumina catalysts. Decrease in the amount of gas products was significant in the presence of *Al-xB* catalysts with respect to the amount of gas product obtained in the presence other catalysts.

At the end of the catalytic thermal degradation reactions, both gas and liquid products were analysed qualitatively and quantitatively, as done in non-catalytic part. The gaseous products obtained from the catalytic thermal degradation reactions are given in Table 6.13.

Table 6.13 The gaseous products obtained from the catalytic thermal degradation of polypropylene (t:30 min.)

| **Gaseous Products** | **CATALYST ID** | | | | | | | |
|---|---|---|---|---|---|---|---|---|
| | Al-0.03A | Al-1A | Al-0.03B | Al-1B | ALS-0.1A | ALS-0.2A | ALS-0.1B | ALS-1B |
| Methane ($CH_4$) | - | - | - | - | - | - | - | - |
| Ethane ($C_2H_6$) | - | - | - | - | - | - | - | - |
| Acetylene ($C_2H_2$) | - | - | - | - | - | - | - | - |
| Ethylene ($C_2H_4$) | ✓ | ✓ | ✓ | ✓ | ✓ | ✓ | ✓ | ✓ |
| Propylene ($C_3H_6$) | ✓ | ✓ | ✓ | ✓ | ✓ | ✓ | ✓ | ✓ |
| n-butane($C_4H_{10}$) | ✓ | ✓ | - | ✓ | ✓ | ✓ | ✓ | ✓ |
| i-butane ($C_4H_{10}$) | ✓ | ✓ | - | ✓ | ✓ | ✓ | - | - |

From this table, it can be said that in the presence of aluminum containing catalysts, methane, ethane and acetylene were not formed. When MCM- type catalysts synthesized using aluminum nitrate were used, $C_2H_4$, $C_3H_6$, n-$C_4H_{10}$ and i-$C_4H_{10}$ were observed as products. When aluminum isopropoxide was used as aluminum source and Al/Si ratio was kept at 0.03, only ethylene and propylene gases were formed. When SBA-type catalysts synthesized using

aluminum sulphate was used, $C_2H_4$, $C_3H_6$, n-$C_4H_{10}$ and i-$C_4H_{10}$ were formed as products. Formation of iso-butane was not observed when aluminum isopropoxide was used as the aluminum source in the synthesis of SBA-type catalysts.

The tabulated values of mole & weight fractions and selectivities of gas products obtained in the presence of catalysts in 30 minutes are given in Appendix G and the variation of gas product mole fractions with respect to aluminum loading and aluminum source in the presence of catalyst is given in Figure 6.37. The results showed that MCM-type catalysts synthesized using aluminum nitrate caused a significant increase in the amount of ethylene when Al/Si ratio was increased from 0.03 to 1. On the other hand, these catalysts caused a significant decrease in the amount of propylene, n-butane and i-butane. When aluminum isopropoxide contained MCM-type catalysts were used in degradation reaction, the amount of ethylene and propylene decreased and formation of n-butane and i-butane was observed with an increase in Al/Si ratio.

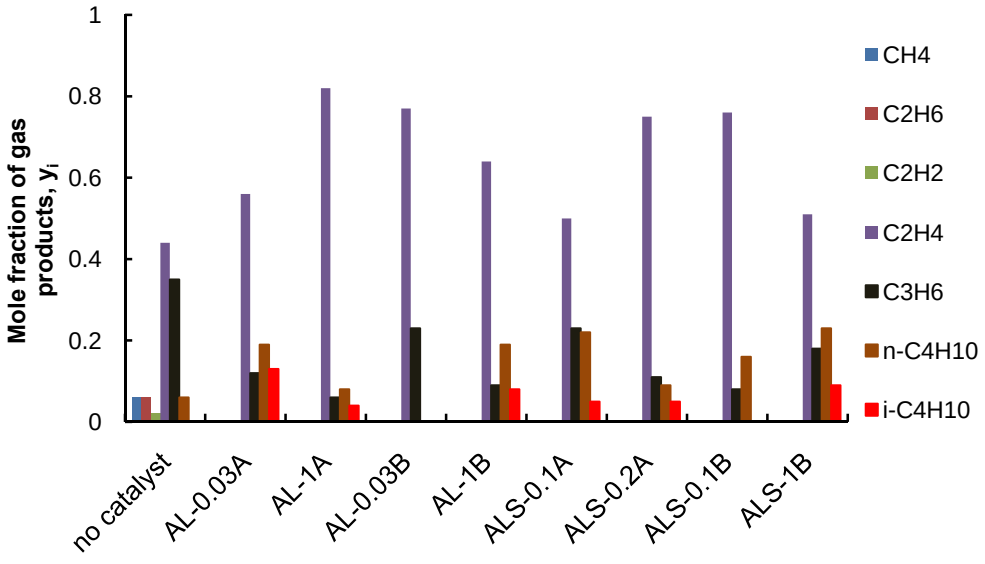


Figure 6.37 Variation of gas mole fractions with respect to aluminum loading and aluminum source in the presence of catalyst ($t_{rxn}$: 30 min)

In the case of using SBA-type catalysts synthesized using aluminum sulphate, the fraction of ethylene increased and the fraction of propylene and n-butane decreased significantly with an increase in Al/Si ratio. On the other hand, the fraction of i-butane remained almost same. When aluminum isopropoxide was used as the aluminum source in the synthesis of aluminum containing SBA-type catalysts, the fraction of ethylene decreased significantly with an increase in Al/Si ratio. On the other hand, the fraction of propylene, n-butane and i-butane increased with an increase in Al/Si ratio.

The variation of gas product selectivities with respect to aluminum loading and aluminum source in the presence of catalyst is given in Figure 6.38. While propylene selectivity was high in the non-catalytic thermal degradation reaction, its selectivity decreased and ethylene selectivity increased significantly in the presence of *Al-1A, Al-0.03B, ALS-0.2A and ALS-0.1B*.

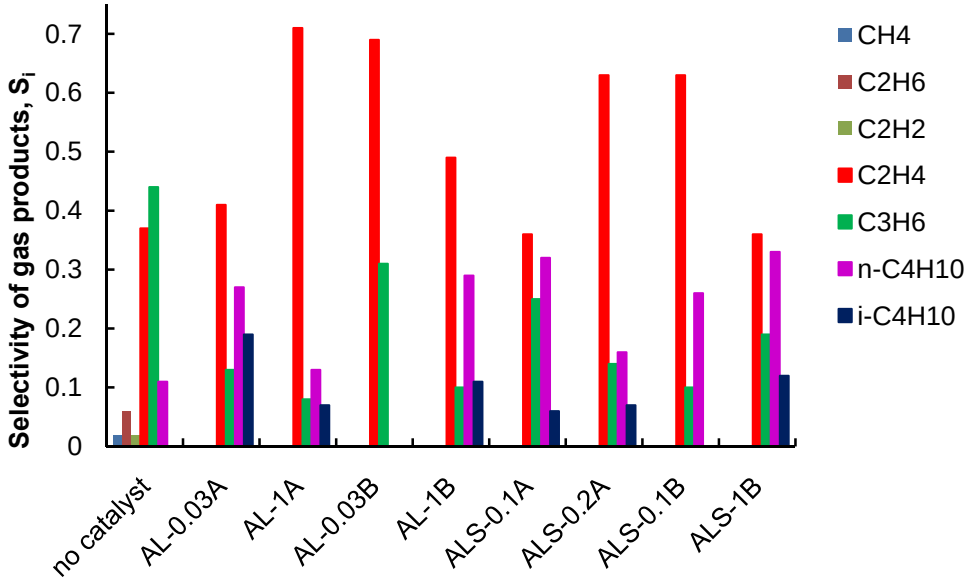


Figure 6.38 Variation of gas selectivities with respect to aluminum loading and aluminum source in the presence of catalyst ($t_{rxn}$: 30 min.)

When aluminum nitrate was used as the aluminum source in the synthesis of MCM-type catalyst, the ethylene selectivity increased significantly with an increase in Al/Si ratio. The amount of aluminum in *Al-1A* is approximately 10 times greater than the amount of aluminum in *Al-0.03* (Table 6.3), therefore increasing the amount of aluminum in catalyst structure increases its acidity [10, 11] and an increase in acidity may cause a rise in ethylene selectivity. When aluminum isopropoxide contained MCM-type catalysts were used, the ethylene and propylene selectivity decreased significantly and n-butane and i-butane selectivity increased Al/Si ratio was raised from 0.03 to 1. Same trend was observed for ethylene selectivity in aluminum containing SBA-type catalysts. In this group, when aluminum isopropoxide was used in the synthesis of SBA-type catalyst, ethylene selectivity decreased with an increase in Al/Si ratio. In Figure 6.27b, both Lewis and Brönsted acid sites became smaller with an increase in Al/Si ratio, so decrease in acidity might cause this decrease in ethylene selectivity.

As a conclusion, both MCM-type and SBA-type catalysts were ethylene selective and these highly ethylene selective catalysts are good for petrochemical industry. For instance, in PETKİM-Aliağa (İzmir/TURKEY) ethylene is used for the production of monoethylene glycol (MEG) and diethylene glycol (DEG) and these products are used in the production of anti-freeze, polyester fibers, plastic bottles and textile products [118].

After a comprehensive analysis of gases, liquid products of degradation reaction were analyzed, extensively. Before carrying out the analyses, calibration experiments were done in order to identify and determine the calibration factors of liquid products. Since there were lots of peaks (>150) in liquid product chromatograms, major peaks and some minor peaks were identified. The other peaks were assumed to belong to isomeric compounds of identified compounds. A sample calculation to determine calibration factors of liquid products are given in Appendix H. Firstly, the liquid products obtained at the end of the non-catalytic thermal degradation reactions were analysed and they are given in terms of total carbon numbers in Table 6.14. From this table, heavy hydrocarbons ($C_n \geq 11$) formed in all temperatures. At 400°C and

425°C, $C_5$, $C_6$, $C_7$, $C_8$ and $C_9$ formation were observed. Finally, at 410°C only heavy hydrocarbons formed ($C_n \geq 11$) at both 15 and 30 minutes reactions.

Table 6.14 The liquid products obtained in the non-catalytic thermal degradation of polypropylene

| Rxn temperature (°C) | 400 | | 410 | | 425 | |
|---|---|---|---|---|---|---|
| Rxn time (min) | 45 | 60 | 15 | 30 | 15 | 30 |
| $C_5$ | ✓ | ✓ | - | - | ✓ | ✓ |
| $C_6$ | ✓ | ✓ | - | - | ✓ | ✓ |
| $C_7$ | - | - | - | - | - | ✓ |
| $C_8$ | ✓ | ✓ | - | - | ✓ | ✓ |
| $C_9$ | ✓ | ✓ | - | - | ✓ | ✓ |
| $C_{10}$ | ✓ | ✓ | ✓ | - | ✓ | ✓ |
| $C_{11}$ | ✓ | ✓ | ✓ | ✓ | ✓ | ✓ |
| $C_{12}$ | ✓ | ✓ | ✓ | ✓ | ✓ | ✓ |
| $C_{13}$ | ✓ | ✓ | ✓ | ✓ | ✓ | ✓ |
| $C_{14}$ | ✓ | ✓ | ✓ | ✓ | ✓ | ✓ |
| $C_{16}$ | ✓ | ✓ | ✓ | ✓ | ✓ | ✓ |
| $C_{18}$ | ✓ | ✓ | ✓ | ✓ | ✓ | ✓ |

After the calculation of calibration factors, the mole and weight fractions and selectivities of liquid products were calculated according to the sample calculation given in Appendix F. Variation of liquid product mole fractions with respect to reaction time at different reaction temperatures are given in Figures 6.39, 6.40 and 6.41. Their tabulated values are given in Appendix I and typical GC spectra are given in Appendix J. According to these results, at 400°C, the amounts of $C_5$, $C_{11}$, $C_{12}$, $C_{14}$, $C_{16}$ and $C_{18}$ hydrocarbons decreased and the amounts of $C_6$ and $C_8$ increased with an increase in time. Additionally, at this temperature, the amount of $C_9$ did not change with an increase in time and very few amount of $C_{10}$ formed at this temperature (Figure 6.39).

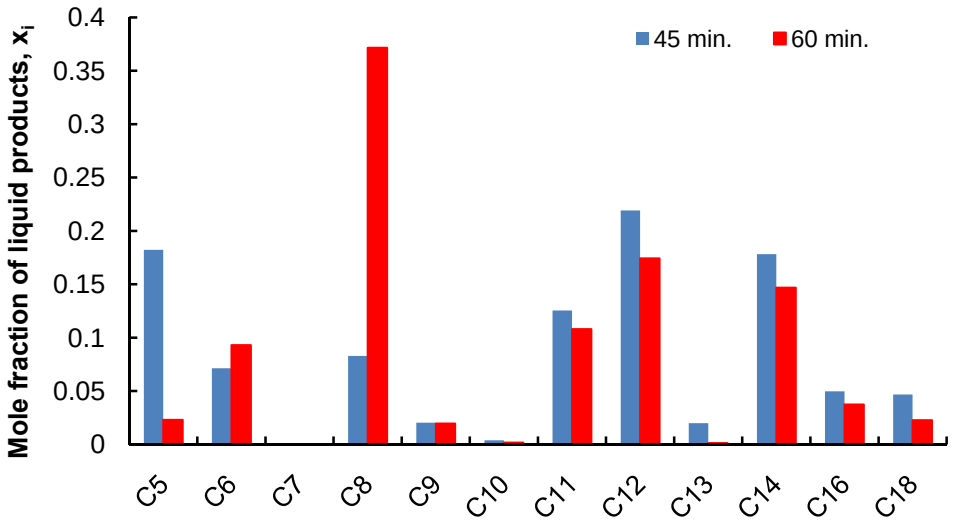


Figure 6.39 Variation of liquid product mole fractions with respect to reaction time at 400°C in the non-catalytic thermal degradation of PP

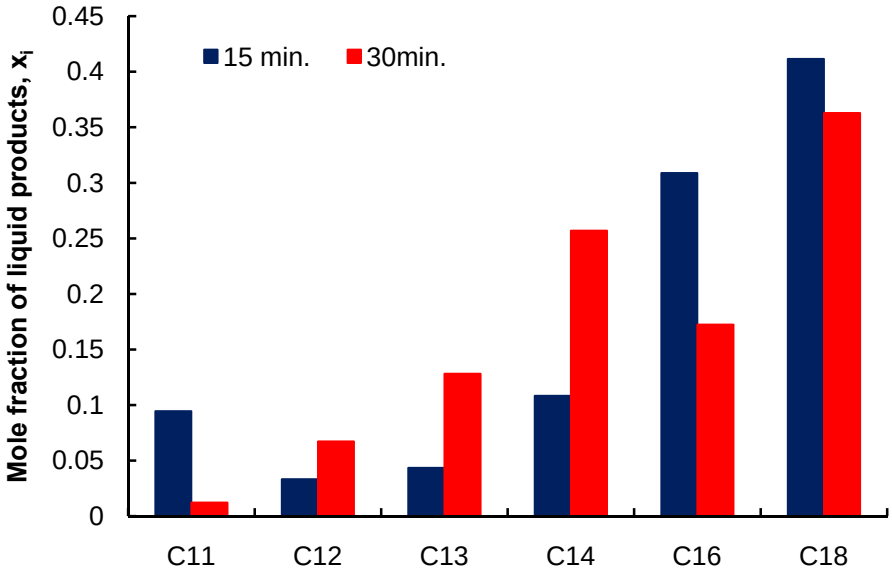


Figure 6.40 Variation of liquid product mole fractions with respect to reaction time at 410°C in the non-catalytic thermal degradation of PP

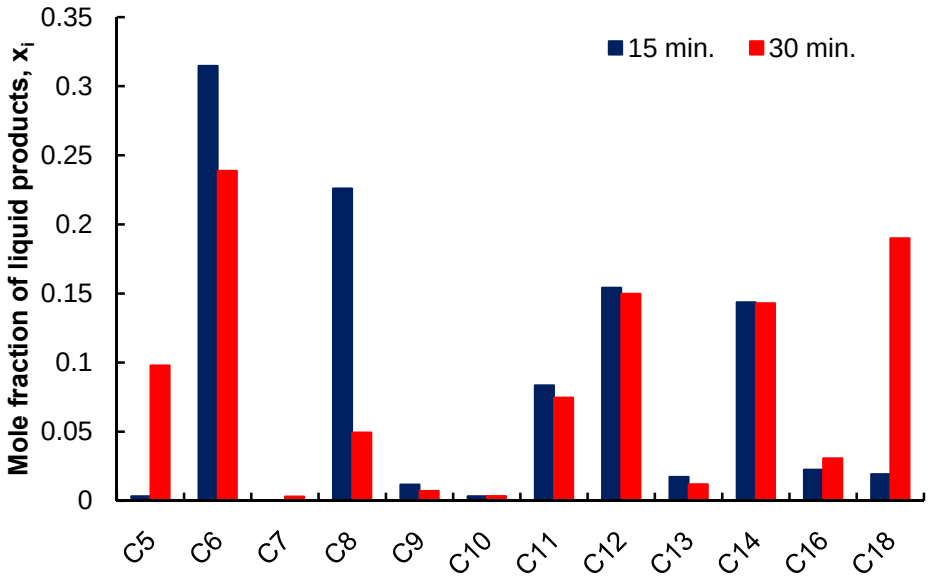


Figure 6.41 Variation of liquid product mole fractions with respect to reaction time at 425°C in the non-catalytic thermal degradation of PP

When the reaction was carried out at 410°C, heavy hydrocarbon formation ($C_n \geq 11$), especially $C_{16}$ and $C_{18}$, was observed. With an increase in reaction time from 15 minutes to 30 minutes, amounts of $C_{12}$-$C_{14}$ hydrocarbons increased, on the other hand the amounts of $C_{11}$, $C_{16}$ and $C_{18}$ hydrocarbons started to decrease (Figure 6.40).

When the reaction temperature was increased to 425°C, the amounts of $C_5$ and $C_{18}$ increased and $C_6$ and $C_8$ decreased significantly with an increase in reaction time. On the other hand, the amounts of $C_{11}$, $C_{12}$ and $C_{14}$ remained almost same with an increase in time. Additionally, few amount of $C_{16}$ formed at 400°C and 425°C, but its amount increased when the reaction was carried out at 410°C. Finally, very few amounts of $C_9$ and $C_{10}$ formed at 425°C.

At 15 minutes of reaction time, the amount of $C_{12}$ and $C_{14}$ hydrocarbons increased and the amount of $C_{16}$-$C_{18}$ hydrocarbons decreased with an increase in temperature. These results showed that heavier hydrocarbons started to

crack within 15 minutes of reaction when temperature was raised from 410°C to 425°C. On the other hand, no liquid product was obtained before 45 minutes when the reaction temperature was kept at 400°C. As a conclusion, in the non-catalytic degradation of polypropylene, it will be better to keep the temperature above 400°C to obtain liquid hydrocarbons within 15 minutes of reaction (Figures 6.40 & 6.41).

Finally, variations of the product selectivities with respect to reaction temperature are given in Figures 6.42 - 6.44. At 400°C, $C_6$ and $C_8$ selectivity increased and $C_5$ selectivity decreased significantly with an increase in the reaction time. On the other hand, $C_{11}$-$C_{18}$ hydrocarbon selectivities decreased when the reaction time was increased from 45 minutes to 60 minutes. Additionally, $C_9$ selectivity did not change with an increase in time. As a conclusion, the non-catalytic thermal degradation of PP which was carried out at 400°C for 60 minutes is highly $C_8$ selective.

At 410°C, $C_{12}$, $C_{13}$ and $C_{18}$ selectivities increased with an increase in the reaction time (Figure 6.43). On the other hand, $C_{11}$, $C_{14}$ and $C_{16}$ selectivities decreased with the reaction time. Alkanes from nonane to hexadecane (cetane) form the major part of diesel and aviation fuel and alkanes from hexadecane to upwards ($C_{18}$) form the most important components of fuel oil and lubricating oil [119]. As a conclusion, higher $C_{16}$ and $C_{18}$ selectivities in 15 minute reaction can be favorable for petroleum industry.

At 425°C, $C_{12}$, $C_{14}$, $C_{16}$ and $C_{18}$ selectivities increased significantly with an increase in the reaction time. Also, smaller hydrocarbons like $C_5$ selectivities increased when the reaction was performed for 30 minutes. On the other hand, $C_8$, $C_{10}$, $C_{11}$ and $C_{13}$ selectivities decreased significantly with an increase in reaction time. Additionally, selectivity of $C_{16}$ did not change so much with time. As a conclusion, this temperature is highly $C_{18}$ selective as observed in results of degradation reaction carried out at 410°C.

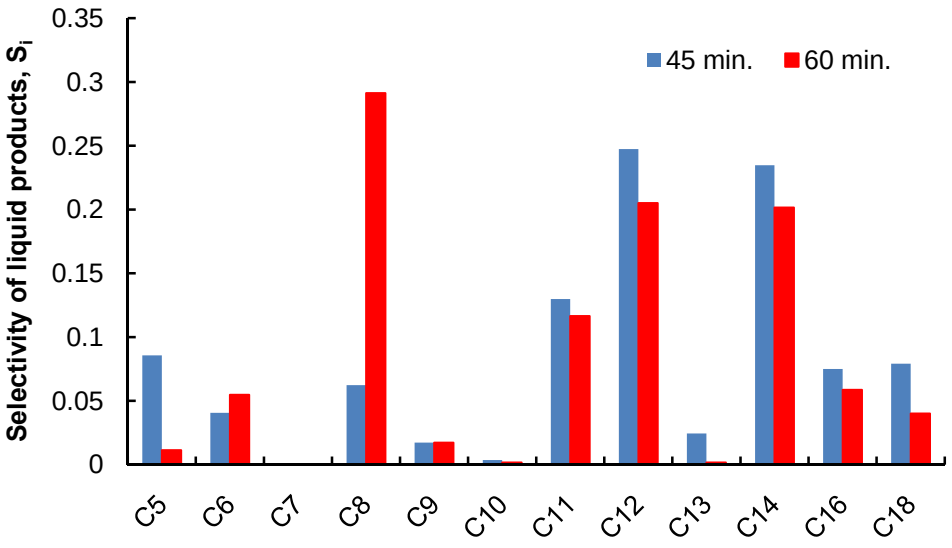


Figure 6.42 Variation of liquid product selectivities with respect to reaction time at 400°C in the non-catalytic thermal degradation of PP

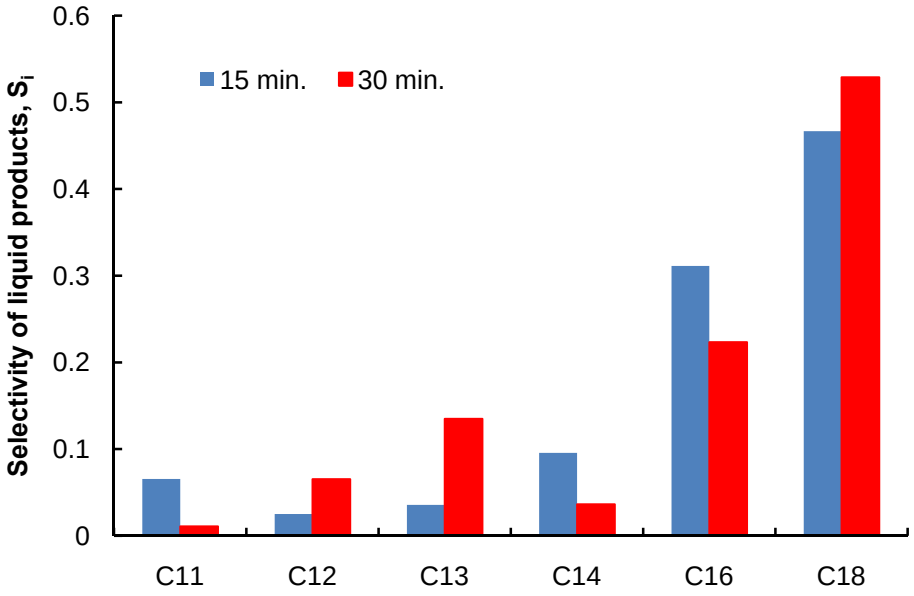


Figure 6.43 Variation of liquid product selectivities with respect to reaction time at 410°C in the non-catalytic thermal degradation of PP

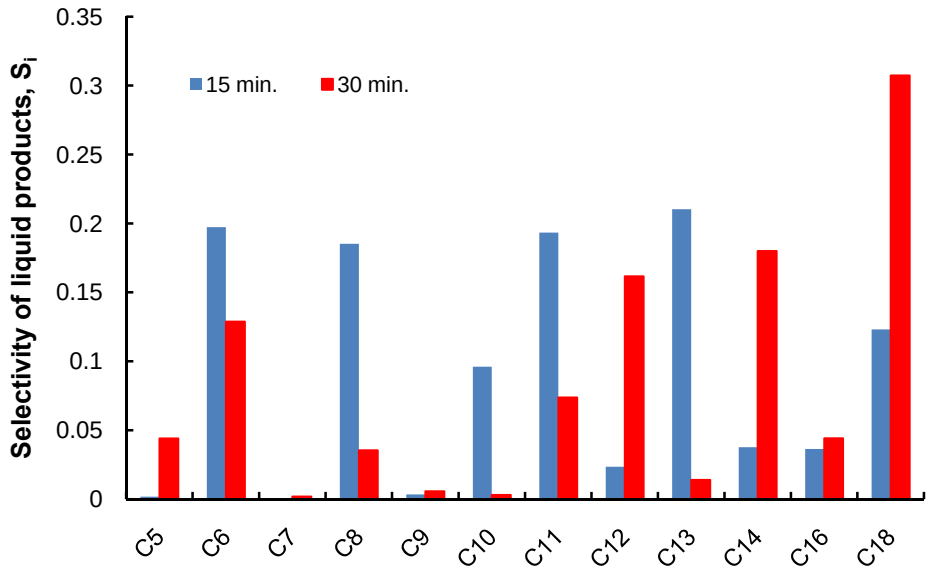


Figure 6.44 Variation of liquid product selectivities with respect to reaction time at 425°C in the non-catalytic thermal degradation of PP

After analyzing liquid products of the non-catalytic degradation reactions, liquid products of catalytic degradation reactions were analysed qualitatively and quantitatively. The liquid products obtained in these catalytic thermal degradation reactions are given in Table 6.15. According to this table, $C_5$ formed in the presence of MCM-type catalysts synthesized using aluminum isopropoxide as the aluminum source. $C_6$ formation was observed only in the presence of MCM-type catalysts synthesized at low aluminum loadings and in the presence of SBA-type catalysts. Almost all the other hydrocarbons formed in the absence and in the presence of catalyst were same.

Table 6.15 The liquid products obtained from the catalytic thermal degradation of polypropylene (t:30 min.)

| Liquid Products | CATALYST ID | | | | | | | |
|---|---|---|---|---|---|---|---|---|
| | Al-0.03A | Al-1A | Al-0.03B | Al-1B | ALS-0.1A | ALS-0.2A | ALS-0.1B | ALS-1B |
| $C_5$ | ✓ | - | ✓ | ✓ | ✓ | - | - | ✓ |
| $C_6$ | ✓ | - | ✓ | - | ✓ | ✓ | ✓ | ✓ |
| $C_7$ | ✓ | ✓ | ✓ | ✓ | ✓ | ✓ | ✓ | ✓ |
| $C_8$ | ✓ | ✓ | ✓ | ✓ | ✓ | ✓ | ✓ | ✓ |
| $C_9$ | ✓ | ✓ | ✓ | ✓ | ✓ | ✓ | ✓ | ✓ |
| $C_{10}$ | ✓ | ✓ | ✓ | ✓ | ✓ | ✓ | ✓ | ✓ |
| $C_{11}$ | ✓ | ✓ | ✓ | ✓ | ✓ | ✓ | ✓ | ✓ |
| $C_{12}$ | ✓ | ✓ | ✓ | ✓ | ✓ | ✓ | ✓ | ✓ |
| $C_{13}$ | ✓ | ✓ | ✓ | ✓ | ✓ | ✓ | ✓ | ✓ |
| $C_{14}$ | ✓ | ✓ | ✓ | ✓ | ✓ | ✓ | ✓ | ✓ |
| $C_{16}$ | ✓ | ✓ | ✓ | ✓ | ✓ | - | ✓ | ✓ |
| $C_{18}$ | ✓ | ✓ | ✓ | ✓ | ✓ | ✓ | ✓ | ✓ |

The variations of liquid product mole fractions obtained in the presence of MCM-type catalysts in 30 minutes are given in Figure 6.45. The tabulated values of mole and weight fractions are given in Appendix I. In the presence of MCM-type catalysts, $C_5$ and $C_7$ formation increased and the amount of heavier hydrocarbons decreased significantly with an increase in Al/Si ratio when aluminum isopropoxide containing MCM-type catalysts were used (Figure 6.45). Therefore, aluminum isopropoxide containing MCM-type catalysts can be considered as active catalysts in degradation of polypropylene to lower hydrocarbons.

On the other hand, high amounts of $C_7$ hydrocarbon formed in the presence of *Al-0.03A* but it decreased with an increase in Al/Si ratio. *Al-1A* catalyst did not show a good efficiency in the production of light liquid hydrocarbons since the amount of $C_{18}$ was higher among the other products, but it was very effective in the production of ethylene gas, as mentioned previously.

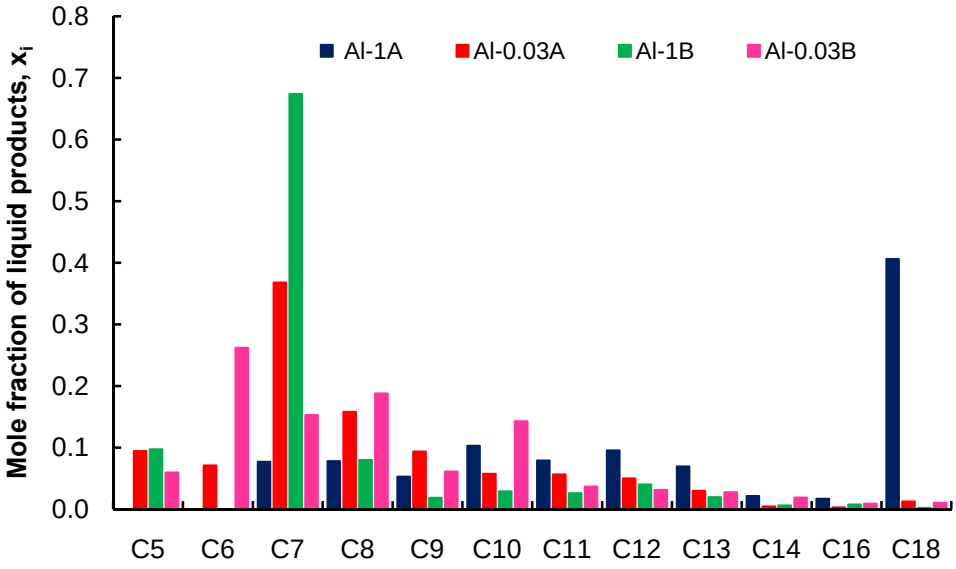


Figure 6.45 Variation of liquid product mole fractions with respect to aluminum loading and aluminum source in the presence of MCM-type catalysts (t:30 min.)

The variations of liquid product mole fractions obtained in the presence of SBA-type catalysts in 30 minutes are given in Figure 6.46. Their tabulated values are given in Appendix I. When aluminum isopropoxide was used as the aluminum source, $C_7$ formation increased among the other products. $C_7$ (e.g. heptane, toluene) is widely applied in laboratories as a solvent. Also, it can be used as a standard in determining octane ratings, and as an anesthetic [120, 121]. On the other hand, when aluminum sulphate was used as the aluminum source, the amount of $C_7$ decreased with an increase in aluminum loading. Additionally, $C_{13}$ formation increased with an increase in aluminum loading in the presence of aluminum sulphate containing SBA-type catalysts. In this catalyst group, both the acidity (Figure 6.27) and the surface area (Table 6.4) decreased with an in increase in aluminum loading and this might cause a decrease in the activity of the catalysts. In both SBA-type catalyst group, few amounts of heavy hydrocarbons formed which means that the polypropylene degraded into smaller molecules in the presence of these SBA catalysts. As a

conclusion, these catalysts are much more active than MCM-type catalysts in degradation reaction. SBA- type catalysts had larger pores and owing to these larger pores, steric hindrances in polypropylene degradation reaction decreased.

Aguado and his co-workers [61] also found that mesoporous catalysts were much more active than zeolites (ZSM-5) in polypropylene degradation reaction due to the steric hindrances large molecules like polymers encountered to enter into the narrow pores of zeolites.

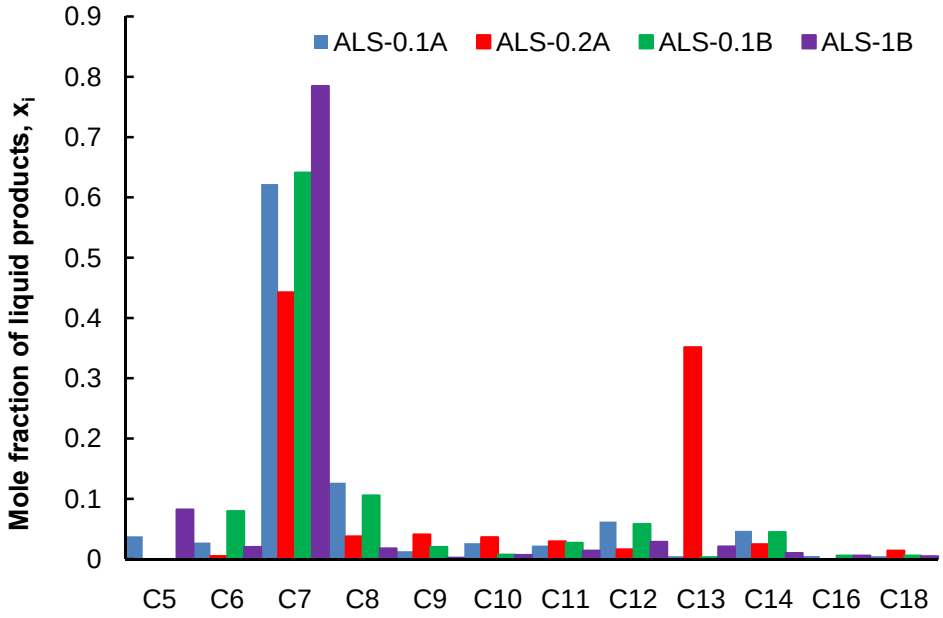


Figure 6.46 Variation of liquid product mole fractions with respect to aluminum loading and aluminum source in the presence of SBA-type catalysts (t:30 min.)

Finally, variations of the liquid product selectivities with respect to aluminum loading and aluminum source in the presence of catalysts are given in Figures 6.47 and 6.48, respectively. In MCM-type catalysts, at high aluminum

loadings, $C_7$ selectivity increased significantly when aluminum isopropoxide was used as the aluminum source. On the other hand, $C_{18}$ selectivity increased at high aluminum loadings in the case of using aluminum nitrate as the aluminum source. In the group of SBA-type catalysts, $C_7$ selectivity increased when Al/Si ratio was increased from 0.1 to 1 in the case of using aluminum isopropoxide as the aluminum source. Same result was obtained in MCM-type catalyst group, as mentioned before. As a conclusion, it can be said that $C_7$ selectivity is dependent on aluminum source used in the synthesis instead of catalyst type (MCM or SBA). When aluminum sulphate was used as the aluminum source in the synthesis of SBA-type catalysts, $C_{13}$ selectivity increased with an increase in Al/Si ratio. $C_{13}$ is used in paper processing industry, rubber industry and jet fuel researches [122].

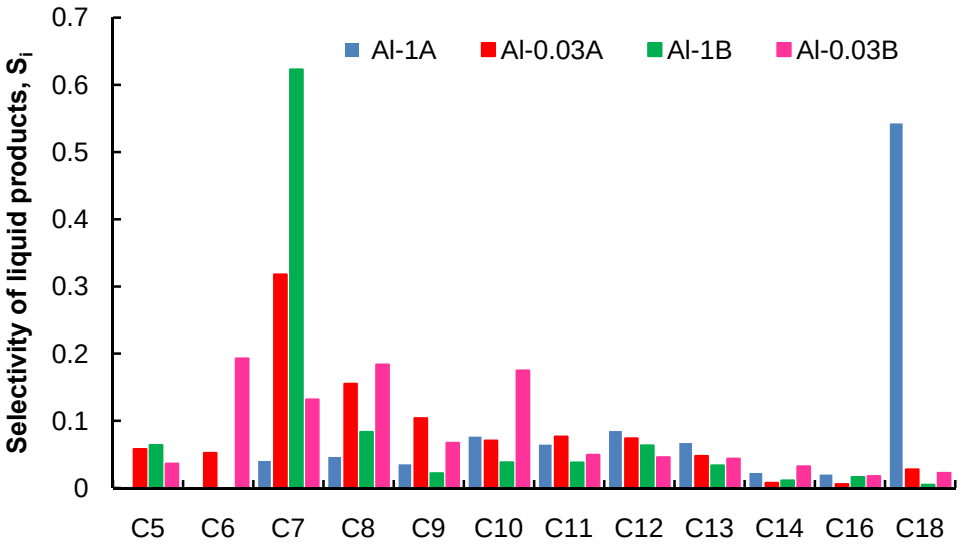


Figure 6.47 Variation of liquid product selectivities with respect to aluminum loading and aluminum source in the presence of MCM-type catalysts (t:30 min.)

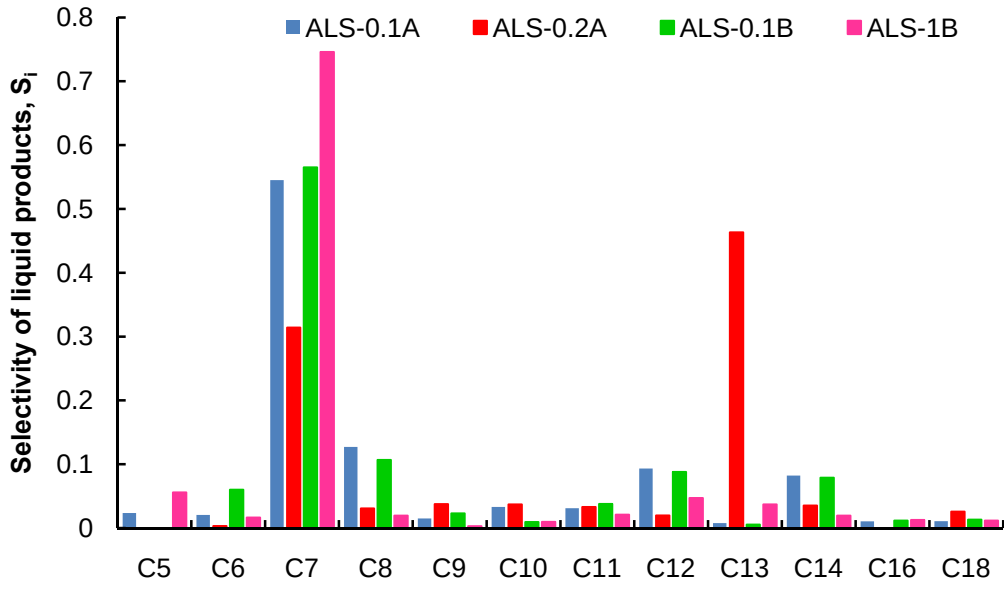


Figure 6.48 Variation of liquid product selectivities with respect to aluminum loading and aluminum source in the presence of SBA-type catalysts (t:30 min.)

To check the consistency of these gas chromatography analyses, two different samples (Al-1B & ALS-1B) obtained at the end of catalytic reactions were analysed qualitatively using GC-MS (Agilent 7890 GC-5975 MS) in Turkish Petroleum Corporation. Sample chromatograms for these samples are given in Appendix J. In both samples, hydrocarbons from $C_6$ to $C_{18}$ were detected in GC-MS and these results were in agrrement with results obtained from GC analysis. Only $C_6$ could not be detected in gas chromatography in the case of using *Al-1B* (Figure 6.45). As a conclusion, the results obtained from gas chromatography were in agreement with the results obtained from GC-MS.

# CHAPTER 7

# CONCLUSIONS AND RECOMMENDATIONS

In this study, the catalytic activity of ordered mesoporous materials*, MCM-type* and *SBA-type*, in polypropylene degradation reaction was investigated. For this purpose, mesoporous *MCM* and *SBA* type catalysts were synthesized and characterized, as described in the experimental part. Before performing catalytic reactions, activation energy value of degradation reaction in the presence of synthesized catalysts were determined by the help of a thermal analyser. After that, the catalytic activity of these catalysts were investigated in polypropylene degradation reaction and products were analysed in gas chromatography. In addition to these catalytic thermal degradation reactions, non-catalytic thermal degradation (blank) reactions were carried out to make a reasonable comparison. Major conclusions reached as a result of this work are:

- In the XRD patterns of the synthesized aluminum containing MCM-type materials, the broader and less intense main peaks were observed due to the structural irregularity caused by aluminum that was incorporated into the structure of the material. These broader peaks are an indication that the pore size distributions of the synthesized mesoporous aluminum contanining *MCM-type* materials were not as narrow as pure *MCM-41* following basic route.

- The MCM-type catalysts synthesized using TEOS and following acidic route catalysts exhibited Type IV isotherms with Type H2 hysteresis loop. Capillary condensation of nitrogen in the mesopores of the

structure may cause this hysteresis formation. When aluminum nitrate was used as the aluminum source, the aluminum was incorporated into the structure more effectively at low Al loadings but at high Al loadings, it can be concluded that most of the aluminum was not incorporated into the structure. On the other hand, when aluminum isopropoxide was used as the aluminum source, aluminum was incorporated into the structure more effectively both at low and high Al loadings.

- The SEM images of MCM-type catalysts showed that when aluminum was incorporated into silica structure, the size of the particles became larger. $^{27}$Al MAS NMR spectra of aluminum containing MCM-type materials exhibited a mixture of tetrahedral and octahedral aluminum.

- When synthesis duration and temperature of SBA-15 was kept 2 days and 100°C, a well-ordered structure was obtained. When aluminum isopropoxide was used as the aluminum source, deformation in the main peak of *SBA-15* was observed which may be due to the structural irregularity, on the other hand, the well ordered structure of *SBA-15* did not deteriorate too much when the level of aluminum was kept low in the case of using aluminum sulphate as the aluminum source.

- All the SBA-type samples showed typical Type IV adsorption/desorption isotherms with a hysteresis loop (H1), which is characteristic of mesoporous materials. This hysteresis loop was broad and the adsorption and desorption branches were parallel in most of the synthesized materials. Additionally, the pore walls of SBA-type catalysts are much thicker than the pore walls of MCM-type catalysts.

- When aluminum isopropoxide was used as the aluminum source in the synthesis of SBA-type catalysts, the aluminum was incorporated into the structure more effectively both at low and high aluminum loadings. On the other hand, when aluminum sulphate was used as the aluminum source, the aluminum was only incorporated into structure more effectively at low loading, not at high loading.

- For the SBA-type materials prepared using aluminum sulphate as the aluminum source, it is clear that Brönsted acid sites are much stronger than Lewis acids. On the other hand, when aluminum isopropoxide was used as the aluminum source, the relative intensities of the bands corresponding to the Lewis and Brönsted acid sites (1489 $cm^{-1}$) increased as the Al/Si ratio increased up to 0.2.

- TEM images of SBA-type materials showed well-ordered hexagonal arrays of uniform mesopores with channels. The materials' pore structure was in honeycomb form that is common for mesoporous materials.

- The activation energy value of degradation was found to be decreased down to about 72-118 kJ/mol for catalysts synthesized using aluminum nitrate as the aluminum source in the synthesis of MCM-type catalysts, while the activation energy of decomposition of polypropylene in the absence of catalyst was about 172 kJ/mol. On the other hand, activation energy values were obtained in the range of 68-126 kJ/mol in the case of catalysts prepared using aluminum isopropoxide as the aluminum source.

- The TGA results showed a marked reduction in the degradation temperature in the presence of aluminum containing SBA-type catalysts. These catalysts caused a significant decrease in the activation energy of the reaction from 172 kJ/mol to a value in the range of 51–89 kJ/mol.

- The results obtained from the non-catalytic thermal degradation of polypropylene showed that the selectivity of methane, ethane and acetylene gases did not change so much with temperature. On the other hand, butane selectivity increased when the reaction temperature was raised to 425°C and the selectivity of propylene increased significantly when the reaction temperature was raised from 400°C to 410°C but it decreased slightly when the temperature was

raised to 425°C. Finally, the ethylene selectivity decreased when the temperature was raised from 400°C to 410°C and became constant.

- When aluminum sulphate was used as the aluminum source in the synthesis of MCM-type catalysts, the ethylene selectivity increased significantly with an increase in Al/Si ratio. When aluminum isopropoxide contained MCM-type catalysts were used, the ethylene and propylene selectivity decreased significantly and n-butane and i-butane selectivity increased with an increase of Al/Si ratio from 0.03 to 1. Same trend was observed for ethylene selectivity in aluminum containing SBA-type catalysts. In this group, when aluminum isopropoxide was used in the synthesis of SBA-type catalyst, ethylene selectivity decreased with an increase in Al/Si ratio.

- In the non-catalytic degradation reaction, at 425°C, $C_{12}$, $C_{14}$, $C_{16}$ and $C_{18}$ selectivities increased with an increase in reaction time. Also, smaller hydrocarbons like $C_5$ and $C_6$ selectivities increased when the reaction performed for 30 minutes. As a conclusion, this temperature is highly $C_{18}$ selective as observed in results of degradation reaction peformed at 410°C.

- At high aluminum loadings, $C_7$ selectivity increased significantly when aluminum isopropoxide was used as the aluminum source. On the other hand, $C_{18}$ selectivity increased at high aluminum loadings in the case of using aluminum nitrate as the aluminum source. In the group of SBA-type catalysts, $C_7$ selectivity increased when Al/Si ratio was increased from 0.1 to 1 in the case of using aluminum isopropoxide as the aluminum source. Same result was obtained in MCM-type catalyst group. As a conclusion, it can be said that $C_7$ selectivity is dependent on aluminum source, not catalyst type (MCM or SBA) used in the synthesis. When aluminum sulphate was used as the aluminum source in the synthesis of SBA-type catalysts, $C_7$ and $C_{13}$ selectivity increased with an increase in Al/Si ratio.

- In the presence of SBA-type catalysts, light hydrocarbon contained products were obtained with respect to the products obtained in the presence of MCM-type catalysts.

In the future studies, to observe the effect of the catalyst on product distribution, pyrolysis reaction may be carried out at different temperatures and reaction times and using the data mathematical modeling may be done. Additionally, more acidic catalysts like heteropolyacid impregnated MCM-41 and SBA-15 may be synthesized and their performances in polypropylene pyrolysis reaction may be tested and their effect on product distribution may be investigated.

# REFERENCES


1) Pinto, F., Costa, P., Gulyurtlu, I., Cabrita, I., "*Pyrolysis of plastic wastes. 1.Effect of plastic waste composition on product yield*", J.Anal.Appl.Pyrol*.,* 51, 1999, p.39-55.

2) Isoda, T., Nakahara, T., Kusakabe, K., Morooka, S., "*Catalytic cracking of polyethylene-liquefied oil over amorphous aluminosilicate catalysts*", Energy&Fuels, 12, 1998, p. 1161-1167.

3) Pinto, F., Costa, P., Gulyurtlu, I., Cabrita, I., "*Pyrolysis of plastic wastes. 2.Effect of catalyst on product yield*", J.Anal.Appl.Pyrol*.,* 51, 1999, p.57-71.

4) Marcilla, A., Gomez-Siurana, A., Berenguer, D., "*Study of the influence of the characteristics of different acid solids in the catalytic pyrolysis of different polymers*", Appl.Catalysis A: Gen., 301, 2006, p.222-231.

5) de la Puente, G., Sedran, U., "*Recycling polystyrene into fuels by means of FCC: performance of various acidic catalysts*", Appl.Catalysis B: Environ., 19, 1998, p.305-311.

6) Van Grieken, R., Serrano, D.P., Aguado, J., Garcia, R., Rojo, C., "*Thermal and catalytic cracking of polyethylene under mild conditions*", J.Anal.Appl.Pyrol*.,* 58-59, 2001, p.127-142.

7) Kaminsky, W., Zorriqueta, I.-J.N., "*Catalytical and thermal pyrolysis of polyolefins*", J.Anal.Appl.Pyrol*.,* 79, 2007, p.368-374.

8) Garcia, R.A., Serrano, D.P., Otero, D., "*Catalytic cracking of HDPE over hybrid zeolitic-mesoporous materials*", J.Anal.Appl.Pyrol*.,* 74, 2005, p.379-386.

9) Aguado, J., Serrano, D.P., San Miguel, G., Escola, J.M., Rodrigues, J.M., "*Catalytic activity of zeolitic and mesostructured catalysts in the cracking of pure and waste polyolefins*", J.Anal.Appl.Pyrol*.,* 78, 2007, p.153-161.

10) Oye G., Sjöblom, J., Stöcker, M., "*Synthesis, characterization and potential applications of new materials in the mesoporous range*", Adv. in Coll. and Inter. Sci., 89-90, 2001, p.439-466.

11) Vartuli, J.C., Shih, S.S., Kresge, C.T., Beck, J.S., "*Potential applications for M41S type mesoporous molecular sieves*", Stud.Surf.Sci.Catal., 117, 1998, p.13-21.

12) Wikipedia, http://eng.wikipedia.org/wiki/Polymer, last accessed date June 30th, 2009.

13) Chymist, http://www.chymist.com/Polymers.pdf, last accessed date June 30th, 2009.

14) Billmeyer, F.W., "*Textbook of Polymer Science*", John Wiley & Sons, 1984, New York, USA.

15) Wikipedia, http://eng.wikipedia.org/wiki/Polyethylene, last accessed date June 30th, 2009.

16) Wikipedia, http://eng.wikipedia.org/wiki/Polypropylene, last accessed date June 30th, 2009.

17) Wikipedia, http://eng.wikipedia.org/wiki/Polystyrene, last accessed date June 30th, 2009.

18) Polymerambassadors,http://www.polymerambassadors.org/ polyethylene.pdf, last accessed date June 30th, 2009.

19) Lenntech, http://www.lenntech.com/Polypropylene.htm, last accessed date June 30th, 2009.

20) Wikimedia,http://upload.wikimedia.org/wikipedia/commons/d/d3/ Propylene.png, last accessed date June 30th,2009.

21) Wikispace,https://reich-chemistry.wikispaces.com/file/view/ polypropylene.jpg, last accessed date June 30th, 2009.

22) Wikimedia,http://upload.wikimedia.org/wikipedia/commons/c/c3/ Styrene_3D.png, last accessed date June 30th, 2009.

23) Wikimedia,http://upload.wikimedia.org/wikipedia/commons/d/d1/ Isotactic-polystyrene-chain-looking-down-axis-from-xtal-3D-vdW.png, last accessed date June 30th, 2009.

24) Britannica,http://www.britannica.com/EBchecked/topic/469114/ polystyrene, last accessed date June 30th, 2009.

25) Wikipedia,http://eng.wikipedia.org/wiki/Polyvinyl_chloride, last accessed date June 30th, 2009.

26) About.com,http://z.about.com/d/chemistry/1/0/Z/o/Vinyl-chloride-3D.jpg, last accessed date June 30th, 2009.

27) Lenntech, http://www.lenntech.com/Polyvinyl-Chloride-PVC.htm, last accessed date June 30th, 2009.

28) Wikipedia,http://eng.wikipedia.org/wiki/Polyethylene_terephthalate, last accessed date June 30th, 2009.

29) Design site, http://www.designinsite.dk/htmsider/m0011.htm, last accessed date June 30th, 2009.

30) Plastics in wiki, http://plastics.inwiki.org/Polyethylene_terephthalate, last accessed date June 30th, 2009.

31) Serrano, D.P., Aguado, J., Escola, J.M., Rodriguez, J.M., Morselli, L., Orsi, R., "*Thermal and catalytic cracking of LDPE-EVA copolymer mixture*", J.Anal.Appl.Pyrolsis, 68-69, 2003, p.481-494.

32) Miskolczi, N., Bartha, L., Deak, G., Jover, B., "*Thermal degradation of municipal plastic waste for production of fuel-like hydrocarbons*", Polym. Degrad. Stab., 86, 2004, p.357-366.

33) Buekens, A.G., Huang, H., "*Catalytic plastics cracking for recovery of gasoline-range hydrocarbons from municipal plastic wastes*", Resourc. Conserv. Recycl., 23, 1998, p.163-181.

34) Gobin, K., Manos, G., "*Polymer degradation to fuels over microporous catalysts as a novel tertiary plastic recycling method*", Polym. Degrad. Stab., 83, 2004, p.267-279.

35) Takuma, K., Uemichi, Y., Sugioka, M., Ayame, A., "*Production of aromatic hydrocarbons by catalytic degradation of polyolefins over H-Gallosilicate*", Ind.Eng.Chem.Res., 40, 2001, p.1076-1082.

36) Uçar, S., Karagöz, S., Karayıldırım, T., Yanık, J., "*Conversion of polymers to fuels in a refinery stream"*, Polym. Degrad. Stab., 75, 2002, p.161-171.

37) Cardona, S., Corma, A., "*Tertiary recycling of polypropylene by catalytic cracking in a semibatch stirred reactor.Use of spent equilibrium FCC commercial catalyst"*, Appl.Catalysis B: Environ., 25, 2000, p.151-162.

38) Serrano, D.P., Aguado, J., Escola, J.M., Garagorri, E., Rodriguez, J.M., Morselli, L., Palazzi, G., Orsi, R., "*Feedstock recycling of agriculture plastic film wastes by catalytic cracking*", Appl.Catalysis B: Environ., 49, 2004, p.257-265.

39) Williams, P.T., Bagri, R., "*Hydrocarbon gases and oils from the recycling of polystyrene waste by catalytic pyrolysis*", Int. J. Energy Res., 28, 2004, p.31-44.

40) Jakab, E., Varhegyi, G., Faix, O., "*Thermal decomposition of polypropylene in the presence of wood-derived materials*", J.Anal.Appl.Pyrolsis, 56, 2000, p.273-285.

41) Gersten, J., Fainberg, V., Hetsroni, G., Shindler, Y., "*Kinetic study of the thermal decomposition of polypropylene, oil shale, and their mixture*", Fuel, 79, 2000, p.1679-1686.

42) Walendziewski, J., Steininger, M., "*Thermal and catalytic conversion of waste polyolefins*", Catalysis Today, 65, 2001, p. 323-330.

43) Walendziewski, J., "*Engine fuel derived from waste plastics by thermal treatment*", Fuel, 81, 2002, p.473-481.

44) Ali, M.F., Siddiqui, M.N., "*Thermal and catalytic decomposition behavior of PVC mixed plastic waste with petroleum residue*", J.Anal.Appl.Pyrolsis, 74, 2005, p.282-289.

45) Sezgi, N.A., Cha, W.S., Smith, J.M., McCoy, B.J., "*Polyethylene pyroysis:Theory and experiments for molecular-weight-distribution kinetics*", Ind.Eng.Chem.Res., 37, 1998, p.2582-2591.

46) Ofoma, I., "*Catalytic pyrolysis of polyolefins*", MSc. Thesis, 2006, Georgia Institute of Technology, Georgia, USA.

47) Peterson,J.D., Vyazovkin, S., Wight, C.A., "*Kinetics of thermal and thermo-oxidative degradation of polystyrene, polyethylene and poly(propylene)*", Macromol.Chem.Phys., 202, 2001, p.775-584.

48) Sharratt, P.N., Lin, Y.-H., Garforth, A.A., Dwyer, J., "*Investigation of the catalytic pyrolysis of high-density polyethylene over a HZSM-5 catalyst in a laboratory fluidized-bed reactor*", Ind.Eng.Chem.Res., 36, 1997, p.5118-5124.

49) Garforth, A., Fiddy, S., Lin, Y.-H., Ghanbari-Siakhali, A., Sharratt, P.N., Dwyer, J., "*Catalytic degradation of high density polyethylene: An evaluation of mesoporous and microporous catalysts using thermal analysis*", Thermochimica Acta, 294, 1997, p.65-69.

50) Ohkita, H., Nishiyama, R., Tochihara, Y., Mizushima, T., Kakuta, N., Morioka, Y., Ueno, A., Namiki, Y., Tanifuji, S., Katoh, H., Sumazuka, H., Nakayama, R., Kuroyanagi, T., "*Acid properties of silica-alumina catalysts and catalytic degradation of polyethylene*", Ind. Eng. Chem. Res., 32, 1993, p.3112-3116.

51) Sakata, Y., Uddin, M.A., Muto, A., "*Degradation of polyethylene and polypropylene into fuel oil by using solid acid and non-acid catalysts*", J.Anal.Appl.Pyrolsis, 51, 1999, p.135-155.

52) Kim, J.R., Kim, Y.A., Yoon, J.H., Park, D.W., Woo, H.C., "*Catalytic degradation of polypropylene: effect of dealumination of clinoptilolite catalyst*", Polym. Degrad. Stab., 75, 2002, p.287-294.

53) Audisio, G., Silvani, A., Beltrame, P.L., Carniti, P., "*Catalytic thermal degradation of polymers. Degradation of polypropylene*", J.Anal.Appl.Pyrolsis, 7, 1984, p.83-90.

54) Sakata, Y., Uddin, M.A., Koizumi, K., Murata, K., "*Catalytic degradation of polypropylene into liquid hydrocarbons using silica-alumina catalyst*", Chem.Lett., 1996, p.245-246.

55) Lee, K.-H., Noh, N.-S., Shin, D.-H., Seo, Y., "*Comparsion of plastic types for catalytic degradation of waste plastics into liquid product with spent FCC catalyst*", Polym. Degrad. Stab., 78, 2002, p.539-544.

56) Serrano, D.P., Aguado, J., Escola, J.M., "*Catalytic cracking of a polyolefin mixture over different acid solid catalysts*", Ind.Eng.Chem.Res., 39, 2000, p.1177-1184.

57) Fukuda, T., Saito, K., Suzuki, S., Sato, H., Hirota, T., "*Processing for producing hydrocarbon oils from plastic wastes"*, US Patent 4851601, 1989.

58) Uemichi, Y., Makino, Y., Kanazuka, T., "*Degradation of polypropylene to aromatic hydrocarbons over Pt- and Fe-containing activated carbon catalysts*", J.Anal.Appl.Pyrolsis, 16, 1989, p.229-238.

59) Uemichi, Y., Makino, Y., Kanazuka, T., "*Degradation of polyethylene to aromatic hydrocarbons over metal-supported activated carbon catalysts*", J.Anal.Appl.Pyrolsis, 14, 1989, p.331-344.

60) Zhou, Q., Zheng, L., Wang, Y.-Z., Zhao, G.-M., Wang, B., "*Catalytic degradation of low-density polyethylene and polypropylene using modified ZSM-5 zeolites*", Polym. Degrad. Stab., 84, 2004, p.493-497.

61) Aguado, J., Sotelo, J.L., Serrano, D.P., Calles, J.A., Escola, J.M., "*Catalytic conversion of polyolefins into liquid fuels over MCM-41: Comparison with ZSM-5 and amorphous $SiO_2$-$Al_2O_3$*", Energy&Fuels, 11, 1997, p.1225-1231.

62) Serrano, D.P., Aguado, J., Escola, J.M., "*Catalytic conversion of polystyrene over HMCM-41, HZSM-5 and amorphous $SiO_2$-$Al_2O_3$: comparison with thermal cracking*", Appl.Catalysis B: Environ., 25, 2000, p.181-189.

63) Lin, Y.-H., Yen, H.-Y., "*Fluidised bed pyrolysis of polypropylene over cracking catalysts for producing hydrocarbons*", Polym. Degrad. Stab., 89, 2005, p.101-108.

64) Seddegi, Z.S., Budrthumal, U., Al-Arfaj, A.A., Al-Amer, A.M., Barri, S.A.I., "*Catalytic cracking of polyethylene over all-silica MCM-41 molecular sieve*", Appl.Catalysis A: Gen., 225, 2002, p.167-176.

65) Obalı, Z., Sezgi, N.A., Doğu, T., "*Performance of acidic MCM-like aluminosilicate catalysts in pyrolysis of polypropylene*", Chem.Eng.Comm., 196, 2009, p.116-130.

66) Taguchi, A., Schüth, F., "*Ordered mesoporous materials in catalysis*", Micropor.Mesopor.Mater., 77, 2005, p. 1-45.

67) Ciesla, U., Schüth, F., "*Ordered mesoporous materials*", Micropor.Mesopor.Mater., 27, 1999, p. 131-149.

68) Weitkamp, J.,"*Zeolites and catalysis*", Solid State Ionics, 131, 2000, p.175-188.

69) Şener,C., "*Synthesis and characterization of Pd-MCM-type mesoporous nanocomposite materials*", MSc Thesis, 2006, Middle East Technical University, Ankara, Turkey.

70) Xu, J., "*Spectroscopic studies of synthesis, modification and characterization of novel mesoporous molecular sieves*", Ph.D. Thesis, 1999, University of Houston, Houston, USA.

71) Linssen, T., Cassiers, K., Cool, P., Vansant, E.F., "*Mesoporous template silicates: an overview of their synthesis, catalytic activation and evaluation of the stability*", Adv. in Coll. and Inter. Sci., 103, 2003, p.121-147.

72) Beck, J.S., Vartuli, J.C., Roth, W.J., Leonowicz, M.E., Kresge, C.T., Schmitt, K.D., Chu, C.T-W., Olson, D.H., Sheppard, E.W., McCullen, S.B., Higgins, J.B., Schlenker, J.L., "*A New Family of Mesoporous Molecular Sieves Prepared with Liquid Crystal Templates*", J.Am.Chem.Soc*.,* 114, 1992, p.10834-10843.

73) Kresge, C.T., Leonowicz, M.E., Roth, W.J., Vartuli, J.C., Beck, J.S., "*Ordered mesoporous molecular sieves synthesized by a liquid-crystal template mechanism*", Nature, 359, 1992, p.710-712.

74) Blin, J.L., Otjacques, C., Herrier, G., Su, B.-L., "*Kinetic study of MCM-41 synthesis*", Int.J.Inorg.Mater., 3, 2001, p.75-86.

75) Schmidt, R., Akporiaye, D., Stöcker, M., Ellestad, O.H., "*Synthesis of a mesoporous MCM-41 material with high levels of tetrahedral aluminum*", J.Chem.Soc., Chem.Commun., 1994, p.1493-1494.

76) Collart, O., "*Nanodesign of an Aluminasilicate Framework in Mesoporous MCM-48 Architecture*", PhD Thesis, 2003, University of Antwerpen, Antwerpen, Belgium.

77) Zhao, D., Nie, C., Zhou, Y., Xia, S., Huang, L., Li, Q.," *Comparison of disordered mesoporous aluminosilicates with highly ordered Al-MCM-41 on stability, acidity and catalytic activity*", Catal.Today, 68, 2001, p.11-20.

78) Katiyar, A., Yadav, S., Smirniotis, P.G., Pinto, N.G., "*Synthesis of ordered large pore SBA-15 spherical particles for adsorption of biomolecules*", J.Chrom.A, 1122, 2006, p.13-20.

79) Vinu, A., Murugesan, V., Böhlmann, W., Hartmann, M., "*An optimized procedure for the synthesis of AlSBA-15 with large pore diameter and high aluminum content*", J.Phys.Chem.B, 108, 2004, p.11496-11505.

80) Zhao, D., Feng, J., Huo, Q., Melosh, N., Fredrickson, G.H., Chmelka, B.F., Stucky, G.D.,"*Triblock copolymer syntheses of mesoporous silica with periodic 50 to 300 angstrom pores*", Science, 279, 1998, p.548-552.

81) Zhao, D., Huo, Q., Feng, J., Chmelka, B.F., Stucky, G.D., "*Nonionic triblock and star diblock copolymer and oligomeric surfactant syntheses of highly ordered, hydrothermally stable, mesoporous silica structures*", J.Am.Chem.Soc., 120, 1998, p.6024-6036.

82) Fulvio, P.F., Pikus, S., Jaroniec, M., "*Short-time synthesis of SBA-15 using various silica sources*", J.Coll.Inter.Sci., 287, 2005, p.717-720.

83) Supriyo Bhattacharya, http://supriyo.net/research1_files/image20.jpg, last accessed date January 27th, 2010.

84) Güçbilmez, Y., "*Vanadium and Molybdenum Incorporated MCM-41 Catalysts for Selective Oxidation of Ethanol*", PhD Thesis, 2005, Middle East Technical University, Ankara, Turkey.

85) Yang, P., Zhao, D., Margolese, D.I., Chmelka, B.F., Stucky, G.D., "*Block copolymer templating syntheses of mesoporous metal oxides with large ordering lengths and semicrystalline framework*", Chem.Mater., 11, 1999, p.2813-2826.

86) Wu, S., Han, Y., Zou, Y.C., Song, J.W., Zhao, L., Di, Y., Liu, S.Z., Xiao, F.S., "*Synthesis of Heteroatom substituted SBA-15 by the "pH-adjusting" method*", Chem.Mater., 16, 2004, p.486-492.

87) Ying, J.Y., Mehnert, C.P., Wong, M.S., "*Synthesis and applications of supramolecular-templated mesoporous materials*", Angew.Chem.Int.Ed., 38, 1999, p.56-77.

88) Galarneau, A., Desplantier-Giscard, D., di Renzo, F., Fajula, F., "*Thermal and mechanical stability of micelle-templated silica supports for catalysts*", Catal.Today, 68, 2001, p.191-200.

89) Igarashi, N., Koyano, K.A., Tanaka, Y., Nakata, S., Hashimoto, K., Tatsumi, T., "*Investigation of the factors influencing the structural stability of mesoporous silica molecular sieves*", Micropor.Mesopor.Mater., 59, 2003, p. 43-52.

90) Ryoo, R., Jun, S., "*Improvement of hydrothermal stability of MCM-41 using salt effects during the crystallization process*", J.Phys.Chem.B, 101, 1997, p.317-320.

91) Kisler, J.M., Gee, M.L., Stevens, G.W., O'Connor, A.J., "*Comparative study of silylation methods to improve the stability of silicate MCM-41 in aqueous solution*", Chem.Mater., 15, 2003, p.619-624.

92) O'Neil, A.S., Mokaya, R., Poliakoff, M., "*Supercritical fluid-mediated alumination of mesoporous silica and its beneficial effect on hydrothermal stability*", J.Am.Chem.Soc., 124, 2002, p.10636-10637.

93) Şener, C., Doğu, T., Doğu, G., "*Effects of synthesis conditions on the structure of Pd incorporated MCM-41 type mesoporous nanocomposite catalytic materials with high Pd/Si ratios*", Micropor. Mesopor. Mater., 94, 2006, p.89-98.

94) Güçbilmez, Y., Doğu, T., Balcı, S., "*Vanadium incorporated high surface area MCM-41 catalysts*", Catal.Today, 100, 2004, p.473-477.

95) Özaydın, Z., Yaşyerli, S., Doğu, G., "*Synthesis and activity comparison of copper-incorporated MCM-41-type sorbents prepared by one-pot and impregnation procedure for $H_2S$*", Ind.Eng.Chem.Res., 47, 2008, p.1035-1042.

96) Tuel, A., "*Modification of mesoporous silicas by incorporation of heteroelements in the framework*", Micropor. Mesopor. Mater., 27, 1999, p.151-169.

97) Zeng, S., Blanchard, J., Breysse, M., Shi, Y., Shu, X., Nie, H., Li, D., "*Post-synthesis alumination of SBA-15 in aqueous solution: a versatile tool for the preparation of acidic Al-SBA-15 supports*", Micropor. Mesopor. Mater., 85, 2005, p.297-304.

98) Jana, S.K., Takahashi, H., Nakamura, M., Kaneko, M., Nishida, R., Shimizu, H., Kugita, T., Namba, S., "*Aluminum incorporation in mesoporous MCM-41 molecular sieves and their catalytic performance in acid-catalyzed reactions*", Appl.Catal.A:General, 245, 2003, p.33-41.

99) Lourenço, J.P., Fernandes, A., Henriques, C., Riberio, M.F., "*Al-containing MCM-41 type materials prepared by different synthesis methods:Hydrothermal stability and catalytic properties*", Micropor. Mesopor. Mater., 94, 2006, p.56-65.

100) Luan, Z., Hartmann, M., Zhao, D., Zhou, W., Kevan, L., "*Alumination and ion-exchange of mesoporous SBA-15 molecular sieves*", Chem.Mater., 11, 1999, p.1621-1627.

101) Cesteros, Y., Haller, G.L., "*Several factors affecting Al-MCM-41 synthesis*", Micropor. Mesopor. Mater., 43, 2001, p.171-179.

102) Sun, Y., Yue, Y., Gao, Z., "*Synthesis and characterization of AlMCM-41 molecular sieves*", Appl.Catal.A:General, 161, 1997, p.121-127.

103) Li, Y., Zhang, W., Zhang, L., Yang, Q., Wei, Z., Feng, Z., Li, C., "*Direct synthesis of Al-SBA-15 mesoporous mater,als via hydrolysis-controlled approach*", J.Phys.Chem.B, 108, 2004, p.9739-9744.

104) Jaroniec, M., Kruk, M., Sayari, A., "*Adsorption methods for characterization of surface and structural properties of mesoporous molecular sieves*", Stud.Surf.Sci.Catal., 117, 1998, , p.325-332.

105) Schmidt, R., Akporiaye, D., Stöcker, M., Ellestad, O.H., "*Synthesis of Al-containing MCM-41 materials: Template interaction and removal*", Stud.Surf.Sci.Catal., 84, 1994, p.61-68.

106) Wachs, I.E., Fitzpatrick, L.E., "*Characterization of Catalytic Materials*", Manning Publications Co., 1992, Greenwich, USA.

107) Corma, A., Grande, M.S., Gonzales-Alfaro, V., Orchilles, A.V., *Cracking activity and hydrothermal stability of MCM-41 and its comparison with amorphous silica-alumina and a USY zeolite*, J.Catal., 159, 1996, p.375-382.

108) Landau, M.V., Titelman, L., Vradman, L., Wilson, P., *Thermostable sulfated 2-4 nm tetragonal $ZrO_2$ with high loading in nanotubes of SBA-15: a superior acidic catalytic material*, Chem.Commun., 2003, p.594-595.

109) Uddin, M.A., Sakata, Y., Muto, A., Shiraga, Y., Koizumi, K., Kanada, Y., Murata, K., *Catalytic degradation of polyethylene and polypropylene into liquid hydrocarbons with mesoporous silica*, Micropor. Mesopor. Mater., 21, 1998, p.557-564.

110) Sakata, Y., Uddin, M.A., Muto, A., Kanada, Y., Koizumi, K., Murata, K., *Catalytic degradation of polyethylene into fuel oil over mesoporous silica (KFS-16) catalyst*, J. Anal.Appl.Pyrolysis, 43, 1997, p.15-25.

111) Mirji, S.A., Halligudi, S.B., Sawant, D.P., Jacob, N.E., Patil, K.R., Gaikward, A.B., Pradhan, S.D., *"Adsorption of octadecyltrichlorosilane on mesoporous SBA-15"*, Appl.Surf.Sci., 2006, 252, p.4097-4103.

112) Kumaran, M.G., Garg, S., Soni, K., Kumar, M., Sharma, L.D., Dhar, G.M., Rama Rao, K.S., *"Effect of Al-SBA-15 support on catalytic functionalities of hydrotreating catalysts. I.Effect of variation of Si/Al*

*ratio on catalytic functionalities*", Appl.Catal.A:General, 305, 2006, p.123-129.

113) Özmen,D., "*Production and Characterization of Boron Nitride Nanotubes*", MSc Thesis, 2008, Middle East Technical University, Ankara, Turkey.

114) Li, Y., Yang, Q., Yang, J., Li C., "*Synthesis of mesoporous aluminosilicates with low Si/Al ratios using a single precursor under acidic conditions*", J.Porous Mater., 13, 2006, p.187-193.

115) Lim, S., and Haller, G.L., "*Preparation of Highly Ordered Vanadium-Substituted MCM-41: Stability and Acidic Properties*",J. Phys. Chem.B,106, 2002, p.8437-8448.

116) Akçay, M., "*The surface acidity and characterization of Fe-montmorillonite probed by in-situ FT-IR spectroscopy of adsorbed pyridine*", Appl. Catal.A: General, 294, 2005, p.156-160.

117) Coats, A.W., Redfern, J.P., "*Kinetic Parameters from Thermogravimetric Data*", Nature, 201, 1964, p.68-69.

118) Repuclic of Turkey Prime Ministry Privatization Administration http://www.oib.gov.tr/portfoy/petkim/ petkim_etilenglikol_fb.htm, last accessed date March 13th, 2010.

119) Wikipedia, http://en.wikipedia.org/wiki/Higher_alkanes, last accessed date March16th, 2010.

120) Home of Wiki & Reference Answers, http://www.answers.com/topic/ heptane, last accessed date March16th, 2010.

121) Wikipedia, http://en.wikipedia.org/wiki/Toluene, last accessed date March16th, 2010.

122) Wikipedia, http://en.wikipedia.org/wiki/Tridecane, last accessed date March16th, 2010.

# APPENDIX A

## CALCULATION OF PORE WALL THICKNESS

From $d_{100}$ value, calculation of lattice parameter *a* in a hexagonal lattice could be done by using the following formula,

$$a = 2 \times d_{100} / \sqrt{3} \quad \text{(A.1)}$$

Here, the lattice parameter referred to the constant distance between unit cells in a crystal lattice and $d_{100}$ value could be obtained from X-ray diffraction pattern of the material using the following equation,

$$n\lambda = 2d_{100} \sin\Theta \text{ (Bragg's law)} \quad \text{(A.2)}$$

where *n* is an integer, $\lambda$ is the wavelength of the X-rays and $\theta$ is the angle between the incident ray and the scattering planes. Here, the most intense peak ($I/I_0$:100) was taken into consideration. In our studies, copper cathode tube was used in X-ray analyses, therefore $\lambda$ was taken as 1.54Å and *n* was taken as 1. After calculation of lattice parameter, *a*, the pore wall thickness, $\delta$, of synthesized catalysts was calculated using the formula given below,

$$\delta = a - 2 \times r \quad \text{(A.3)}$$

where *r* is the pore radius.

A.1 Sample Calculation

Pore wall thickness calculation for catalyst *ALS-0.03A*:

$2\theta$ = 1° (read from X-ray diffraction pattern) → $\sin\theta$ = 0.0087 & $\lambda_{Cu}$ = 0.154 Å

$$\Rightarrow \quad d_{100} = 0.154/2\sin(0.5) = 8.8nm$$

By using this value, lattice parameter (*a*) was calculated from equation A.1,

$$\Rightarrow \quad a = 2\times 8.8/\sqrt{3} = 10.2nm$$

From equation A.3,

$$\Rightarrow \quad \delta = 10.2 - 5.4 = 4.8nm$$

where 5.4 nm is diameter (2xr) of *ALS-0.03A* and this value was taken from Table 6.4.

# APPENDIX B

## EDS RESULTS OF MCM-TYPE CATALYSTS

EDS spectra of the MCM-type catalysts are given in Figures B.1-B.5.

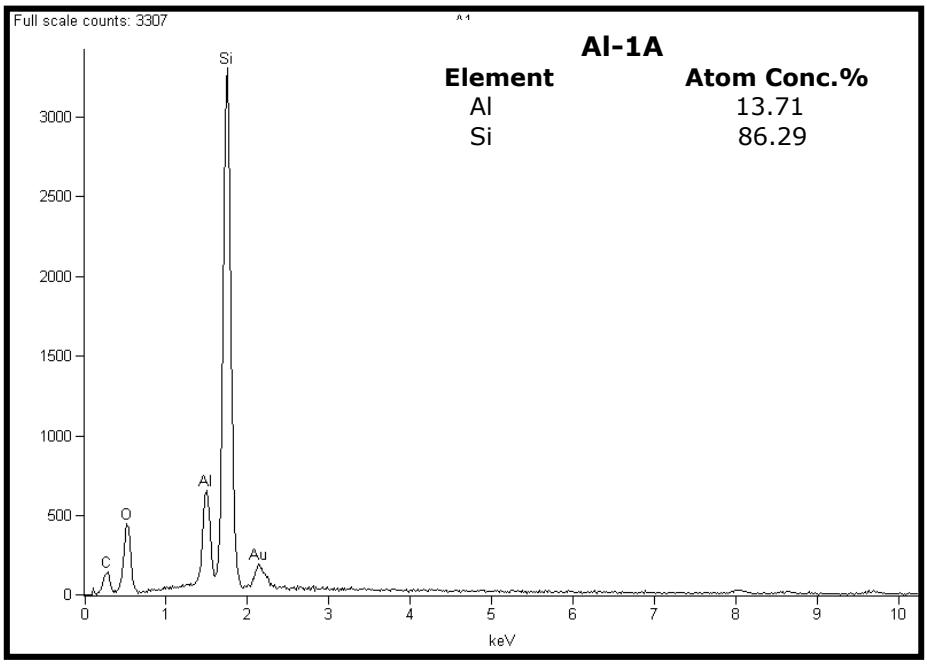


Figure B.1 EDS spectrum of *Al-1A* sample

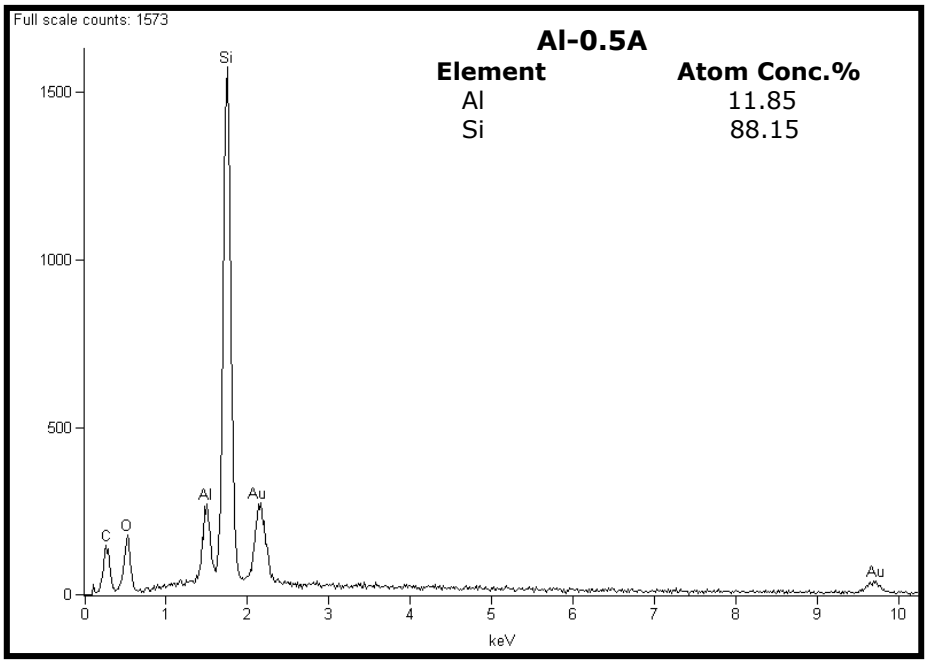


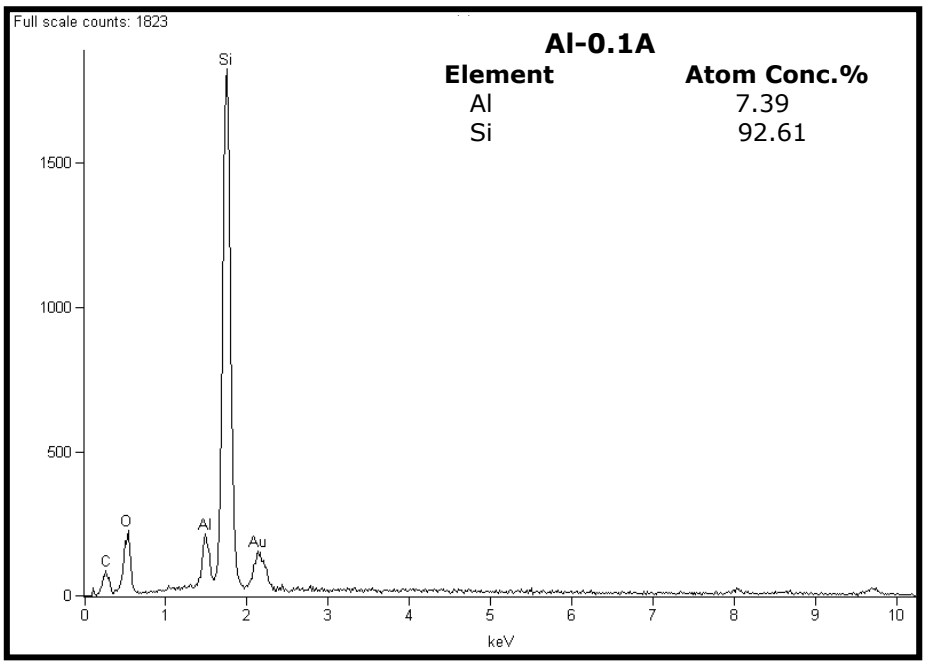


Figure B.2 EDS spectra of *Al-0.5A* and *Al-0.1A* samples

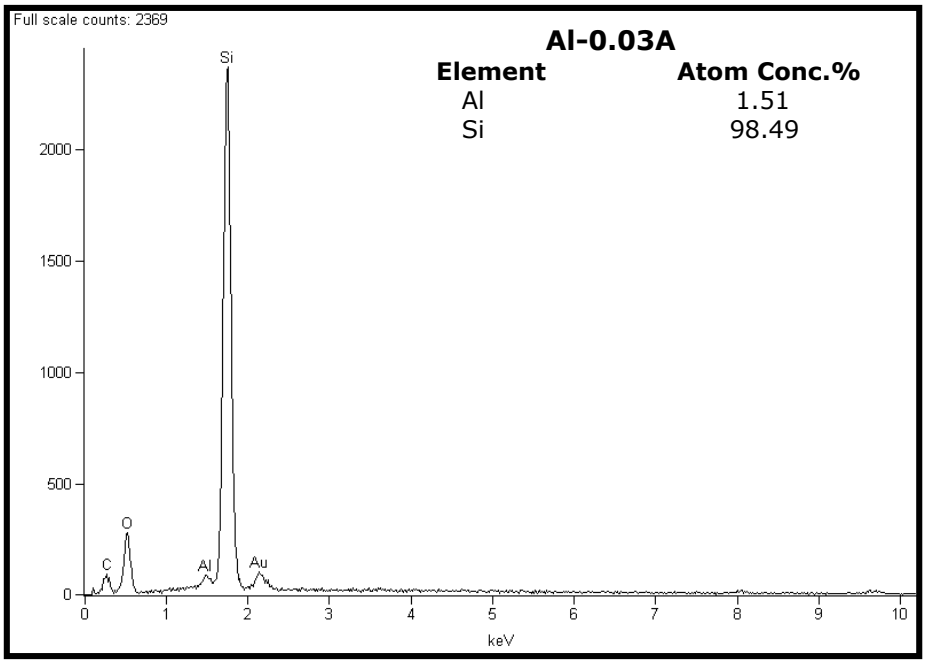


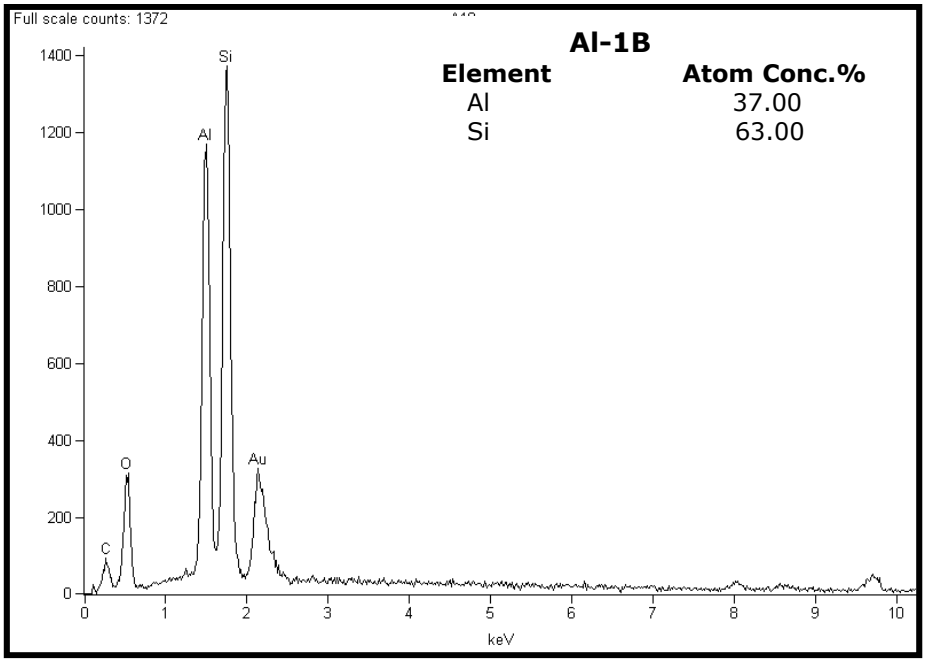


Figure B.3 EDS spectra of *Al-0.03A* and *Al-1B* samples

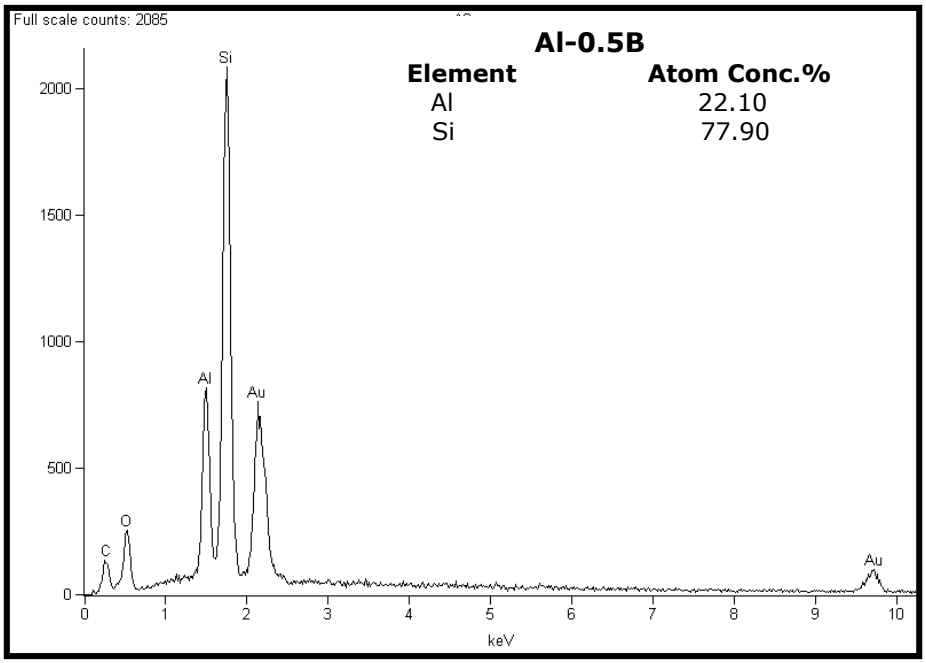


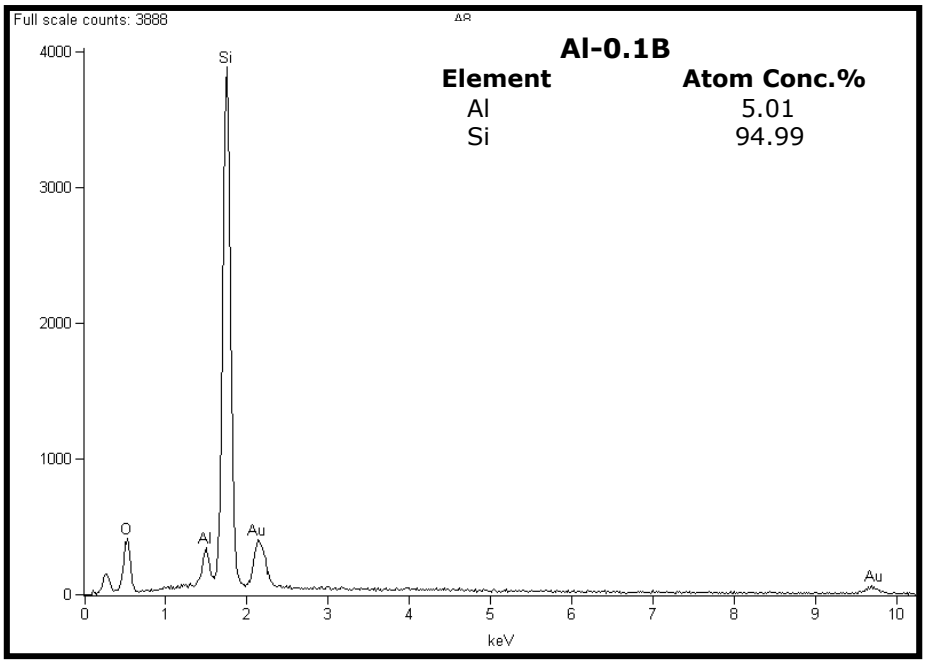


Figure B.4 EDS spectra of *Al-0.5B* and *Al-0.1B* samples

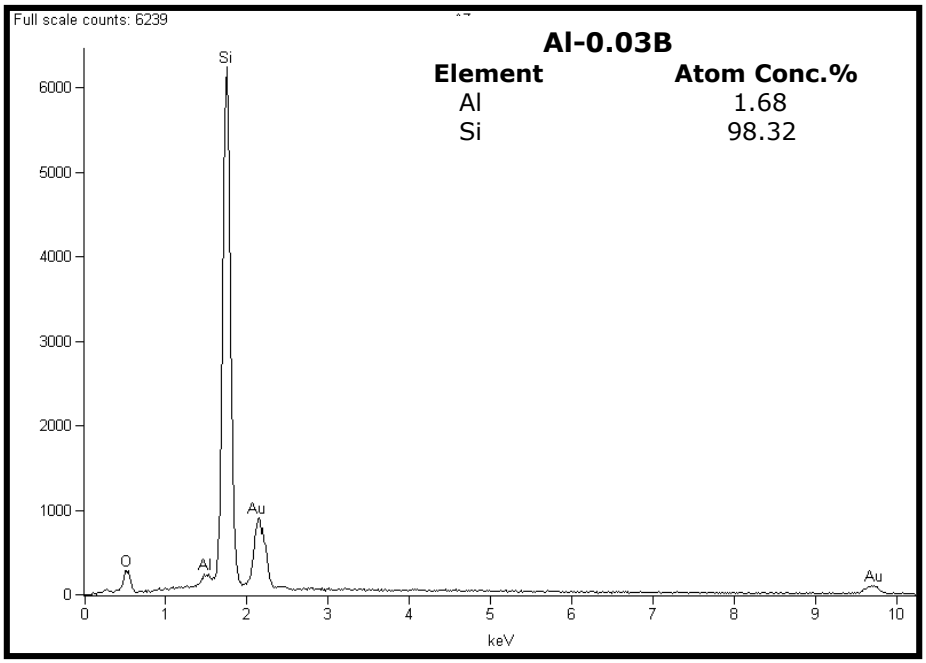


Figure B.5 EDS spectra of *Al-0.03B* samples

# APPENDIX C

## EDS RESULTS OF SBA-TYPE CATALYSTS

EDS spectra of the SBA-type catalysts are given in Figures C.1-C.6.

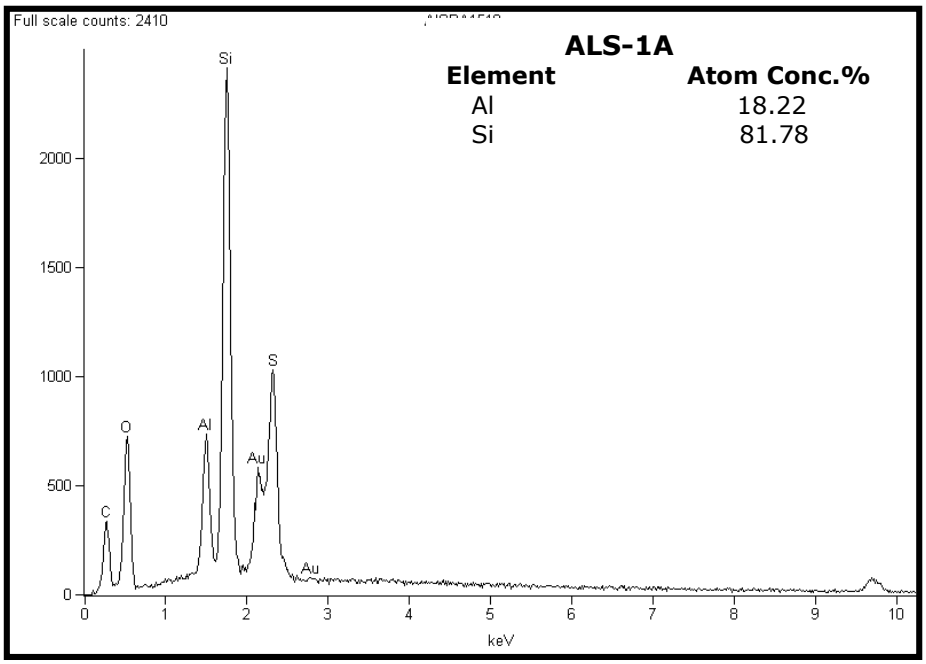


Figure C.1 EDS spectrum of *ALS-1A* samples

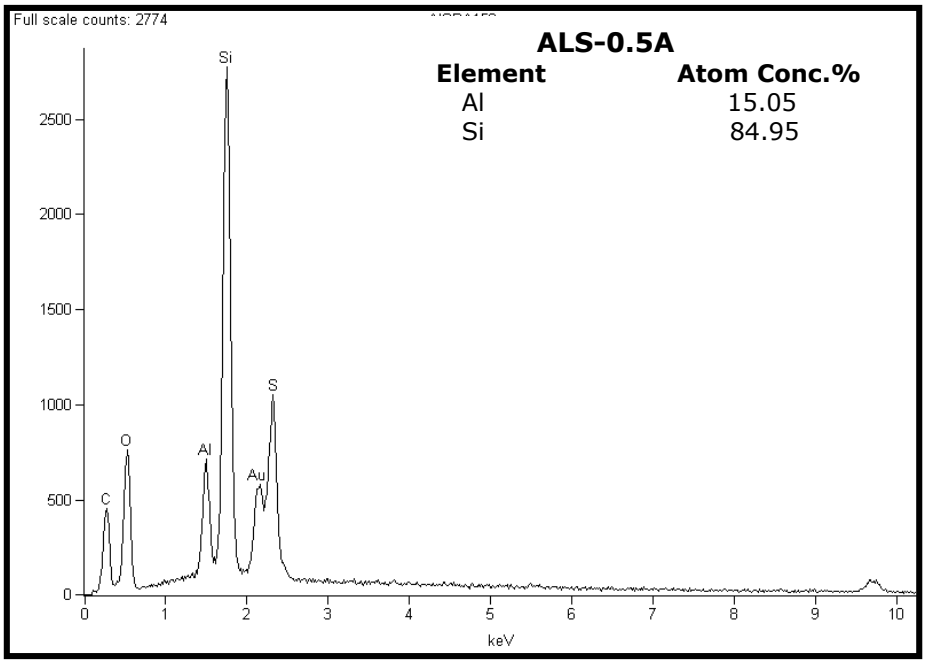


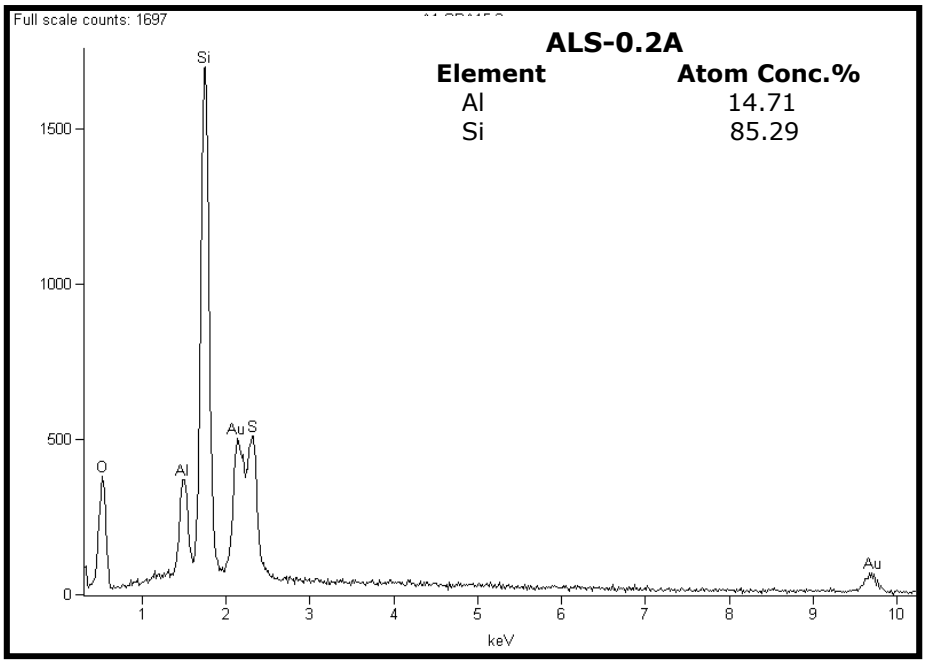


Figure C.2 EDS spectra of *ALS-0.5A* and *ALS-0.2A* samples

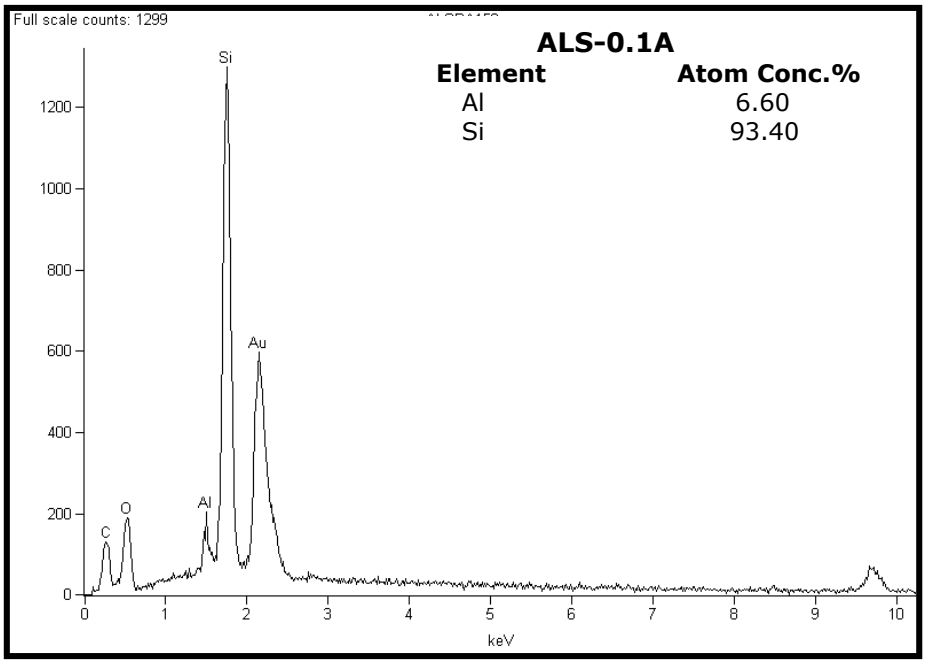


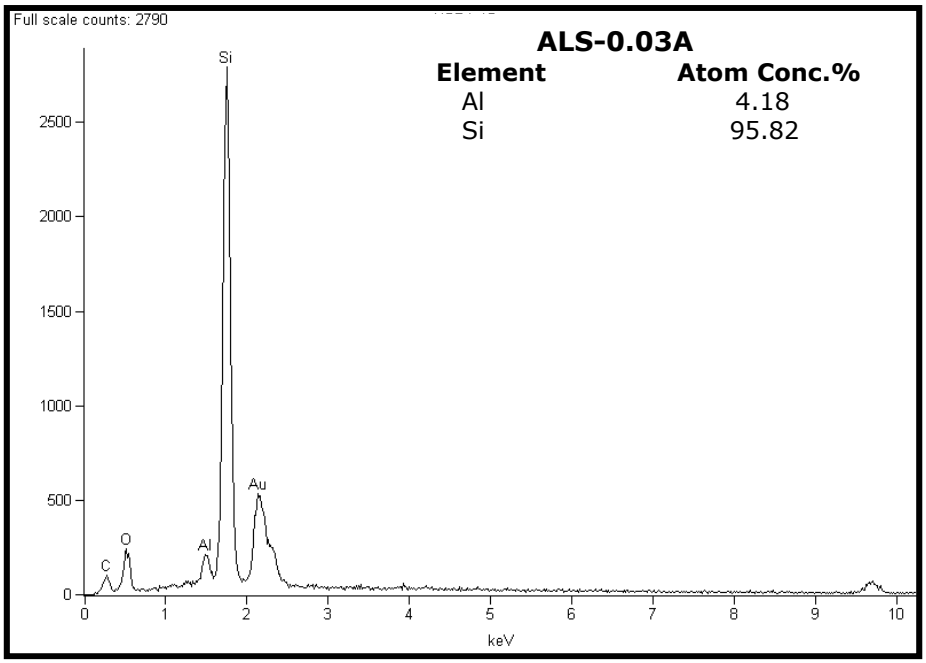


Figure C.3 EDS spectra of *ALS-0.1A* and *ALS-0.03A* samples

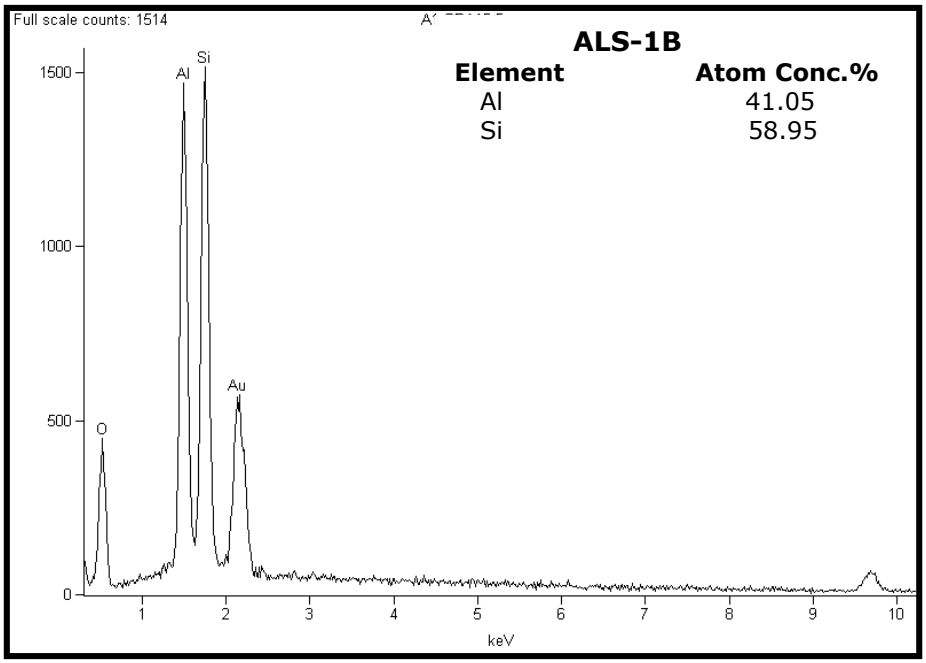


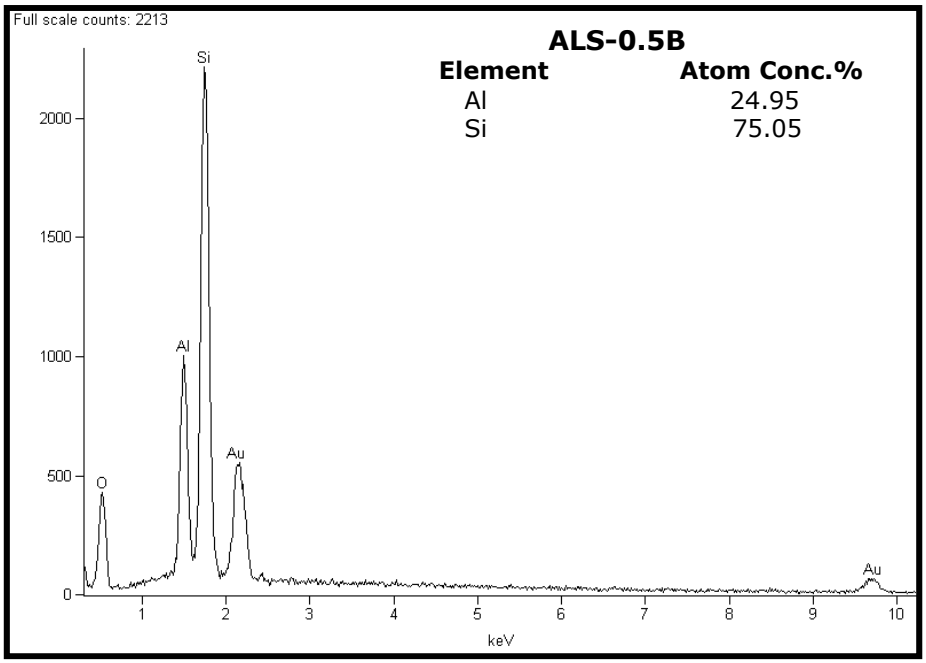


Figure C.4 EDS spectra of *ALS-1B* and *ALS-0.5B* samples

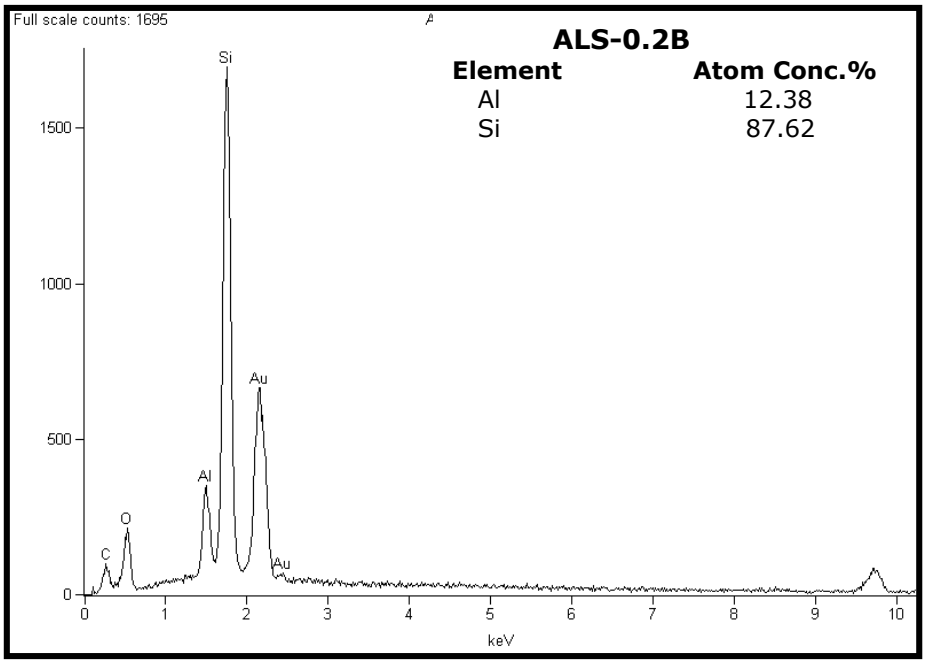


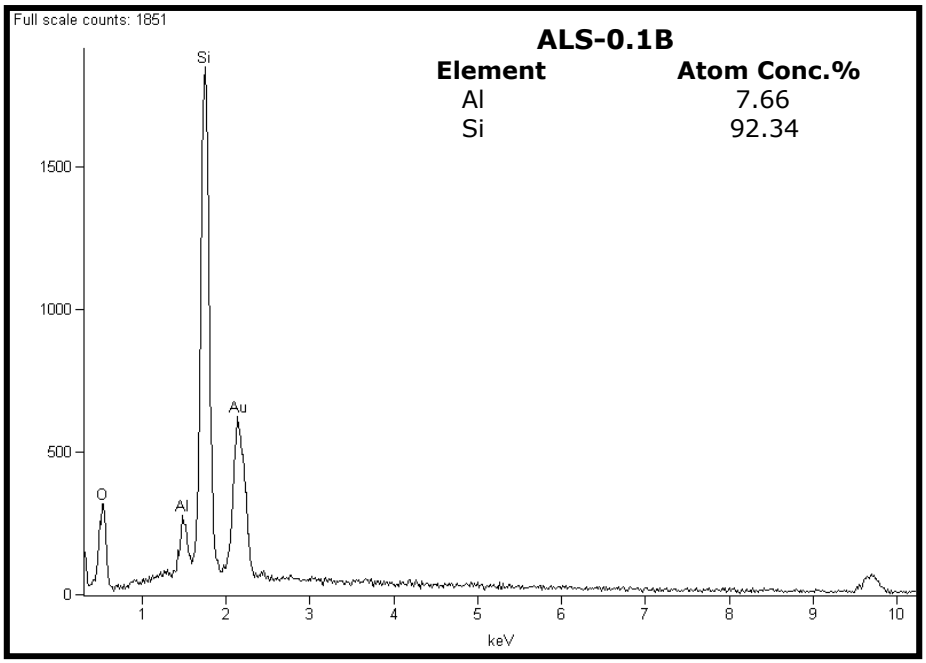


Figure C.5 EDS spectra of *ALS-0.2B* and *ALS-0.1B* samples

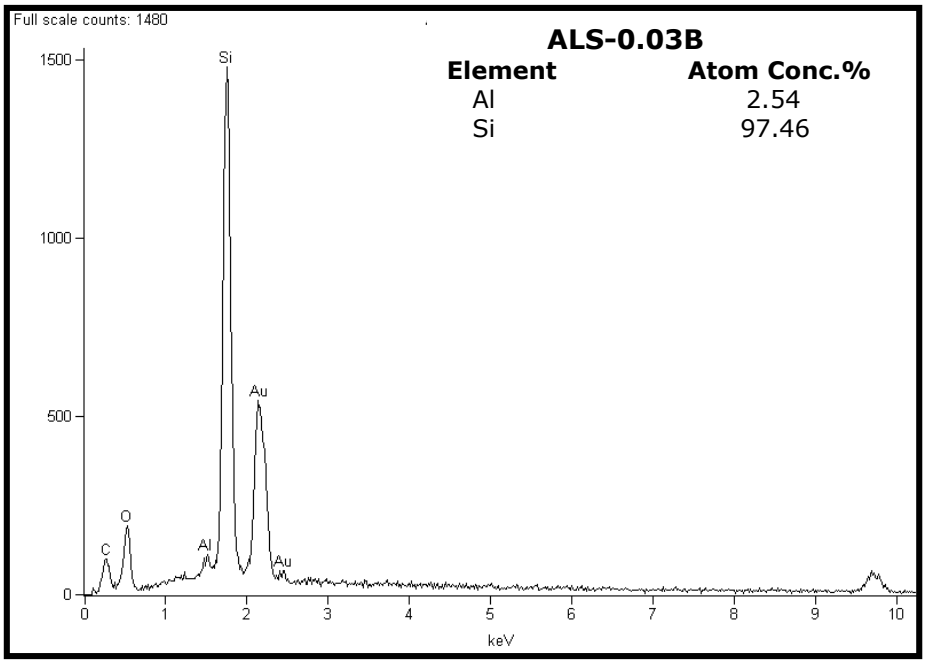


Figure C.6 EDS spectrum of *ALS-0.03B* samples

# APPENDIX D

## CALCULATION OF ACTIVATION ENERGY OF POLYMER DEGRADATION REACTION

The following solid state reaction takes place in polymer cracking,

$$aA_{(s)} \rightarrow bB_{(s)} + cC_{(g)}$$

The rate of disappearence of A is expressed as

$$\frac{d\alpha}{dt} = k_{avg}(1-\alpha)^n \qquad \text{(D.1)}$$

where $\alpha$ is the fraction of A decomposed at time $t$, $n$ is the overall reaction order and $k_{avg}$ is the rate constant. Here $\alpha$ is defined as,

$$\alpha = \frac{1-f_t}{1-f_\infty} \qquad \text{(D.2)}$$

where $f_t$ and $f_\infty$ are the instantaneous and final values of the weight fractions, respectively. The rate constant $k_{avg}$ is described by Arrhenius temperature dependency

$$k_{avg} = A\exp^{-E/RT} \qquad \text{(D.3)}$$

where *A* and *E* are the pre-exponential factor and activation energy of the reaction, respectively. The temperature at any time is written as,

$$T = T_0 + qt \tag{D.4}$$

where *q* is the heating rate, $T_0$ is the initial temperature and *t* is time.
By inserting equations (D.3) and (D.4) into equation (D.1), rearranging, the rate expression for the decomposition becomes as

$$\frac{d\alpha}{(1-\alpha)^n} = \frac{A}{q}\exp\left(\frac{-E}{RT}\right)dT \tag{D.5}$$

The right-hand side of equation (D.5) has no exact integral, but by making the substitution $u=E/RT$ and using the following relation,

$$\int_u^\infty e^{-u}u^{-b}du = u^{1-u}\sum_{n=0}^{\infty}\frac{(-1)^n(b)_n}{u^{n+1}}$$

equation D.5 is integrated with the boundary conditions of $\alpha=0$ for $T=T_0$ and $\alpha=\alpha$ for $T=T$. For the case of $n\neq1$, the following equation is obtained by ignoring the higher order terms of the series,

$$\frac{1-(1-\alpha)^{(1-n)}}{(1-n)T^2} = \frac{AR}{qE}\left(1-\frac{2RT}{E}\right)\exp\left(\frac{-E}{RT}\right) \tag{D.6}$$

This equation is simplified if it is assumed 2RT<<E, and by taking natural logarithm of both sides, the following equation is used for estimating the kinetic parameters from TGA data:

$$\ln\frac{1-(1-\alpha)^{(1-n)}}{(1-n)T^2} = \ln\frac{AR}{qE} - \frac{E}{RT} \tag{D.7}$$

Integration of equation D.5 for the first order reaction (n=1) gives:

$$\ln \frac{-\ln(1-\alpha)}{T^2} = \ln \frac{AR}{qE} - \frac{E}{RT} \qquad \text{(D.8)}$$

By using the $\alpha$ values, a plot of left hand side of equations D.7 and D.8 versus 1/T should give straight lines for a value of *n*. The conventional Arrhenius parameters, *A* and *E*, can be estimated from the intercept and the slope of this line. For first order and second order reactions, equation D.7 was plotted and the results showed that best $R^2$ value was obtained when the reaction order was estimated as 1 (Figure D.1). These plots were drawn using TGA results of non-catalytic thermal degradation reaction. The same calculations were done for catalytic thermal degradation reactions and found that when *n*=1, best $R^2$ value was obtained.

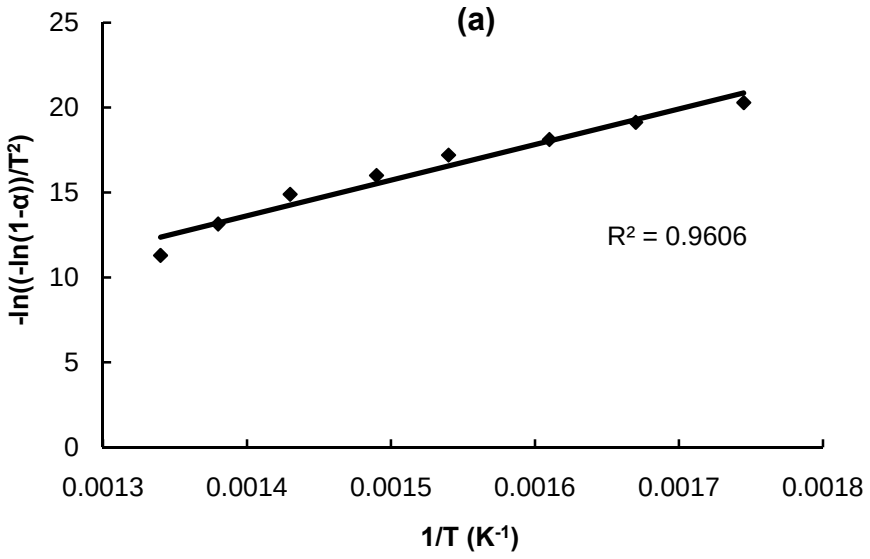


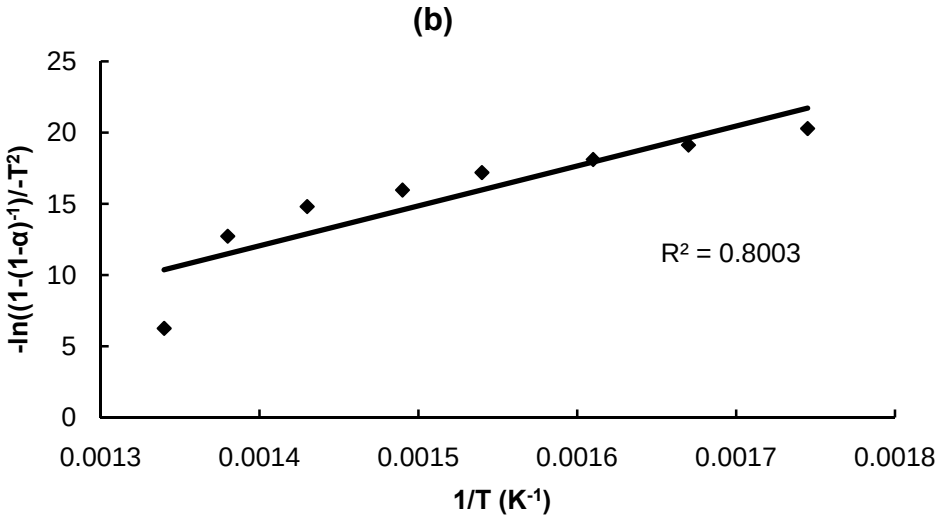


Figure D.1 Determination of the degradation reaction order
(a) for n=1, (b) for n=2

# APPENDIX E

## CALCULATION OF GAS CHROMATOGRAPHY CALIBRATION FACTORS OF GASEOUS PRODUCTS

To identify the products obtained from both the non-catalytic and catalytic degradation reaction of polypropylene, calibration experiments were performed. From these experiments, retention times and calibration factors of the products were determined. For the gaseous products, two different calibration gas mixtures were used. The content of these calibration mixtures are given in Table E.1.

Table E.1 Gas mixtures used in calibration

| 1. Mixture | | 2. Mixture | |
|---|---|---|---|
| **Gas ID** | **Mole (%)** | **Gas ID** | **Mole (%)** |
| CO | 1 | $CH_4$ | 1 |
| $CO_2$ | 1 | $C_2H_6$ | 1 |
| $CH_4$ | 1 | $C_3H_6$ | 1 |
| $C_2H_6$ | 1 | $C_3H_8$ | 1 |
| $C_2H_4$ | 1 | $C_4H_{10}$ | 1 |
| $C_2H_2$ | 1 | $N_2$ | 95 |
| $N_2$ | 94 | | |

## E.1 Sample Calculation for Finding Calibration Factors of Gaseous Products

The calculation procedure for calibration factor is given in the following (via second calibration gas mixture):

A: $CH_4$; B: $C_2H_6$; E: $C_3H_6$; F: $C_3H_8$; G:n-$C_4H_{10}$

$A_i$ : Area belongs to ith component (obtained from GC)

$\beta_i$ : Calibration factor of ith component

$y_i$ : Mole fraction of ith component

$n_i$ : Mole of ith component, $A_i\beta_i$

<u>$N_2$ free basis calculation</u>:

$$A_A\beta_A + A_B\beta_B + A_E\beta_E + A_F\beta_F + A_G\beta_G = n_{total} \quad \text{(E.1)}$$

$$\Downarrow$$

$$y_A = \frac{n_A}{n_{total}} = \frac{A_A\beta_A}{A_A\beta_A + A_B\beta_B + A_E\beta_E + A_F\beta_F + A_G\beta_G} \quad \text{(E.2)}$$

$$\Downarrow$$

$$\frac{y_A}{y_B} = \frac{n_A}{n_B} = \frac{A_A\beta_A}{A_B\beta_B} \quad \text{(E.3)}$$

Since methane ($CH_4$) and ethane ($C_2H_6$) are common in both calibration gas mixtures, methane was arbitrarily assigned a calibration factor ($\beta_A$) of 1.0. From equation E.3, $\beta_B$ can be calculated since $A_A$, $A_B$ and $\beta_A$ are known. Same calculations were done for the other gases. All the retention times, average areas obtained from gas chromatography and calibration factors of gases are given in Table E.2. Average areas were taken as a result of six injection from each gas mixture.

Table E.2 Retention times, average areas and calibration factors of gas products obtained in degradation of polypropylene

| Gas ID | Retention time (minutes) | $A_{average}$ (mVolt.sec) | Calibration Factor,β |
|---|---|---|---|
| $CH_4$ (A) | 0.58 | 13.2 | 1 |
| $C_2H_6$ (B) | 2.1 | 19.2 | 0.69 |
| $C_2H_2$ (C) | 1.57 | 29.8 | 0.44 |
| $C_2H_4$ (D) | 3.14 | 31.7 | 0.42 |
| $C_3H_6$ (E) | 6.97 | 24.7 | 0.54 |
| $C_3H_8$(F) | 7.91 | 23.7 | 0.56 |
| $C_4H_{10}$(G) | n-$C_4H_{10}$: 28.9<br>i-$C_4H_{10}$ : 26.1 | 22.6 | 0.59 |

# APPENDIX F

## CALCULATION OF MOLE & WEIGHT FRACTIONS AND SELECTIVITIES OF PRODUCTS

F.1 Sample Calculation for determination of product molar & weight fractions and selectivities

Reaction temperature: 425°C & Reaction time: 30 min.

A: $CH_4$; B: $C_2H_6$; C: $C_2H_2$; D: $C_2H_4$;

E: $C_3H_6$; G:n-$C_4H_{10}$

Mole fraction of $CH_4$:

$$y_A = \frac{n_A}{n_{total}} = \frac{A_A \beta_A}{A_A \beta_A + A_B \beta_B + A_C \beta_C + A_D \beta_D + A_E \beta_E + A_G \beta_G} \qquad (F.1)$$

Weight fraction of $CH_4$:

$$w_A = \frac{m_A}{m_{mixture}} = \frac{y_A MWt_A}{y_A MWt_A + y_B MWt_B + y_C MWt_C + y_D MWt_D + y_E MWt_E + y_G MWt_G} \qquad (F.2)$$

Carbon balance was done for selectivity calculations.

Selectivity of $CH_4$:

$$S_A = \frac{n_A}{n_A + 2n_B + 2n_C + 2n_D + 3n_E + 4n_G} \qquad (F.3)$$

Area of peaks, calibration factors and moles of gas products are given in Table F.1.

Table F.1 Area of peaks, calibration factors and moles of gas products (T:425°C & t:30 min.)

| Gas ID | $A_{average}$ (mVolt.sec) | Calibration Factor,β | Mole n |
|---|---|---|---|
| $CH_4$ (A) | 1.33 | 1 | 1.33 |
| $C_2H_6$ (B) | 2.15 | 0.69 | 1.48 |
| $C_2H_2$ (C) | 1.14 | 0.44 | 0.50 |
| $C_2H_4$ (D) | 24.3 | 0.42 | 10.2 |
| $C_3H_6$ (E) | 15 | 0.54 | 8.10 |
| $C_4H_{10}$(G) | 2.4 | 0.59 | 1.42 |

From this table mole fraction of methane can be calculated as given below,

$$y_A = \frac{n_A}{n_{total}} = \frac{1.33}{1.33 + 1.48 + 0.50 + 10.2 + 8.10 + 1.42} = 0.06$$

Weight fraction of methane was calculated using equation F.2,

$$w_A = \frac{m_A}{m_{mixture}} = \frac{0.06 \times 16}{0.06 \times 16 + 0.06 \times 30 + 0.02 \times 26 + 0.44 \times 28 + 0.35 \times 42 + 0.06 \times 58} = 0.03$$

From equation F.3, selectivity of methane at 425°C was calculated as,

$$S_A = \frac{1.33}{1.33 + 2 \times 1.48 + 2 \times 0.5 + 2 \times 10.2 + 3 \times 8.1 + 4 \times 1.42} = 0.02$$

# APPENDIX G

## MOLE & WEIGHT FRACTIONS AND SELECTIVITY VALUES OF GASEOUS PRODUCTS

Mole and weight fractions and selectivities of gas products were tabulated in Tables G.1-G.4.

Table G.1 Mole & weight fractions and selectivities of gas products obtained at 400°C

| | | Reaction time (min) | | |
|---|---|---|---|---|
| Mole & weight fractions and selectivities of gas products | | 30 | 45 | 60 |
| Ethane | y | 0.06 | 0.06 | 0 |
| | **w** | **0.06** | **0.06** | **0** |
| | *S* | *0.06* | *0.06* | *0* |
| Ethylene | y | 0.69 | 0.69 | 0.81 |
| | **w** | **0.61** | **0.61** | **0.75** |
| | *S* | *0.61* | *0.61* | *0.75* |
| Propylene | y | 0.25 | 0.25 | 0.19 |
| | **w** | **0.33** | **0.33** | **0.25** |
| | *S* | *0.33* | *0.33* | *0.25* |

Table G.2 Mole & weight fractions and selectivities of gas products obtained at 410°C

Reaction time (min)

| Mole & weight fractions and selectivities of gas products | | 15 | 30 |
|---|---|---|---|
| Ethane | y | 0.09 | 0.08 |
| | **w** | **0.08** | **0.07** |
| | *S* | *0.08* | *0.07* |
| Ethylene | y | 0.54 | 0.53 |
| | **w** | **0.45** | **0.44** |
| | *S* | *0.45* | *0.44* |
| Propylene | y | 0.37 | 0.39 |
| | **w** | **0.47** | **0.49** |
| | *S* | *0.47* | *0.49* |

Table G.3 Mole & weight fractions and selectivities of gas products obtained at 425°C

Reaction time (min)

| Mole & weight fractions and selectivities of gas products | | 15 | 30 |
|---|---|---|---|
| Methane | y | 0.07 | 0.06 |
| | **w** | **0.04** | **0.03** |
| | *S* | *0.03* | *0.02* |
| Ethane | Y | 0.09 | 0.06 |
| | **w** | **0.08** | **0.06** |
| | *S* | *0.07* | *0.05* |
| Acetylene | y | 0.02 | 0.02 |
| | **w** | **0.02** | **0.02** |
| | *S* | *0.02* | *0.02* |
| Ethylene | y | 0.38 | 0.44 |
| | **w** | **0.32** | **0.36** |
| | *S* | *0.32* | *0.37* |
| Propylene | y | 0.44 | 0.35 |
| | **w** | **0.55** | **0.43** |
| | *S* | *0.56* | *0.44* |
| n-butane | y | 0 | 0.06 |
| | **w** | **0** | **0.11** |
| | *S* | *0* | *0.10* |

Table G.4 Mole & weight fractions and selectivities of gas products obtained in the presence of catalysts (t:30 min.)

| | **CATALYST ID** | | | | | | | |
|---|---|---|---|---|---|---|---|---|
| | Al-0.03A | Al-1A | Al-0.03B | Al-1B | ALS-0.1A | ALS-0.2A | ALS-0.1B | ALS-1B |
| $y_{ethylene}$ | 0.56 | 0.82 | 0.77 | 0.64 | 0.50 | 0.75 | 0.76 | 0.51 |
| $\mathbf{w_{ethylene}}$ | **0.40** | **0.71** | **0.69** | **0.48** | **0.36** | **0.63** | **0.63** | **0.36** |
| $S_{ethylene}$ | *0.41* | *0.71* | *0.69* | *0.49* | *0.36* | *0.63* | *0.63* | *0.36* |
| $y_{propylene}$ | 0.12 | 0.06 | 0.23 | 0.09 | 0.23 | 0.11 | 0.08 | 0.18 |
| $\mathbf{w_{propylene}}$ | **0.13** | **0.08** | **0.31** | **0.10** | **0.25** | **0.14** | **0.10** | **0.19** |
| $S_{propylene}$ | *0.13* | *0.08* | *0.31* | *0.10* | *0.25* | *0.14* | *0.10* | *0.19* |
| $y_{n\text{-}butane}$ | 0.19 | 0.08 | 0 | 0.19 | 0.22 | 0.09 | 0.16 | 0.23 |
| $\mathbf{w_{n\text{-}butane}}$ | **0.28** | **0.14** | **0** | **0.30** | **0.33** | **0.16** | **0.27** | **0.33** |
| $S_{n\text{-}butane}$ | *0.27* | *0.13* | *0* | *0.29* | *0.32* | *0.16* | *0.26* | 0.33 |
| $y_{i\text{-}butane}$ | 0.13 | 0.04 | 0 | 0.08 | 0.05 | 0.05 | 0 | 0.09 |
| $\mathbf{w_{i\text{-}butane}}$ | **0.19** | **0.08** | 0 | **0.12** | **0.07** | **0.08** | **0** | **0.12** |
| $S_{i\text{-}butane}$ | *0.19* | *0.07* | *0* | *0.11* | *0.06* | *0.07* | *0* | *0.12* |

# APPENDIX H

# CALCULATION OF GAS CHROMATOGRAPHY CALIBRATION FACTORS FOR LIQUID PRODUCTS

To identify the products obtained from both the non-catalytic and catalytic degradation reaction of polypropylene, calibration experiments were performed. From these experiments, retention times and calibration factors of the products were determined. For the liquid products, five different paraffin mixtures were used. The content of these calibration mixtures are given in Tables H.1 and H.2, respectively.

Table H.1 Paraffin mixtures ($C_5$-$C_{12}$) used in calibration

| 1. Mixture | | 2. Mixture | | 3. Mixture | |
|---|---|---|---|---|---|
| **Liq. ID** | **Weight (%)** | **Liq. ID** | **Weight (%)** | **Liq. ID** | **Weight (%)** |
| n-$C_5H_{12}$ | 25 | n-$C_7H_{16}$ | 25 | n-$C_9H_{20}$ | 25 |
| n-$C_6H_{14}$ | 25 | n-$C_8H_{18}$ | 25 | n-$C_{10}H_{22}$ | 25 |
| n-$C_7H_{16}$ | 25 | n-$C_9H_{20}$ | 25 | n-$C_{11}H_{24}$ | 25 |
| n-$C_8H_{18}$ | 25 | n-$C_{10}H_{22}$ | 25 | n-$C_{12}H_{26}$ | 25 |

Table H.2 Paraffin mixtures ($C_{12}$-$C_{18}$) used in calibration

| 4. Mixture | | 5. Mixture | |
|---|---|---|---|
| **Liq. ID** | **Weight (%)** | **Liq. ID** | **Weight (%)** |
| n-$C_{11}H_{24}$ | 25 | n-$C_{12}H_{26}$ | 25 |
| n-$C_{12}H_{26}$ | 25 | n-$C_{14}H_{30}$ | 25 |
| n-$C_{13}H_{28}$ | 25 | n-$C_{16}H_{34}$ | 25 |
| n-$C_{14}H_{30}$ | 25 | n-$C_{18}H_{38}$ | 25 |

Additional calibration mixtures were prepared in equal volumes. One of the compounds was taken as n-hexane in preparing these mixtures. These mixtures are given in Table H.3. 2 ml of mixture was prepared.

Table H.3 Prepared calibration mixtures

| |
|---|
| n-hexane+isooctane |
| n-hexane+diisobutylene |
| n-hexane+cyclohexane |
| n-hexane+benzene |
| n-hexane+xylene |
| n-hexane+toluene |
| n-hexane+ethylbenzene |

H.1 Sample Calculation for Finding Calibration Factors of Liquid Products

The calculation procedure for calibration factor is given in the following (via first calibration paraffin mixture):

A: n-$C_5H_{12}$; B: n-$C_6H_{14}$; C:n-$C_7H_{16}$; D:n-$C_8H_{18}$

$A_i$ : Area belongs to ith component (obtained from GC)

$\beta_i$ : Calibration factor of ith component

$z_i$ : Volume fraction of ith component

$x_i$ : Mole fraction of ith component

$n_i$ : Mole of ith component, $A_i\beta_i$

$$A_A\beta_A + A_B\beta_B + A_C\beta_C + A_D\beta_D = n_{total} \quad \text{(H.1)}$$

$$\Downarrow$$

$$x_A = \frac{n_A}{n_{total}} = \frac{A_A\beta_A}{A_A\beta_A + A_B\beta_B + A_C\beta_C + A_D\beta_D} \quad \text{(H.2)}$$

$$\Downarrow$$

$$\frac{x_A}{x_B} = \frac{n_A}{n_B} = \frac{A_A\beta_A}{A_B\beta_B} \quad \text{(H.3)}$$

Volume fraction of the component can be found from the following relation, if necessary

$$z_A = x_A \frac{MW_A}{\rho_A} \quad \text{(H.4)}$$

In calibration of liquids, n-hexane was arbitrarily assigned a calibration factor ($\beta_B$) of 1.0. From equation E.3, $\beta_A$ can be calculated since $A_A$, $A_B$ and $\beta_B$ are known. Calibration factors of components in the other mixtures were calculated by using the values obtained from the first calibration mixture. All the retention times, average areas obtained from gas chromatography and calibration factors of gases are given in Table H.4.

Table H.4 Retention times and calibration factors of liquid products obtained in degradation of polypropylene

| | **Retention Time (min)** | **Calibration Factor, β** |
|---|---|---|
| n-Pentane ($C_5H_{12}$) | 3.39 | 2.98 |
| n-Hexane ($C_6H_{14}$) | 4.16 | 1.0 |
| Cyclohexane ($C_6H_{12}$) | 6.03 | 0.51 |
| Benzene ($C_6H_6$) | 6.11 | 0.87 |
| n-Heptane ($C_7H_{16}$) | 6.56 | 0.93 |
| isooctane (i-$C_8H_{18}$) | 7.07 | 0.79 |
| Diisobutylene($C_8H_{16}$) | 7.97 | 0.75 |
| Toluene ($C_7H_8$) | 11.7 | 0.78 |
| n-Octane (n-$C_8H_{18}$) | 12.9 | 0.87 |
| Ethylbenzene($C_8H_{10}$) | 17.4 | 0.51 |
| m,p-xylene($C_6H_4(CH_3)_2$) | 17.9 | 0.51 |
| o-xylene($C_6H_4(CH_3)_2$) | 18.2 | 0.51 |
| n-Nonane ($C_9H_{20}$) | 18.4 | 0.64 |
| n-Decane($C_{10}H_{22}$) | 23.3 | 0.56 |
| n-Undecane($C_{11}H_{24}$) | 27.0 | 0.45 |
| n-Dodecane($C_{12}H_{26}$) | 30.7 | 0.42 |
| n-Tridecane($C_{13}H_{28}$) | 33.9 | 0.33 |
| n-Tetradecane($C_{14}H_{30}$) | 38.1 | 0.41 |
| n-Hexadecane($C_{16}H_{34}$) | 51.2 | 0.69 |
| n-Octadecane($C_{18}H_{38}$) | 69.4 | 0.90 |

# APPENDIX I

## MOLE & WEIGHT FRACTIONS AND SELECTIVITY VALUES OF LIQUID PRODUCTS

Mole and weight fractions and selectivities of liquid products were tabulated in Tables I.1-I.14.

Table I.1 Mole & weight fraction and selectivity values of liquid products at *400℃* and t:45 minutes

| Product ID | Mole fraction, x | Weight fraction, w | Selectivity, S |
|---|---|---|---|
| $C_5$ | 0.182 | 0.087 | 0.086 |
| $C_6$ | 0.071 | 0.040 | 0.040 |
| $C_8$ | 0.083 | 0.060 | 0.063 |
| $C_9$ | 0.020 | 0.017 | 0.017 |
| $C_{10}$ | 0.004 | 0.004 | 0.004 |
| $C_{11}$ | 0.125 | 0.130 | 0.130 |
| $C_{12}$ | 0.219 | 0.248 | 0.247 |
| $C_{13}$ | 0.020 | 0.024 | 0.024 |
| $C_{14}$ | 0.178 | 0.235 | 0.235 |
| $C_{16}$ | 0.050 | 0.075 | 0.075 |
| $C_{18}$ | 0.047 | 0.079 | 0.079 |

Table I.2 Mole & weight fraction and selectivity values of liquid products at *400℃* and t:60 minutes

| Product ID | Mole fraction, x | Weight fraction, w | Selectivity, S |
|---|---|---|---|
| $C_5$ | 0.023 | 0.012 | 0.011 |
| $C_6$ | 0.093 | 0.053 | 0.055 |
| $C_8$ | 0.371 | 0.285 | 0.291 |
| $C_9$ | 0.020 | 0.018 | 0.017 |
| $C_{10}$ | 0.002 | 0.002 | 0.002 |
| $C_{11}$ | 0.108 | 0.118 | 0.117 |
| $C_{12}$ | 0.174 | 0.207 | 0.205 |
| $C_{13}$ | 0.001 | 0.002 | 0.002 |
| $C_{14}$ | 0.147 | 0.203 | 0.202 |
| $C_{16}$ | 0.037 | 0.059 | 0.059 |
| $C_{18}$ | 0.023 | 0.040 | 0.040 |

Table I.3 Mole & weight fraction and selectivity values of liquid products at 410°C and t:15 minutes

| Product ID | Mole fraction, x | Weight fraction, w | Selectivity, S |
|---|---|---|---|
| $C_{11}$ | 0.094 | 0.066 | 0.065 |
| $C_{12}$ | 0.033 | 0.025 | 0.025 |
| $C_{13}$ | 0.044 | 0.036 | 0.036 |
| $C_{14}$ | 0.108 | 0.096 | 0.096 |
| $C_{16}$ | 0.309 | 0.311 | 0.311 |
| $C_{18}$ | 0.412 | 0.466 | 0.467 |

Table I.4 Mole & weight fraction and selectivity values of liquid products at *410℃* and t:30 minutes

| Product ID | Mole fraction, x | Weight fraction, w | Selectivity, S |
|---|---|---|---|
| $C_{11}$ | 0.012 | 0.009 | 0.011 |
| $C_{12}$ | 0.067 | 0.052 | 0.065 |
| $C_{13}$ | 0.128 | 0.108 | 0.135 |
| $C_{14}$ | 0.257 | 0.232 | 0.036 |
| $C_{16}$ | 0.172 | 0.178 | 0.223 |
| $C_{18}$ | 0.363 | 0.421 | 0.529 |

Table I.5 Mole & weight fraction and selectivity values of liquid products at *425℃* and t:15 minutes

| Product ID | Mole fraction, x | Weight fraction, w | Selectivity, S |
|---|---|---|---|
| $C_5$ | 0.003 | 0.002 | 0.002 |
| $C_6$ | 0.315 | 0.192 | 0.197 |
| $C_8$ | 0.226 | 0.184 | 0.185 |
| $C_9$ | 0.012 | 0.011 | 0.003 |
| $C_{10}$ | 0.003 | 0.004 | 0.096 |
| $C_{11}$ | 0.084 | 0.098 | 0.193 |
| $C_{12}$ | 0.154 | 0.197 | 0.024 |
| $C_{13}$ | 0.017 | 0.024 | 0.210 |
| $C_{14}$ | 0.144 | 0.213 | 0.038 |
| $C_{16}$ | 0.023 | 0.038 | 0.036 |
| $C_{18}$ | 0.019 | 0.037 | 0.123 |

Table I.6 Mole & weight fraction and selectivity values of liquid products at *425℃* and t:30 minutes

| Product ID | Mole fraction, x | Weight fraction, w | Selectivity, S |
|---|---|---|---|
| $C_5$ | 0.098 | 0.045 | 0.044 |
| $C_6$ | 0.239 | 0.131 | 0.129 |
| $C_7$ | 0.003 | 0.002 | 0.002 |
| $C_8$ | 0.049 | 0.034 | 0.035 |
| $C_9$ | 0.007 | 0.006 | 0.006 |
| $C_{10}$ | 0.003 | 0.003 | 0.003 |
| $C_{11}$ | 0.075 | 0.074 | 0.074 |
| $C_{12}$ | 0.150 | 0.162 | 0.162 |
| $C_{13}$ | 0.012 | 0.014 | 0.014 |
| $C_{14}$ | 0.143 | 0.180 | 0.180 |
| $C_{16}$ | 0.031 | 0.044 | 0.044 |
| $C_{18}$ | 0.190 | 0.306 | 0.307 |

Table I.7 Mole & Weight Fraction and Selectivity values of liquid products in the presence of *Al-1A* catalyst (t:30 min)

| Product ID | Mole fraction, x | Weight fraction, w | Selectivity, S |
|---|---|---|---|
| $C_5$ | 0.000 | 0.000 | 0.000 |
| $C_6$ | 0.000 | 0.000 | 0.000 |
| $C_7$ | 0.077 | 0.039 | 0.040 |
| $C_8$ | 0.078 | 0.045 | 0.046 |
| $C_9$ | 0.053 | 0.036 | 0.035 |
| $C_{10}$ | 0.103 | 0.077 | 0.076 |
| $C_{11}$ | 0.079 | 0.065 | 0.065 |
| $C_{12}$ | 0.095 | 0.085 | 0.085 |
| $C_{13}$ | 0.069 | 0.067 | 0.067 |
| $C_{14}$ | 0.022 | 0.022 | 0.022 |
| $C_{16}$ | 0.017 | 0.020 | 0.020 |
| $C_{18}$ | 0.406 | 0.543 | 0.543 |

Table I.8 Mole & weight fraction and selectivity values of liquid products in the presence of *Al-0.03A* catalyst (t:30 min)

| Product ID | Mole fraction, x | Weight fraction, w | Selectivity, S |
|---|---|---|---|
| $C_5$ | 0.095 | 0.060 | 0.058 |
| $C_6$ | 0.071 | 0.053 | 0.052 |
| $C_7$ | 0.368 | 0.315 | 0.318 |
| $C_8$ | 0.158 | 0.153 | 0.155 |
| $C_9$ | 0.094 | 0.105 | 0.104 |
| $C_{10}$ | 0.058 | 0.071 | 0.071 |
| $C_{11}$ | 0.057 | 0.077 | 0.077 |
| $C_{12}$ | 0.050 | 0.074 | 0.074 |
| $C_{13}$ | 0.030 | 0.048 | 0.048 |
| $C_{14}$ | 0.005 | 0.008 | 0.008 |
| $C_{16}$ | 0.003 | 0.006 | 0.006 |
| $C_{18}$ | 0.013 | 0.028 | 0.028 |

Table I.9 Mole & weight fraction and selectivity values of liquid products in the presence of *Al-1B* catalyst (t:30 min)

| Product ID | Mole fraction, x | Weight fraction, w | Selectivity, S |
|---|---|---|---|
| $C_5$ | 0.097 | 0.066 | 0.064 |
| $C_7$ | 0.674 | 0.619 | 0.623 |
| $C_8$ | 0.080 | 0.084 | 0.084 |
| $C_9$ | 0.019 | 0.022 | 0.022 |
| $C_{10}$ | 0.029 | 0.039 | 0.038 |
| $C_{11}$ | 0.026 | 0.039 | 0.038 |
| $C_{12}$ | 0.040 | 0.064 | 0.064 |
| $C_{13}$ | 0.020 | 0.034 | 0.034 |
| $C_{14}$ | 0.006 | 0.011 | 0.011 |
| $C_{16}$ | 0.008 | 0.017 | 0.016 |
| $C_{18}$ | 0.002 | 0.005 | 0.005 |

Table I.10 Mole & weight fraction and selectivity values of liquid products in the presence of *Al-0.03B* catalyst (t:30 min)

| Product ID | Mole fraction, x | Weight fraction, w | Selectivity, S |
|---|---|---|---|
| $C_5$ | 0.060 | 0.038 | 0.037 |
| $C_6$ | 0.262 | 0.197 | 0.193 |
| $C_7$ | 0.153 | 0.124 | 0.132 |
| $C_8$ | 0.188 | 0.180 | 0.184 |
| $C_9$ | 0.061 | 0.069 | 0.068 |
| $C_{10}$ | 0.143 | 0.178 | 0.175 |
| $C_{11}$ | 0.037 | 0.050 | 0.050 |
| $C_{12}$ | 0.031 | 0.047 | 0.046 |
| $C_{13}$ | 0.028 | 0.045 | 0.044 |
| $C_{14}$ | 0.019 | 0.033 | 0.032 |
| $C_{16}$ | 0.009 | 0.018 | 0.018 |
| $C_{18}$ | 0.010 | 0.023 | 0.023 |

Table I.11 Mole & weight fraction and selectivity values of liquid products in the presence of *ALS-0.1A* catalyst (t:30 min)

| Product ID | Mole fraction, x | Weight fraction, w | Selectivity, S |
|---|---|---|---|
| $C_5$ | 0.038 | 0.024 | 0.024 |
| $C_6$ | 0.027 | 0.021 | 0.021 |
| $C_7$ | 0.622 | 0.541 | 0.545 |
| $C_8$ | 0.127 | 0.125 | 0.127 |
| $C_9$ | 0.013 | 0.015 | 0.015 |
| $C_{10}$ | 0.026 | 0.034 | 0.033 |
| $C_{11}$ | 0.023 | 0.031 | 0.031 |
| $C_{12}$ | 0.062 | 0.095 | 0.093 |
| $C_{13}$ | 0.005 | 0.008 | 0.008 |
| $C_{14}$ | 0.047 | 0.083 | 0.082 |
| $C_{16}$ | 0.005 | 0.010 | 0.010 |
| $C_{18}$ | 0.005 | 0.011 | 0.011 |

Table I.12 Mole & weight fraction and selectivity values of liquid products in the presence of *ALS-0.2A* catalyst (t:30 min)

| Product ID | Mole fraction, x | Weight fraction, w | Selectivity, S |
|---|---|---|---|
| $C_5$ | 0.000 | 0.000 | 0.000 |
| $C_6$ | 0.005 | 0.003 | 0.003 |
| $C_7$ | 0.443 | 0.304 | 0.314 |
| $C_8$ | 0.038 | 0.028 | 0.031 |
| $C_9$ | 0.041 | 0.038 | 0.037 |
| $C_{10}$ | 0.037 | 0.038 | 0.037 |
| $C_{11}$ | 0.030 | 0.034 | 0.033 |
| $C_{12}$ | 0.016 | 0.020 | 0.020 |
| $C_{13}$ | 0.352 | 0.471 | 0.464 |
| $C_{14}$ | 0.025 | 0.036 | 0.035 |
| $C_{16}$ | 0.000 | 0.000 | 0.000 |
| $C_{18}$ | 0.014 | 0.026 | 0.026 |

Table I.13 Mole & weight fraction and selectivity values of liquid products in the presence of *ALS-0.1B* catalyst (t:30 min)

| Product ID | Mole fraction, x | Weight fraction, w | Selectivity, S |
|---|---|---|---|
| $C_5$ | 0.000 | 0.000 | 0.000 |
| $C_6$ | 0.080 | 0.059 | 0.060 |
| $C_7$ | 0.641 | 0.569 | 0.565 |
| $C_8$ | 0.106 | 0.104 | 0.106 |
| $C_9$ | 0.020 | 0.023 | 0.023 |
| $C_{10}$ | 0.008 | 0.009 | 0.009 |
| $C_{11}$ | 0.027 | 0.038 | 0.038 |
| $C_{12}$ | 0.058 | 0.088 | 0.088 |
| $C_{13}$ | 0.003 | 0.006 | 0.006 |
| $C_{14}$ | 0.045 | 0.079 | 0.079 |
| $C_{16}$ | 0.006 | 0.012 | 0.012 |
| $C_{18}$ | 0.006 | 0.013 | 0.013 |

Table I.14 Mole & weight fraction and selectivity values of liquid products in the presence of *ALS-1B* catalyst (t: 30 min)

| Product ID | Mole fraction, x | Weight fraction, w | Selectivity, S |
|---|---|---|---|
| $C_5$ | 0.082 | 0.057 | 0.056 |
| $C_6$ | 0.020 | 0.016 | 0.017 |
| $C_7$ | 0.785 | 0.746 | 0.746 |
| $C_8$ | 0.018 | 0.020 | 0.020 |
| $C_9$ | 0.002 | 0.003 | 0.003 |
| $C_{10}$ | 0.007 | 0.010 | 0.010 |
| $C_{11}$ | 0.014 | 0.021 | 0.021 |
| $C_{12}$ | 0.029 | 0.047 | 0.047 |
| $C_{13}$ | 0.021 | 0.037 | 0.037 |
| $C_{14}$ | 0.010 | 0.020 | 0.020 |
| $C_{16}$ | 0.006 | 0.013 | 0.013 |
| $C_{18}$ | 0.005 | 0.012 | 0.012 |

# APPENDIX J

## SAMPLE CHROMATOGRAMS

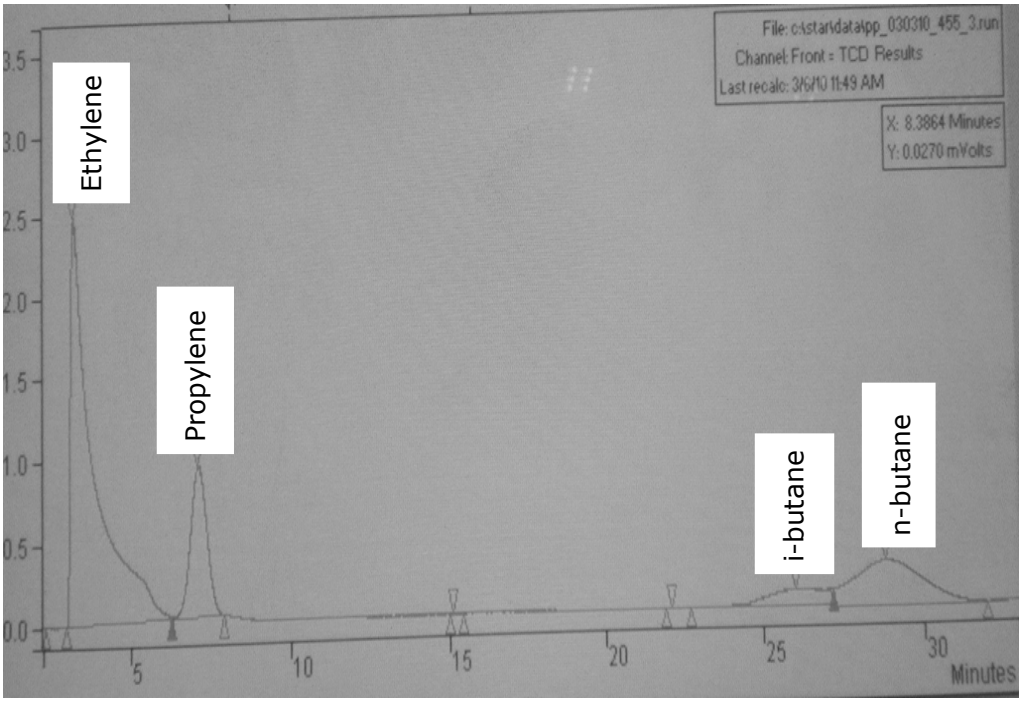


Figure J.1 GC Chromatogram of gas products obtained in the presence of *ALS-1B*

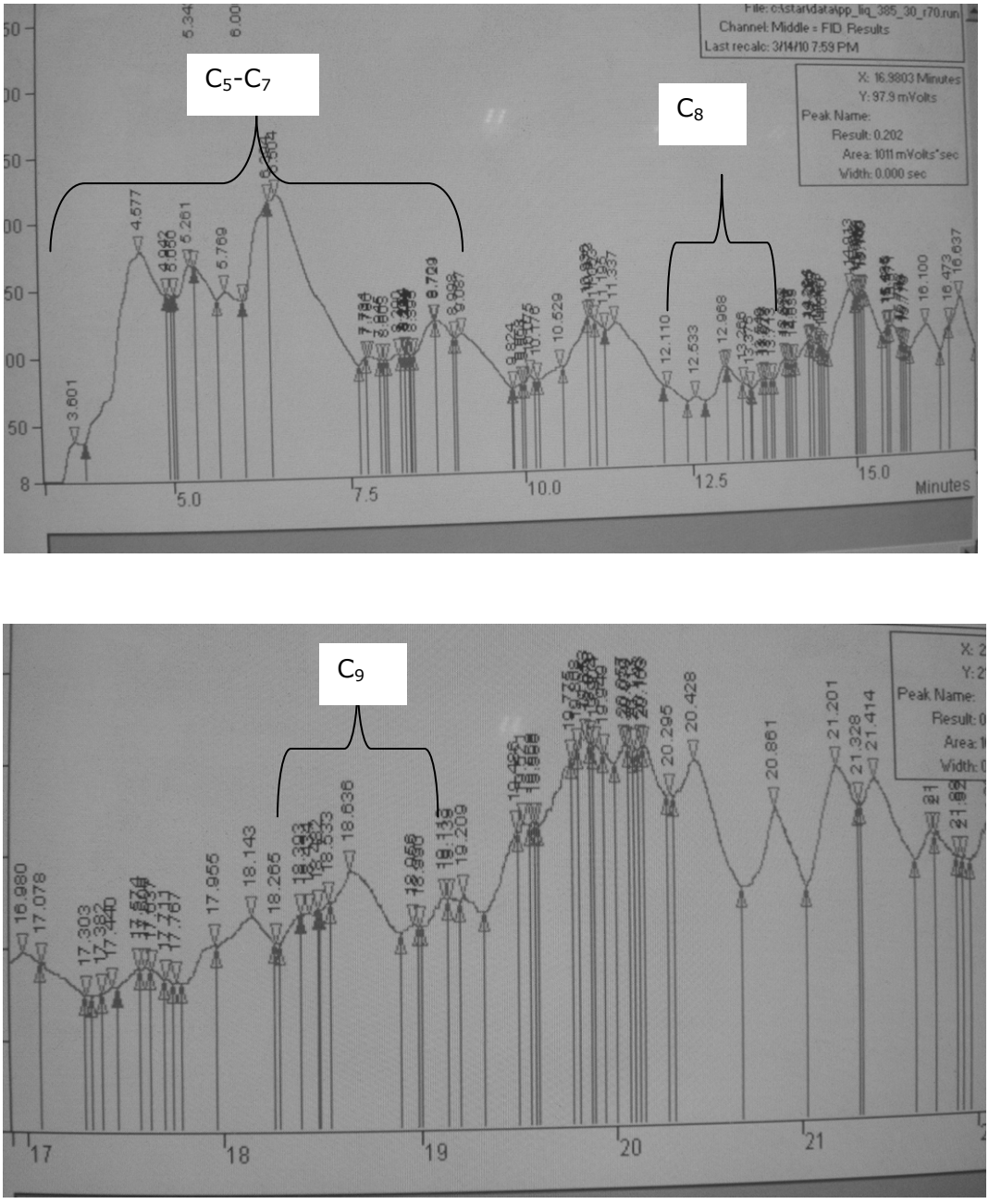


Figure J.2 GC Chromatogram of liquid products obtained in the presence of *Al-1B (t:*3-22 min)

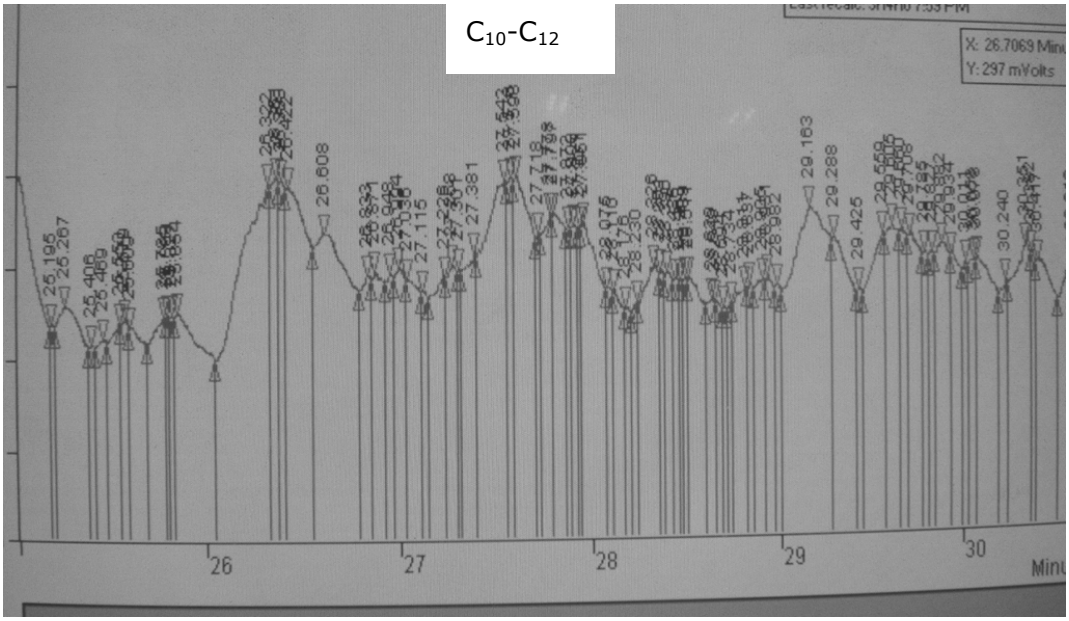


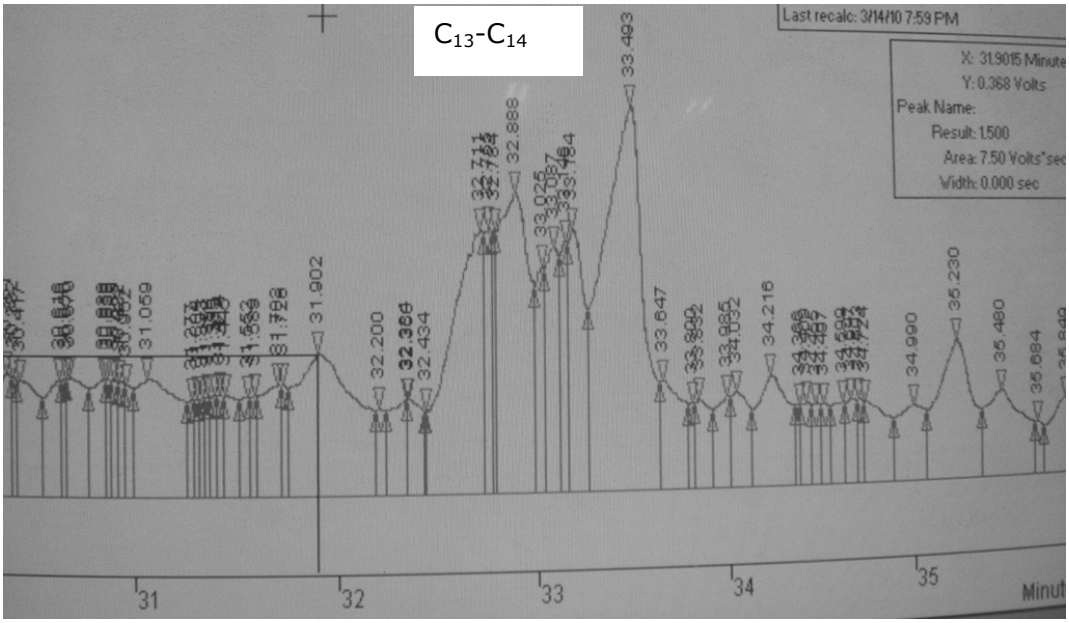


Figure J.3 GC Chromatogram of liquid products obtained in the presence of *Al-1B (t:*25-36 min)

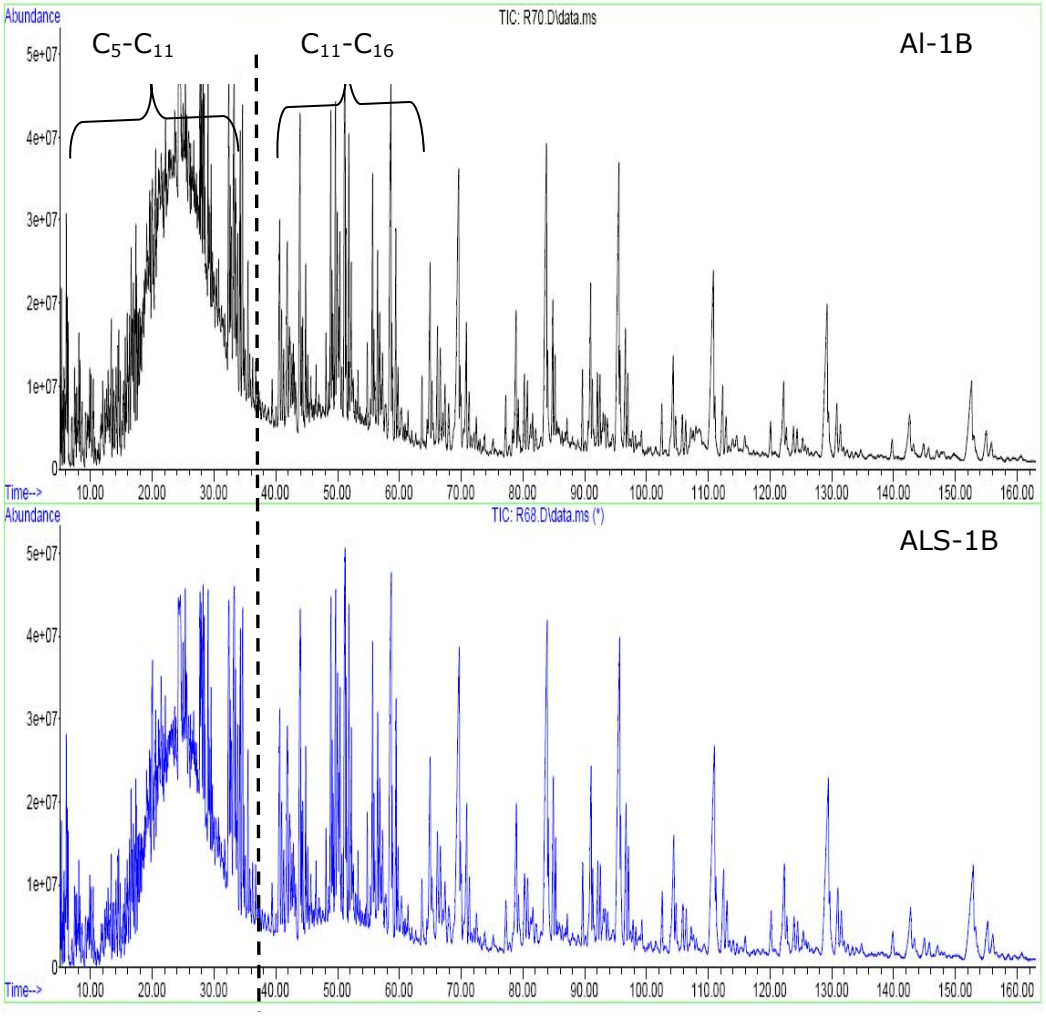


Figure J.4 GC-MS Chromatograms of *Al-1B* & *ALS-1B*

# CURRICULUM VITAE

## PERSONAL INFORMATION

Surname, Name: Obalı, Zeynep
Nationality: Turkish (TC)
Date and Place of Birth: 26 August 1978, Ankara
Marital Status: Single
Phone: +90 312 210 43 63
Fax: +90 312 210 26 00
email: z_obali@yahoo.com

## EDUCATION

- **Ph.D.** (Chemical Engineering) C.GPA: 3.79/4.00
  **[September 2003 –April 2010]**
  Middle East Technical University, Department of Chemical Engineering, Ankara, Turkey
  **Dissertation title:** Synthesis of Aluminum Incorporated Mesoporous Catalysts for Pyrolysis of Polypropylene
  **Supervised by:** Assoc. Prof. Dr. Naime Aslı Sezgi & Prof. Dr. Timur Doğu

- **M.Sc** (Chemical Engineering) C.GPA: 3.50/4.00
  **[September 2000 – September 2003]**
  Middle East Technical University, Department of Chemical Engineering, Ankara, Turkey
  **Dissertation title:** Heteropolyacid Catalysts for Etherification of Isoolefins
  **Supervised by:** Prof.Dr. Timur Doğu

- **B.Sc** (Chemical Engineering) C.GPA: 3.82/4.00
  **[September 1996 – June 2000]**
  Middle East Technical University, Department of Chemical Engineering, Ankara, Turkey

**PROFESSIONAL EXPERIENCE**

- **Teaching Assistant** (Chemical Engineering)
  **[September 2000 – September 2007 ]**
  Middle East Technical University, Department of Chemical Engineering, Ankara, Turkey.
  (Assistanship to undergraduate and graduate courses namely, Engineering Thermodynamics, Process Control, Chemical Reaction Engineering, Chemical Engineering Economics, Chemical Technology, Chemical Engineering Laboratory, Transport Phenomena and Chemical Engineering Mathematics).

- **Training Experience** (Chemical Engineering)
  **[July 1998 – August 1998]**
  AKKİM, Yalova, Turkey

**COMPUTER/LANGUAGE SKILLS**

- Programming Language: Fortran
- Commercial Software Package: Microsoft Office (Word, Excel, PowerPoint), Polymath, Matlab
- Proficient in written and spoken English.

**SCHOLARSHIPS AND AWARDS**

- Middle East Technical University High Honor Roll (Fall 1997, Spring 1998, Fall 1998, Fall 1999, Spring 2000)

- Middle East Technical University Honor Roll (Spring 1999)

## JOURNAL ARTICLES COVERED BY SCIENCE CITATION INDEX

- Obalı Z., Doğu T., **"**Activated carbon-tungstophosphoric acid catalysts for the synthesis of tert-amyl ethyl ether(TAEE)", *Chemical Engineering Journal*, 2008, **138**, 548-555.

- Obalı Z., Sezgi N.A., Doğu T., "Performance of Acidic MCM-like Aluminosilicate catalysts in pyrolysis of polypropylene", *Chemical Engineering Communications*, 2009, **196**, 116-130.

## INTERNATIONAL CONFERENCES ATTENDED

- Obalı Z., Doğu T., "Activated carbon-tungstophosphoric acid catalysts for the synthesis of tert-amyl ethyl ether", II.International Symposium on Carbon for Catalysis, OP-II-11, 11-13 July 2006, St.Petersburg, Russia.

- Obalı Z., Sezgi N.A., Doğu T., "Recycling of polypropylene by catalytic cracking over acidic MCM-like aluminosilicate catalysts", 1. International Congress on Green Process Engineering, Book of Abstracts, p. 290, 24-26 April 2007, Toulouse, France.

- Obalı Z., Sezgi N.A., Doğu T., "Performance of acidic MCM-like aluminosilicate catalysts in pyrolysis of polypropylene", 1.Somer Symposium Series, Somer-S-26, 14-15 May 2007, Ankara, Turkey.

- Obalı Z., Sezgi, N.A., Doğu, T., "Synthesis and Characterization of SBA-type Catalysts and Their Applicability to the Degradation of Polypropylene", 2.International Congress on Green Process Engineering, Book of Extended Abstracts, P54, 14-17 June 2009, Venice, Italy.

## NATIONAL CONFERENCES ATTENDED

- Obalı Z., Doğu T., " Heteropoliasit katalizörlerin tersiyer amil etil eter üretimindeki aktifliği", 6.Ulusal Kimya Mühendisliği Kongresi, RM-36, 7–10 Eylül 2004, İzmir,Türkiye

- Obalı Z., Sezgi, N.A., Doğu T., " Polipropilenin Katalizörlü Ortamda Parçalanması", XX.Ulusal Kimya Kongresi, SKS-03, 4-8 Eylül 2006, Kayseri, Türkiye

- Obalı Z., Sezgi N.A., Doğu T., " Catalytic degradation of polypropylene with a mesoporous aluminosilicate catalyst", I.National Catalysis Conference, C-3, 17-20 January 2007, Güzelyurt, KKTC

- Obalı Z., Sezgi N.A., Doğu T., " Catalytic degradation of polypropylene with SBA-type catalysts", II.National Catalysis Conference, P2, 18-21 June 2008, Erzurum, Turkey

- Obalı Z., Sezgi N.A., Doğu T., " SBA-tipi katalizörlerin sentezlenmesi ve polipropilenin parçalanma reaksiyonundaki performansı", XXII.Ulusal Kimya Kongresi, FKP201, 6-10 Ekim 2008, Mağusa, KKTC

**PROJECTS ATTENDED**

- Doğu T., Obalı Z., "İzoolefinlerin Eterifikasyonunda Kullanılan Heteropoliasit Katalizörleri", AFP-2001-07-02-00-33, ODTÜ, Ankara, 2001-2003.

- Doğu T., Boz N., Obalı Z., Varışlı D., "Benzin Oktan Yükselticileri ETBE,TAME,TAEE üretimi için katalizör geliştirilmesi ve kinetik çalışmalar", BAP-03-04-DPT.2002K120540-19, ODTÜ, Ankara, 2002-2005.

- Sezgi N.A., Doğu T., Obalı Z., "Polipropilen Plastik Atığının Katalitik İndirgenmesiyle Değerli Kimyasallar ve Sıvı Yakıt Üretimi", BAP-2007-03-04-08, ODTÜ, Ankara, 2007-2009.

- Sezgi N.A., Doğu T., Obalı Z., "Polipropilen Plastik Atıklarının Katalitik Parçalanması ile Değerli Kimyasallar ve Sıvı Yakıt Üretimi", TÜBİTAK,107M303, Ankara, 2007-2009.